UNIVERSIDAD DE GRANADA

FACULTAD DE CIENCIAS

Departamento de Química Analítica

Grupo de investigación FQM-297 "Control Analítico, Ambiental, Bioquímico y Alimentario"

TESIS DOCTORAL

DESARROLLO DE NUEVAS FASES SENSORAS ÓPTICAS PARA EL CONTROL DE OXÍGENO MOLECULAR CON APLICACIONES BIOTECNOLÓGICAS, INDUSTRIALES Y CLÍNICAS

Marta Marín Suárez del Toro

Granada, septiembre de 2012

Editor: Editorial de la Universidad de Granada
Autor: Marta Marín Suárez del Toro
D.L.: GR 350-2013
ISBN: 978-84-9028-363-9

UNIVERSIDAD DE GRANADA
FACULTA DE CIENCIAS
DEPARTAMENTO DE QUÍMICA ANALÍTICA

DESARROLLO DE NUEVAS FASES SENSORAS ÓPTICAS PARA EL CONTROL DE OXÍGENO MOLECULAR CON APLICACIONES BIOTECNOLÓGICAS, INDUSTRIALES Y CLÍNICAS

Memoria presentada por Marta Marín Suárez del Toro para optar al grado de Doctor Internacional en Química.

Granada, septiembre de 2012

Marta Marín Suárez del Toro

LOS DIRECTORES DE LA TESIS

Dr. D. Alberto Fernández Gutiérrez
Profesor Catedrático del Departamento de Química Analítica

Dr. D. Jorge Fernando Fernández Sánchez
Profesor Titular del Departamento de Química Analítica

Departamento de Química Analítica
"Profesor Fermín Capitán García"
Campus Universitario Fuentenueva
18071 Granada. España

El Prof. Dr. D. Alberto Fernández Gutiérrez, Catedrático del Departamento de Química Analítica "Profesor Fermín Capitán" de la Facultad de Ciencias, y Director del grupo de investigación FQM-297 "Control analítico, ambiental, bioquímico y alimentario", de la Universidad de Granada,

CERTIFICA QUE:

El trabajo que se presenta en esta tesis doctoral con el título: **"DESARROLLO DE NUEVAS FASES SENSORAS ÓPTICAS PARA EL CONTROL DE OXÍGENO MOLECULAR CON APLICACIONES BIOTECNOLÓGICAS, INDUSTRIALES Y CLÍNICAS",** que ha sido realizado bajo mi dirección y la del Prof. Dr. D. Jorge F. Fernández Sánchez en los laboratorios que el grupo FQM-297 tiene en el Departamento de Química Analítica y también, parcialmente, en el Institute of Robotics and Intelligent Systems (IRIS), del Swiss Federal Institute of Technology (ETH) de Zurich (Suiza), y en el Institute of Analytical Chemistry and Food Chemistry, de Graz University of Technology (Austria), reúne todos los requisitos legales, académicos y científicos para hacer que la doctoranda Dña. Marta Marín Suárez del Toro pueda optar al grado de Doctor Internacional en Química.

Y para que así conste, expido y firmo el presente certificado en Granada a 1 de septiembre de 2012:

Esta tesis doctoral ha sido realizada gracias a una beca predoctoral asignada al Proyecto de Excelencia P07-FQM- 02625, y a la financiación con cargo a fondos del grupo FQM-297 "Control Analítico, Ambiental, Bioquímico y Alimentario" del Plan Andaluz de Investigación de la Junta de Andalucía, procedentes de diferentes contratos, proyectos y subvenciones de la Administración central y autonómica y plan propio de investigación de la UGR.

AGRADECIMIENTOS

DEDICATORIA

Nuestras horas son minutos
cuando esperamos saber,
y siglos cuando sabemos
lo que se puede aprender.

(A. Machado)

ÍNDICE

Justificación y Objetivos

La importancia del oxígeno para estimar y evaluar una gran variedad de parámetros físico-químicos de gran interés para la vida, la medicina, el medio ambiente o la industria, junto al impulso que la Nanotecnología ha dado a los sensores ópticos, han dado lugar a un creciente interés por la determinación de oxígeno a través de estos métodos. Esto ha permitido desarrollar sofisticados y robustos sistemas de detección de fácil aplicabilidad y que dan solución a problemas complejos presentes en la Química Analítica. Así, el objeto principal de esta memoria es el desarrollo de fases sensoras ópticas para la determinación de oxígeno con aplicación biotecnológica y médica, tanto mediante la caracterización de fase sensoras ópticas como mediante la optimización y el desarrollo de nuevas estrategias de deposición.

En primer lugar, se pretende profundizar a nivel teórico y experimental en el desarrollo de fases sensoras ópticas para la determinación de oxígeno y progresar en el conocimiento de la relación de sus componentes con parámetros analíticos (sensibilidad). Para ello, el primer objetivo de este memoria es la caracterización y evaluación de fases sensoras ópticas sensibles a oxígeno basadas en nuevos complejos de Ir(III) que cubran diferentes longitudes de onda de emisión del espectro visible y que presenten alta sensibilidad a oxígeno. Además, el segundo objetivo es valorar la habilidad de soportes nanoestructurados de óxido hidróxido de aluminio para mejorar las propiedades luminiscentes y de sensibilidad de estos nuevos (en especial de los complejos de carácter neutro que nunca antes se habían combinado con este tipo de soportes), y evaluar su aplicabilidad en la detección de concentraciones bajas de oxígeno.

Por otro lado, el diseño de fases sensoras con propiedades específicas constituye hoy en día uno de los principales desafíos de la Ciencia de los Materiales y de la Química Analítica, lo que se ve reflejado en dos aspectos de esta memoria: la necesidad de sintetizar nuevos materiales a la carta y de controlar el procesado de los mismos

(formación y deposición de la fase sensora). Por tanto, otro de los objetivos es resaltar la importancia de las técnicas de polimerización controlada en el diseño y desarrollo de (co)polímeros con propiedades ópticas, en concreto mediante polimerización radical por transferencia de átomo. Del mismo modo, se pretende evaluar la utilidad de la metodología de superficie de respuesta (SRM) para modelizar las propiedades morfológicas de las fases sensoras nanopartículadas y en especial para el desarrollo de nanopartículas híbridas sensibles a oxígeno con polidispersidad y tamaño controlado.

Otro de los objetivos principales de esta tesis es el desarrollo de una fase sensora fácilmente implementable sobre un microrrobot inalámbrico para la detección de oxígeno *in vivo* en el líquido ocular. Para ello, primero se pretende evaluar fases sensoras de diferente naturaleza (planares y nanopartículadas) usando instrumentación adaptada a las medidas reales. De este estudio y debido a la morfología tridimensional del microrrobot, surge como objetivo la necesidad de desarrollar métodos de deposición fácilmente adaptables a formas irregulares y escala micrométrica, sin que se pierda el control sobre las propiedades de la fase sensora (fotoestabilidad, sensibilidad y tiempo de respuesta).

El último objetivo de esta Memoria consiste en demostrar la versatilidad de la técnica de deposición electroforética, que ha sido previamente aplicada para desarrollar una fase sensora de oxígeno, para desarrollar otro tipo de fases sensoras ópticas. Se hace por tanto uso de todos los conocimientos adquiridos en la etapa predoctoral con el objetivo de iniciar una nueva línea de investigación en el Grupo de Investigación en el cual se ha desarrollado esta Tesis. Esta línea versa sobre la detección óptica de oxígeno como sistema de transducción para la determinación indirecta de parámetros bioquímicos, usando en este caso la glucosa como modelo de parámetro bioquímico, y evaluando diversas estrategias para la generación de fases sensoras con transducción óptica de O_2.

Resumen

Esta **Memoria** presenta los resultados obtenidos durante la realización de la Tesis Doctoral titulada "Desarrollo de nuevas fases sensoras ópticas para el control de oxígeno molecular con aplicaciones biotecnológicas, industriales y clínicas".

La Memoria se ha dividido en dos secciones principales: introducción y parte experimental.

La **introducción** recoge, en primer lugar, una visión general de la importancia de la determinación de oxígeno en diferentes campos de la Ciencia, así como las técnicas existentes para realizar dicha determinación. En segundo lugar, se detalla más información sobre la determinación de oxígeno por atenuación de la luminiscencia y el diseño de fases sensoras ópticas. Para ello, se describen tanto los fundamentos de la luminiscencia molecular como los diferentes métodos existentes para su detección, haciendo un especial hincapié sobre las partes que componen un sensor óptico y sus diferentes configuraciones. Tras estas nociones sobre sensores ópticos de oxígeno se describen los componentes de la fase sensora: indicador y matriz; señalando cuales son los materiales más utilizados en el desarrollo de fases sensoras ópticas de oxígeno, algunas de sus características y como éstas influyen sobre la sensibilidad de la fase sensora obtenida. En el último apartado de la introducción se resume la importancia de los sensores ópticos de oxígeno, resaltando aspectos generales del diseño y la caracterización, los motivos que han impulsado el desarrollo de estos dispositivos, así como sus ventajas e inconvenientes. Por último se realiza una revisión sobre las aplicaciones más relevantes que utilizan la atenuación de la luminiscencia para obtener información de importancia analítica sobre paramétros de diferente naturaleza.

La segunda parte, denominada **experimental,** recoge los resultados obtenidos durante la realización de la presente Tesis Doctoral y la discusión de los mismos; se divide en cuatro bloques (cada uno compuesto de uno o dos capítulos) con una breve introducción sobre la temática y consideraciones más importantes.

El **primer bloque** se centra en la caracterización de fases sensoras ópticas basadas en complejos de Ir(III) depositados en membranas poliméricas de diferente viscosidad, así como en el soporte nanoestructurado. Este bloque fue desarrollado en colaboración con el *Laboratory for Photonics and Interfaces del Institute of Chemical Sciences and Engineering* del *École Polytechnique Fédérale de Lausanne* (EPFL) en Suiza y recoge la caracterización de nuevos complejos de iridio con diferentes combinaciones de ligandos derivados de la piridina que emiten a longitudes de onda comprendidas entre 470 nm y 625 nm.

En total se han caracterizado 4 complejos catiónicos y 3 complejos neutros. Estos complejos fueron depositados sobre poliestireno con diferentes cantidades de plastificante y sobre un soporte nanoestructurado basado en óxido hidróxido de aluminio. Para la evaluación de las fases sensoras y su compatibilidad con los soportes en función de las características del complejo, se determinaron sus constantes de Stern-Volmer, rendimientos cuánticos de luminiscencia y tiempo de respuesta; los complejos mostraron una alta sensibilidad a oxígeno para bajas concentraciones cuando son incorporados a la matriz de óxido hidróxido de aluminio. Los resultados obtenidos de esta caracterización se muestran en los **Capítulos 1 y 2.**

El **segundo bloque** versa sobre la importancia del desarrollo de fases sensoras ópticas con propiedades específicas. Este control de propiedades puede hacerse atendiendo a dos aspectos: la síntesis de materiales a la carta o el control sobre las propiedades morfológicas de la fase sensora. Así, en el **Capítulo 3** se llevó a cabo una revisión bibliográfica de la técnica de polimerización radical controlada como herramienta para la obtención de nuevos materiales con propiedades especificas que potencien su aplicación en el desarrollo de fases sensoras ópticas. Y en el **Capítulo 4** se aplica un diseño de experimentos basados en la metodología de superficies de respuesta (RSM) para modelizar el tamaño y polidispersidad de nanopartículas poliméricas obtenidas mediante el método de miniemulsión-evaporación. Este trabajo fue realizado en colaboración con el Departamento de Química Analítica de la Universidad de Extremadura. La aplicación de esta metodología resulta útil para simplificar la búsqueda de las condiciones experimentales que dan lugar a nanopartículas con un determinado valor de tamaño y polidispersidad, y puede hacerse extensible a la modelización de otros parámetros. Además, la metodología de superficies de respuesta permite obtener un catalogo de tamaños y polidispersidad

realizando un mínimo número de experimentos. En concreto, el modelo obtenido fue aplicado en el desarrollo de nanopartículas híbridas de poli(estireno-co-anhídrido maleico) y magnetita que poseían el indicador de oxígeno (pentafluorofenilporirina de Pt(II), (PtTFPP)) encapsulado en su interior, con la intención de producir nanopartículas que fueran fácilmente recolectables con un imán. Para ello, se fijó un tamaño objetivo de 200 nm y la mínima polidispersidad alcanzable por las condiciones experimentales. De este modo, haciendo uso de Matlab y las ecuaciones obtenidas de la aplicación del RSM, se encontraron las condiciones de síntesis (concentración de polímero y volumen de disolvente) más adecuadas para obtener dicho tamaño de partícula en polímeros de tres pesos moleculares diferentes.

El **tercer bloque** se llevó a cabo en colaboración con el *Swiss Federal Institute of Technology* de Zurich (ETH Zurich), Suiza. El contenido de este bloque está relacionado con el desarrollo de un sensor inalámbrico para determinación de oxígeno en líquido ocular. Así, en el **Capítulo 5** se comparan dos fase sensoras, una membrana clásica y otra particulada, basadas en poliestireno y el complejo octaetilporifirina de Pt(II). Ambas tipos de fases son depositadas sobre un chip recubierto de oro que simula la superficie del sensor intraocular usado para esta aplicación. La comparación de su sensibilidad y tiempo de respuesta muestran las ventajas que ofrece la Nanotecnología para disminuir el tiempo de respuesta. A continuación, en el **Capítulo 6** se desarrolla un método de deposición de estas partículas basado en la deposición electroforética, lo que no solo permite el control sobre la deposición de la fase sensora sino que también permite la deposición en superficies micrométricas no planas. Para desarrollar este método se optimizó, en primer lugar, la síntesis de nanopartículas mediante precipitación-evaporación con el complejo PtTFPP encapsulado físicamente, y se acotó el intervalo óptimo de voltaje y tiempo para llevar a cabo la deposición. A continuación se realizó la deposición electroforética sobre diferentes chips de oro, a diferentes tiempos y voltajes, y se analizaron las propiedades de las fases sensoras, mostrando una buena sensibilidad a oxígeno. Además, el tiempo de respuesta de las fases varió entre 4 y 8 segundos, lo cual es importante en aplicaciones *in vivo*. El análisis de los chips mediante microscopia electrónica de barrido también proporcionó información sobre la cantidad de partículas depositadas (mayor cantidad para tiempo y voltajes mayores). El agarre de las partículas sobre la superficie de oro fue evaluado haciendo

pasar un flujo de agua durante 12 horas, demostrando la aplicabilidad de esta técnica de deposición para la generación de fases sensoras ópticas.

Por último el **bloque 4**, que consta de un único capítulo, se dedica íntegramente al desarrollo de un biosensor de glucosa con transducción óptica de oxígeno. Así, en el **Capítulo 7** se desarrolla una fase sensora sensible a glucosa mediante la deposición electroforética de la enzima glucosa oxidasa y nanopartículas poliméricas que contenían el indicador PtTFPP covalentemente unido. La síntesis del polímero indicador se llevó a cabo en el *Institute of Analytical Chemistry and Food Chemistry* de la *Graz University of Technology* de Graz (Austria), a partir de un polímero y complejo comerciales y condiciones suaves de reacción. Las nanopartículas obtenidas por precipitación-evaporación a partir de este polímero fueron depositadas sobre un chip de oro junto con la enzima siguiendo varias estrategias (concentración, voltaje y tiempo aplicado, orden de deposición de los diferentes reactivos). El chip que mostró una mejor respuesta fue evaluado frente a diferentes concentraciones de glucosa, mostrando una buena sensibilidad para concentraciones entre 0.5 y 3 mM. Estos resultados también demuestran la idoneidad de la deposición electroforética para el desarrollo de biosensores con transducción óptica.

Summary

This Manuscript shows the results obtained during the realization of the Doctoral Thesis entitled "Development of new optical oxygen sensing phases with biotechnological, industrial and clinic applications". The report has been divided in two main parts: introduction and experimental part.

In the **introduction**, an overview of the relevance of oxygen in different fields of Science and the available techniques for its determination is first shown. Secondly, the determination of oxygen by luminescence quenching is detailed. For this reason, the fundaments of molecular luminescence and the available methodologies for its detection are described paying special attention to the components and different configuration of an optical sensing device. Following this concepts, the components of an optical oxygen sensing layer are described: indicator dye and matrix, pointing to the materials more frequently used and those aspects more relevant in the development of this type of sensing layer, such as their influence in the final sensitivity of the film. In the last section of the introduction, a general vision of the design, advantages and disadvantages of optical sensors and the reason of their recent development are described. Finally, main applications making use of the optical detection of oxygen in different fields are summarized.

The second part of the Manuscript, so-called **experimental part**, shows the results obtained during the Doctoral Thesis. This part is divided in four thematic sections, each one having one or two chapters, with a general introduction. Note that numbering of the chapters is consecutive, regardless of the section they belong to.

The **first section** deals with the characterization of optical sensing films based on Ir(III) complexes immobilized in matrix of different viscosity and in a nanostructured support. This first thematic entity was carried out in collaboration with the Laboratory for Photonics and Interfaces of the Institute of Chemical Sciences and Engineering of the *École Polytechnique Fédérale de Lausanne* (EPFL), Switzerland, and collects the

characterization of new iridium dyes based of different pyridine ligands, with emission wavelengths ranging from the 470 nm to 625 nm.

A total of four cationic and three neutral iridium dyes were studied. They were immobilized in a polystyrene matrix with different amount of plasticizer and in an aluminum oxide hydroxide nanostructured support in order to evaluate their compatibility with the properties of the dyes. For the evaluation of the sensing films, the Stern-Volmer constants, the response time and luminescence quantum yield were determined. All the dyes showed an improvement of their sensitivity for low oxygen concentration when they were immobilized in the nanostructured support. These results are collected in **Chapter 1** and **2** of this report.

The **second section** concerns to the importance of controlling specific properties in optical sensing layers. This control can be accomplished regarding to either the synthesis of materials upon request, or by controlling the morphologic properties of the sensing phase. Thus, **Chapter 3** reviews recent works published in the field of Atom Transfer Radical Polymerization (ATRP) as a tool to develop materials with specific properties that increased their performance as optical sensing layers. In **Chapter 4** an experimental design based on the response surface methodology (RSM) was applied in order to modelize both size and polydispersity of polymeric nanoparticles developed by miniemulsión-solvent evaporation. This work was carried out in collaboration with the Department of Analytical Chemistry of the University of Extremadura (Spain). This methodology can be useful to explore the experimental conditions leading to nanoparticles with specific size and polydispersity, and can be apply to the modelization of many other parameters. In adittion, the RSM allows to obtain a catalogue of size and polydispersity with a minimum number of experiments. Specifically, this model was applied for the development of hybrid magnetic nanoparticles based on poly(styrene-co-maleic anhydride) (PSMA), magnetite and the dye Pt(II) pentafluorophenyl porphyrine (PtTFPP). With the aim that these particles were easily collected with a magnet, a size of 200 nm and the minimum polydispersity achievable were set as target values. From the equation obtained with the application of RSM and making use of Matlab it was possible to obtain the synthesis conditions (polymer concentration and volume of organic phase) more suitable for the target size and polydisperstiy.

The **third section** was carried out in collaboration with the Swiss Federal Institute of Technology of Zurich (ETH Zurich), Switzerland. The results presented in this section are related to the development of a wireless microrobot for *in vivo* oxygen determination inside the eye. Therefore, in **Chapter 5** two different sensing phases based on polystyrene and the complex Pt(II) octaethyl porphyrine were compared. The phases were developed by spin-coating or by depositing nanoparticles onto a gold coated chip, which simulates the surface of a microrrobot used for intraocular measurements. The phases were compared in terms of sensitivity and response time, confirming the suitability of Nanotechnology to decrease the response time. Consequently, in **Chapter 6** a method based on electrophoretic deposition (EPD) of polymeric nanoparticles was developed in order to create sensing films at micrometric non-planar surfaces. The first step was the optimization of the synthesis conditions of the nanoparticles produced by precipitation-evaporation using PSMA and the polymer PtTFPP, as well as to delimit the deposition time and potential range to carry out the EPD. The properties of sensing phases developed on gold coated chips by applying different times and potential within the delimited range were subsequently studied, showing good sensitivity to oxygen in all the cases. The response time was between 4 and 8 seconds, which is of great interest for biomedical applications. By analyzing the chips surface with scanning electron microscopy, information about the amount of nanoparticles was obtained, confirming an increase when either time or voltage are increased. The attachment of the nanoparticles to the gold surface was also corroborated by applying a water flow during 12 hours, which confirms the suitability of this technique for the fabrication of optical sensing films.

Finally, the **fourth section**, composed only by **Chapter 7**, concerns exclusively to the development of a biosensor for deteriming glucose by optical oxygen transduction. In this chapter, EPD was used to immobilise both the enzyme glucose oxidase and polymeric nanoparticles with the oxygen indicator PtTFPP covalently attached. This polymer was obtained by chemical modification of a commercial polymer of PSMA and the dye PtTFPP during a stay in the Institute of Analytical Chemistry and Food Chemistry of the Graz University of Technology (Austria). The nanoparticles obtained from this polymer were immobilized along with the enzyme following different strategies (concentration, voltage, time, order of the reactives during a step deposition, etc.). The chip with the best response was evaluated for different glucose concentration within the physiological range, showing the best sensitivity for concentrations between

0 and 4 mM. These results confirm the suitability of EPD to developed biosensor with optical transductions.

Introducción

1. El oxígeno como analito de especial interés

1.1. La importancia del oxígeno

El oxígeno es uno de los elementos más abundantes en la Tierra (un 50,3% en peso incluyendo agua y atmósfera), y está presente tanto como constituyente de moléculas en la corteza terrestre y océanos, como en su forma molecular más frecuente: el O_2. A temperatura ambiente, el oxígeno molecular o dioxígeno es un gas incoloro e inodoro formado por moléculas de dos átomos de oxígeno.

El oxígeno molecular es el segundo gas atmosférico más abundante en la tierra después del nitrógeno, encontrándose con un porcentaje del 20.95% en volumen. La principal fuente de oxígeno atmosférico es la producción a partir de dióxido de carbono, agua y luz durante el proceso de fotosíntesis. Pero además, el oxígeno también es incorporado a la atmósfera mediante fotolisis de las moléculas de monóxido de nitrógeno y vapor de agua presentes en la atmosfera, y está presente en océanos, mares y ríos como oxígeno disuelto, siendo la principal fuente de vida de seres acuáticos, tanto animales como plantas.[1]

El descubrimiento del oxígeno se asigna a Priestley (1733-1804) ya que fue el primer científico capaz de aislarlo, casi al mismo tiempo que Scheele (1742-1786). Lavoisier (1743-1794) también reconocía la importancia del oxígeno, demostrando que la combustión es un proceso en el que se produce la combinación de una sustancia con oxígeno, y que a su vez éste juega un papel importante en la respiración de las plantas y los animales. Hasta entonces el oxígeno se conocía como "flogisto", y fue Lavoiser quien acuñó el término "oxígeno", con la idea errónea de que todos los ácidos contenían este tipo de gas (de la raíz griega *oxus geinomais,* generador de ácido).[2]

En 1877 Cailletet y Pictet consiguieron licuar el oxígeno por primera vez, aunque la producción industrial no comenzó hasta 1902 gracias al proceso de licuación del aire de

Linde. Hasta 1961 el oxígeno fue usado como elemento de referencia para la asignación de masas atómicas relativas, cuando fue sustituido por el carbono 12.[1]

La molécula de O_2 se caracteriza por sus propiedades únicas comparada con otros gases diatómicos. Es un gas paramágnetico y sus electrones desapareados dan lugar a un estado triplete fundamental muy estable, representado por $^3\Sigma_g O_2$ [3] La situación cambia, cuando en lugar de $^3\Sigma_g O_2$, el oxígeno es convertido a su estado singlete $^1\Delta_g O_2$, mucho más reactivo. Así pues, puede decirse que el oxígeno es por un lado indispensable para la vida, pues es necesario para obtener energía, mientras que por otro lado es el responsable del daño oxidativo en sistemas biológicos que irremediablemente llevan a la muerte.

En cualquiera de los casos, el oxígeno molecular es fundamental para la vida y su concentración en la Tierra es el resultado de un balance bioquímico y fisiológico entre los animables que lo consumen y las plantas que lo generan a través de la fotosíntesis. Así, el O_2 interviene en reacciones biológicas de diferente escala molecular, desde seres microscópicos como las bacterias hasta seres macroscópicos, ya sea en la respiración celular o en la fotosíntesis. Además, el oxígeno presenta una gran aplicación en multitud de reacciones industriales, por lo que su monitorización en diferentes entornos lo han convertido en un parámetro de gran interés.

El oxígeno en el metabolismo celular

El análisis de las poblaciones de células, su viabilidad y el metabolismo celular juegan un papel muy importante en la biología celular moderna, la medicina y la biotécnologia.[4] El principal objetivo de la respiración celular es generar energía en forma de ATP (del inglés *adenosine triphosphate*), donde por cada dos molécula de ATP se consume una molécula de oxígeno.[5, 6]

Por tanto, una adecuada presencia de O_2 es importante para el crecimiento y desarrollo de las células, lo que lo convierte en un metabolito clave tanto en células aeróbicas como en organismos mayores. Así, su concentración es un marcador muy útil de su estado metabólico y salud, proporciona información sobre su respuesta frente a estímulos externos e internos.[7] Por ejemplo, se puede correlacionar el suministro de oxígeno con el desarrollo del tejido en términos de composición bioquímica, apariencia

y propiedades, y es un parámetro necesario para la optimización de los sistemas de cultivo.[8-10]

El oxígeno en el sector médico y clínico: hipoxia e hiperoxia en los tejidos

La importancia del oxígeno para las células hace que el suministro y difusión de oxígeno en los tejidos sea indispensable para la vida. La hipoxia resulta como consecuencia de un balance negativo entre la demanda de oxígeno de los tejidos y la capacidad del sistema vascular para suministrarlo. Diversas patologías como la diabetes, la inflamación o el cáncer pueden afectar de forma negativa la oxigenación de los tejidos.[11]

La hipoxia se encuentra presente en desórdenes vasculares, inflamaciones agudas o crónicas [12] y en el crecimiento de tumores malignos, donde se relaciona con un crecimiento agresivo, riesgo de metástasis e incluso una mayor resistencia del tumor a la radio y la quimioterapia.[13-15]

Una disminución de oxígeno en el tejido durante un trasplante puede producir daños irreparables o incluso la pérdida del órgano trasplantado. Los tejidos, y en especial el tejido muscular, son muy sensibles a la isquemia producida por la perdida transitoria del riego sanguíneo durante el trasplante.[16]

El suministro inadecuado de oxígeno en los tejidos del cuerpo humano también se relaciona con la aparición de cierto tipo de enfermedades, como por ejemplo oculares.[17] La determinación de oxígeno en otras situaciones también puede resultar útil para, por ejemplo, determinar la viabilidad de los fetos.[18] Sin embargo, tanto condiciones de hipoxia como de hiperoxia durante el desarrollo fetal pueden desencadenar daños durante el desarrollo cerebral del bebé. [19]

De hecho, un exceso de oxígeno puede provocar la muerte de tejidos debido al estrés oxidativo y la formación de especies reactivas (ROS, de sus siglas en inglés *Reactive Oxygen Species*).[20, 21] Estos radicales libres intervienen en el envejecimiento celular y en la estabilidad oxidativa y pueden tener influencia en enfermedades neurodegenerativas.[22] Otro ejemplo de daño por hiperoxia se encuentra en muchas enfermedades crónicas como la arterioesclerosis o las enfermedades pulmonares [23] La

toxicidad del oxígeno puede ocurrir en muchos pacientes sometidos a terapias hiperbáricas con oxígeno[24], bebes prematuraos[25, 26] e incluso submarinistas. [27]

Precisamente por los daños que la situaciones de hipoxia e hiperoxia pueden producir, el control de oxígeno también es hoy en día indispensable en las unidades de cuidados intensivos de los hospitales y durante la anestesia.[28]

Pero además, en el sector médico y clínico, diversos tipos de reacciones enzimáticas monitorizadas a través del consumo o producción de oxígeno pueden servir para la determinación de otros analitos de gran interés. Un ejemplo es la determinación de glucosa, una de las áreas con mayor aplicación de la Química Analítica. La cuantificación de glucosa supone un 40% de todos los análisis de sangre,[29] y además tiene gran aplicación en biotecnología y en la producción y procesado de diferentes tipos de alimentos.

El oxígeno en el sector alimentario

La influencia de la disponibilidad de oxígeno sobre el crecimiento bacteriano también influye en la cinética de las fermentaciones que se llevan a cabo en biorreactores. Debio a que estas reacciones se llevan a cabo normalmente en medio acuoso, donde la solubilidad a oxígeno es baja, y los microorganismo lo consumen rápidamente, la introducción de oxígeno, bien a través de técnicas de aireación o producción de oxígeno *in situ*, hace que su monitorización sea importante.[30] Además, el estudio de la tasa de transferencia de oxígeno (*Oxygen Transfer Rate*, OTR)[31] de los diferentes cultivos también puede ayudar a optimizar los procesos, conocer el comportamiento de crecimiento bacteriano, y contribuir en el escalado de biorreactores. [32, 33]

Las enzimas también son muy usadas en la industria alimentaria, tanto para el control del procesado (control de la temperatura mediante la termoestabilidad de enzimas), como para la determinar los constituyentes (proteínas, vitaminas, etc.), o incluso determinar la calidad de los alimentos (insecticidas y bacterias que puedan estar presentes en la muestra, o subproductos provenientes de la degradación de los alimentos).[34] Muchas de estas enzimas producen o consumen oxígeno como resultados de las reacciones que catalizan. La aplicación de control de oxígeno con el uso de

enzimas, también permite analizar otros parámetros, como el contenido en etanol de bebidas alcoholicas.[35]

La presencia de oxígeno junto con otros factores como la temperatura, puede alterar el sabor de determinados alimentos, como el que ocurre debido a la oxidación de los lípidos durante la etapa de maceración de la cerveza.[36] Asi, los sensores para la determinación de oxígeno disuelto pueden servir para determinar el grado de descomposición de los alimentos en controles de calidad.[37]

La transferencia del oxígeno a través de la comida influye en el valor nutricional, características organolépticas y maduración de alimentos, frutas y verduras, [38] sobre todo en alimentos envasados. Del mismo modo que el oxígeno interviene durante el procesado de los alimentos, la estabilidad oxidativa de los compuestos lipídicos es fundamental para determinar las condiciones de almacenamiento, donde el control del oxígeno presente es importante.[39, 40] Del mismo modo, su concentración también es vital en envases al vacío o con atmósferas modificadas (MAP, *Modified Atmoshphere Package*) para garantizar la frescura y conservación de los alimentos. [41-44]

El papel del oxígeno en aplicaciones industriales y tecnológicas

El oxígeno, al ser un gas altamente reactivo, oxida una gran cantidad de elementos, lo cual hace que tenga una gran aplicación en la industria.[1] En 2004 el oxígeno fue el cuarto producto químico más producido en Estados Unidos y el primero en Europa, con 19539 y 13672 millones de metros cúbicos respectivamente.[45] Como dato anecdótico, la primera misión espacial del programa Apollo de la NASA (*National Aeronautics and Space Administration*) en 1969 (alunizaje del Apollo 11), usó 1270 m^3 de oxígeno líquido para oxidar unos 550 toneladas de combustible.[1] Pero además, la detección de trazas de oxígeno es hoy en día uno de los aspectos más importantes a controlar en el combustible de hidrógeno usado por la NASA en algunos de sus cohetes[46] y la detección de posibles filtraciones de oxígeno es muy importante por razones económicas y de seguridad. [47]

Del mismo modo, la determinación de oxígeno puede servir para evitar la emisión de sustancias perjudiciales y mejorar el rendimiento de los motores en la industria automovilística mediante un control de la relación aire/fuel.[48]

La detección de oxígeno también puede servir para monitorizar la presión del aire a lo largo del tiempo en diferentes superficies mediante el uso de pinturas sensibles a la presión (*pressure-sensitive paint*s, PSP), lo cual es de gran utilidad en la mecánica de fluidos y estudios aerodinámicos como por ejemplo el diseño de vehículos espaciales[49], optimización de rotores[50, 51] o aplicaciones tecnológicas.[52]

Además, en la industrica metalúrgica, la formación de oxígeno en los electrodos durante procesos de electrodeposición (*oxygen evolution reaction*, OER) es también un parámetro muy importante que se relaciona con resistencia a la corrosión del material. Su determinación permite controlar las propiedades de los materiales, [53] especialmente sobre su estructura y propiedades ópticas. [54]

El oxígeno no solo es importante para el control de procesos industriales donde se consuma o produzca este gas, por ejemplo en procesos de combustión[55, 56] o fermentaciones anaerobias como la producción de biogas,[57] sino que también tiene un papel destacado en sistemas de seguridad de plantas químicas y petroquímicas (como por ejemplo, el control de posibles explosiones) o en plantas de residuos peligrosos.[58, 59]

Por otro lado, el control de oxígeno disuelto sirve para evitar los posibles procesos de corrosión en instalaciones de calderas de vapor o sistemas refrigerantes que se pueden producir debido al poder oxidante del oxígeno.[60, 61] La presencia de ciertos niveles de oxígeno en las aguas en estos sistemas, no solo puede dañar la instalación, con la consiguiente pérdida en la calidad en el producto manufacturado, sino que en determinados casos puede suponer un riesgo si por ejemplo, restos de óxido llegan a un reactor nuclear.

El oxígeno disuelto y el medio ambiente

La concentración de oxígeno es unos de los parámetros más importantes a considerar en la calidad de las aguas. La concentración de oxígeno depende de la temperatura y la profundidad y suele ser de unos 8 ppm a 1 atm de presión y 20 ^{o}C. Así, el O_2 es esencial para los organismo marinos, lo cuales requieren diferente cantidad de oxígeno para su metabolismo.[62]. Gracias a este oxígeno, los microorganismos aeróbicos son capaces de eliminar los contaminantes del medio. Sin embargo, si la cantidad de contaminantes es alta, esto puede producir una reducción significativa de los niveles de oxígeno afectando negativamente a los organismos

acuáticos. [63] Por la misma razón, es interesante monitorizar el oxígeno en piscifactorías para obtener una reproducción óptima y evitar su mortalidad debido a un suministro inadecuado de O_2.

Por otro lado, el control de las propiedades fisicoquímicas y microbiológicas en aguas potables es fundamental para proteger a los consumidores. En la mayoría de los países desarrollados, existe legislación sobre las aguas potables, donde se establecen los niveles máximos de elementos tóxicos admitidos en el agua de consumo. En este sentido, la cantidad de oxígeno disuelto es un indicador importante de la calidad del agua, pues como hemos visto indica el nivel de contaminación. Así, la medida de la demanda biológica de oxígeno (DBO) y la demanda química de oxígeno (DQO) son parámetros ampliamente utilizados para la caracterización de la calidad de las aguas. El primero, suministra información sobre la cantidad de oxígeno requerida para la biodegradación de materia orgánica presente en el agua, a través de la actividad metabólica de los microorganismos que la digieren. Por otro lado, la DQO corresponde a una oxidación química de las sustancias oxidables presentes en el agua, por lo que también suministra información sobre la materia inorgánica no biodegradable,[63] permitiendo en cualquier caso un mejor control sobre el tratamiento de las aguas residuales.[64, 65]

En oxígeno en botánica

Teniendo en cuenta que la rotura de las moléculas de agua durante la fotosíntesis conlleva la formación de oxígeno, su determinación también es interesante en el campo de la botánica.[3, 66] Al contrario que los animales, las plantas no tienen un sistema de suministro de oxígeno en sus tejidos, por lo que la concentración de este gas va a depender del balance entre el consumo celular y su producción vía fotosíntesis.[67] Además, la permeabilidad del tejido de las plantas tanto a oxígeno como a monóxido de carbono es un factor importante en su desarrollo y crecimiento,[68] mientras que una correcta aireación de las raíces es un factor importante en el crecimiento de vegetales y plantas.[69]

1.2. Técnicas generales de determinación de oxígeno

A continuación se van a describir de forma general los métodos de determinación de oxígeno más comunes encontrados en bibliografía, comentando en cada caso sus

ventajas e inconvenientes, así como su campo de aplicación. La **Tabla 1** recoge un resumen de estos métodos y sus características. .

Análisis gravimétrico

Este método permite evaluar el oxígeno adsorbido por una muestra determinada, simplemente mediante diferencia de pesada, y en relación a los cambios de temperatura. Para realizar este tipo de análisis hace falta una microbalanza de precisión para monitorizar el aumento o disminución de peso. Aunque este instrumento de medida es sencillo, debe estar aislado herméticamente para que la muestra pueda ser desgasificada antes de comenzar el análisis, y su temperatura y humedad perfectamente controladas.

Se trata por tanto de una técnica global, que no permite conocer la concentración de oxígeno localmente. Además, cuando la concentración de oxígeno es muy baja las variaciones de masa detectadas debido a elementos volátiles (entre ellos el vapor de agua) no pueden ser diferenciados del oxígeno.[70] Esta técnica ha sido especialmente usada para la determinación de la estabilidad oxidativa de ciertos alimentos[71] y para la determinación de la constante de difusión e isotermas de adsorción de materiales. Aunque hoy en día existen balanzas de gran precisión, la gravimetría ha sido sustituida por otras técnicas como las electroquímicas o las ópticas.

Detección manométrica

Este tipo de análisis se basa en la cuantificación de oxígeno mediante la disminución de presión de un sistema. De este modo, la diferencia entre las presiones de entrada y salida del sistema se puede relacionar con la cantidad de oxígeno consumida por los microorganismos o adsorbida en una determinada muestra. Las diferentes variantes de este principio son esencialmente usadas para evaluar tasas metabólicas a partir de la estimación de un consumo de oxígeno,[72-74] aunque también para conocer la solubilidad del oxígeno y la capacidad antioxidante de determinados alimentos.[70]

Tabla 1. Comparación entre los principales métodos de determinación de oxígeno. G:gas, L:líquido; S: sólido

Método	**Gravimétrico**	**Manométrico**	**Cromatografía de gases**	**Winkler**	**Electrodo Clark**	**EPR**	**Óptico luminiscente**
Parámetro estimado	Masa	Presión	Área de pico/intensidad	Moles	Corriente	Ancho pico/Intensidad	Disminución intensidad/tiempo de vida
Medio de medida	L/S	L/S	G/L/S	L	G/L/S	G/L/S	G/L/S
Contacto con la muestra	No	No	No	Destructivo	Invasivo	No	Invasivo
Necesidad de calibración	No	Sí	Sí	No	Sí	Sí	Sí
Reversible	No	No	Si	No	Si	Si	Si
Consumo de oxígeno	No	No	Sí	Sí	Sí	No	No
Tiempo de medida	Horas	Horas	Minutos	Minutos	Segundos	Minutos	Segundos
Tipo de media	Global	Global	Global	Global	Local/Global	Distribución O_2	Local/Global/Distribución O_2)
Miniaturización	No	Si	No	No	Si	No	Si
Medida *in situ*	No	No	No	No	Si	No	Si
Aplicación típica	Adsorción de O_2 alimentos	Tasas metabólicas organismos	O_2 en muestras gaseosas	Oxígeno disuelto en aguas	Variada	Imágenes tejidos	Variada
Referencia	70	75	76	77	78	15, 79	80

Cromatografía de gases

La cromatografía de gases es una técnica muy eficaz para la determinación de oxígeno gaseoso, el cual se separa del resto de gases mediante el uso de columnas de distintos tipos. El detector que se acopla al cromatógrafo de gases suele ser de conductividad térmica,[64, 81, 82] aunque también es posible el uso de otros detectores.[76, 83]

Principalmente su uso está dirigido a la determinación de oxígeno en muestras gaseosas, puesto que su principal desventaja en matrices sólidas o acuosas es que requiere recoger la atmósfera que rodea a la muestra analizada y conducirla hasta el cromatógrafo, lo cual puede perturbar el equilibro de la muestra.

Valoración Química (Método Winkler)

El método más antiguo para la determinación de oxígeno disuelto es la valoración colorimétrica o método Winkler, y aún hoy en día es el procedimiento volumétrico más exacto y fiable para analizar oxígeno disuelto en agua. Este método requiere la fijación del oxígeno disuelto en forma de hidróxido de manganeso mediante la adición de un exceso de Mn(II) y una base fuerte, que producirán la aparición de un precipitado marrón de $Mn(OH)_3$.

$$MnSO_4 + O_2 + OH^- + 2H_2O \rightarrow Mn(OH)_3 + {SO_4}^{-2}$$

La posterior adición de iones yoduro en medio ácido, permite la reducción del Mn(III) and Mn(II) a costa de la oxidación del ión yoduro a triyoduro (I_3^-), en una concentración proporcional a la concentración inicial de oxígeno disuelto.

$$Mn(OH)_3 + I^- + H^+ \rightarrow I_3^- + 6H_2O + 2Mn^{2+}$$

Por tanto, la valoración del triyoduro formado con un patrón de tiosulfato sódico, permite determinar la concentración de oxígeno. El punto final de la valoración se puede detectar tanto visualmente, utilizando almidón como indicador, o bien mediante técnicas potenciométricas o espectroscópicas, las cuales permiten una automatización más sencilla. [84-87]

Así, las técnicas espectroscópicas permiten una aproximación más simple, ya que evitan usar tiosulfato y realizan la medida directa de la absorbancia del ión triyoduro

I_3^-.[88, 89] Sin embargo, este tipo de técnicas no son tan precisas como la valoración química, y solamente han demostrado utilidad para concentraciones bajas de oxígeno.[90]

En general, el método Winkler es muy usado para la calibración de otros instrumentos que miden oxígeno, aunque solamente puede ser aplicado a muestras líquidas y asegurando que no se pierde ni introduce oxígeno durante las diferentes etapas. Además, la muestra debe estar libre de otros compuestos que puedan reducir u oxidar el yoduro.[77] Debido a que el análisis produce la destrucción de la muestra de agua, la determinación mediante este método está especialmente dirigida a volúmenes grandes de agua.

Técnicas electroquímicas (Electrodo de Clark)

Los métodos electroquímicos se basan en el uso de un electrolito para reducir al oxígeno y crear una corriente eléctrica entre dos electrodos, la cual se correlaciona con la concentración de oxígeno.

Los sensores electroquímicos para oxígeno se pueden agrupar en función de los parámetros electroquímicos que transmite la información como *potenciométricos*, si lo que se mide es una diferencia de potencial, *amperométricos*, donde lo que se detecta es una corriente eléctrica, o *conducimétricos*, si se mede la conductividad. [91, 92]

Dentro de cada tipo de sensor, se pueden encontrar diversas clasificaciones y subclases en función de la configuración de las celdas, aislamiento de los electrodos, polarización de la muestra, potencial o corriente constantes, etc.[91, 93] Algunos de estos tipos de sensores electroquímicos se pueden encontrar comercialmente, como el conocido electrodo de Clark, mientras que otros aún están en etapa de desarrollo.[91, 94]

Por su importancia y robustez, nos centraremos en el electrodo de Clark,[95] un sensor amperométrico donde la intensidad de la corriente se mide en función de un potencial aplicado. Aunque menos extendidos, también existen sensores potenciométricos para medir oxígeno[96, 97] asi como otros tipos de métodos amperométricos.[98]

En el electrodo de Clark, los electrodos se encuentran aislados del medio mediante una membrana, lo cual lo diferencia del resto de sensores amperométricos.[91] Las reacciones que tienen lugar son:

Cátodo Pt: $\frac{1}{2}O_2 + 2e^- + H_2O \rightarrow 2OH^-$

Ánodo Ag: $2Ag + 2Cl^- \rightarrow 2AgCl + 2e^-$

Como se puede deducir de las reacciones, una desventaja de este método es el consumo de oxígeno en el cátodo y la obstrucción del ánodo a lo largo del tiempo debido al cloruro de plata formado.[70, 78] Además, debido al uso de una membrana es necesario una agitación continua y la difusión de oxígeno puede ser lenta, resultando en tiempos de respuesta largos.[78] Por otro lado el consumo del electrolito requiere que este sea reemplazado cada cierto tiempo.

A pesar de estas desventajas, la detección de oxígeno mediante el electrodo de Clark es ampliamente usada debido a su robustez y flexibilidad. Diversas variantes adaptadas a diferentes ambientes han sido y están siendo desarrolladas para detectar oxígeno bajo diferentes configuraciones, incluyendo el uso de microelectrodos.[5, 6, 35, 37, 44, 65, 66, 69, 99]

Resonancia paramagnética electrónica (EPR)

El método más utilizado en la determinación de oxígeno es la resonancia paramagnética electrónica (RPE de sus siglas en español o más conocido como EPR del ingés *Electron Paramagnetic Resonance*).[79] La EPR es análoga a las técnicas de resonancia magnética nuclear (*Nuclear Magnetic Resonance,* NMR), pero en lugar de la excitación del núcleo atomico, la intereacción se produce con el spin de los electrones. La mayoría de las moléculas tienen sus electrones apareados, por lo que esta técnica ofrece una gran especificidad, teniendo en cuenta los electrones desapareados que posee el oxígeno. Debido a las características no invasivas de este tipo de métodos, [15]principalmente se ha usado para obtener imágenes de alta resolución de la distribución de oxígeno en tejidos celulares[14, 15, 79]

Además, también se puede hacer uso de las técnicas de RMN para obtener imágenes de resonancia magnética nuclear (*Magnetic Resonance Imaging*, MRI) y detectar situaciones de hipoxia en tejidos haciendo uso de biomarcadores de hipoxia, sondas fluoradas, o mediante las propiedades de la desoxihemoglobina.[15, 79, 100]

Métodos ópticos

Sensores fotométricos

La absorción por parte de las moléculas de oxígeno ocurre en el infrarojo cercano (IR ceracano), en torno a 760 nm, donde no se conocen interferencias de otros gases. Esta característica permite detectar este gas mediante medida de la absorbancia. Para ello es necesario un láser a la longitud de onda adecuada, de modo que conforme aumenta la concentración de oxígeno en el gas, la intensidad de luz del laser que llega al detector es menor pues parte es absorbida por las moléculas de oxígeno. La mayoría de las aplicaciones de espectrometría de absorción de diodo láser son de carácter industrial[58, 101] o médico. [102-104]

Sensores luminiscentes

Los sensores ópticos basados en la atenuación de la luminiscencia han tenido un gran desarrollo y aplicación en los últimos años, y son el método óptico de detección de oxígeno más ampliamente usado junto con los métodos polarográficos.[80, 105, 106] Estos sensores se basan en la disminución de luminiscencia de una molécula orgánica en presencia de oxígeno, de modo que esta atenuación puede relacionarse con la concentración del gas presente en el medio. En la **Figura 1** se esquematiza el proceso de atenuación de la luminiscencia producido por el oxígeno. El primero en observar que el oxígeno podía atenuar la fluorescencia de ciertos complejos fue Kautsky en 1939.[107] Sin embargo, se tardaron más de 25 años en desarrollar el primer sensor óptico de medida de oxígeno.[108]

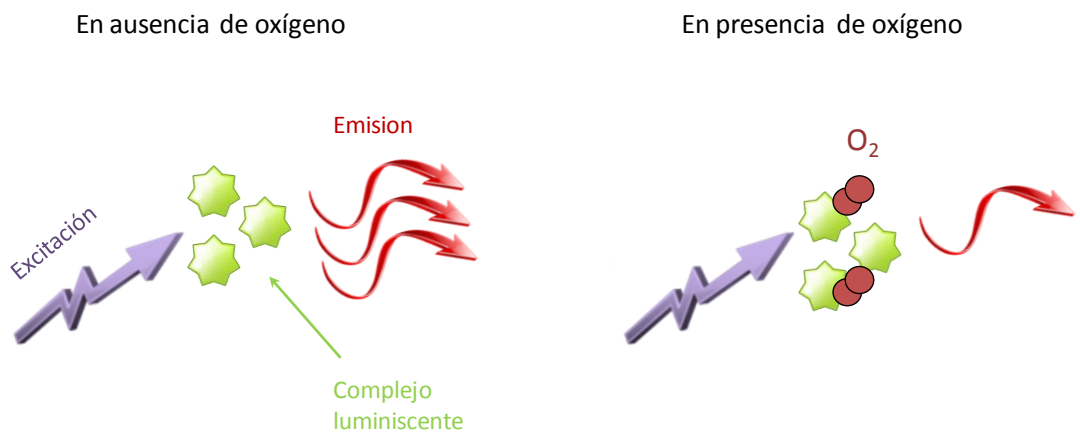

Figura 1. Proceso esquemático simplificado de la atenuación de la luminiscencia de un complejo luminiscente ante la presencia de oxígeno.

La principal ventaja de estos sensores frente al electrodo de Clark es que no consumen oxígeno. Los sensores ópticos ofrecen una gran selectividad comparada con otros sensores químicos. Además, permiten el uso de fibra óptica para unir la zona de análisis con los dispositivos de medida, lo cual permite realizar medidas remotas, incluso en ambientes potencialmente peligrosos. Asimismo, a ser un proceso reversible, permite monitorizar la concentración de oxígeno a lo largo del tiempo.

Al ser el objeto de esta memoria, en las siguientes secciones se analizan más detalladamente los sensores ópticos de oxígeno basados en la atenuación de la luminiscencia, empezando por las bases de este fenómeno y sus diferentes métodos de medida. A continuación nos centrarnos en los componentes y características de una fase sensora para oxígeno. Como conclusión, se establece un resumen sobre el desarrollo de los sensores de este tipo, y algunos de los últimos trabajos encontrados en literatura donde se pone de manifiesto la determinación de oxígeno con este tipo de sensores en diversos tipos de aplicaciones.

2. Determinación de oxígeno por atenuación de la luminiscencia

Los sensores ópticos luminiscentes basan su funcionamiento en la detección de la emisión de luz luminiscente, aunque no siempre esta proceda del analito de interés, sino de una molécula indicadora como es el caso de los sensores ópticos de oxígeno. Por este motivo en primer lugar se va a describirá el fenómeno luminiscente, así como su utilidad en la determinación de oxígeno molecular y los métodos de detección empleados con este fin.

2.1. El fenómeno luminiscente

La luminiscencia molecular es una rama de la espectroscopia de emisión en la que intervienen, fundamentalmente, los estados electrónicos de una molécula. Por tanto, las técnicas luminiscentes son aquellas en las que existe una interacción entre la radiación electromagnética y la materia, existiendo procesos de absorción y/o emisión de dicha radiación. Concretamente, dentro del nombre de este colectivo se encuentran tres tipos de fenómenos luminiscentes relacionados entre sí: fluorescencia, fosforescencia y quimioluminiscencia. Estos tres fenómenos están basados en la emisión de radiación electromagnética tras la formación de una especie excitada, bien

mediante una reacción química (quimioluminiscencia) o mediante la absorción de fotones (fluorescencia y fosforescencia).

La fluorescencia y la fosforescencia se diferencian básicamente en las transiciones electrónicas implicadas en la emisión de la radiación electromagnética, que confieren, a cada fenómeno unas características determinadas. Así, si la molécula se desactiva desde el primer estado excitado singlete al estado fundamental emitiendo un fotón, esta transición se denomina fluorescencia; mientras que si por el contrario el electrón pasa al primer estado triplete excitado, produciéndose un cambio en la multiplicidad de espín, y posteriormente la molécula pasa al estado fundamental emitiendo un fotón, se denomina fosforescencia. Esta última transición está prohibida por las reglas de selección y se caracteriza por su larga duración (10^{-6} s-min.), mientras que la fluorescencia ocurre en tiempos del orden de entre 10^{-11}-10^{-7} s. Esto hace que las medidas de fosforescencia sean más sensibles que las de fluorescencia, ya que la concentración de desactivador necesaria para alcanzar la misma eficiencia de desactivación que en la fluorescencia es unas 10^{3}-10^{5} veces inferior debido al largo tiempo de vida.[109] Además, como los niveles de energía implicados en uno y otro proceso son diferentes, la fosforescencia suele presentarse en longitudes de onda mayores que la fluorescencia.

Todo proceso fotoluminiscente comienza con la absorción de luz (**A**) como resultado de la interacción del campo eléctrico de la luz excitatriz con los electrones débilmente asociados de la molécula a excitar, lo que provoca que la energía sea cedida por el campo eléctrico de la luz a la molécula, alterándose la distribución electrónica de la misma. La intensidad de luz absorbida viene dada por la Ley de Lambert-Beer (ecuación 1):

$$I_a = I_0 - I = I_0\left(1 - 10^{-\varepsilon b C}\right) \qquad (1)$$

donde I_a es la intensidad de luz absorbida, I_0 e I son respectivamente las intensidades de la luz incidente y transmitida, ε es la absortividad molar (la cual representa la probabilidad de absorción de cada especie molecular), C es la concentración molar de la sustancia absorbente y b es el espesor en centímetros de la muestra que atraviesa el haz de luz.

Las transiciones electrónicas que tienen lugar y que explican el fenómeno luminiscente se pueden representar mediante el diagrama de Jablonski (**Figura 2**) donde se muestran las diferentes transiciones radiantes y no radiantes en una molécula después de su excitación a un estado singlete.

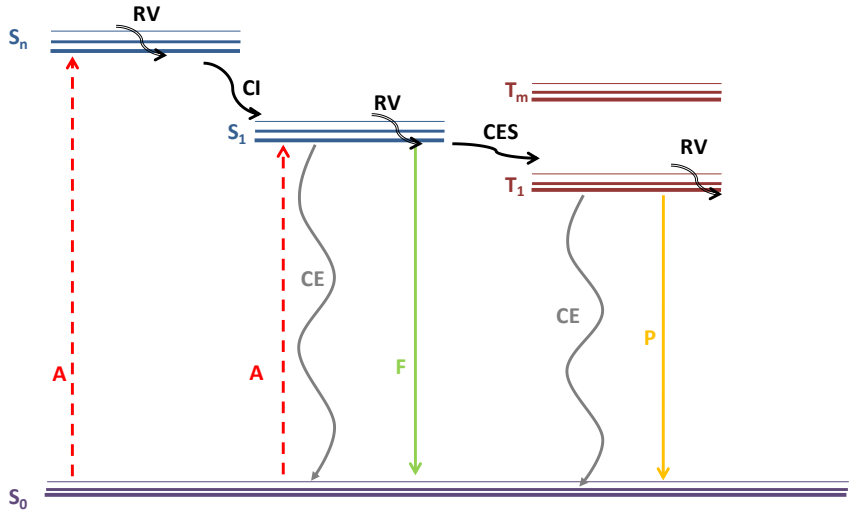

Figura 2. Diagrama de Jablonski donde se observan las transiciones electrónicas involucradas en la excitación de una molécula. S_0: estado singlete fundamental; S_n: estado singlete excitado de mayor energía; S_n: estado singlete excitado de menos energía; T_1: estado triplete excitado de menor energía; RV: relajación vibracional; CI: conversión interna; CE: Conversión externa; CES: cruzamiento entre sistemas; A: absorción; F: fluorescencia; P: fosforescencia.

Como cada estado electrónico molecular tiene varios estados vibracionales asociados, a temperatura ambiente casi todas las moléculas se encuentran en el estado vibracional más bajo del estado electrónico fundamental S_0. Al excitar con una radiación electromagnética de la zona del UV o del visible, la molécula es promovida a un estado vibracional de un estado electrónico excitado ($\mathbf{S_0 \rightarrow S_n}$). La pérdida del exceso de energía vibracional y electrónica en la molécula ocurre inmediatamente y esta energía es absorbida por moléculas en fase condensada (moléculas del disolvente que se encuentran en constantes colisión con el soluto excitado). Esta desactivación térmica se llama **relajación vibracional (RV)**, cuando pierde la energía vibracional dentro de un estado electrónico dado, o **conversión interna (CI)** cuando sufre una transición sin radiación desde un estado electrónico superior al estado electrónico excitado de la misma multiplicidad de espín pero de menor energía ($\mathbf{S_n \rightarrow S_{n-1}}$). Por tanto, la RV y la CI llevan a la molécula al nivel vibracional más bajo del estado

singlete excitado de menor energía ($\mathbf{S_n \rightarrow S_1}$) sin que ello conlleve la emisión de luz. Este proceso se lleva a cabo en un periodo de tiempo de 10^{-14} a 10^{-12} s.

Muchas moléculas regresan de nuevo al estado electrónico fundamental por desactivación térmica ($\mathbf{S_1 \rightarrow S_0}$), proceso denominado **conversión externa (CE)**. Sin embargo, en algunas moléculas, concretamente aquellas con estructura molecular rígida, el retorno desde el estado excitado singlete de menor energía al estado electrónico fundamental por CE está desfavorecido (debido a bajas probabilidades o a una duración excesiva). En estas moléculas, el retorno al estado electrónico fundamental ocurre por mecanismos más lentos. Uno de estos mecanismos implica emisión directa de radiación UV-vis cuyas frecuencias y longitudes de onda vienen dadas por la diferencia de energía entre el estado excitado singlete de menor energía y el estado electrónico fundamental. La transición radiativa entre estos estados se llama **fluorescencia (F)** y ocurre entre 10^{-11} y 10^{-7} s después de la excitación inicial. El hecho de que el estado electrónico fundamental de la molécula tenga varios niveles vibracionales provoca que su fluorescencia no ocurra a una única longitud de onda. De hecho, la fluorescencia se manifiesta sobre un amplio rango de longitudes de onda las cuales corresponden a varias transiciones vibracionales que son componentes de una única transición electrónica.

Existe otro mecanismo por el cual una molécula se puede desactivar desde su estado singlete excitado de menor energía y que, normalmente, ocurre al mismo tiempo que la fluorescencia. Este mecanismo implica el **cruzamiento entre sistemas (CES)** entre el estado singlete excitado más bajo al estado triplete excitado de menor energía de la molécula ($\mathbf{S_1 \rightarrow T_1}$). El CES está acompañado por un cambio en el espín del momento angular, lo cual viola la ley de conservación del momento angular. El hecho de que esto ocurra es un millón de veces menos probable (más lento) que la CE (cambio de estado singlete a singlete). El CES ocurre a una velocidad comparable a la de fluorescencia, por lo tanto, compite con ella por la desactivación del estado singlete más bajo. Las moléculas que se desactivan por medio del CES llegarán por RV al nivel vibracional más bajo del estado triplete. Desde este estado, las moléculas pueden pasar al estado fundamental ($\mathbf{T_1 \rightarrow S_0}$) con o sin emisión de radiación. Si lo hacen mediante radiación, esta emisión se denomina **fosforescencia (P)**, la cual también está prohibida y se caracteriza por su larga duración (10^{-6} s a min).

2.2. Atenuación de la luminiscencia

A la hora de desarrollar un sensor basado en medidas de luminiscencia, es posible diferenciar tres casos: (1) el analito es un luminóforo, (2) el reactivo indicador presenta propiedades luminiscentes que varían como resultado de la interacción de éste, en el estado fundamental, con el analito, y (3) la emisión luminiscente del reactivo varía debido a la interacción de éste, en el estado excitado, con el analito[110], como es el caso de la detección de oxígeno.

Se define por tanto atenuación o "*quenching*" de la luminiscencia a cualquier proceso que disminuya la fluorescencia o fosforescencia de una molécula luminiscente. Durante estos fenómenos de atenuación de los estado singlete y triplete por parte del oxígeno en su estado fundamental, $^3\Sigma_gO_2$, se generan estados excitados del oxígeno, $^1\Sigma_gO_2^+$ y $^1\Delta_gO_2$ respectivamente.[111] Los mecanismos fisicoquímicos por los que el oxígeno desactiva o atenúa estos procesos luminiscentes y la relación con del estado excitado de estas moléculas sobre la producción de oxígeno singlete ha sido ampliamente estudiados.[111-114] Comprender completamente este proceso requiere tener en cuenta una gran variedad de procesos fotofísicos relacionados con el oxígeno, así como la influencia sobre la efectividad de la atenuación.[111]

En general, los procesos que pueden producir una atenuación de la luminiscencia son:[115, 116]

- Reacciones en estado excitado (transferencia oxidativa o reductiva de electrones)
- Transferencias de energía por resonancia (*Fluorescence Resonance Energy Transfer*, FRET)
- Atenuación estática (*Static Quenching*, SQ).
- Atenuación colisional o dinámica (*Dynamic Quenching*, DQ)

La atenuación de la luminiscencia por los procesos citados resulta en una disipación de la energía del luminóforo en forma de calor y no en forma lumínica. Para que esto tenga lugar es necesario un contacto molecular entre el luminóforo y el atenuador. La principal diferencia radica en la forma de contactos entre dichas moléculas: en el caso de FRET, existe una transferencia de energía entre un donor (luminóforo) y un aceptor (atenuador) que se realiza a largas distancias. En cambio, SQ y DQ son procesos de corto alcance (< 2 Å). En la SQ el contacto entre el luminóforo y el atenuador (oxígeno) se debe a la formación de un complejo. En cambio, la DQ

implica un choque entre ambas moléculas, de ahí que en algunas ocasiones se denomine también "desactivación colisional". Dado que la SQ implica que la atenuación ocurre cuando el oxígeno forma un complejo con el indicador, el decaimiento de la luminiscencia tiene lugar sin necesidad de que exista difusión. En cambio, la DQ está gobernado por la difusión del oxígeno en el medio donde se encuentre el luminóforo, lo cual es necesario para que se produzcan la colisión entre las moléculas.

El oxígeno es uno de los desactivadores dinámicos de la luminiscencia más eficaces y de ahí que la detección de oxígeno mediante este método haya experimentado un aumentado en los últimos años.[80, 117] En el Esquema 1 se muestran los procesos involucrados en la excitación y emisión de un indicador, donde pueden coexistir hasta cuatro tipos reacciones: absorción, desactivación luminiscente, desactivación por el oxígeno y desactivación térmica.

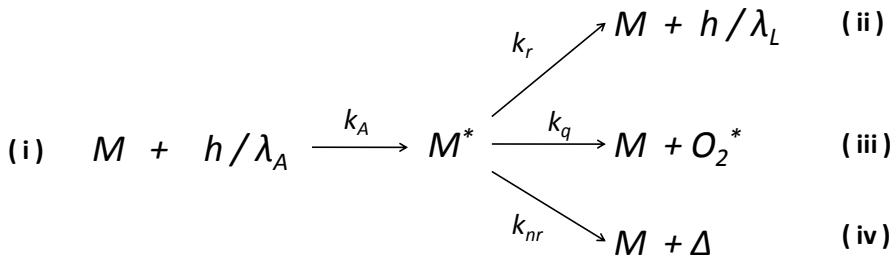

Esquema 1. Representación de las reacciones implicadas en la excitación y emisión de un indicador. (i) Absorción de luz y excitación del luminóforo; (ii) Desactivación luminiscente; (iii)Desactivación por el oxígeno; (iv)Desactivación no radiativa

M y M* es el luminóforo en su estado fundamental y excitado respectivamente, O_2 es el atenuador, λ_A y λ_L son las longitudes de onda de absorción y emisión respectivamente, y Δ el término de energía por desactivación no radiativa. Las constantes involucradas en cada proceso se definen a continuación y nos sirven para describir y entender una serie de parámetros relacionados con la luminiscencia.

El tiempo de vida τ del estado excitado se define como el tiempo medio que la molécula pasa en su estado excitado antes de volver al estado fundamental por cualquiera de los mecanismo citados en los procesos (ii) y (iv). [116] El tiempo de vida engloba tanto a procesos radiativos como no radiativos, y en general se define sin tener en cuenta los procesos de desactivación (iii):

$$\tau = \frac{1}{k_{nr} + k_r} \tag{2}$$

donde k_r es la constante de la emisión radiativa del luminóforo, y k_{nr} es la constante de los procesos no radiativos.

Del mismo modo el tiempo de vida de un luminóforo en ausencia de procesos no radiativos (es decir, cuando toda su energía se desactiva en forma lumínica según el proceso (ii)) se denomina tiempo de vida natural o intrínseco, τ_n, y es igual a:

$$\tau_n = \frac{1}{k_r} \tag{3}$$

Se puede definir el rendimiento cuántico (*Quantum Yield*, QY) de la luminiscencia como la relación entre la cantidad de energía absorbida (número de fotones absorbido) y la cantidad de energía emitida en forma luz (número de fotones emitidos), en ausencia de atenuador:

$$QY = \frac{fotones\ emitidos}{fotones\ absorbidos} = \frac{k_r}{k_A} = \frac{k_r}{k_r + k_{nr}} \tag{4}$$

donde k_A es la constante del proceso de absorción de fotones.

Esta definición nos permite calcular el tiempo de vida natural a partir del rendimiento cuántico y el tiempo de vida (ecuaciones 2, 3 y 4), como:

$$\tau_n = \frac{\tau}{QY} \tag{5}$$

Debido a los procesos no radiativos τ_n es normalmente menor que τ. Sin embargo, si la constante de los procesos no radiativos es mucho menor que la emisión lumínica ($k_{nr} << k_r$), el rendimiento cuántico será muy cercano a la unidad. En este caso tenemos una luminiscencia muy efectiva, donde todos los fotones absorbidos son reemitidos en forma lumínica, y por tanto, el tiempo de vida del luminóforo será íntegramente el tiempo de vida natural del mismo.

Precisamente una forma de diferenciar entre SQ y DQ es mediante el tiempo de vida media de la luminiscencia, ya que para la desactivación estática, donde existe una interacción continua entre atenuador y luminóforo, no hay cambio en el tiempo de vida media sino solo una disminución en la población de luminóforos, de modo que

aquellos que emiten lo hacen de la misma forma. Sin embargo, en la DQ, aquellos luminóforos que tardan más en emitir tienen más probabilidad de ser atenuados por una colisión con el oxígeno, como resultado, el tiempo de vida media de la población disminuye.

Ademas, debido a que la DQ depende de un proceso difusional, se ve afectada por cualquier efecto que varíe el coeficiente de difusión del atenuador en el material, lo que también puede servir para diferenciar la DQ de la SQ. Así, un aumento de la temperatura produce un aumento en el coeficiente de difusión y, por tanto, un aumento de la DQ. Al mismo tiempo, un aumento de la temperatura produce una disminución de la estabilidad del complejo luminóforo-atenuador, lo que provoca una disminución de la SQ. Por otro lado, un aumento de la viscosidad produce una disminución del coeficiente de difusión, lo que provoca una disminución de la DQ, mientras que la SQ, normalmente, no se ve afectada.

Demas y Carraway no encontraron evidencias de atenuación estática en el uso de sensores ópticos para la determinación de oxígeno. [118, 119] En cualquier caso como ya se ha mencionado, la desactivación estática ocurre cuando el luminóforo y el atenuador forman un complejo en su estado fundamental, el cual no es luminiscente, por lo que las medidas de tiempo de vida no se ven afectadas. Además, esta desactivación es muy rápida (picosegundos o inferior) [120], por lo que en medidas de intensidad tomadas con un cierto tiempo de retardo entre la excitación y la recolección de intensidad, tampoco van a ser afectadas por este fenómeno.

La ecuación de Stern-Volmer

El tiempo de vida de luminiscencia permite la resolución de una gran cantidad de problemas analíticos, mediante su relación con la concentración de oxígeno (analito). Así, normalmente se utiliza el subíndice "*0*" para indicar el valor del tiempo de vida en ausencia de oxígeno. Así, el tiempo de vida τ_0 sería exclusivamente:

$$\tau_0 = \frac{1}{k_{nr} + k_r} \tag{6}$$

Mientras que en presencia de atenuador [O_2], contemplando los procesos (ii), (iii) y (iv), sería de la forma:

$$\tau = \frac{1}{k_{nr} + k_r + k_q[O_2]} \tag{7}$$

donde k_q es la constante de desactivación bimolecular. Dividiendo las expresiones 6 y 7 se obtiene:

$$\frac{\tau_0}{\tau} = 1 + \frac{k_q[O_2]}{k_{nr} + k_r} = 1 + k_q\,\tau_0[O_2] \implies \frac{\tau_0}{\tau} = 1 + k_{SV}[O_2] \tag{8}$$

La ecuación 8 es la ecuación de Stern-Volmer y relaciona los cambios producidos en el tiempo de vida del estado excitado (τ) con la concentración de oxígeno ($[O_2]$) mediante la constante de Stern-Volmer (k_{SV}). Aunque esta cinética fue desarrollada para procesos en disolución, su aplicación en fase sólida también es posible, como veremos más adelante.

De un modo similar es posible relacionar la intensidad de la luminiscencia con la concentración de oxígeno. Cuando no existe oxígeno en el medio, la variación del número de moléculas en el estado excitado ($[M^*]_0$) a lo largo del tiempo vendrá dada por las constantes de desactivación de los procesos radiativos y no radiativos:

$$-\frac{d[M^*]_0}{dt} = k_A[M]_0 - k_{nr}[M^*]_0 - k_r[M^*]_0 \tag{9}$$

Mientras que en presencia de oxígeno hay que considerar la constante de atenuación k_q de modo que:

$$-\frac{d[M^*]}{dt} = k_A[M] - k_{nr}[M^*] - k_r[M^*] - k_q[M^*][O_2] \tag{10}$$

Una vez alcanzado el estado estacionario, no habrá variación en el número de moléculas del estado excitado tanto en ausencia como en presencia de oxígeno:

$$\frac{d[M^*]_0}{dt} = 0; \qquad \frac{d[M^*]}{dt} = 0$$

Por lo que se puede obtener la concentración de moléculas en el estado excitado en ausencia de oxígeno despejando de la ecuación 9:

$$[M]_0 = \frac{k_{nr}[M^*]_0 + k_r[M^*]_0}{k_A} = \frac{(k_{nr} + k_r)[M^*]_0}{k_A} \tag{11}$$

como en presencia de oxígeno, despejando de la ecuación 10:

$$[M] = \frac{k_{nr}[M^*] + k_r[M^*] + k_q[M^*][O_2]}{k_A} = \frac{\left(k_{nr} + k_r + k_q[O_2]\right)[M^*]}{k_A} \qquad (12)$$

Teniendo en cuenta que la intensidad de luminiscencia (I) es proporcional al número de moléculas que emiten en el estado excitado, dividiendo las expresiones 11 y 12, se obtiene:

$$\frac{I_0}{I} = \frac{\propto [M^*]_0}{\propto [M^*]} = \frac{k_{nr} + k_r + k_q[O_2]}{k_{nr} + k_r} = 1 + \frac{k_q[O_2]}{k_{nr} + k_r} \quad \rightarrow$$

$$\rightarrow \quad \frac{I_0}{I} = 1 + k_q\,\tau_0[O_2] = 1 + k_{SV}[O_2] \qquad (13)$$

donde I_0 e I son la intensidades de emisión en ausencia y presencia de desactivador respectivamente, $[O_2]$ es la concentración del desactivador (oxígeno), k_{SV} es la denominada constante de Stern-Volmer, y representa la sensibilidad. La ecuación de Stern-Volmer (ecuación 13) es la encargada de relacionar la concentración de atenuador (O_2) con la intensidad de luminiscencia (I).[116]

Cabe destacar que las ecuaciones 8 y 13 solo serán equivalentes cuando el decaimiento de la luminiscencia sea exponencial, lo que en la práctica casi nunca ocurre.

Desviaciones de la ecuación de Stern-Volmer

En principio, la ecuación de Stern-Volmer se puede usar para conocer la concentración de oxígeno o cualquier otro atenuador. Sin embargo, debido a que un gran número de moléculas pueden actuar como atenuadores de la luminiscencia (iones metálicos, oxidantes, reductores, surfactantes, proteínas, etc.)[116], para la detección de oxígeno es necesario que el luminóforo o molécula indicadora se encuentre aislada de los posibles interferentes, normalmente mediante el uso de membranas permeables a oxígeno.[115, 117, 121] La principal desventaja del uso de soportes sólidos es que añaden un grado de heterogeneidad, la cual se manifiesta en desviaciones de la linealidad de la ecuación de Stern-Volmer y en decaimientos del tiempo de vida no exponenciales.

Estas desviaciones se pueden explicar en base a modelos que suponen que, dentro de un mismo sistema, existen sitios o ambientes donde el luminóforo presenta

diferente comportamiento hacía el oxígeno, siendo el modelo de dos sitios el más simple.[122] Algunos de estos modelos consideran que la desviación de la ecuación de Stern-Volmer atiende a una difusión no homogénea del oxígeno dentro de la fase que soporta al indicador.[119] Por ejemplo, en soportes de naturaleza poliméricas, la teoría de Adsorción Dual (*Dual Mode Sorption Theory*) postula dos tipos de sitios con diferente dependencia de la presión parcial de oxígeno, uno de ellos donde la penetración de oxígeno sigue la ley de Henry, y otro donde el oxígeno se adsorbe siguiendo la isoterma de Langmuir.[120]

En cualquier caso, estos modelos simplemente tratan de dar una explicación matemática a un proceso de naturaleza fisicoquímica, sin que ello conlleve que sean ciertos. Probablemente, las desviaciones de la linealidad respondan a una mezcla de factores. Otros modelos de ajuste que no contemplan parámetros físicos se basan en distribuciones Gausianas, exponenciales, Gamma, Max-Boltzmann, etc., pero todos ellos suelen presentar un peor ajuste que el modelo de sitios múltiples o multiestado. [123, 124]

En el modelo multiestado, la interpretación matemática de este fenómeno se puede hacer considerando cada ambiente como una fracción del total de sitios, de modo que en cada uno de ellos el luminóforo se atenúa siguiendo la ecuación de Stern-Volmer, con su constante correspondiente:[122]

$$\frac{I_0}{I} = \left[\sum_{i=1}^{m} \frac{f_i}{1 + k_{SVi}[O_2]}\right]^{-1} \qquad (14)$$

donde m es el número de ambientes diferentes, k_{SVi} es la constante de Stern-Volmer asociada a cada ambiente, $[O_2]$ es la concentración de atenuador (oxígeno) y f_i es la fracción del total de sitios con la que contribuye cada ambiente, de donde se deriva que $\sum f_i = 1$.

Por regla general, los modelos con dos ambientes, es decir $m=2$, suelen presentar un buen ajuste de los datos. Estos modelos fueron propuestos por Demas y Lehrer y se describen a continuación:

Modelo de Demas: en cada uno de los dos ambientes el luminóforo está expuesto de forma desigual al atenuador y por tanto k_{SV1} y k_{SV2} tienen valores diferentes pero ambos mayores que cero:

$$\frac{I_0}{I} = \left[\frac{f_1}{1 + k_{SV1}[Q]} + \frac{f_2}{1 + k_{SV2}[Q]}\right]^{-1} \quad (15)$$

Modelo de Lehrer: hay dos ambientes diferentes, pero en este caso el luminóforo localizado en uno de los ambientes, por lo que no se ve afectado por el atenuador, y por tanto k_{SV2} es igual a cero:

$$\frac{I_0}{I} = \left[\frac{f}{1 + k_{SV}[Q]} + (1 - f)\right]^{-1} \quad (16)$$

La sensibilidad en los sensores luminiscentes

La sensibilidad de un sensor viene dada por la pendiente de la respuesta del sensor dentro del intervalo dinámico de trabajo. Esta pendiente de la recta de calibrado es la constante de Stern-Volmer (k_{SV}). Además, existen otros parámetros que se pueden tomar como guías de la sensibilidad a oxígeno, tales como la intensidad o el tiempo de vida relativo en ausencia y en presencia de oxígeno (I_0/I *y* τ_0/τ) , *o* la presión de oxígeno necesaria para alcanzar un 50% ($I_0/2$) del decaimiento total de la luminiscencia ($pO_2(S=1/2)$).

Para conocer qué parámetros tienen incidencia sobre la sensibilidad, se puede considerar la ecuación de Stern-Volmer (ecuación 8 o 13) y relacionarla con una serie de parámetros fisicoquímicos. [120, 125] De este modo, teniendo en cuenta que en procesos de atenuación dinámica o controlados por los procesos de difusión, la constante bimolecular de la atenuación, k_q, se puede relacionar mediante la ecuación 17 con la eficiencia del atenuador, es decir, con la proporción de colisiones que atenúan efectivamente ($\propto$) y con la accesibilidad del luminóforo al atenuador, dada por k_{dif}.[116]

$$k_q = \alpha k_{dif} \quad (17)$$

$\propto$ es 1 para compuestos fluorescentes, mientras que para compuestos fosforescentes está probabilidad queda reducida a 1/9 debido a que la fluorescencia implica transiciones prohibidas.[126]

k_{dif} es la constante bimolecular de difusión dada por la ecuación de Smoluchowski [127]:

$$k_{dif} = \frac{4\pi RND}{1000} \tag{18}$$

donde R es el radio colisional, N el número de Avogadro, y D es la suma de los coeficientes de difusión del atenuador y del luminóforo. En procesos controlados por la difusión del atenuador, $D \approx D_{O2}$.

Por tanto, teniendo en cuenta las ecuaciones 17 y 18, se obtiene que la constante bimolecular de atenuación, k_q es igual a:

$$k_q = \alpha \frac{4}{1000} \pi R D_{O_2} \tag{19}$$

En interfaces en equilibrio, la concentración de oxígeno $[O_2]$ es proporcional a la presión parcial de oxígeno (p_{O_2}) según la Ley de Henry:

$$[O_2] = S_{O_2} p_{O_2} \tag{20}$$

donde S_{O_2} es la constante de solubilidad de oxígeno en el medio.

Y sustituyendo las ecuaciones 19 y 20 en la ecuación de Stern-Volmer (ecuación 12):

$$\frac{I_0}{I} = 1 + k_{SV}[O_2] = 1 + \tau_0 k_q [O_2] = 1 + \tau_0 \alpha \frac{4}{1000} \pi R D_{O_2} S_{O_2} p_{O_2} \tag{21}$$

De donde se obtiene que la constante de Stern-Volmer, k_{SV}, es de la forma

$$k_{SV} = \tau_0 \alpha \frac{4}{1000} \pi R D_{O_2} S_{O_2} \tag{22}$$

Teniendo en cuenta que la constante de difusión en disolución, D, se puede calcular usando la ecuación de Stokes–Einstein:[127]

$$D = \frac{kT}{6\pi\eta R} \tag{23}$$

donde k es la constante de Boltzman, η la viscosidad del disolvente y T la temperatura, se puede decir que la constante de Stern-volmer, ergo, la sensibilidad de una fase sensora es proporcional a:

$$k_{SV} \propto \tau_0 \frac{T}{\eta} S_{O_2} \quad (24)$$

De la ecuación 24 se pueden deducir los factores que influyen sobre la sensibilidad de los sensores ópticos (k_{SV}), los cuales vienen determinados tanto por el luminóforo (tiempo de vida) como por las propiedades del disolvente que lo rodee (viscosidad y solubilidad a oxígeno), así como por la temperatura. A continuación, se detalla la influencia de estos parámetros sobre la sensibilidad, y el apartado 3.3 se pueden encontrar más detalles de cómo influyen cada uno de los componentes de un sensor sobre su sensibilidad.

Tiempo de vida luminóforo (τ_0)

Como ya se ha comentado, tiempos de vida largos suelen dar lugar a valores más alto de sensibilidad puesto que al permanecer más tiempo en el estado excitado las moléculas tienen más tiempo (y por tanto mayor probabilidad) de desactivarse al chocar con el oxígeno. No obstante, para un luminóforo con un tiempo de vida dado, hay que tener en cuenta qué procesos puede influir en la magnitud de éste, como por ejemplo autoatenuación debido a agregación por problemas de solubilidad, procesos de transferencia de carga con otras moleculas, etc.

Temperatura (T)

Como se observa en la ecuación 24, la k_{SV} es directamente proporcional a la temperatura. Esto es debido, a que a temperaturas más altas, el coeficiente de difusión a oxígeno del medio que rodea al indicador aumenta (ec. 23) aumentando el contacto entre el atenuador (oxígeno) y el indicador. Sin embargo, hay que tener en cuenta que los procesos luminiscentes se ven menos favorecidos a temperaturas altas debido a la desactivación no radiativa (térmica) de la luminiscencia.[128]

Viscosidad (η)

Como se deduce de la ecuación de Stokes-Einstein (ec. 23), la influencia de la viscosidad tiene un marcado efecto sobre el coeficiente de difusión. Esto hace que, un aumento de la viscosidad del medio disminuya la sensibilidad pues indirectamente se está variando la difusión al O_2 al disminuir la movilidad de las moléculas.

Solubilidad a oxígeno (S_{O2})

La solubilidad a oxígeno es importante cuando el indicador se encuentra en disolventes de diferente naturaleza; por ejemplo, la solubilidad del oxígeno en disolventes orgánicos es mayor que en agua, y a su vez, la solubilidad en agua es 100 veces mayor que en la mayoría de las matrices rígidas.[125]

2.3. Métodos de detección luminiscente para la determinación de oxígeno

La detección de la luminiscencia de una determinada molécula puede hacerse mediante la determinación de la intensidad de la luminiscencia o del tiempo de vida.[116] A continuación se describen los métodos más usados para la determinación de oxígeno molecular.

Medidas de intensidad de luminiscencia

En este tipo de medidas la **intensidad** de emisión de la molécula se registra de **forma continua** a una longitud de onda determinada. Una medida de intensidad es simplemente un valor promedio de la luminiscencia que presenta el luminóforo, la cual decae en función del tiempo, de modo que, para un decaimiento monoexponencial de la luminiscencia $I(t) = I_0 e^{-\frac{t}{\tau}}$ integrando se obtiene:

$$I = \int_0^\infty I_0 e^{-\frac{t}{\tau}} dt = I_0 \tau \qquad (25)$$

El valor de I_0 depende de la concentración de luminóforo y de los parámetros instrumentales y se puede considerar constante. Sin embargo hay que tener en cuenta que cuando el decaimiento no es monoexponencial, es necesario usar aproximaciones, donde la curva de decaimiento será la suma de diferentes términos exponenciales y por tanto la intensidad registrada:

$$I(t) = \sum_j \alpha_j \, e^{-\frac{t}{\tau_j}} \qquad (26)$$

donde τ_j es el tiempo de vida de cada uno de los decaimientos monoexponenciales y α_j es la fracción del tiempo de vida total del luminóforo que presente un decaimiento monoexponencial de $\tau = \tau_j$

En cualquier caso en las medidas de intensidad se puede decir que la intensidad registrada en estado estacionario es proporcional al tiempo de vida, cualquiera que sea

la forma de su decaimiento. Así, si la intensidad luminescente de la molécula es atenuada en presencia de oxígeno, el tiempo de vida tomará valores más corto, de forma que la intensidad registrada será menor. Un ejemplo se puede observar en la **Figura 3** para concentraciones de oxígeno entre 0 y 10%. Así, las medidas de intensidad promedio obtenidas para cada concentración de oxígeno puede ser relacionadas de forma directa con la concentración de oxígeno mediante la ecuación de Stern-Volmer (ver ec.13). [116]

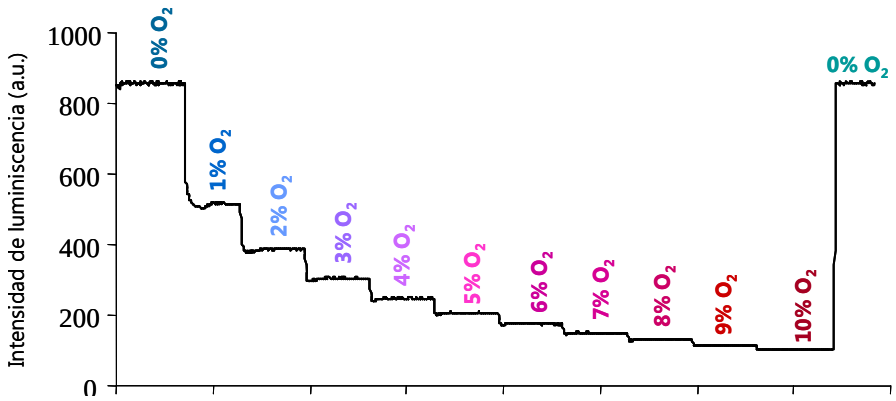

Figura 3. Medidas de intensidad directa a diferentes concentraciones de atenuador (oxígeno)

Las medidas de intensidad son relativamente simples y precisas en el laboratorio, sin embargo presentan algunas desventajas en aplicaciones reales ya que son muy sensibles a una serie de factores:[129]

- Parámetros extrínsecos a la fase sensora, como fluctuaciones en la fuente de excitación o sensibilidad del detector empleado.
- Perdidas de luz entre el indicador y el detector, debido a la orientación de las medidas y a la distancia al detector (sobre todo si no se manteiene constante o se utiliza fibra óptica).
- Concentración, fotodegradación o lixiviación de la molécula indicadora

Esta serie de factores influyen en la intensidad recolectada en el detector, que varía entre muestra y muestra, obligando a tener especial cuidado en la posición de la medida y a realizar recalibraciones continuas. No obstante, la instrumentación que se

requiere en este tipo de medidas es simple comparada con la instrumentación necesaria en las medidas de tiempo de vida.[130] Esto ha hecho que su uso nunca haya desaparecido y que se hayan desarrollado otros métodos basados en las medidas de intensidad que sean menos sensibles a cambios extrínsecos a la fase sensora. Tal es el caso de los métodos relativos, los cuales basan su funcionamiento en el uso de una referencia interna.[130, 131] Esta referencia es una molécula luminiscente no sensible a oxígeno coinmovilizada junto al indicador, o bien un luminóforo que presenten dos longitudes de onda de emisión, siendo solo una sensible a oxígeno.[130, 132] De este modo, el espectro de emisión presentará una región espectral no atenuada por el oxígeno (generalmente la asociada a fluorescencia) tal como se observa en la **Figura 4,** lo cual permite el uso de medidas relativas más robustas que las medidas de intesidad directas a una sola longitud de onda.

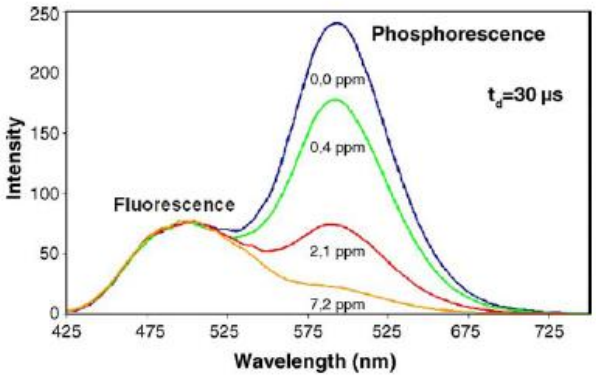

Figura 4. Medidas relativas donde se observa la región espectral no afectada por el oxígeno.[130]

Otro tipo de medidas relativas menos desarrolladas son las basadas en la detección polarizada, donde en lugar de usar una relación de intensidad a diferentes longitudes de onda, la medida relativa se consigue entre las componentes verticales y horizontales de una emisión polarizada. [132] Este método se basa en las propiedades de anisotropía de la emisión luminiscente[116, 132, 133] y pueden ser usadas en sistemas viscosos y con concentraciones de indicador mayores que las medidas de intensidad directa.

Medidas de tiempo de vida

El tiempo de vida de emisión (τ) se define como el tiempo medio que una molécula pasa en el estado excitado antes de volver a su estado fundamental.[116] Este tiempo de vida es un valor medio del tiempo que las moléculas pasan en el estado excitado, pues no todas las moléculas emiten en el preciso instante de tiempo t = τ.

Así, el valor de tiempo de vida es el valor en el que la intensidad inicial en ausencia de oxígeno ha decaído 1/e su valor inicial(**Figura 5**). De acuerdo a la ecuación 26 esto quiere decir que el 63% de la moléculas habrá perdido su luminiscencia para t inferiores a τ, mientras que el 27% lo harán para t > τ.

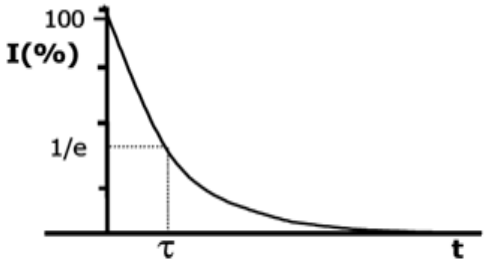

Figura 5. Decaimiento monoexponencial de la luminiscencia. El instante *t* donde la intensidad decae 1/e es el tiempo de vida *τ*.

Por tanto los cambios producidos en el tiempo de vida del estado excitado se pueden usar como parámetro analítico para la medida de la constante de Stern-Volmer (ecuación 8).

En los experimentos de tiempo de vida lo que se observa es una intensidad de emisión proporcional al número de moléculas, de donde el tiempo de vida puede ser calculado a partir del decaimiento de la luminiscencia, la cual en el caso más simple sigue un decaimiento monoexponencial (ecuación 27)

$$I(t) = I_0 e^{-\frac{t}{\tau}} \qquad (27)$$

Sin embargo, como ya se ha mencionado, la mayoría de las veces el decaimiento de la luminiscencia no es monoexponencial, debido a que la atenuación tiene lugar en varias etapas (cada una de ellas siendo exponencial), o simplemente por procesos cuya atenuación no es exponencial (como es el caso del proceso de desactivación colisional por las moleculaes del disolvente o transferencia de energía entre moléculas).[134] Teniendo en cuenta la ecuación 26, si la constante de radiación (k_r) es la misma para cada decaimiento, cada uno de los decaimientos monoexponenciales responderá a la ecuación de Stern-Volmer:

$$\frac{\tau_{j0}}{\tau_j} = 1 + k_{SVj}[O_2] \qquad (28)$$

donde τ_j es el tiempo de vida de cada uno de los decaimientos monoexponenciales los cuales presenta una constante de Stern-Volmer de k_{SVj}.

Muchos de los problemas asociados a las medidas de intensidad absoluta pueden minimizarse usando medidas de tiempo de vida, [135] aunque la instrumentación requerida es normalmente compleja y de mayor coste. El tiempo de vida es una propiedad intrínseca del luminóforo, y por tanto es virtualmente independiente de perturbaciones externas que sí afectan a las medidas de intensidad absoluta. Así, como (1) el tiempo de vida es independiente de la concentración del luminóforo, la variación de su concentración (por fotodescomposición o lixiviación del indicador) no afecta a la señal analítica; (2) el tiempo de vida no se ve afectado por las posibles derivas instrumentales de la fuente de radiación o el detector; (3) permite emplear fibras ópticas de gran longitud (hasta de 1 Km), sin que varíe la precisión o exactitud de la medida del tiempo de vida.

El tiempo de vida del indicador luminiscente puede ser cuantificado por dos métodos distintos: mediante medidas en el dominio del tiempo o mediante medidas en el dominio de la frecuencia.[116]

i) Medidas en el dominio del tiempo (tiempo resuelto). En este tipo de medidas la muestra se excita con un pulso de luz corto, registrándose la disminución de la intensidad de emisión en función del tiempo, que normalmente sigue un decaimiento monoexponencial. La **Figura 6** muestra los diferentes parámetros de tiempo que presenta un pulso de luz utilizado en las medidas de luminiscencia de tiempo resuelto:

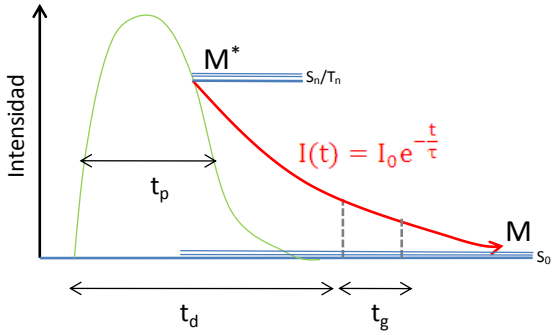

Figura 6. Medida de tiempo resuelto; t_p es el tiempo medio que tarda el pulso de la lámpara, t_d es el tiempo de demora ("*delay time*") que transcurre entre que se inicia el pulso de la lámpara y se toma la medida, y t_g es el tiempo de medida ("*gate time*") durante el cual se registra la intensidad en función del tiempo. M* y M representan el indicador en su estado excitado y fundamental respectivamente.

Los tiempos de vida típicos de los compuestos fluorescentes varían entre 2-20 ns, mientras que los tiempos de vida de los compuestos fosforescentes son relativamente mayores, del orden de 1 µs - 10 s. Como en este tipo de medidas es preciso registrar la variación de intensidad a lo largo del tiempo tras un pulso corto de la lámpara, es necesario el uso de detectores de alta velocidad, sobre todo si nos encontramos ante procesos fluorescentes.[116] Por ello, en los últimos años hay un considerable interés por la búsqueda de indicadores con tiempos de vida relativamente largos (del orden de µs o mayores), de forma que se pueda reducir el coste de los dispositivos de medida empleados. [130]

Aun así, este tipo de medidas son ideales para eliminar interferencias (luminiscencia de fondo y dispersión de luz[136]) y en los últimos años ha habido un gran desarrollo en la instrumentación, haciéndose en general más simple y barata.[131]

Diferentes modalidades de medida, como por ejemplo el método de determinación rápida de tiempos de vida (*Rapid Lifetime Determination Method*, RLD),[137] donde el tiempo de vida es calculado en dos instantes temporales diferentes de la curva de decaimiento, permite una monitorización de oxígeno autoreferenciada.[138, 139] Otra posibilidad es la obtención de imágenes de fluorescencia (*Fluorescence Lifetime Imaging*, FLIM) haciendo uso del método de conteo de fotones individuales correlacionados con el tiempo (*Time-Correlated Single-Photon Counting*, TCSPC).[140]

ii) Medidas en el dominio de la frecuencia (fase resuelta). Las medidas de tiempo de vida mediante este método no suelen requerir una instrumentación tan compleja como las del dominio del tiempo.[141, 142] Este tipo de medidas se basan en un método de modulación de la fase, donde la excitación de la fase sensora se realiza con una fuente de luz modulada a una frecuencia fija (generalmente una señal con forma de onda sinusoidal o cuadrada), la cual produce una emisión luminiscente modulada a la misma frecuencia. Sin embargo, debido al tiempo de vida intrínseco de la molécula indicadora (cuyo valor varía en función de la concentración de oxígeno), dicha emisión sufre un retraso respecto a la señal de excitación. Este retraso puede ser cuantificado bien a través del desfase (Φ, en radianes) o de la magnitud (R, en voltios) de la señal de emisión respecto a la señal de excitación, la cual se usa como referencia.[143] En la **Figura 7** se representa un esquema de la señal de excitación y emisión para este tipo de medidas.

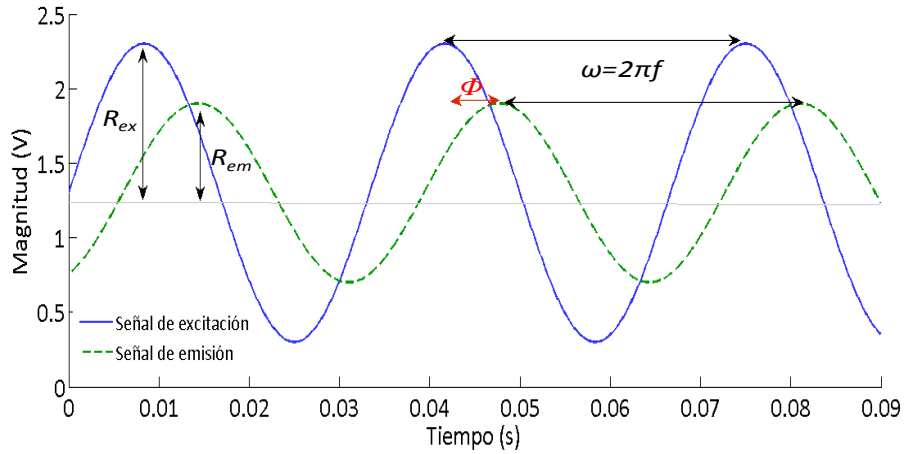

Figura 7. Medida de modulación de fase, donde se observa el desfase Φ de la señal de excitación y emisión, ambas a una frecuencia de modulación f, y la magnitud R de la señal de emisión y excitación (R_{ex} y R_{em})

Tanto el desfase como la magnitud pueden ser usados para calcular el tiempo de vida. [116, 143] Sin embargo, en la práctica, la medida del desfase es más usada que la de la magnitud, ya que esta última, al igual que las medidas de intensidad, se ve más afectada por los niveles de intensidad de fondo, fluctuaciones, degradación del complejo, etc.

Si el decaimiento es monoexponencial, el tiempo de vida (τ) se puede calcular a partir del desfase observado Φ (en radianes) y la frecuencia de modulación f (Hz) según la ecuación 29 [116, 144].

$$\tau = \frac{tan\phi}{2\pi f} \tag{29}$$

El método clásico para seleccionar la frecuencia óptima de modulación consiste en determinar el valor de frecuencia donde la sensibilidad alcanza el máximo, lo cual teniendo en cuenta ecuación 29 corresponde a un desfase de 45º (tan 45º=1). [116, 145] Sin embargo, la selección de la frecuencia de modulación optima debe hacerse cuidadosamente, puesto que si bien al aumentar la frecuencia de modulación la sensibilidad de la fase sensora aumenta, la relación señal-ruido (*Signal to Noise Ratio*, SNR) decrece.[116]

En cualquier caso, la selección de una frecuencia óptima viene determinada por el intervalo dinámico que requiera una aplicación concreta. De este modo, la frecuencia

suele elegirse de forma que se maximice el desfase (y por tanto la diferencia de tiempos de vida) entre los extremos de intervalo de medida elegido.

Precisamente una de las principales ventajas de este tipo de medidas es que permite disminuir en gran medida la SNR cuando el sensor se enfrenta a escenarios de medida hostiles mediante la selección de frecuencias de modulación bajas, siempre y cuando el intervalo dinámico requerido para la aplicación lo permita.

3. Sensores ópticos luminiscentes para el control de oxígeno

En los siguiente apartado veremos un resumen sobres las generalidades de un sensor ópticos de oxígeno, es decir, los diferentes elementos de que se compone y su configuración, y la instrumentación requerida para le medida de la luminiscencia, haciendo especial hincapié en el desarrollo sufrido por los sensores ópticos en los últimos 20 años. En el apartado 3.2 nos centramos en los componentes de una fase sensora óptica sensible a oxígeno, y por último se analizan los elementos a considerar en el diseño de un sensor óptico de oxígeno y algunas de sus aplicaciones en diferentes campos.

3.1. Generalidades de un sensor óptico

Un sensor químico es definido por la IUPAC (International Union of Pure and Applied *Chemistry*) como un dispositivo que transforma la información química en una señal analítica útil.[146] Por tanto, los sensores ópticos son aquellos sensores químicos donde la información química es transformada en una señal de naturaleza óptica. Así, la interacción del analito con la zona receptora o de reconocimiento del sensor produce un cambio en las propiedades ópticas del sistema, ya sea transmitancia, trasflectancia, reflexión interna atenuada, índice de refracción, o como hemos visto en el caso de los sensores de oxígeno, un cambio en las propiedades luminiscentes (intensidad de emisión y tiempo de vida).

Por tanto, los sensores ópticos de oxígeno se basan en el uso de fases sensoras químicamente activas que se implementan en dispositivos de medida. Las partes en que se divide un sensor óptico están esquematizadas en la **Figura 8** y se describen a continuación:

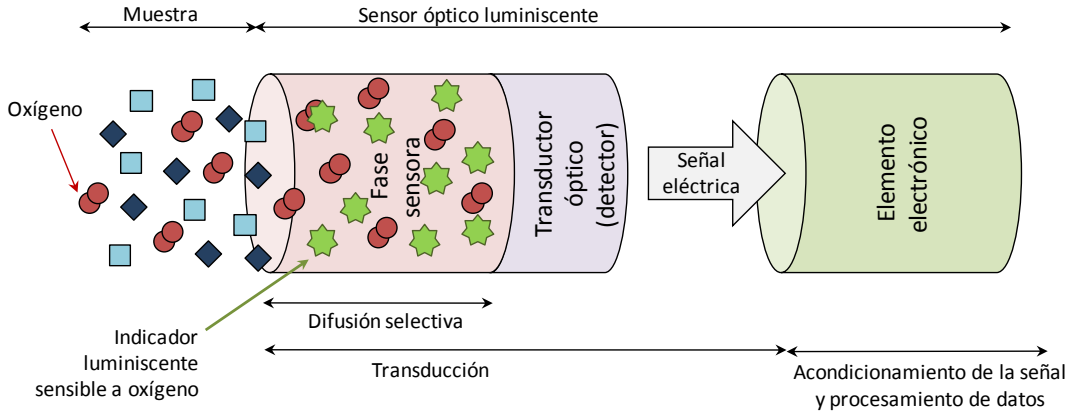

Figura 8. Esquema general de un sensor óptico luminiscente para determinación de oxígeno

- En primer lugar, podemos diferenciar la *fase sensora o zona de reconomiento* del sensor, que es donde se produce la interacción selectiva entre el analito de interés y el elemento indicador luminiscente. Esta interacción produce un cambio en una propiedad del sistema cuya magnitud es proporcional a la concentración del analito, lo que constituye la primera etapa del proceso de transducción. En los sensores químicos óptico esta traducción es de carácter físico (cambio en las propiedades espectroscópicas), si bien este cambio puede estar asociado a una reacción química, como ocurre en los biosensores enzimáticos con transducción de oxígeno.

  En cualquier caso, la fase sensora consta de dos partes: un indicador luminiscente y un soporte físico que además puede aportar propiedades de selectividad al analito de interés. Si bien es posible usar un indicador sensible a oxígeno (o estructuras supramoleculares derivadas de éste) directamente sobre la matriz a analizar,[147, 148] el uso de una matriz que aísle al indicador del medio mejora las propiedades de sensibilidad y estabilidad, y en aplicaciones biológicas evita citotoxicidad asociada a este tipo de compuestos.[138]
- A continuación podemos encontrar un elemento *transductor*, que es el encargado de transformar las propiedades de la fase sensora en una señal analítica útil (normalmente eléctrica). En los sensores ópticos de oxígeno, el elemento transductor es normalmente un detector de carácter óptico, el cual transforma la radiación recibida de la fase sensora en una señal de naturaleza eléctrica.
- Por último, esta señal eléctrica llega a un *elemento electrónico*, que es el encargado del acondicionamiento de la señal analógica y posterior procesamiento de los datos. En el caso de los sensores de oxígeno, este elemento es el encargado de

generar un valor de intensidad o de desfase (en función de las propiedades de la señal eléctrica generada por el detector). Este elemento electrónico está normalmente integrado en el sensor, de modo que la magnitud de la señal física obtenida se relaciona con la concentración de analito mediante un calibrado previo.

Configuración de un sensor óptico

Tradicionalmente se han definido tres tipos de los sensores químicos atendiendo a la posición de la fase sensora (en el interior de una celda de flujo, depositada sobre una fibra óptica o más recientemente sensores planares donde la fase sensora se deposita directamente sobre el detector).[109, 149] La **¡Error! No se encuentra el origen de la eferencia.** muestra un esquema de esta clasificación, donde se ha añadido un cuarto grupo de sensores denominados "inalámbricos", ya que debido a la naturaleza inalámbrica la transducción óptica hoy en día es común el uso de fases sensoras incorporadas directamente sobre la muestra, de forma que la concentración de oxígeno puede ser monitorizada *inálmbricamente* desde una cierta distancia, bien haciendo uso de un detector o de una fibra óptica. A continuación se describen cada uno de ellos:

- *Sensores tipo célula de flujo (optosensores).* En este tipo de sensores la fase sensora se encuentra empaquetada en una celda de flujo. El término optosensor fue introducido por Ruzicka y Hansen[150] para definir un nuevo principio de detección en análisis por inyección de flujo (*Flux Injection Analysis*, FIA) basado en el cambio de las propiedades ópticas de una superficie activa situada en el paso de un flujo.

La celda de flujo con la fase sensora puede estar situada en el compartimento de muestra del propio equipo, dando lugar a un *optosensor convencional*, o en el exterior del mismo (*optosensor no convencional*). En este último caso, a veces es preciso el uso de guías de ondas que permitan el transporte de luz hasta el sitio de medida[109].

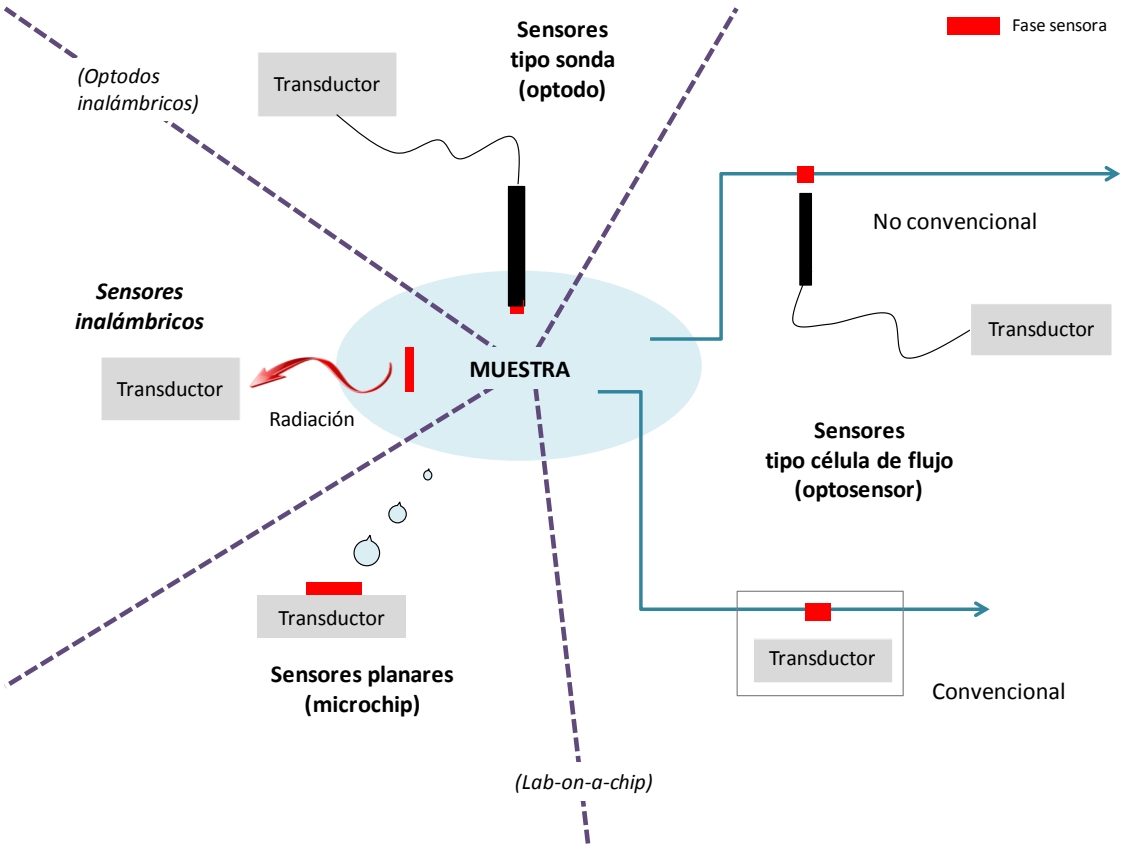

Figura 9. Tipos de sensores según la posición de la fase sensora respecto a la matriz de medida y el transductor

- *Sensores tipo sonda (optodos).* Están constituidos por una fase ópticamente activa situada en una guía de ondas, normalmente de forma cilíndrica (fibra óptica), aunque también existen de morfología plana. Estos sensores han recibido el nombre de optodos[151] (del griego "*óptico*" y "*camino*"), aunque también se conocen como optrodos (del ingles "*optical electrode*") a pesar de que la señal es óptica y no eléctrica.[152]

- *Sensores planares (tipo microchip).* En ellos, la fase sensora se encuentra inmovilizada directamente sobre el transductor o sobre un soporte inerte instalado en un microchip, que posee todos los componentes necesarios para realizar la medida (fuente de excitación, detector, filtros ópticos, etc). Además, la aparación de este tipo de sensores ha aumentado la posibilidad de miniaturización, dando lugar a sensores de gran flexibilidad.[80, 91]

- *Sensores inalámbricos.* Es el caso de aquellas configuraciones cuya zona de reconocimiento se encuentra incorporada en el ambiente de medida y su detección

se hace de forma externa a una cierta distancia de ésta, bien mediante el uso de un detector o de una fibra óptica.

Esta clasificación no es cerrada y puede depender de otros muchos aspectos, dando lugar a una serie de subclasificaciones. Por ejemplo, optodos de multifibra óptica para el análisis simultáneo en diferentes puntos con una sola fuente de excitación y un detector.[153] Además, la miniaturización de la fibra óptica permite hoy en día el desarrollo de optodos tipo catéter para aplicaciones *in vivo*[34, 154], mientras que los sensores planares, donde el indicador luminiscente se encuentra directamente depositado sobre el detector, han permitido el diseño de equipos compactos de medida. [155, 156]

Prueba de que muchas veces no es posible discernir entre un tipo de sensor y otro de sensor, es el caso de los microsistemas de flujo (μFIA) integrados en un chip (*Lab-on-a-chip*)[157] los cuales podrían considerarse una configuración híbrida entre sensor tipo chip y optosensor convencional.

Por otro lado, los sensores inalámbricos son muy versátiles. Permiten una lectura puntual de la concentración de oxígeno,[158] aunque en muchas ocasiones se combinan con una matriz de fases sensoras(por ejemplo, en 96 pocillos) o con el uso de nanoparticulas que son dispersadas en el interior de la muestra donde se desea medir el O_2. [159] A su vez pueden combinarse con el uso fibras ópticas para guiar la luz hasta el transductor (lo que bien podría considerarse como un optodo inalámbrico), cámaras CCDs que abarcan una mayor superficie y dan lugar a imágenes en dos dimensiones, o incluso hacer uso de una cámara digital de un teléfono móvil con tecnología CMOS como detector.[160]

En cualquier caso, la posición relativa de la fase sensora/transductor/muestra es un aspecto a tener en cuenta a la hora de desarrollar una fase sensora para la medida de oxígeno, la cual debe poder adaptarse a situaciones concretas de implementación y medida que puedan requerir un determinado tipo de configuración.

Instrumentación para el desarrollo de sensores ópticos

La instrumentación utilizada en el desarrollo de sensores ópticos puede ser simple o compleja dependiendo de la aplicación concreta y del principio de medida empleado. En general, los componentes básicos para el desarrollo de un sistema de medida para sensores ópticos aparecen representados en la **Figura 10**. El reciente desarrollo sufrido por los sensores ópticos está directamente relacionado con el desarrollo tecnológico de la instrumentación y nuevos métodos espectroscópicos.

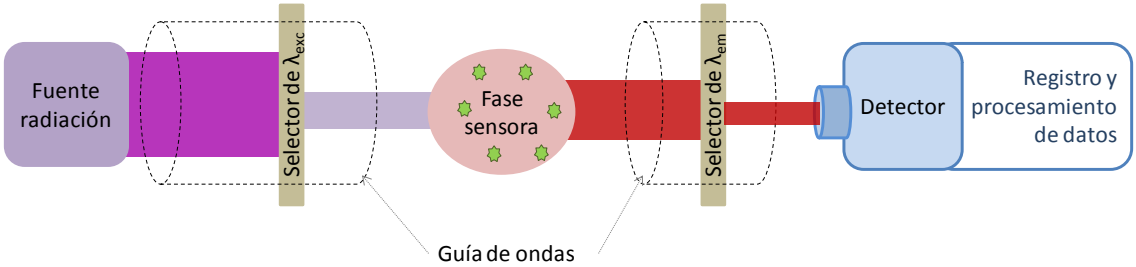

Figura 10. Componentes básico para el desarrollo de un sensor óptico luminiscente. La línea de puntos indica la posibilidad de utilizar una guía de ondas para conducir el haz de luz. (λ_{exc} y λ_{em} son las longitudes de onda de excitación y emisión de la fase sensora respectivamente).

A continuación se describen los distintos componentes mencionados anteriormente. Una descripción más detallada de los mismos puede ser encontrada en publicaciones especializadas.[93, 109, 116]

Fuente de radiación: debe ser capaz de proporcionar un haz de luz lo suficientemente intenso y estable para excitar adecuadamente la fase sensora. Actualmente se dispone de una amplia variedad de fuentes de luz: lámparas de wolframio-halógeno, de hidrógeno, de xenón pulsadas o continuas, lámparas de mercurio, láseres y diodos emisores de luz (*Light Emitting Diodes*, LEDs). La elección de la fuente luminosa depende en gran medida de las características espectroscópicas de la fase sensora y dek tipo de aplicación, así como del tipo de medida y configuración. Por ejemplo, para medidas de tiempo de vida en el dominio del tiempo es imprescindible el uso de una lámpara de pulsos, mientras que sensores que utilizan fibra óptica para largas distancia es preferible el uso de láseres.

La existencia de nuevas fuentes de radiación, como es el caso de láseres y LEDs, que permiten la excitación del analito prácticamente en toda la región del espectro visible, y evitan en muchos casos el uso de filtro y monocromadores, con la

consiguiente disminución del coste y tamaño del dispositivo de medida. En concreto el uso de LEDs se ha incrementado notablemente en los últimos años, debido a su bajo coste, pequeño tamaño, a su facilidad de uso y al hecho de que proporcionan una emisión relativamente monocromática e intensa en el intervalo UV-vis.

Guía de ondas: en muchas ocasiones se puede emplear una guía de ondas para conducir la radiación electromagnética (luz) desde la fuente de radiación hasta la fase sensora y desde ésta hasta el detector. Aunque existen guía de ondas planas, normalmente se utilizan guías cilíndricas como la fibra óptica , la cual está compuesta por un núcleo central *(core*), un revestimiento *(cladding*) que rodea al núcleo y un recubrimiento *(coating*), consistente en una capa de material plástico o metálico que la protege. Gracias a los índices de refracción de los materiales que la componen permite que la energía luminosa introducida en la fibra se propague de forma guiada a través del núcleo, sin escapar por el revestimiento.

Los materiales empleados en la fabricación de fibras ópticas dependen, en parte, del tipo de radiación que se pretende transmitir a través de ellas. Así, las fibras de núcleo de sílice fundida o de cuarzo, transmiten luz en el UV-vis-IR (190-1300 nm), mientras que las de vidrio o plástico, más económicas, lo hacen solo en el visible (450-700 nm). El recubrimiento de la fibra se fabrica siempre con materiales resistentes al medio externo donde vaya a operar. Las fibras ópticas de cuarzo son resistentes a medios fuertemente ácidos o moderadamente alcalinos. La máxima temperatura a la que se puede trabajar con la mayoría de las fibras ópticas está limitada por la resistencia del material que constituye la "envoltura protectora" y suele ser de unos 125 ^{o}C.

Por otro lado, cuando se decide emplear fibra óptica normalmente es necesario el uso de acopladores ópticos (en general, lentes de vidrio o cuarzo) para lograr reducir al máximo las posibles pérdidas de radiación luminosa mediante el enfoque del haz luminoso.

Además, hoy en día la industria de las telecomunicaciones ha logrado la comercialización de fibra óptica de bajo coste y que permita cubrir largas distancias, con buena transmisión en todo el espectro UV e IR.[161, 162] Esto abre nuevas posibilidades para medidas de oxígeno en atmósferas explosivas o lugares remotos.

Selectores de longitud de onda. Los selectores de longitud de onda (filtros ópticos y monocromadores) sirven, por un lado, para acortar la banda de excitación perteneciente a una fuente luminosa, especialmente si ésta presenta un intervalo de emisión muy ancho, y por otro, para discriminar la señal óptica de interés analítico de la luz interferente que habitualmente la acompaña (restos de la excitación, emisión Raman y dispersión Rayleigh, principalmente). La elección entre el empleo de monocromadores o filtros ópticos depende en gran parte del tipo de medida, el coste y la resolución espectral requeridos.

Los filtros ópticos de absorción son la elección más idónea cuando se pretende construir un sistema sencillo y barato. Se clasifican en función del intervalo de longitudes de onda que dejen pasar. Así, podemos encontrar filtros "paso banda" (*band pass*), los cuales dejan pasar una determinada banda del espectro electromagnético, filtros de corte (*cutt-off*), los cuales dejan pasar todo el rango de longitudes de onda que queda por encima (filtros "paso larga") o por debajo (filtros "paso corto") de un determinado valor umbral.

En cambio, para aquellas aplicaciones en las que se requiera una selección muy precisa de la longitud de onda, el uso de monocromadores constituye la única solución. Estos dispositivos constan de una *rendija de entrada* de luz, una *lente* o *espejo colimador*, que produce un haz de luz paralelo, un *prisma* o *red de difracción* que descompone la luz en sus diferentes componentes espectrales, y un *espejo cóncavo,* que conduce la radiación imagen hasta el denominado *plano focal*, donde se encuentra situada la *rendija de salida*, encargada de aislar la banda espectral deseada. Si se requiere una gran resolución espectral es preferible usar una apertura pequeña de las rendijas, teniendo en cuenta que este estrechamiento también supondrá una disminución significativa de la potencia óptica de la señal.

Detector: se basan en el efecto fotoeléctrico, es decir, la conversión espontánea de la luz incidente en corriente eléctrica La selección del detector óptico adecuado será siempre un compromiso entre la sensibilidad requerida para el sistema y los factores económicos. Idealmente, un detector debe poseer una alta sensibilidad en un amplio intervalo de longitudes de onda, rápidos tiempos de respuesta y una señal de salida mínima en ausencia de iluminación externa (corriente de oscuridad). De entre la gran

variedad de detectores existentes en el mercado, a continuación se detallan los más utilizado en el desarrollo de sensores ópticos de oxígeno.

- Tubos fotomultiplicadores (PMT, *Photomultiplier tube*). Los tubos PMTs son muy sensibles a la radiación UV-vis y su tiempo de respuesta es muy rápido. Los PMT contienen una serie de electrodos, llamados *dínodos*, que se utilizan como sistema de amplificación. Estos sistemas suelen venir implementados en equipos comerciales alojados convenientemente en compartimentos cerrados, ya que una luz intensa genera un daño irreversible en la superficie fotoeléctrica, razón por la cual se utilizan para medir radiaciones ópticas de muy baja potencia.

- Fotodiodos. De pequeños tamaño y bajo coste, están especialmente diseñados para medir radiaciones de media a alta intensidad, por lo que su sensibilidad es inferior a la de los PMT.

- Dispositivos de carga acoplada (*Charge Coupled Device*, CCD). Aunque de mayor coste que los PMTs, son junto a éstos los detectores multicanal más sensibles que se conocen actualmente. Un circuito integrado que contiene un número determinado de condensadores enlazados o acoplados permite amplificar la señal, de modo que la alta sensibilidad permite disminuir el nivel de iluminación necesario para su excitación, prolongando la vida útil del indicador fotodegradable.

  La alternativa digital a las CCD son los dispositivos CMOS *(Complementary Metal Oxide Semiconductor).* En los sensores ópticos de oxígeno el uso de cámaras color (tanto CCD de color como CMOS) ha abierto nuevas alternativas sobre las medidas de tiempo de vida o intensidad tradicionales, permitiendo incluso obtener imágenes de la distribución de oxígeno. [160, 163-165]

Registro y procesamiento de datos: en esta etapa se produce el registro y procesamiento de la señal eléctrica recibida para proporcionar un valor numérico. Por ejemplo, en las medidas de tiempo de vida por modulación de fase es necesario el uso de un detector sensible a la fase (*Phase sensitive Detector*, PSD), como un *lock-in amplifier*, encargado de transformar internamente la radiación recibida en un valor numérico de desfase. En algunos casos se puede requerir el acondicionamiento de las señales eléctricas (amplificación y/o filtrado de las mismas). Además, el procesamiento de

imágenes está tomando hoy en día más importancia debido al uso de microscopios y CCDs para obtener distribuciones de oxígeno. La aparición de microprocesadores de pequeño tamaño que han permitido mejorar el procesamiento y almacenamiento de datos, disminuyendo no solo el coste sino el tamaño de los dispositivos de medida.

Por otro lado, el gran desarrollo sufrido por las técnicas espectroscópicas permite hoy en día realizar medidas más precisas, versátiles y sensibles, tanto para la medida de la intensidad de la luminiscencia como para el tiempo de vida.[80, 166] Los amplificadores y osciloscopios desarrollados también permiten hoy en día aumentar la sensibilidad y velocidad de los métodos de medida de tiempo de vida en el dominio de la frecuencia, contribuyendo a disminuir el ruido de fondo que constituye una de sus principales desventajas.

En la **Figura 11** se resumen los aspectos de la instrumentación cuyo desarrollo ha indicido en el avance sufrido por los sensores ópticos, así como la influencia de la Ciencia de los Materiales sobre el desarrollo de los mismos.

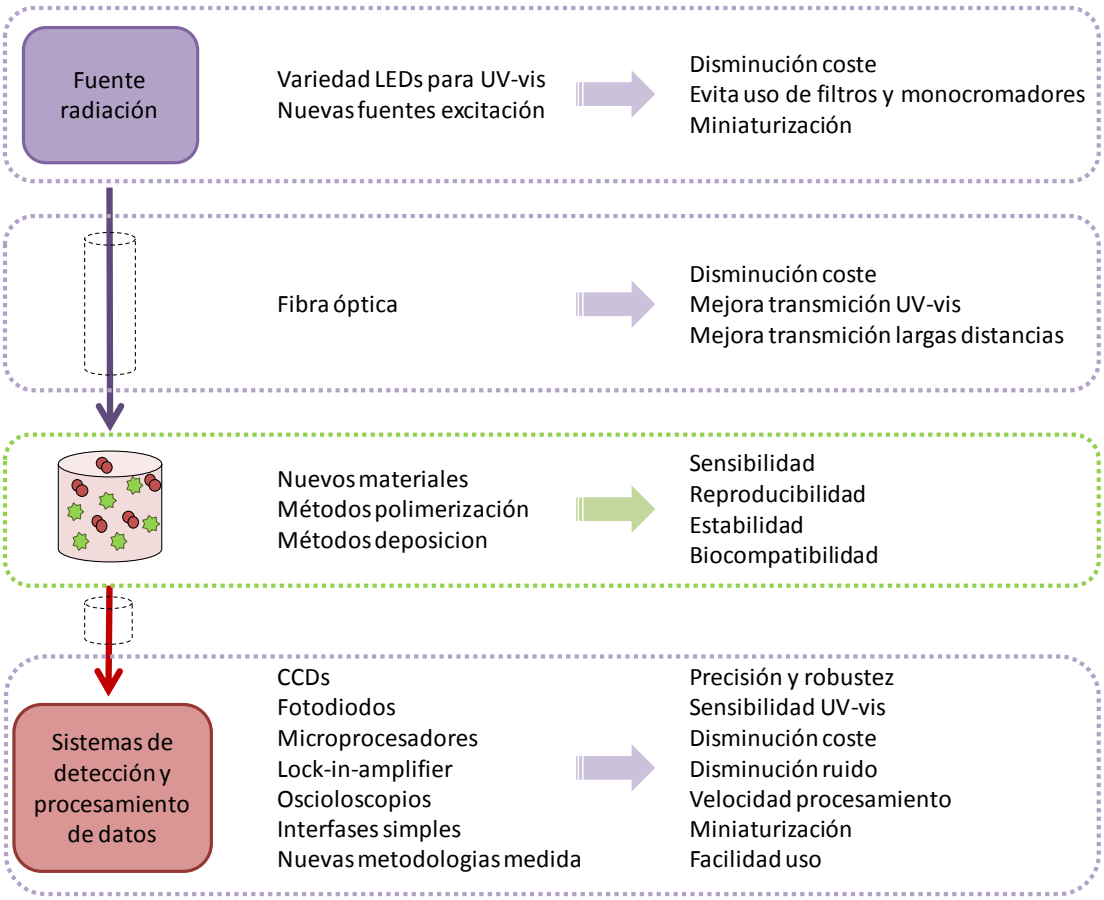

Figura 11. Influencia del desarrollo de la espectroscopia y síntesis de materiales sobre las partes de un sensor óptico.

En el desarrollo producido por los sensores ópticos en general, no hay que olvidar la influencia de la ciencia de los materiales sobre la fase sensora. De este modo, resulta muy importante el estudio de nuevas fases sensoras cuyas características estén próximas a las demandas exigidas. En este sentido, tanto la síntesis de nuevos complejos con tiempo de vida largos y fotoestabilidad mejorada, como el desarrollo de nuevos materiales[117] y técnicas de polimerización controlada[167] ha permitido mejorar la naturaleza de la fases sensoras. Esta mejora no solo ha permitido un aumento de la estabilidad y propiedades mecánicas, y mejora de la selectividad y sensibilidad del sensor, sino también la posibilidad de realizar un diseñar *a la carta* del mejor candidato para la medida de oxígeno molecular. Además, la creación de materias biocompatibles, y la química de la inmovilización de biomoléculas también han contribuido a aumentar el interés por este tipo de sensores. [161]

3.2. Componentes de una fase sensora óptica para oxígeno

Como ya se ha comentando, una fase sensora sensible a oxígeno consta de 2 partes: una molécula indicadora cuyas propiedades luminiscentes cambian en función de la concentración de oxígeno en el medio y un material o matriz donde éste se inmoviliza de forma que quede aislado del medio. A continuación se realiza una descripción más detallada de los tipos de elementos que componen una fase sensora.

Indicadores sensibles al oxígeno

Diversos compuestos como los hidrocarburos aromáticos policíclicos (PAHs), el ácido 1-pirenobutirico (PBA)[168] o el decacicleno (DCY),[121] han sido usados como indicadores sensibles a oxígeno. Otro tipo de materiales, como el fullereno C70[169], ftalocianinas[170] o los quelatos de aluminio,[171] también han demostrado utilidad en fases sensoras de oxígeno.

Sin embargo, las buenas propiedades luminiscentes de los complejos organometálicos (*Organometalic Compounds*, OMCs) de metales de transición han hecho que este grupo constituya hoy en día la principal fuente de indicadores luminiscentes sensibles a oxígeno, y por tanto se detallan a continuación. En general la configuración electrónica d^6 es capaz de producir una mayor cantidad de complejos luminiscentes que cualquier otra, [172] por lo que los metales más utilizado en OMCs para la detección luminiscente de oxígeno son principalmente Ru(II) e Ir(III), aunque también Re(I)[173], Os(III)[174, 175], Eu(III)[176] e incluso Pt(II).[177]

Otra clase muy utilizada de indicadores luminiscentes son las metaloporfinas (sobre todo de Pd(II) y Pt(II)) compuestas por un anillo tetrapirrólico con diferentes sustituyentes. Los derivados de la porfirinas (cetonas, lactonas, etc.) son muy versátiles ya que permiten diferentes modificaciones de su estructura. Otra clase de complejos basados en complejos de Pt o Pd son las azotetrabenzoporfirinas, las cuales ocupan una posición intermedia entre las porfirinas y la ftalocianinas.[178] La **Figura 12** muestra la estructura básica de los complejos organometálicos y las metaloporfirinas.

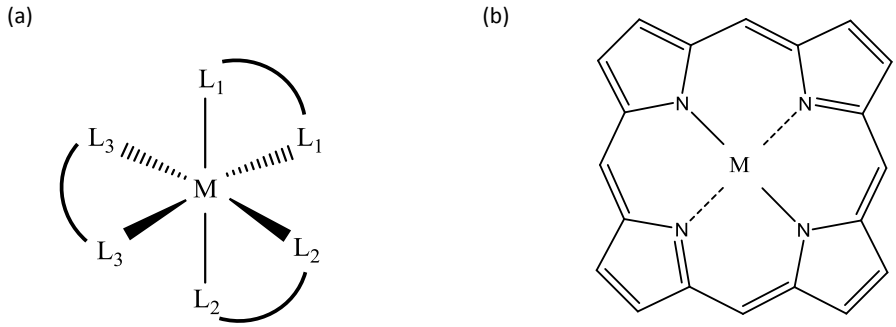

Figura 12. Estructura básica de a) complejo organometálico octaédrico donde L_1, L_2 y L_3 pueden ser ligandos de diferente naturaleza b) Anillo tetrapirrólico de la porfirina. M representa a cualquier de los metales de transición.

Por su importancia, en la **Tabla 2** se recogen los complejos metálicos de Ru(II) e Ir(III), y porfirinas de Pt(II) y Pd(II) más usados en el desarrollo de fases sensoras ópticas con matrices de diferente naturaleza, muchos de los cuales pueden encontrarse comercialmente.

La principal ventaja de los metales de transición es que poseen orbitales *d* parcialmente ocupados. La formación de complejos con diferentes tipo de ligandos (ver **Figura 13**) hace que este orbital *d* se divida en dos niveles de energía, lo cual posibilita la absorción de luz a determinadas frecuencias. La diferencia de energía en esta división, su ocupación y orden determinan sus propiedades emisivas, por lo que tanto el ligando, como el catión y la geometría del complejo formado influyen en las propiedades luminiscentes y de atenuación con el oxígeno. [115]

Además, la modificación de los ligandos de estos complejos puede ser útil para variar el carácter lipofílico del complejo, permitiendo solubilizarlo en materiales de diferente naturaleza, sobre todo aquellos de carácter apolar como las siliconas y

polímeros.[117] Del mismo modo, la solubilidad del contraión de los complejos cargados también puede contribuir a mejorar esta solubilidad.[179]

Tabla 2. Complejos organométalicos y porfirinas usadas en el desarrollo de sensores luminiscentes para oxígeno

Complejo	Soporte	λ_{abs} (nm)	λ_{em}(nm)	$\tau_{soporte}$ (μs)[a]	$\tau_{disolución}$ (μs)[b]	Ref
$Ru(bpy)_3^{2+}$	PMMA/CAB/Si	460	610	0.90-1.53	0.62	180, 181
$Ru(dpp)_3^{2+}$	PS/Ormosil/Si	450	615	4.2-7.5	-	181-183
$Ru(Phen)_3^{2+}$	PS	450	590	3	-	181
$Ir(ppy)_3$	PS	376	512	-	<2.0	184
$Ir(ppy)_2(dptNH_2)^+$	pPEGMA	380	500/550	1.3	.	185
$Ir(ppy_2)(mp\text{-}bpy)^+$	PS	318, 494	665	112	<12	186
PtOEP	PS/pPEGMA	384, 505, 535	646	84-90	17	182, 187, 188
PtTFPP	PS/Si	398, 508, 540	650	56-71	-	181, 189, 190
PtOEPK	PS/PVC	398, 592	759	62	-	191, 192
PdOEP	PS/pPEGMA/Si	393, 512, 546	663	770-1000	20	181, 188
PdOEPK	PS/PVC	410, 602	792	440-480	-	191, 192
PdTFPP	PS	405, 525, 565	670	930	-	189

[a] Tiempo de vida del indicador inmovilizado en soporte y en ausencia de oxígeno. [b] Tiempo de vida del indicador inmovilizado en disolución y en ausencia de oxígeno.

PMMA: poli metil metacrilato; CAB: butirato acetato de celulosa Si: sílice; Ormosil: Silicatos modificados orgánicamente; S: Silicona; PS:Poliestireno; pPEGMA: poli(etilenglicol)etiléter metacrilato;$dptNH_2$: 4-amino-3,5-di-2-piridil-H4-l,2,4-triazol; mp-bpy:2(4,4'-bis(2-(4-N,N-metilhexilaminofenil)etenil)-2,2'-bipiridina); PtOEP: Octaetilporfirina de Pt(II); PtTFPP: Pentafluorofenil porfirina de Pt(II); PtOEPK: Octaetilporfirina cetona de Pt(II); PVC: Policloruro de vinilo; PdOEP: Octaetilporfirina de Paladio (II), PdTFPP: Pentafluorofenilporfirina de Pd(II); PdOEPK: Octaetilporfirina cetona de Pd(II). (Ver Figura 13)

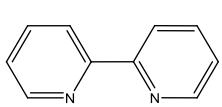

bpy: 2,2'-bipiridina

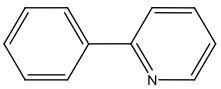

ppy: 2-fenilpiridina

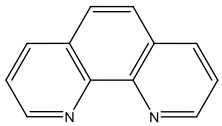

Phen: 1,10-fenantrolina

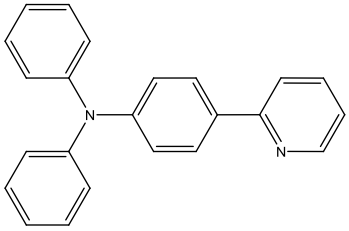

Ppy-NPh_2: difenilamina fenilpiridina

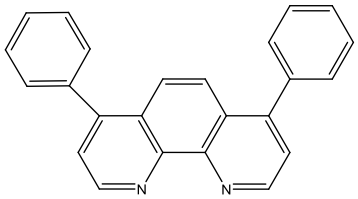

dpp: 4,7-difenil-1,10-fenantrolina

Figura 13. Ligandos más comunes usados en los OMCs de metales de transición.

En general, el indicador seleccionado debe poseer propiedades que le permita ser inmovilizado en una matriz rígida sin que ello afecte a sus propiedades físico-químicas. En general, el efecto de las matrices donde se encuentra el luminóforo tiene una gran influencia sobre el espectro de absorción y emisión de los complejos. Cuando el indicador se encuentra en disolución, el disolvente puede ser capaz de disminuir la energía del estado excitado, lo cual influye en la longitud de onda de emisión y en el tiempo de vida, debido a que la relajación de las moléculas en un disolvente es rápida (alta movilidad que presentan en estado líquido). Sin embargo, en sistemas rígidos, las rotaciones intramoleculares son más difíciles, por lo que el tiempo de vida de una molécula aumenta cuando ésta se inmoviliza en un soporte rígido comparado con el tiempo de vida en disolución, [109] tal como se observa para algunos complejos mostrados en la Tabla 2. Este es el principal motivo de que cuando el indicador es inmovilizado en una matriz rígida, aumenta su sensibilidad a oxígeno, puesto que como se comentó, la k_{SV} es directamente proporcional al τ_0.

Otro factor importante para el desarrollo de fases sensoras es la concentración del indicador, ya que si se realizan medidas de intensidad de la luminiscencia, ésta se va a ver afectada por la cantidad de indicador inmovilizado. Además, la concentración también es importante incluso en medidas de tiempo de vida, puesto que una alta concentración de complejo indicador puede dar lugar a fenómenos de precipitación y autoatenuación, que disminuyen el tiempo de vida, y por tanto la sensibilidad[183]

Un requisito deseable en los indicadores de oxígeno es que estos posean un brillo alto, entendiendo como tal el producto del coeficiente de absorción molar y el rendimiento cuántico, lo que se refleja en un aumento de luz absorbida y/o emitida. Esta característica no va a afectar a la sensibilidad de la fase sensora, pero incrementará la cantidad de luz que recibe el fotodetector,[193] facilitando su implementación en dispositivos ópticos.

Los complejos de Ru(II), ampliamente usados y estudiados,[194, 195] poseen tiempos de vida que aunque relativamente largos (del orden de unos pocos μs) dan lugar a una sensibilidad menor comparada con otro tipo de complejos como las porfirinas, que presentan tiempo de vida cercanos a los 100 μs (ver Tabla 2). Además, los complejos de rutenio se ven más afectado por la desactivación térmica, por lo que su sensibilidad a oxígeno se puede variar con la temperatura.[195] Aún así, los complejo de Ru(II) suelen

poseer una banda muy ancha de absorción en la región azul del espectro, lo que junto con un gran desplazamiento de Stokes, ha dado lugar a una gran variedad de aplicaciones.[117, 121, 138, 196]

Menos sensibles a la temperatura que los complejos de Ru(II) son los complejos de Ir(III). Modificaciones de los complejos mostrados en la Tabla 2 han dado lugar a una gran variedad de estructuras.[197-199] También se pueden encontrar complejos de Ir(III) con ligandos coumarínicos[193] o incluso porfirinas de Ir.[200] En general, los complejos de Ir(III) han demostrado buena capacidad para modificar su espectro de emisión en todo la región UV,[201, 202] aunque en la mayoría de los casos también poseen tiempo de vida del orden de los µs.

El uso de diferentes tipos de ligandos no solo permite modificar las propiedades espectroscópicas del complejo (longitud de onda de excitación y/o emisión, tiempo de vida, ver Tabla 2), sino que también influye sobre su fotoestabilidad. La estabilidad fotoquímica es muy importante para su empleo en fases sensoras ópticas de oxígeno, debido a que la fotodescomposición del reactivo inmovilizado puede producirse por la exposición prolongada a la radiación electromagnética. Por tanto, la modificación de los indicadores también contribuye a mejorar la fotoestabilidad del luminóforo. Un ejemplo lo encontramos en los complejos PtOEP y PdOEP. La modificación del anillo tetrapirrólico con un grupo cetónico, no solo produce un desplazamiento en la longitud de onda del rojo del espectro de emisión, sino que mejora las estabilidad química y fotodegradación del complejo.[191] Del mismo modo, la introducción de sustituyentes fluorados incrementa aún más la estabilidad, como ocurre con el complejo PtTFPP,[190] el cual es ampliamente usado como indicador de oxígeno.

Tipos de matrices

Según la morfología de la fase sensora donde se inmoviliza el indicador, podemos encontrar fases sensoras ópticas basados en dos tipos principales de formatos:

- Fase sensoras planares o membranas. Históricamente, las membranas fueron los primeros soportes sólidos usados en el desarrollo de fases sensoras ópticas, debido a la posibilidad de formar películas sensoras delgadas donde se pueden inmovilizar diferentes reactivos.
- Nanopartículas. Combinan la flexibilidad de los indicadores disueltos con las ventajas de las membranas. Estas nanopartículas a veces se denominan PEBBLEs

(*probes encapsulated by biological localized embedding*) cuando la determinación de oxígeno (u otro analitos) es intracelular.[203]

El desarrollo de un sensor ópticos requiere normalmente la deposición de la fase sensora en diferentes tipos de soporte donde llevar a cabo la medida óptica. La obtención de membranas lleva implícita la deposición de la fase sensora sobre un soporte. Sin embargo, las nanopartículas pueden constituir en si mismas el soporte al ser usadas directamente en el medio, o bien pueden ser depositadas para obtener una membrana nanoparticulada. Tanto membranas como nanopartículas presentan diferentes ventajas e inconvenientes y la selección del mejor formato vendrá determinado por la aplicación concreta, además de por el material de fabricación.

Los métodos de obtención de fases sensores más comunes en el campo de los sensores ópticos de oxígeno están recogidos en la **Tabla 3**. La elección final del formato y método de fabricación dependerá del material de la fase sensora y de la configuración (optosensor, optodo, inálmbrico, microchip) utilizada para realizar la medida.

Tabla 3. Principales formatos y métodos de obtención de fases sensoras.

Formato	Método de fabriación	Ref.
Membrana	*Spin-coating*	197, 204
	Dip-coating	205
	Knife-coating	206
Nanopartículas	*Nano spray-drying*)	207 208
	Precipitación	209, 210
	Miniemulsión	211, 212

En cualquier de los formatos de matrices que vamos a tratar (membranas y nanopartículas) la inmovilización del indicador puede hacerse física o químicamente:

Inmovilización física: el luminóforo sensible a oxígeno que se quiere retener se puede añadir con el cóctel a depositar mediante los métodos anteriores. Si se lleva a cabo una polimerización durante la formación de la fase sensora, el indicador puede añadirse junto a los monómeros quedando atrapada en el interior del material. También es posible llevar a cabo una inmovilización física en materiales porosos mediante la evaporación del disolvente,[213] o por impregnación o hinchamiento de la fase sensora.[214, 215]

Inmovilización química: mediante la formación de enlaces covalentes entre el indicador y la matriz. Precisamente la inmovilización química permite mejorar la estabilidad y evitar la migración de los complejos.[216] Esta inmovilización puede llevarse a cabo durante la síntesis del material, y luego ser depositado sobre un soporte, o bien llevarse a cabo la reacción cuando la fase sensora ya se ha depositado. En cualquier caso, la posibilidad de realizar una inmovilización química del indicador va a depender de los grupos funcionales que dispongan tanto la molécula como el material de la matriz, y de las condiciones de reactividad que estos sean capaces de soportar.

El uso de soportes de diferente naturaleza, así como el de plastificantes, tienen una enorme influencia en la sensibilidad de la fase sensora.[217] En general, el uso de diferentes materiales influye sobre la difusión de oxígeno, que como vimos está directamente relacionado con la sensibilidad k_{SV}. A continuación se detallan las matrices más utilizadas en el desarrollo de fases sensoras,[117, 121, 218] algunas de los cuales han sido aplicados en el desarrollo de esta memoria.

Membranas poliméricas

Este tipo de membranas, normalmente de carácter hidrofóbico suele proteger al indicador del acceso de otros posibles atenuadores de la luminiscencia, como especies iónicas. Sin embargo, debido al carácter apolar de algunas de estas membranas poliméricas pueden existir problemas de solubilidad del complejo, lo que produce lixiviación del complejo cuando la fase sensora entra en contracto con agua, o problemas de agregación del mismo en la fase sensora con la consiguiente disminución de sensibilidad.

Para comprender la influencia del material sobre la sensibilidad a oxígeno, se puede tener en cuenta la permeabilidad a oxígeno (P_{O2}), que directamente se relaciona con el coeficiente de difusión (D_{O2}) y la solubilidad a oxígeno del material (S_{O2}) mediante la ecuación 29:

$$P_{O2} = D_{O2}S_{02} \tag{29}$$

Según el trabajo de Mills *et al.*[125] la magnitud con que la solubilidad influye sobre la permeabilidad es mucho menor a como lo hace la difusión, por lo que en la mayoría de las fases sensoras, la S_{O2} puede considerarse aproximadamente igual, y se puede hablar

de difusión y permeabilidad indistintamente, aunque su significado físico no sea el mismo. Así, el valor de permeabilidad puede tomarse como guía de la sensibilidad a oxígeno de una fase sensora. Diversos factores influyen de una forma u otra sobre la permeabilidad a oxígeno de un polímero, como por ejemplo, su polaridad, grado de entrecruzamiento, humedad, grosor de la película, etc., que además no solo van a influir en la sensibilidad sino en otras propiedades como el tiempo de respuesta.

Además, como se vio en la sección 2.2 (pag. 35, ec. 23) un parámetro a considerar en la inmovilización del indicador es la viscosidad (η), la cual afecta directamente al coeficiente de difusión de oxígeno (D_{O2}) de la membrana, mejorando la sensibilidad de la fase sensora para valores de viscosidad más bajos. En este sentido, la temperatura de transición vítrea (T_g) del material polimérico es un parámetro a considerar. Por debajo de la T_g, el polímero se vuelva duro y quebradizo, mientras que por encima pasa a un estado blando y flexible. Por tanto, un polímero con una T_g alta va a ser más rígido que otro con un T_g baja. Así, polímeros con T_g más bajas tienen una mayor movilidad de sus cadenas poliméricas, y por tanto van a presentar una mejor difusión al oxígeno.

Una comparación entre soportes de diferente viscosidad demuestra mejores resultados en aquellos menos viscosos.[188] Sin embargo, aunque la difusión esté favorecida a bajas T_g, hay que tener en cuenta que la T_g también influye en las propiedades mecánicas del polímero, previene la migración del indicador e indica la posibilidad de realizar esterilización.

Además, el tamaño y distribución de las cadenas del polímero juega un papel importante en la viscosidad del mismo, ya que polímeros con un peso molecular más alto poseen una viscosidad mayor que el mismo polímero con un peso molecular menor.[219]

Entre los diferentes materiales poliméricos empleados en la elaboración de fases sensores ópticas para oxígeno podemos encontrar siliconas, polímeros orgánicos y derivados de la celulosa. La **Tabla 4** muestra algunos de los polímeros más usados en el desarrollo de fases sensoras con su correspondiente temperatura de transición T_g y coeficientes de permeabilidad (P_{O2}). De esta tabla se puede deducir, que en general la sensibilidad a oxígeno sigue la siguiente tendencia siliconas>celulosas>polímeros orgánicos. Sin embargo, los polímeros orgánicos son lo más usados ya que cubren un amplio intervalo de permeabilidad y pueden ser modificaciones para aumentar su

difusión, la cual va a depender en gran medida de los grupos funcionales que posean en su estructura. A continuación de describen algunas características y ejemplo de cada tipo de material.

Tabla 4. Tipos de polímeros utilizados en el desarrollo de fases sensores.

Tipo	Polímero	Acrónimo	*Tg* (ºC)[a]	[a,b] $P_{O2}\,10^{13}$ (cm^3 cm cm^{-2} s^{-1} Pa^{-1})	Ejemplos
Siliconas	Siliconas (varias)	-		376 (Ref.[125])	125, 220, 221
	Poli(dimetilsiloxano)	PDMS	-123	695 (35ºC)	215, 222
Polímeros orgánicos	Poli(1-trimetilsilil-1-propino)	PTMSP	-	5790 (30º) (Ref.[223])	224
	Poliacrilamida	PAA	165		225
	Poliacetato de vinilo	PVAc	32	0.367	226
	Poliacrilonitrilo	PAN	125	0.00015	206
	Policloruro de vinilo	PVC	≈74	0.034	192, 217, 226
	Poli(metilmetacrilato)	PMMA	≈105	0.06-0.116 (35 ºC)	226, 227
	Poli(2-hidroxietil metacrilato)	PHEMA	85	2.32-5.43 (35ºC)	225
	Poli(decil metacrilato)	PDMA	-66		228
	Poli(trifluoroetil metacrilato)	PTFEM	69		229
	Poli(etilenglicol)etil eter metacrilato	PEGMA	-40 (Ref.[185])		185, 188
	Poliestireno (PS)	PS	100	2	191-193, 198, 226, 230-232
	Poli(estireno-*co*-acrilonitrilo)	PScoPAN	-	0.0032-0.35	233
	Poly(pentafluoroestireno)	PFS	47		216
	Poli(estireno-*co*-divinilbenceno)	PScoDVB			234
	Polisulfona	PSF	186	0.0711	232, 235, 236
Celulosas	Acetato de celulosa	CA	200	0.585 (30ºC)	237
	Acetato butirato de celulosa	CAB		3.56 (34ºC)	217 226, 227
	Etil celulosa	EC	43	11	206, 217

[a] Valores obtenidos de la referencia [219] o específicado; [b] Valores a 25 ºC o especificado

Siliconas

Las siliconas o polisiloxanos se consideran polímeros inorgánicos puesto que contienen átomos de silicio y de oxígeno en su cadena principal. Pertenecen al grupo de los elastómeros, por lo que la flexibilidad de su cadena principal es muy alta. Así, debido a la alta permeabilidad a oxígeno y baja T_g comparada con otros polímeros (ver Tabla 4), las siliconas han sido ampliamente usadas en el desarrollo de fases sensores ópticas de oxígeno. [117, 121]

Las siliconas se pueden encontrar comercialmente como un líquido viscoso que solidifica durante la etapa de curación. Se pueden diferenciar entre siliconas de un componente o de dos componentes, en función del número de prepolímeros usados para su formación, lo cual influye notablemente en las propiedades. Las siliconas de un solo componente, que se caracterizan por la especie química liberada durante su etapa de curación, han mostrado mejores resultados con respecto a la sensibilidad a oxígeno[122, 220, 221]

Sin embargo, algunas siliconas, aunque altamente permeables a oxígeno, carecen de propiedades mecánicas cuando son depositadas como membranas, precisamente debido a su baja temperatura de transición vítrea. Además, la permeabilidad a oxígeno debe ser analizada cuidadosamente, puesto que esto pueden conllevar permeabilidad a otros gases y vapores[238] que actúen como atenuadores de la luminiscencia.

Polímeros orgánicos

El reactivo utilizado en fases sensoras ópticas se inmoviliza, preferentemente, en polímeros que sean rígidos y ópticamente transparentes. En este sentido los polímero cristalinos como el poliestireno o el poli(metilmetacrilato), los cuales presentan una T_g ≥ 100 ºC (ver Tabla 4), aunque poseen menos permeabilidad a oxígeno que las siliconas, tienen una alta capacidad de adhesión a diferentes tipo de superficies. Esto junto a su permeabilidad selectiva a oxígeno que evita que otros atenuadores entren en contacto con el luminóforo, ha hecho que se utilicen en el desarrollo de este tipo de fases sensoras. Además, el hecho de que posean una temperatura de transición vítrea alta, permite someter a la fase sensora a determinados procesos de esterilización, como en el caso de la alta T_g (186 ºC) que presenta la polisulfona.[232, 235]

En especial poliestireno está especialmente indicado para el desarrollo de fases sensoras y es normalmente usado como material de referencia ya que ha demostrado buena compatibilidad con un gran número de complejos. Además su alta T_g previene la migración del mismo, evitando obtener agregados incluso tras largos periodos de tiempo.

El copolímero poli(estireno-*co*-acrilonitrilo) posee un permeabilidad intermedia, en función del porcentaje de PAN, entre el PAN y el PS ($0.00015\ 10^{-13}$ y $2\ 10^{-13}$ $cm^3\ cm\ cm^{-2}\ s^{-1}\ Pa^{-1}$ respectivamente). De hecho el PAN tiene muy mala difusión al oxígeno, por lo

que a menudo se ha usado para evitar la sensibilidad cruzada a este gas en sensores de temperatura o para aislar complejos de referencia en medidas relativas. [206]

La mejor permeabilidad a oxígeno la encontramos en el poli(1-trimetilsilil-1-propino) (PTMSP).[223] Este polímero posee un grupo trimetilsilil responsable de crear rigidez a la vez que aumentar el espacio libre en su estructura. Así, el PTMSP muestra un valor de coeficiente de difusión similar a la silicona PDMS, lo cual ha sido usada para fases sensoras a baja concentración de oxígeno.[224]

En general, la presencia de fluoruros en el material, al igual que en los complejos, aumenta la estabilidad y evitan la degradación de la fase sensora. La longitud del enlace C-F es menor que la C-H, por lo que su energía es mayor, lo que unido al carácter electronegativo del fluor, mejora el potencial redox del polímero a la vez que induce una mayor afinidad por el oxígeno. [229]

En muchos casos, la fomación de un copolímero permite adecuar las propiedades de difusión de la fases sensoras, por ejemplo, se puede añadir acrilamida para hacerlas permeables a otros iones de interés analítico.[225] En general, el uso de monómeros más polares permite aumenta la hidrifilicidad del polímero, lo cual puede dar lugar a la formación hidrogeles, los cuales presentan una mejor biocompatibilidad para el caso de sensores implantables.[239-243]

Derivados de la celulosa

La celulosa es un polímero natural formado por unidades repetidas del monómero glucosa, y entre sus derivados más ampliamente usados en el desarrollo de fases sensoras a oxígeno se pueden encontrar el acetato de celulosa(CA), el butirato acetato de celulosa (CAB) o la etil celulosa(EC).[117, 121] Estos polímeros difieren considerablemente en su coeficientes de permeabilidad (ver Tabla 4), que en general es alto. En el caso de la etil celulosa su permeabilidad puede variar en función del contenido en etoxi de la misma.[244]

Las celulosas presentan una mayor hidrofilicidad que las siliconas y los polímeros orgánicos, por lo que muchas veces se utilizan para la formación de hidrogeles.[117] Estos hidrogeles son insolubles en agua, pero suficientemente hidrofílicos para que sufran procesos de hinchamiento en medios acuosos, mejorando la biocompatibilidad de la fase sensora.

Estrategias para mejorar la sensibilidad de las membranas poliméricas

Los problemas de linealidad y sensibilidad asociados con la compatibilidad matriz-indicador pueden mejorar mediante el uso de copolímeros, cuya polaridad optimice las propiedades del polímero para solubilizar el indicador.[215]

Sin embargo, la estrategia más ampliamente utilizada es el uso de plastificantes para aumentar el coeficiente de difusión de los polímeros, y puede puede ayudar a compatibilizar material e indicador. En la **Figura 14** se muestran las estructuras de los plastificantes más usados en el desarrollo de sensores ópticos de oxígeno. Aún así, hay que tener en cuenta que los plastificantes también modifican la T_g y por tanto la viscosidad de la matriz, lo cual puede tener efecto negativo.[198, 245] Por ejemplo, plastificantes como el *o*-CPOE o el *o*-NPOE pueden producir una disminución de sensibilidad en función del indicador, matriz y concentración de plastificante utilizados. En muchos casos, se produce una disminución inicial de la sensibilidad para concentraciones de palstificante hasta el 10%, mientras que para concentraciones mayores mayores la sensibilidad aumenta.[198, 218] A pesar de esta mejorar en la sensibilidad para concentraciones altas, hay que tener en cuenta que las propiedades de adhesión del polímero pueden verse afectadas negativamente. Del mismo modo, diversos tipos de plastificantes pueden afectar de diferentes forma la fotodegración del complejo a lo largo del tiempo o cuando éste es sometido a procesos de esterilización.[197]

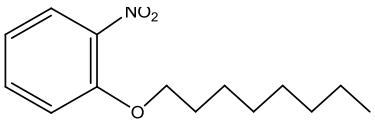

o-NPOE: *orto*-nitrofeniloctileter

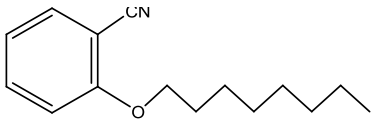

o-CPOE: *orto*-cianofeniloctileter

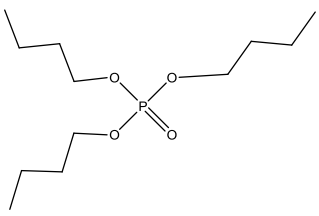

TBP: Tributilfosfato

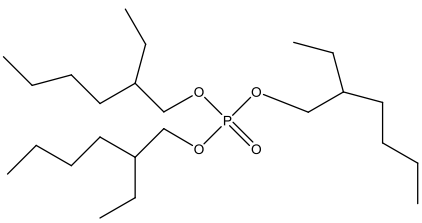

TOP: Tris(2-etilhexil) fosfato

Figura 14. Estructuras de los plastificantes más comunmente usados en el desarrollo de fases sensoras ópticas para oxígeno.

En otras ocasiones, para mejorar la solubilidad del complejo en la fase sensora polimérica se hace uso de nanopartículas de óxidos metálicos donde el indicador está adsorbido o encapsulado, de modo que estos se dispersan en la matriz polimérica mejorando su sensibilidad a oxígeno mientras que el carácter polimérico permite su deposición en diferentes substratos. [120, 246, 247] Estas nanopartículas sólidas también mejoran la señal de intensidad de luminiscencia debido a la dispersión de la luz que producen.[236] En muchos casos, se añaden partículas de TiO_2[120] o SiO_2 (sílice).[215]

Membranas sol-gel

El uso de procesos sol-gel para producir fases sensoras ópticas ha tomado un gran interés en los últimos años, sobre todo por su flexibilidad en el diseño y facilidad de fabricación.[208] El material sol-gel se utiliza para crear un soporte microporoso encargado de atrapar (con diferentes mecanismos) al indicador luminóforo a la vez que permite la difusión del oxígeno para que interactúe con este.

Un sol-gel se produce por la hidrólisis y condensación de tetraalcoxilanos del tipo $Si(OR)_4$, donde R es un grupo alquilo. [117] Lo más utilizados son el tetrametoxisilano (TMOS), metiltrimetoxisilano (MTMOS) o tetraetoxisilano (TEOS). Estos organosilicatos producen una suspensión coloidal (sol) que al condensar a temperatura ambiente gelifica para producir un entramado de moléculas (gel). El secado posterior produce una densificación del gel que da lugar a una película porosa. En la **Figura 15** se esquematizan las dos etapas del proceso sol-gel. De este modo, variando el tipo de catálisis, así como la temperatura y concentraciones utilizadas, se pueden modificar las propiedades del material nanoestructurado formado.

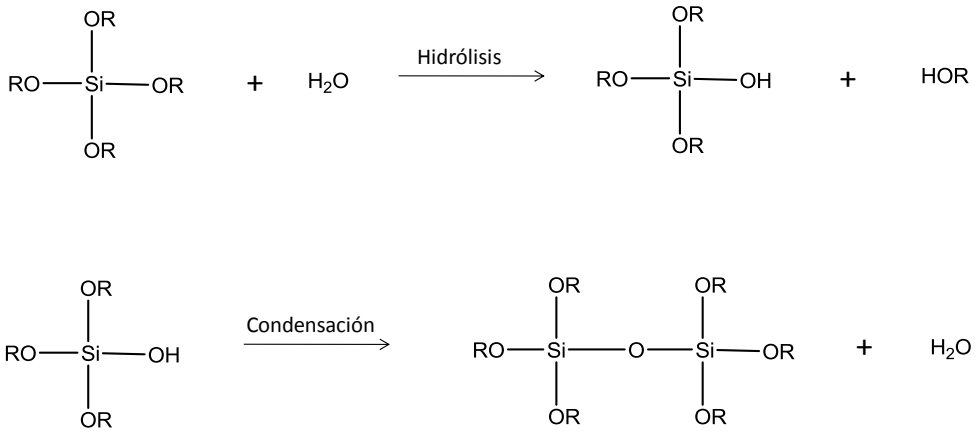

Figura 15. Etapas de hidrólisis y condensación del proceso sol gel.

Para sensores gaseosos, los silicatos modificados orgánicamente (*ORganically MOdified SILicates*, ORMOSIL) funcionan particularmente bien. Estos organosilicatos se basan en el uso de algún precursor modificado orgánicamente, como el feniltrimetoxisilano, con cualquiera de los alcoxidos de silicio mencionados anteriormente. La policondensación de estas moléculas ha producido materiales con propiedades de estabilidad y permeabilidad mejoradas.[182, 248] Añadiendo un indicador sensible a oxígeno durante la etapa *sol* se pueden producir fases sensoras sobre una variedad de substratos, tanto fibras ópticas como superficies planas. [204] Además, muchos de ellos son solubles en disolventes, lo cual permite su deposición con diferentes métodos[208]

Óxidos metálicos nanoestructurados

Los óxidos nanoestructurados permiten crear membranas inorgánicas de tamaño, porosidad y transparencia perfectamente controlables. Su obtención está ampliamente desarrollada debido al gran interés que despiertan estos materiales en campos tan relevantes como la microinformática, robótica, sensores electroquímicos, etc. Este tipo de material permite crear multitud de materiales con características totalmente diferentes en función del óxido metálico usado así como el proceso de síntesis. Además, la reducción del tamaño de partícula en este tipo de fases y el control de la difusión del gas ha hecho que estas fases presenten propiedades mejoradas para su uso como sensores de gas. [34]

Para el uso de este tipo de óxidos como fases sensoras de oxígeno se pueden seguir dos estrategias:

- La propia nanoestructura de óxido es el material sensible, de modo que cuando se expone a un gas se produce un cambio en sus propiedades eléctricas[249] u ópticas.[250]
- La nanoestructura se usa para inmovilizar una especie luminiscente, en este caso sensible a oxígeno, de modo que se mejora la interacción de éste con el gas.[213]

Estos nuevos materiales nanoestructurados están basados en la dispersión de nanopartículas de óxidos metálicos en un soporte inerte (alcohol polivinílico, PVA). [251], siendo los óxidos más utilizados los de aluminio, silicio, zirconio y titanio. Su

fabricación es muy simple y económica, pues se pueden conseguir 200 m^2 de material por minuto mediante "*curtain coating*" (deposición en cortina o cascada) y pudiendo generar membranas de 1 a 30 ml/m^2 de volumen total de poros con diámetros que oscilan entre 1 y 50 nm.

Los óxidos metálicos de óxido hidróxido de aluminio (AlOOH) desarrollados por la empresa Ilford Imaging[252] han dado muy buenos resultados en el desarrollo de fases sensoras ópticas para detección de oxígeno. Las membranas generadas con este tipo de óxidos son nanoporosas, pudiendo controlar el tamaño, volumen y carga de los poros, lo cual permite incorporar indicadores o otros reactivos.[213] Las membranas desarrolladas con AlOOH han demostrado mejorar las propiedades de las fases sensoras cuando se inmovilizan indicadores sensibles a oxígeno.[198, 213] En la Figura **16** se muestran varias imágenes de microscopio de las nanoestructuras AlOOH

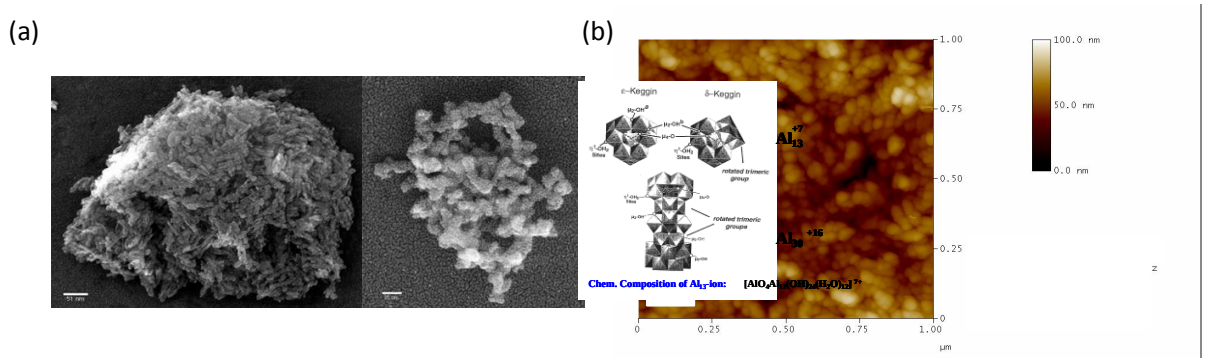

Figura 16. Fotografía de: a) microscopio de electrónico de barrido (SEM) de las partículas de AlOOH, b) microscopio de fuerza atómica (AFM) de estas partículas depositadas sobre PVC para formar la nanoestructura de óxido hidróxido de aluminio.

Las partículas de óxido de este material se aglomeran formando nanoporos en el interior, mientas que el espacio entre estos aglomerados da lugar a la existencia de macroporos.[253] Esta heterogeneidad da lugar a la formación de dos ambientes dentro de la fase sensora que hacen que la respuesta de la fase sensora a oxígeno no sea lineal, y normalmente requiera un ajuste según el modelo de Demas. Sin embargo, esta arquitectura de los poros también parece ser responsable de que las fuerzas capilares conduzcan al oxígeno rápidamente hacia el interior de los poros, mejorando la sensibilidad a oxígeno de la fase sensora, que puede mejorar hasta 100 veces respecto al mismo indicador inmovilizado en una membrana clásica de poliestireno.

Al mismo tiempo, la distribución del indicador en los nano- y macro- poros formados proporcionan a la fase sensora una gran estabilidad frente a la

fotodescomposición debido a un mayor aislamiento de estos reactivos, lo que disminuye la probabilidad de formación de aglomerados y precipitación del mismo.[253] Esta característica también permite la coincorporación de dos o más reactivos sin que se produzcan aglomerados, evitando procesos físico-químicos reversibles entre ellos, como procesos de transferencia de energía (FRET) y de transferencia de protones[252] lo que abre nuevas posibilidades en el desarrollo de sensores ópticos.

Nanopartículas poliméricas

Aunque se pueden encontrar gran variedad de nanopartículas de naturaleza inorgánica, [210, 254, 255] en este apartado nos centramos en un nuevo formato de fase sensora: partículas poliméricas de tamaño nanométrico que llevan el indicador sensible a oxígeno inmovilizado en su interior. Estas partículas (NPs) se utilizan dispersadas en el medio, pero también es posible su (co)inmovilización en soportes para realizar medidas en fase gaseosa.

A ser de naturaleza polimérica, ofrecen las mismas ventajas que una membrana polimérica, pero además poseen una serie de características que pueden hacer interesante su uso, como son una gran relación superficie/volumen, la posibilidad de ser dispersadas en el medio (incluso intracelularmente) para realizar medidas inalámbricas, evitan procesos de transferencia de carga entre moléculas del indicador y evitan la aglomeración del mismo.

La combinación de NPs con propiedades magnéticas permiten guiar las mismas hacia la región de interés,[256] mientras que si son recolectadas con un imán, se puede mejorar la sensibilidad de la fase sensora evitando también interferencias con la matriz.[257] Estas propiedades magnéticas suelen conseguirse mediante la adicion de magnetita (Fe_3O_4) durante el procesado de la nanopartícula. El contenido en magnetita debe ser optimizado, puesto que como consecuencia de su color negro ésta absorbe parte de la radiación, disminuyendo la señal que llega al detector. La **Figura 17** muestran una fibra óptica especialmente diseñada con un imán en la punta para llevar a cabo la recolección de NPs.

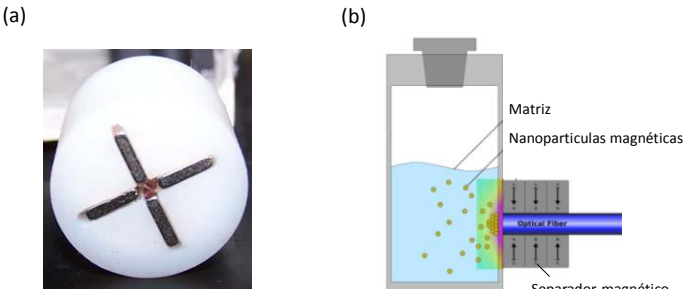

Figura 17. (a) Imán en la punta de la fibra óptica para permitir la recolección de las nanopartículas magnéticas (b) Recolección de las nanopartículas con fibra óptica.[258]

Aparte de las propiedades ópticas, la caracterización de estas NPs se hace principalmente en base al tamaño de partícula (d, nm), la polidispersidad (PdI) u homogeneidad de tamaños, y el potencial zeta (, en mV). La influencia de estos parámetros sobre las características de la fase sensora no se conoce por completo, sin embargo hay que tener en cuenta que

- El ζ da información sobre la cantidad y signo de la carga superficial de la partícula, indicando la estabilidad de la dispersión formadas. Esto tiene interés para medidas acuosas o bien si se desea recolectar las partículas mediante un campo magnético, ya que va a influir sobre el tiempo de recolección y por tanto de respuesta del sensor. Además, el valor de potencial zeta es útil si se pretende modificar la superfie de la partícula, bien mediante técnicas capa-a-capa (LbL, *Layer by Layer*) o gracias a la información que se puede obtener de este parámetro sobre la cantidad de grupos funcionales disponibles.[259]
- Por otro lado, tamaños más pequeños dan lugar a una mayor relación volumen/área superficial, de modo que la sensibilidad puede verse aumentada al mejorar la difusión de oxígeno sobre el indicador. Además, diferente tamaño de partícula pueden ser útiles en diferentes aplicaciones, por ejemplo, para aplicaciones *in vivo* es necesario que las partículas sean inferiores a 60 nm,[259] mientras que para una buena separación magnéticas, además del potencial zeta el tamaño de partícula debe ser lo suficientemente grande.

Las NP pueden ser entrecruzadas o bien estar formadas por aglomeración de un (co)polímero lineal. Las NP permiten usar cualquiera de los métodos de inmovilización

del indicador: este puede ser añadido en la mezcla de monómeros durante la síntesis de polímero, mezclado con el polímero antes de la etapa de formación de la partícula, o a posteriori. Si las NPs son entrecruzadas, el indicador también puede quedar retenido físicamente durante la etapa de síntesis. Otros métodos se basan en la impregnación de las NPs mediante hinchamiento de las mismas al sumergirlas en un disolvente donde se encuentre el indicador.[214]

En este apartado nos centraremos en la inmovilización física como forma de inmovilizar el indicador en las NPs. La preparación de este tipo de nanofases sensoras mediante este mecanismo se basa en el procesado de un cóctel que contiene el polímero lineal, indicador y magnetita adecuadamente disueltos o dispersados. Los polímeros lineales utilizados pueden ser previamente sintetizados u obtenidos de forma comercial. Mediante los métodos de miniemulsión y precipitación de este cóctel se pueden conseguir partículas micro y nanométricas de diferente polidispersidad.

Precipitación-evaporación

Este es el método de formación de NPs más simple y versátil, ya que basta con la precipitación bajo agitación de un cóctel que contiene tanto el polímero como el indicador disueltos, sobre una cantidad de otro disolvente donde ni polímero ni indicador son solubles. La **Figura 18** muestra un esquema de la síntesis de NPs mediante precipitación evaporación. El primer paso es la mezcla de los componentes en el cóctel (1) que formaran la fase orgánica o discontinua. Este cóctel es vertido bajo agitación sobre otro disolvente, normalmente agua (2), el cual constituye la fase acuosa o continua. Para una adecuada formación de partículas, es imprescindible que ambos disolventes sean miscibles de modo que cuando el polímero entra en contacto la fase acuosa donde no es soluble, se produzca la aglomeración de las cadenas de polímero formando la partícula con el indicador atrapado dentro. La posterior evaporación del disolvente orgánico (3) produce una dispersión de NPs las cuales contienen el indicador y magnetita retenidos en su interior.

El tipo de disolventes y polímeros que se pueden utilizar es muy amplio, obteniéndose diferentes tamaños en función de la carga y concentración de polímero utilizado.[209] Entre los disolventes más usados en este tipo de precipitación están la dimetilformamida (DMF), dimetilsulfoxido (DMS), acetona, tetrahidrofurano (THF),

acetonitrilo (ACN), etanol…etc., siento agua el medio sobre el que se lleva a cabo la precipitación.

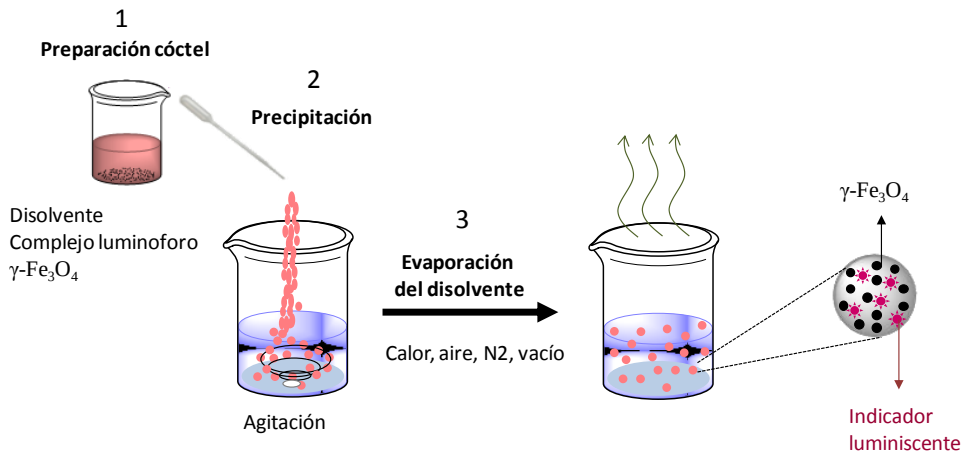

Figura 18. Procedimiento de precipitación-evaporación utilizado para la producción de NP poliméricas

En todo caso la elección de disolvente dependerá de la polaridad del polímero elegido y del disolvente sobre el que se va a llevar a cabo la precipitación. Por ejemplo, se puede conseguir formar partículas de polímeros apolares como el PS usando disolventes polares como el metanol o muy apolares como el hexano.

Del mismo modo, la carga del polímero puede dar lugar a mayor o menor estabilidad de las NP en medio acuoso: por ejemplo, un polímero de PSMA puede formar dispersiones extremadamente estables, con un potencial zeta muy negativo (<-30mv), debido a la apertura de los grupos maleico del polímero al entrar en contacto con el agua, tal como se muestra en la **Figura 19**:

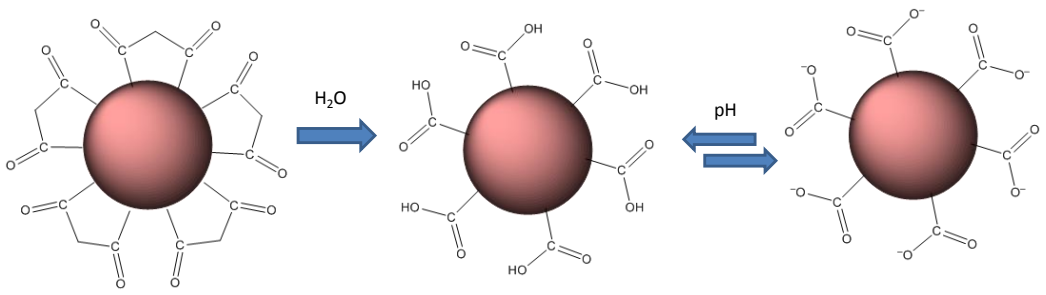

Figura 19. Apertura de los grupos maleico del PSMA cuando la NP entra en contacto con agua. La carga negativa de la superficie es responsable de su alta estabilidad (ζ < -30m V) y depende del pH del medio.

La adición de propiedades magnéticas puede resultar más complicada que en otros métodos que hacen uso de surfactantes, debido a que los disolventes donde la magnetita puede dispersarse es más limitado. En este caso es conviene optimizar el

recubrimiento de magnetita para facilitar su dispersión en el cóctel. Comercialmente existen diferentes tipos de magnetitas cuya dispersión cubre un amplio rango de disolventes, incluso agua.

Miniemulsion-evoparación

Esta técnica se basa en la preparación de miniemulsiones agua/disolvente (*water/oil, w/o*) o disolvente/agua (*o/w*) en las cuales la fase discontinua es el cóctel que contiene el polímero e indicador. La **Figura 20** muestra un esquema del procedimiento de preparación de nanopartículas sensoras magnéticas mediante miniemulsión o/w. Para conseguir la miniemulsión es necesaria la adición de un surfactante en concentración inferior a la micelar crítica (CMC). Una vez mezcladas las dos fases (1), la miniemulsión se consigue mediante sonicación de alta energía. (2) con diferentes ciclos de enfriamiento. Una vez formada la miniemulsión se procede la evaporación del disolvente (3), lo que produce la formación de nanopartículas poliméricas que incluyen en su estructura el indicador para el reconocimiento óptico.

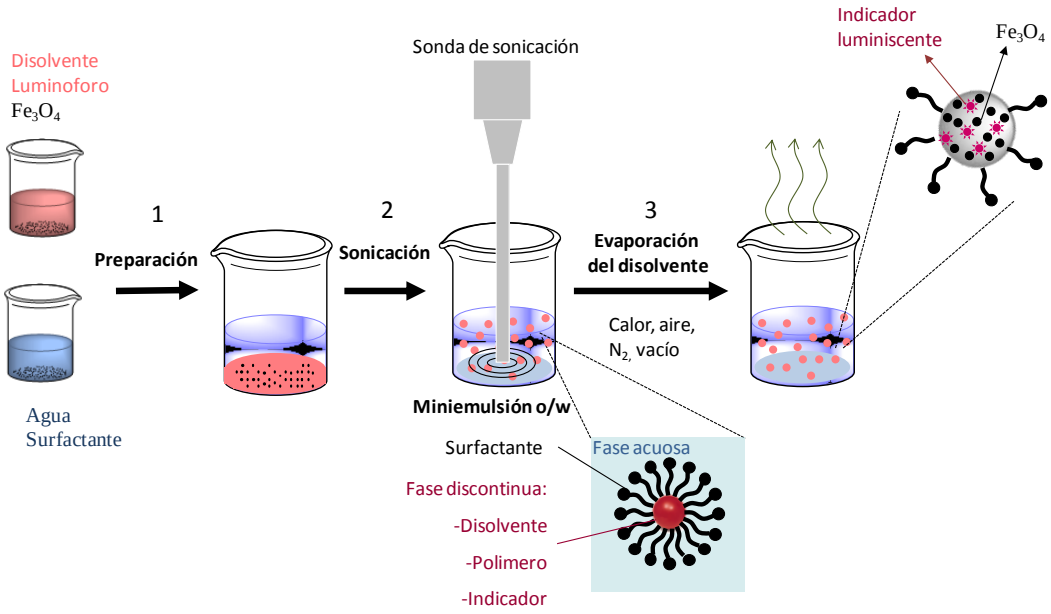

Figura 20. Procedimiento de miniemulsión-evaporación utilizado para la síntesis de NP poliméricas.

Las propiedades magnéticas se consiguen añadiendo al cóctel un ferrofluido que es preparado a partir de nanopartículas magnéticas lipofílicas (*Lipophilic Magnetic Nanoparticles*, LMNP). Este ferrofluido se obtiene dispersando magnetita, de entre 15 y 25 nm, estabilizadas con ácido oleico para mejorar la interacción con el disolvente.

El principal problema de esta técnica de fabricación de NPs es la presencia de surfactante, el cual puede ser dañino para aplicaciones biológicas. Tras la evaporación del disolvente es necesario lavar las NPs con sucesivos pasos de recolección y redispersión en agua, pero en la mayoría de las ocasiones es muy difícil eliminar la totalidad del surfactante.

No obstante, resulta una técnica bastante simple que permite obtener partículas en un amplio rango de tamaños. El tamaño de partícula y la polidispersidad de las mismas depende de las condiciones de síntesis como la cantidad de polímero, su peso molecular, relación *o/w*, la cantidad de surfactante usado y condiciones de sonicación.[211]

3.3. Diseño y aplicaciones de los sensores ópticos de oxígeno

En este apartado se va a recoger a modo resumen consideraciones generales sobre el diseño de fases sensoras ópticas de oxígeno considerando todos los elementos vistos. A continuación se hará un recorrido sobre sus ventajas e inconvenientes así como las últimas aplicaciones encontradas con este tipo de sensores.

Aspectos generales del diseño

Conocidos los componentes de la fase sensora y sus características principales, vale la pena destacar la relación de estos elementos en el diseño de una fase sensora, y como algunos de estos aspecto deben ser compatibles para lograr su implementación sobre un dispositivo óptico para la resolución de un problema analítico concreto.

La **Figura 21** muestra la interdependencia entre los distintos aspectos a considerar en el desarrollo de un sensor óptico, donde la flecha indica la dependencia directa de un elemento sobre otro. Así, la definición del problema analítico va a influir en tres aspectos claves: el formato de fase sensora (1), la elección de los materiales (indicador y matriz) (2) y la configuración del sensor (3). La fase sensora va a influir sobre las propiedades analíticas, mientras que el formato y configuración deben poder adaptarse a la situación real de medida, y de ahí que dependan directamente de la aplicación que se le vaya a dar al sensor. Si por ejemplo, se quiere desarrollar un sensor enzimático con transducción óptica de oxígeno, es necesario bien elegir un material que posea determinados grupos funcionales para crear enlaces covalentes con la enzima o un formato de fase sensora que permita crear estructuras porosas donde inmovilizar la enzima físicamente.

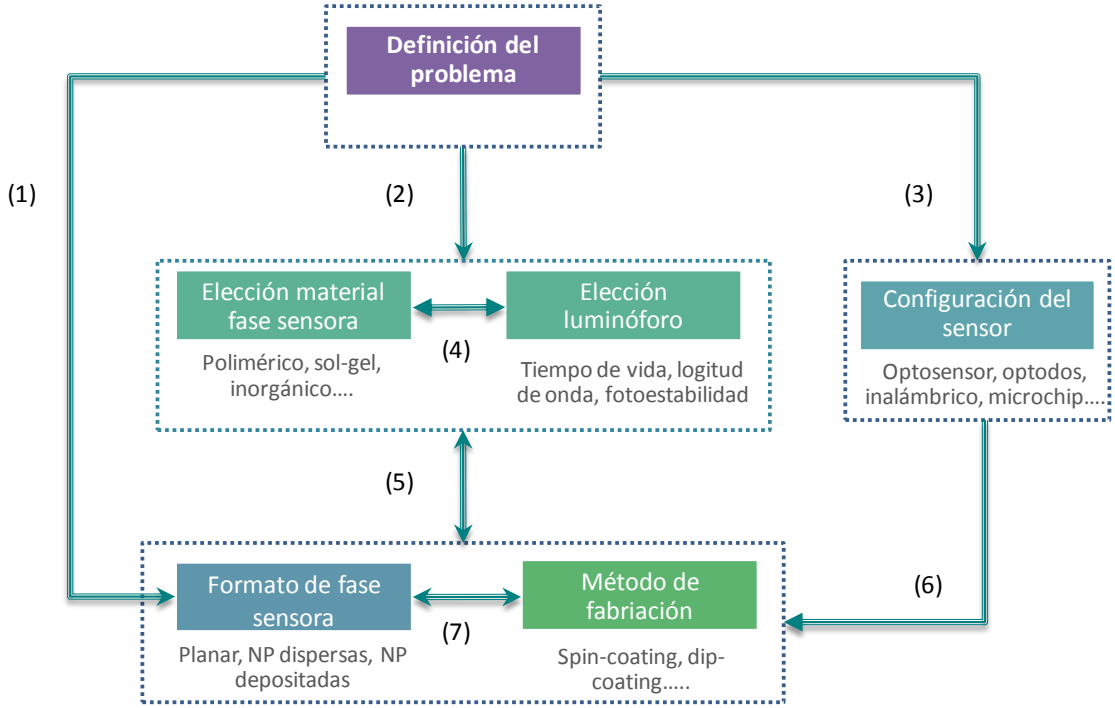

Figura 21. Interrelación entre las diferentes componentes del diseño de un sensor óptico de oxígeno.

Como se ha ido resaltando a lo largo de la memoria, el tipo de matriz donde se inmoviliza el indicador influye sobre las propiedades de éste, por lo que su elección debe hacerse de forma conjunta para resolver una determinado problema (4). Además, la elección de una fase sensora determinada debe ser compatible con un determinado formato y método de fabricación (5). Por ejemplo si se desea un material biocompatible, deben tenerse en cuenta las propiedades de adhesión del mismo asi como su capacidad de formar membranas o NP. Afortunadamente, el gran desarrollo de las Ciencia de los Materiales permite aumentar la versatilidad de los mismos permitiendo adaptarse a casi cualquier situación.

Por otro lado, la configuración también debe ser compatible con el formato de fase sensora y sobre todo, con el método de fabricación de la misma; pero en cualquier caso la configuración, determinada por el problema analítico, es la que influye sobre estos dos aspectos (6). Así, el método de fabricación de la fase sensora va a venir también impuesto por estos dos aspectos: su relación con la configuración (6) y su compatibilidad con el formato (7).

La situación puede ser compleja con ciertos problemas analíticos, por ejemplo, si se desea desarrollar un sensor multiparamétrico, la compatibilidad entre indicadores es prioritaria y puede influir de forma notable sobre el formato de fase sensora (es

preferible usar NPs para evitar procesos de transferencia de carga) y el método de fabricación (que a su vez debe permitir coinmobilización), independientemente de su sencillez y bajo coste, los cuales son también aspectos deseables.

Por tanto, el diseño de una fase sensora no puede hacer de forma secuencial, sino que debe hacerse teniendo en cuenta todos los aspectos mencionados y en muchos casos requiere adaptarse e inclusos renunciar a ciertos aspectos deseables en el sensor en pro de otro con el cual es incompatible.

En este sentido, Wolfbeis propone una serie de preguntas que denomina "*killer criteria*"[117] los cuales pueden ser útiles para la elección y diseño de una fase sensora atendiendo a estos aspectos.

Ventajas e inconvenientes de un sensor óptico

El desarrollo de los sensores ópticos es consecuencia de la evolución de la Química Analítica y el creciente interés y demanda de análisis móviles, instrumentación y automatización monitorización de procesos, donde el análisis online está principalmente basado en el uso de sensores. En este sentido, las ventajas inherentes a los sensores ópticos han servido para impulsar su uso frente a otro tipo de sensores. Estas ventajas que se han ido mencionando a lo largo de esta memoria, se resumen a continuación:

- ✓ La señal óptica no está sujeta a interferencias eléctricas.
- ✓ No se requiere un sistema de referencia.
- ✓ No hay consumo de oxígeno por parte de la fase sensora, lo cual es de gran importancia en aplicaciones biotecnológicas y médicas.
- ✓ La fase sensora no necesita estar en contacto directo con el sistema óptico de medida. Esto implica que se puedan hacer medidas no invasivas o mínimamente invasivas.
- ✓ No hay consumo de oxígeno por parte de la fase sensora, lo cual es de gran importancia en aplicaciones biotecnológicas y médicas.
- ✓ Permite realizar medidas multiparamétricas de varios analitos, lo cual iimplica una reducción del coste permitiendo el análisis rápido de diversos analitos con un mismo equipo.

- ✓ Son susceptibles de ser miniaturizados
- ✓ El uso de sensores de fibra óptica permite monitorizar el oxígeno en largas distancias.[260]
- ✓ En medidas biomédicas *in vivo*, los sensores ópticos son más seguros pues se evitán el riesgo de un *shock* eléctrico.
- ✓ La gran mayoría de fases sensoras son esterizables.

Precisamente las características de portabilidad, miniaturización y facilidad de uso, son también muy importantes para el éxito final del sensor óptico, ya que permite desarrollar dispositivos muy económicos (desechables o reutilizables) que pueden ser separados del instrumento de medida, lo que junto con su capacidad de medida continua e *in situ*, está permitiendo el desarrollo de sensores ópticos con aplicaciones médicas capaces de ser usados directamente *in vivo*. Precisamente en el campo biotecnológico es donde los sensores ópticos han despertado un gran interés en los últimos años. En este sentido, hay que recordar que los sensores ópticos presentan una serie de ventajas como inmunidad frente a interferencias electromagnéticas e imposibilidad de *shock* eléctrico.

Sin embargo, a pesar de estas ventajas y del desarrollo sufrido décadas de investigación en la tecnología de los sensores ópticos solo una pequeña parte de los sistemas ha logrado una salida comercial. Por tanto, ha sido y sigue siendo necesario contrarrestar o mejorar algunas de las desventajas que poseen los sensores de este tipo, como puede ser:

- × Falta de sensibilidad o intervalo lineal de las fases sensoras para determinado tipo de aplicaciones.
- × Desarrollo de nuevos materiales y complejos que mejoren las propiedades de la fase sensora, y donde se pueda ejercer un control sobre sus características finales
- × Instrumentación más sensible en todo el rango del UV-vis-IR, así como indicadores cuyas longitudes de onda de emisión no se solapen.
- × Desarrollo de materiales y/o técnicas de deposición que se puedan adaptar a diferentes configuraciones sin perder el control sobre las propiedades de la membrana.[115]

- Aunque el tiempo de respuesta de los sensores de oxígeno suele ser en torno a los segundos, en algunos casos como los sensores enzimático con transducción óptica de oxígeno, este tiempo puede verse incrementado considerablemente.
- Para dar una salida comercial a estos sensores existe la necesidad de desarrollar dispositivos robustos, con interfases simples y mantenimiento mínimo.

Aplicaciones de los sensores ópticos de oxígeno

La importancia del oxígeno y la gran cantidad de aplicaciones donde su determinación es importante ha quedado manifiesta. A lo largo de esta memoria también se han descrito la diversidad de fases sensoras ópticas de oxígeno encontradas en literatura. Como conclusión parece necesario recoger algunos ejemplos concretos de aplicaciones de sensores ópticos basadas en la atenuación de la luminiscencia, y que más allá de su caracterización y potencial aplicabilidad han resultados útiles en situaciones de diferente naturaleza.

La **Tabla 5** recoge las principales aéreas de aplicación de los sensores ópticos de oxígeno. Cabe destacar que se han obviado muchas aplicaciones biotecnológicas y médicas de obtención de imágenes *in vivo* haciendo uso del indicador directamente disuelto en el objeto de análisis. [147, 261-263] Ruslan *et al.* realizaron una revisión que incluye este tipo de "sondas moleculares" para oxígeno[148]. Debido a la gran cantidad de información y trabajos publicados, se han tomado lo más representativos encontrados en los últimos años. Más información puede encontrarse en revisiones sobre el tema.[29, 70, 138, 148]

El primer ejemplo lo podemos encontrar en el campo de los alimentos, donde los sensores ópticos presentan una gran aplicabilidad y versatilidad.[70] Papkovsky *et al*.[264] optimizaron un sensor desechable de oxígeno basado en el complejo PtOEPK para medir oxígeno en envases de alimentos. De un modo similar, Hempel *et al.* [265] estudiaron la capacidad de sensores ópticos de oxígeno para detectar fugas en el empaquetamiento de quesos. El procedimiento que se siguió fue depositar el complejo de platino PtOEPK sobre papel de filtro Durapore de modo que la fase sensora fuese fácilmente incluida en zonas visibles durante el proceso de empaquetamiento del

queso. Este mismo dispositivo fue usado para cuantificar la permeabilidad a gases de gelatinas animales.[266]

Tabla 5. Principales áreas de aplicación de la detección de oxígeno mediante atenuación de la luminiscencia.

Área	Aplicación	Configuración	Detector	Fase sensora	Ref
Alimentos	Fugas en envase de queso	Optodo inalámbrico	Comercial	PtOEPK/PS sobre papel filtro	265
	O_2 en bolsas ensaladas	Optodo inalámbrico	Comercial	Comercial	158
Biotecnología	Actividad respiratoria en mitocondrias	Inalámbrico	PMT	Micro partículas PtTFPP/PS depositadas en 96 pocillos	267
	Monitorización paralela en células	Optodo inalámbrico	Comercial	Tira comercial	268
Medicina	Monitorización actividad embriones	Inalámbrico	CCD	PtOEP/PS depositado en micropocillos	269
	Hipoxia *in vitro* (células tumorales)	Inalámbrico	CCD	PdTPTBP en NP de PS funcionalizadas	159
	Hipoxia *in vivo* (ratones)	Inalámbrico	PMT		
	Oxigenación durante perfusión de tejido *exvivo*	Optodo(tipo catéter)	Comercial	Comercial	270
		Célula de flujo	Comercial	Comercial	270
	Presión parcial O2 in vivo conejos lesión pulmonar agua	Optodo (tipo catéter)	CCD	$Ru(dpp)_3(PF_6)_2$ / pMPCcoBMA	34
Medio ambiente	O_2 intracelular de algas	Optodo inalámbrico	PMT	PtTFPP en NP de PS carboxilado.	67
	Consumo O_2 raíces	Microchip	Fotodiodo	PtOEP sobre circuito impreso	156
	Transporte O_2 acuíferos	Celelula flujo	Comercial	Comercial	271
	Evaluación *in situ* respiración y fotosíntensis algas	Optodo	Comercial	Comercial	272
Industrial y tecnológica	O_2 en procesos combustión baja Tª	Optodo	PMT	PSP comercial	*56*
	Rotor	Inalámbrico	CCD	PtTFPP en polímero/cerámica	50
	Disco duro	Inalámbrico	CCD	$PySO_3H$ / silica-gel	52
	Evaluación refrigeración turbinas	Inalámbrico	CCD	PSP comercial	51

PtOEPK: Octaetilporfirina cetona de Pt(II); PMT: fotomultiplicador; PtTFPP: Pentafluorofenilporfirina de Pt(II); PS: Poliestireno; CCD: detector de carga acoplada; PtOEP: Octaetil porfirina de Pt(II); NP: Nanopartículas; PdTPTBP: meso-tetrafenil-tetrabenzoporfirina de Pd(II); $Ru(dpp)_3(PF_6)_2$; Hexafluorofosfato de [tris(4,7-difenil-1,10-fenantrolina)] de rutenio(II); p-MPCcoBMA:poli(2-metacriloiloxietil fosforilcolina-co-butilmetacrilate); PSP: Pintura sensible a la presión; $PySO_3H$: Ácido 1-pirenosulfónico;

Borchert *et al.* [158] también han estudiado la capacidad de un sensor óptico comercial (OpTech™) para medir el oxígeno residual de 206 bolsas de ensalada empaquetadas bajo diferentes atmósferas modificadas, y almacenadas a 4ºC durante 10 días. Los resultados obtenidos fueron comparados con otros métodos destructivos tradicionales, mostrando una buena correlación y demostrando su aplicabilidad en el control de atmósferas modificadas.

Sin embargo, puede decirse que la mayor aplicación de los sensores ópticos de oxígeno está en el campo biotecnológico y médico, como es el control de oxígeno en cultivos celulares, o directamente en el interior de las células. En este sentido, Hellen *et al.* [267] han investigado la habilidad de los sensores ópticos de oxígeno incorporados en pocillos para determinar la actividad respiratoria de células. Otro ejemplo de aplicación de este tipo de sensores en cultivos celulares fue llevado a cabo por Soley *et al*. [268], quienes implementaron varios parches comerciales fluorescentes en un sistema de seis minirreactores capaz de llevar a cabo una monitorización paralela del oxígeno y otros parámetros.

En otro trabajo, Dragu *et al*. [270] analizaron la saturación de oxígeno en tejidos *exvivo.* Para ello, compararon el uso de dos tipos de sensores ópticos comerciales, uno tipo aguja aplicado directamente en el tejido, y otro tipo célula de flujo que monitorizaba la presión parcial de oxígeno en las venas y arterias durante la perfusión del tejido. De los resultados se deduce la necesidad de un suministro adicional de oxígeno durante la perfusión de tejidos trasplantandos para prevenir situaciones de hipoxia.

Por otro lado, Napp *et al*. [159] analizaron la hipoxia en células tumorales mediante el uso de NPs de poliestireno funcionalizadas. Estas NPs poseían un indicador sensibles a oxígeno (Meso-tetrafenil-tetrabenzoporfirina de Pd(II)) y un complejo de referencia, y fueron dispersadas en el medio de cultivo e inyectadas en ratones para comprobar su potencialidad para obtener imágenes *in vivo* en 2 dimensiones.

Wang *et al*. [34] caracterizaron y evaluaron un optodo de fibra óptica para la monitorización de oxígeno *in vivo*. Para ello recubrieron la punta de una fibra óptica tipo catéter con el complejo $Ru(dpp)_3(PF6)_2$ inmovilizado en un copolímero de poli(2-metacriloiloxietil fosforilcolina-co-butilmetacrilate) (p-MPC-co-BMA) y lo aplicaron en arterias de conejos con lesión pulmonar aguda. Los resultados se compararon con otro

método de medida de oxigenación arterial, análisis de gas en sangre (*blood gas analysis*, BGA) sugiriendo su utilidad para aplicaciones clínicas.

Komori *et at*. [269] encontraron relación entre el número y tamaño de células embrionarias y la intensidad de luminiscencia de una fase sensora. Para ello emplearon el complejo luminiscente PtOEP inmovilizada en PS y monitorizaron el consumo de oxígeno de embriones con el objetivo de seleccionarlos para mejorar la tasa de embarazos en problemas de infertilidad.

Un estudio preliminar sobre la producción de oxígeno por la fotosíntesis fue llevado a cabo usando NP de PS y el complejo PtTFPP. Gracias al largo tiempo de vida de este complejo y su espectro de absorción, se evitó la interferencia de la autoflorescencia del alga *Chara corallina.* [67] Las NPs fueron inyectadas en el interior de las células con un microcapilar de vidrio. Estas células fueron sometidas a diferentes condiciones de luz, observándose cambios en la concentración de oxígeno mediante la técnica de modulación de fase.

Gevaert *et al*.[272] compararon un sistema automatizado basado en medidas de tiempo de vida con un electrodo tipo Clark para medir la respiración y fotosíntesis de algas en su hábitat natural frente a cambios de luz solar, temperatura o nutrientes, y a lo largo de diferentes épocas del año. En otro estudio, [271] se usó una fibra óptica para obtener un perfil vertical de la distribución de oxígeno en la franja capilar y la zona saturada de acuíferos. Las fases sensoras comerciales colocadas en el interior de una cámara de flujo eran analizadas externamente mediante un detector de fibra óptica. Otra aplicación en campo ambiental es la de Martinez-Olmos *et al*.[156], quienes depositaron el complejo PtOEP (y otros dos indicadores para temperatura y humedad) sobre un circuito impreso para monitorizar la presencia de oxígeno durante diferentes ciclos de riego y el consumo por parte de las raíces.

En procesos de combustión suele ser menos común el uso de sensores ópticos de oxígeno, debido a las condiciones extremas que pueden destruir la fase sensora. Sin embargo, Sarner *et al*.[56] usaron una pintura sensible a la presión basada en la atenuación de la luminiscencia para medir el oxígeno en cámaras de procesos de combustión de baja temperatura, demostrando su utilidad para monitorizar oxígeno por debajo de 180ºC.

Precisamente este tipo de pinturas sensibles a la presión son usadas en numerosos estudios aerodinámicos, pues permite analizar la distribución de la presión en una superficie. Juliano et al. [50] usaron una pintura sensible a la presión basada en el complejo PtTFPP en un matriz cerámico-polimérica para observar la distribución de presión no estacionaria en palas de un modelo de hélice de aeroplano. Uno de los inconvenientes en este tipo de estudios es la temperatura, que debe ser corregida. Para evitar el efecto de la temperatura sobre la sensibilidad del complejo, Kameya *et al*. [52] emplearon ácido 1-pirenosulfónico como indicador insensible a los cambios de temperatura, y estudiaron la distribución de presión sobre en una unidad de disco duro (*hard drive disk*).

Pero además, este tipo de pinturas también permite evaluar la efectividad de la refrigeración en turbinas de gas, estableciendo una analogía calor/masa.[273] En este tipo de experimentos, la corriente principal de gas es aire (20.9 % en O_2), mientras que el gas refrigerante es cualquier otro que no posea oxígeno. [51]

Como se ha visto, la determinación de oxígeno por métodos ópticos encuentra aplicación en una gran variedad de campos. Estos ejemplos intentan barrer las diferentes aplicaciones dentro de cada área, asi como las configuraciones y formatos fases sensores existentes, intentando reflejar la importancia que este tipo de sensores ha tomado hoy en día.

Referencias

1. Greenwood, N. N.; Earnshaw, A., *Chemistry of the Elements*. 2nd Edition ed.; Elsevier: 1997.

2. Magner, L. N., *A History of the Life Sciences*. Third ed.; Marcel-Dekker Inc. : New York - Basel, 2005.

3. Renger, G.; Hanssum, B., Oxygen detection in biological systems. *Photosynthesis Research* **2009,** 102, (2), 487-498.

4. Alderman, J.; Hynes, J.; Floyd, S. M.; Krüger, J.; O'Connor, R.; Papkovsky, D. B., A low-volume platform for cell-respirometric screening based on quenched-luminescence oxygen sensing. *Biosensors and Bioelectronics* **2004,** 19, (11), 1529-1535.

5. Thedinga, E.; Kob, A.; Holst, H.; Keuer, A.; Drechsler, S.; Niendorf, R.; Baumann, W.; Freund, I.; Lehmann, M.; Ehret, R., Online monitoring of cell metabolism for studying pharmacodynamic effects. *Toxicology and Applied Pharmacology* **2007,** 220, (1), 33-44.

6. Li, Z.; Graham, B. H., Measurement of Mitochondrial Oxygen Consumption Using a Clark Electrode In *Mitochondrial Disorders*, Wong, L.-J. C., Ed. Springer New York: 2012; Vol. 837, pp 63-72.

7. O'Mahony, F. C.; O'Donovan, C.; Hynes, J.; Moore, T.; Davenport, J.; Papkovsky, D. B., Optical Oxygen Microrespirometry as a Platform for Environmental Toxicology and Animal Model Studies. *Environmental Science & Technology* **2005,** 39, (13), 5010-5014.

8. Kellner, K.; Liebsch, G.; Klimant, I.; Wolfbeis, O. S.; Blunk, T.; Schulz, M. B.; Göpferich, A., Determination of oxygen gradients in engineered tissue using a fluorescent sensor. *Biotechnology and Bioengineering* **2002,** 80, (1), 73-83.

9. O'Driscoll, S. W.; Fitzsimmons, J. S.; Commisso, C. N., Role of oxygen tension during cartilage formation by periosteum. *Journal of Orthopaedic Research* **1997,** 15, (5), 682-687.

10. Radisic, M.; Malda, J.; Epping, E.; Geng, W.; Langer, R.; Vunjak-Novakovic, G., Oxygen gradients correlate with cell density and cell viability in engineered cardiac tissue. *Biotechnology and Bioengineering* **2006,** 93, (2), 332-343.

11. Carreau, A.; Hafny-Rahbi, B. E.; Matejuk, A.; Grillon, C.; Kieda, C., Why is the partial oxygen pressure of human tissues a crucial parameter? Small molecules and hypoxia. *Journal of Cellular and Molecular Medicine* **2011,** 15, (6), 1239-1253.

12. Kiss, J.; Kirchberg, J.; Schneider, M., Molecular oxygen sensing: implications for visceral surgery. *Langenbeck's Archives of Surgery* **2012,** 397, (4), 603-610.

13. Brahimi-Horn, M.; Chiche, J.; Pouysségur, J., Hypoxia and cancer. *Journal of Molecular Medicine* **2007,** 85, (12), 1301-1307.

14. Elas, M.; Ahn, K.-H.; Parasca, A.; Barth, E. D.; Lee, D.; Haney, C.; Halpern, H. J., Electron Paramagnetic Resonance Oxygen Images Correlate Spatially and Quantitatively with Oxylite Oxygen Measurements. *Clinical Cancer Research* **2006,** 12, (14), 4209-4217.

15. Pacheco-Torres, J.; López-Larrubia, P.; Ballesteros, P.; Cerdán, S., Imaging tumor hypoxia by magnetic resonance methods. *NMR in Biomedicine* **2010,** 24, (1), 1-16.

16. Dragu, A.; Taeger, C.; Buchholz, R.; Sommerfeld, B.; Hübner, H.; Birkholz, T.; Kleinmann, J.; Münch, F.; Horch, R.; Präbst, K., Online oxygen measurements in ex vivo perfused muscle tissue in a porcine model using dynamic quenching methods. *Archives of Orthopaedic and Trauma Surgery* **2012**, 1-7.

17. Lange, C. A. K.; Stavrakas, P.; Luhmann, U. F. O.; de Silva, D. J.; Ali, R. R.; Gregor, Z. J.; Bainbridge, J. W. B., Intraocular Oxygen Distribution in Advanced Proliferative Diabetic Retinopathy. *American Journal of Ophthalmology* **2011,** 152, (3), 406-412.e3.

18. Macnab, A.; Shadgan, B.; Janssen, P.; Rurak, D., Fetal oxygenation measurement using wireless near infrared spectroscopy. *Proc. SPIE* **2012,** 8229, 822902.

19. Heldt, T.; Kashif, F. M.; Sulemanji, M.; O'Leary, H. M.; Du Plessis, A. J.; Verghese, G. C., Continuous quantitative monitoring of cerebral oxygen metabolism in neonates by ventilator-gated analysis of NIRS recordings. In *Acta Neurochirurgica, Supplementum*, 2012; pp 177-180.

20. Acosta, M. A.; Ymele-Leki, P.; Kostov, Y. V.; Leach, J. B., Fluorescent microparticles for sensing cell microenvironment oxygen levels within 3D scaffolds. *Biomaterials* **2009,** 30, (17), 3068-3074.

21. Ross, R. E., Age-specific decrease in aerobic efficiency associated with increase in oxygen free radical production in Drosophila melanogaster. *Journal of Insect Physiology* **2000,** 46, (11), 1477-1480.

22. Bunik, V.; Schloss, J.; Pinto, J.; Gibson, G.; Cooper, A., Enzyme-Catalyzed Side Reactions with Molecular Oxygen may Contribute to Cell Signaling and Neurodegenerative Diseases. *Neurochemical Research* **2007,** 32, (4), 871-891.

23. Grinnell, K.; Duong, H.; Newton, J.; Rounds, S.; Choudhary, G.; Harrington, E. O., Heterogeneity in apoptotic responses of microvascular endothelial cells to oxidative stress. *Journal of Cellular Physiology* **2012,** 227, (5), 1899-1910.

24. Dennog, C.; Hartmann, A.; Frey, G. n.; Speit, G. n., Detection of DNA damage after hyperbaric oxygen (HBO) therapy. *Mutagenesis* **1996,** 11, (6), 605-609.

25. Saugstad, O. D., Oxygen Toxicity in the Neonatal Period. *Acta Pædiatrica* **1990,** 79, (10), 881-892.

26. Weinberger, B.; Laskin, D. L.; Heck, D. E.; Laskin, J. D., Oxygen Toxicity in Premature Infants. *Toxicology and Applied Pharmacology* **2002,** 181, (1), 60-67.

27. Wilmshurst, P., Diving and Oxygen *BMJ, ABC of oxygen* **1998,** 317, (7164), 996-999.

28. Gopal Mandal, N., Measurement of gas concentrations: oxygen, carbon dioxide, nitrogen, nitrous oxide and volatile anaesthetic agents. *Anaesthesia & Intensive Care Medicine* **2008,** 9, (12), 559-563.

29. Steiner, M.-S.; Duerkop, A.; Wolfbeis, O. S., Optical methods for sensing glucose. *Chemical Society Reviews* **2011,** 40, (9), 4805-4839.

30. Suresh, S.; Srivastava, V. C.; Mishra, I. M., Techniques for oxygen transfer measurement in bioreactors: a review. *Journal of Chemical Technology & Biotechnology* **2009,** 84, (8), 1091-1103.

31. Suresh, S.; Srivastava, V. C.; Mishra, I. M., Techniques for oxygen transfer measurement in bioreactors: A review. *Journal of Chemical Technology and Biotechnology* **2009,** 84, (8), 1091-1103.

32. Peña, C.; Peter, C. P.; Büchs, J.; Galindo, E., Evolution of the specific power consumption and oxygen transfer rate in alginate-producing cultures of Azotobacter vinelandii conducted in shake flasks. *Biochemical Engineering Journal* **2007,** 36, (2), 73-80.

33. Ge, X.; Rao, G., Real-time monitoring of shake flask fermentation and off gas using triple disposable noninvasive optical sensors. *Biotechnology Progress* **2012,** 28, (3), 872-877.

34. Wang, Y.; Meng, S.; Song, Y.; Zhong, W.; Jiang, J.; Chen, S.; Bai, C., Fluorescence optical fibre sensor provides accurate continuous oxygen detection in rabbit model with acute lung injury. *Respirology* **2010,** 15, (1), 99-106.

35. Pisoschi, A. M.; Pop, A.; Serban, A. I.; Negulescu, G. P., Ethanol determination by an amperometric bienzyme sensor based on a Clark-type transducer. *Journal of Electroanalytical Chemistry* **2012,** 671, (0), 85-91.

36. Arts, M. J. T. J.; Grun, C.; de Jong, R. L.; Voss, H.-P.; Bast, A.; Mueller, M. J.; Haenen, G. R. M. M., Oxidative Degradation of Lipids during Mashing. *Journal of Agricultural and Food Chemistry* **2007,** 55, (17), 7010-7014.

37. Numata, M.; Funazaki, N.; Ito, S.; Asano, Y.; Yano, Y., Flow-injection analysis for hypoxanthine in meat with dissolved oxygen detector and enzyme reactor. *Talanta* **1996,** 43, (12), 2053-2059.

38. Pénicaud, C.; Guilbert, S.; Peyron, S.; Gontard, N.; Guillard, V., Oxygen transfer in foods using oxygen luminescence sensors: Influence of oxygen partial pressure and food nature and composition. *Food Chemistry* **2012,** 123, (4), 1275-1281.

39. O'Keefe, S. F.; Pike, O. A., *Food Analysis* Fourth Edition ed.; Springer: New York Dordrecht Heidelberg London, 2010.

40. Lopes, P.; Saucier, C.; Teissedre, P. L.; Glories, Y., Main routes of oxygen ingress through different closures into wine bottles. *Journal of Agricultural and Food Chemistry* **2007,** 55, (13), 5167-5170.

41. O'Mahony, F. C.; O'Riordan, T. s. C.; Papkovskaia, N.; Kerry, J. P.; Papkovsky, D. B., Non-destructive assessment of oxygen levels in industrial modified atmosphere packaged cheddar cheese. *Food Control* **2006,** 17, (4), 286-292.

42. Smiddy, M.; Fitzgerald, M.; Kerry, J. P.; Papkovsky, D. B.; O' Sullivan, C. K.; Guilbault, G. G., Use of oxygen sensors to non-destructively measure the oxygen content in modified atmosphere and vacuum packed beef: impact of oxygen content on lipid oxidation. *Meat Science* **2002,** 61, (3), 285-290.

43. Soliva-Fortuny, R. C.; Martín-Belloso, O., New advances in extending the shelf-life of fresh-cut fruits: a review. *Trends in Food Science & Technology* **2003,** 14, (9), 341-353.

44. Lammertyn, J.; Scheerlinck, N.; Verlinden, B. E.; Schotsmans, W.; M. Nicolä, B., Simultaneous determination of oxygen diffusivity and respiration in pear skin and tissue. *Postharvest Biology and Technology* **2001,** 23, (2), 93-104.

45. Facts & Figures for the Chemical Industry. *Chemical & Engineering News* **2005,** 83, (28).

46. Tripathi, M. M.; Eseller, K. E.; Yueh, F. Y.; Singh, J. P., An optical sensor for multi-species impurity monitoring in hydrogen fuel. *Sensors and Actuators, B: Chemical* **2012**.

47. Beshay, M.; Garon, S.; Ruiz, D.; Kempen, L. U. In *Intrinsically safe oxygen and hydrogen optical leak detector*, Proceedings of SPIE - The International Society for Optical Engineering, 2011; 2011.

48. Takeuchi, T., Oxygen sensors. *Sensors and Actuators* **1988,** 14, (2), 109-124.

49. Yang, L.; Zare-Behtash, H.; Erdem, E.; Kontis, K., Investigation of the double ramp in hypersonic flow using luminescent measurement systems. *Experimental Thermal and Fluid Science* **2012,** 40, (0), 50-56.

50. Juliano, T. J.; Disotell, K. J.; Gregory, J. W.; Crafton, J.; Fonov, S., Motion-deblurred, fast-response pressure-sensitive paint on a rotor in forward flight. *Measurement Science and Technology* **2012,** 23, (4).

51. Han, C.; Ren, J.; Jiang, H.-d., Multi-parameter influence on combined-hole film cooling system. *International Journal of Heat and Mass Transfer* **2012,** 55, (15-16), 4232-4240.

52. Kameya, T.; Matsuda, Y.; Yamaguchi, H.; Egami, Y.; Niimi, T., Pressure-sensitive paint measurement on co-rotating disks in a hard disk drive. *Optics and Lasers in Engineering* **2012,** 50, (1), 82-86.

53. Li, Y.; Jiang, L. X.; Lv, X. J.; Lai, Y. Q.; Zhang, H. L.; Li, J.; Liu, Y. X., Oxygen evolution and corrosion behaviors of co-deposited Pb/Pb-MnO2 composite anode for electrowinning of nonferrous metals. *Hydrometallurgy* **2011,** 109, (34), 252-257.

54. Hasan, N. B.; Haider, A. J.; Al-Amar, M. A., Effect of Oxygen pressure on the structural, morphology and optical properties of Nanocrystalline TiO 2 thin films prepared by Pulsed Laser Deposition. *European Journal of Scientific Research* **2012,** 69, (4), 520-526.

55. Santos, A. Á. B.; Goldstein Jr, L.; Ferrari, C. A., An experiment on the effect of oxygen content and air velocity on soot formation in acetylene laminar diffusion flame produced in a burner with a parallel annular coaxial oxidizer flow. *International Communications in Heat and Mass Transfer* **2009,** 36, (5), 445-450.

56. Särner, G.; Göransson, U.; Lindén, J.; Richter, M.; Aldén, M., Using oxygen-quenched pressure-sensitive paint for oxygen concentration measurements in low-temperature combustion environments. *Measurement Science and Technology* **2008,** 19, (8), 085307.

57. Brglez, P.; Holobar, A.; Pivec, A.; Belsak, N.; Kolar, M., Determination of oxygen by means of a biogas and gas-interference study using an optical tris (4,7-diphenyl-1,10-phenanthroline) ruthenium(II) dichloride complex sensor. *Acta Chimica Slovenica* **2012,** 59, (1), 50-58.

58. Linnerud, I.; Kaspersen, P.; Jaeger, T., Gas monitoring in the process industry using diode laser spectroscopy. *Applied Physics B: Lasers and Optics* **1998,** 67, (3), 297-305.

59. Nakamura, Y.; Ito, D.; Yokoyama, T.; Okazaki, S.; Nakagawa, H.; Arai, T., Development of a Fiber-Optic Oxygen Sensor for Long-Term Corrosion Monitoring of Radioactive-Waste Repository. *Sensor Letters* **2008,** 6, (6), 951-955.

60. Makarenko, V.; Shatilo, S.; Gumerskii, K.; Belyaev, V., Effect of oxygen and hydrogen sulfide on carbon dioxide corrosion of welded structures of oil and gas installations. *Chemical and Petroleum Engineering* **2000,** 36, (2), 125-130.

61. Liu, B.; Wu, D.; Sun, Q. L.; Zheng, W. Y.; Lu, J. D.; Lin, G. X.; Li, X. M., Maintenance of water-cooled generator stator coils during outage. *Corrosion Science and Protection Technology* **2009,** 21, (3), 305-307.

62. Gouin, J. F.; Baros, F.; Birot, D.; André, J. C., A fibre-optic oxygen sensor for oceanography. *Sensors and Actuators B: Chemical* **1997,** 39, (13), 401-406.

63. Ballance, R., Field Testing Methods. In *Water Quality Monitoring*, First Edition ed.; Bartram, J.; Ballance, R., Eds. E&FN Spon: London, 1996.

64. Mu, J.; Zhang, F.; Zhu, X.; Dong, X., A gas chromatography method established for oxygen transfer efficiency measurement. *Journal of Environmental Sciences* **2009,** 21, Supplement 1, (0), S146-S148.

65. Plekhanova, Y.; Reshetilov, A.; Manolov, T.; Taranova, L., Biosensor monitoring of microbial treatment of wastewater from nonylphenol polyethoxylates under flow-through conditions. *Applied Biochemistry and Microbiology* **2011,** 47, (9), 846-851.

66. Woelfel, J.; xf; rensen, K.; Warkentin, M.; Forster, S.; Oren, A.; Schumann, R., Oxygen evolution in a hypersaline crust: in situ photosynthesis quantification by microelectrode profiling and use of planar optode spots in incubation chambers. *Aquatic Microbial Ecology* **2009,** 56, (2-3), 263-273.

67. Schmäzlin, E.; Van Dongen, J. T.; Klimant, I.; Marmodée, B.; Steup, M.; Fisahn, J.; Geigenberger, P.; Löhmannsröben, H. G., An optical multifrequency phase-modulation method using microbeads for measuring intracellular oxygen concentrations in plants. *Biophysical Journal* **2005,** 89, (2), 1339-1345.

68. Liddiard, V.; Carman, J., Simulating in ovulo osmotic potentials and O2 tensions normalize growth and pigmentation of immature cotton embryos. *Plant Cell, Tissue and Organ Culture* **2010,** 102, (1), 1-8.

69. Shimamura, S.; Yamamoto, R.; Nakamura, T.; Shimada, S.; Komatsu, S., Stem hypertrophic lenticels and secondary aerenchyma enable oxygen transport to roots of soybean in flooded soil. *Annals of Botany* **2010,** 106, (2), 277-284.

70. Pénicaud, C.; Peyron, S.; Gontard, N.; Guillard, V., Oxygen Quantification Methods and Application to the Determination of Oxygen Diffusion and Solubility Coefficients in Food. *Food Reviews International* **2012,** 28, (2), 113-145.

71. García Mesa, J. A.; de Castro, M. D. L.; Valcárcel, M., Determination of the oxidative stability of olive oil by use of a robotic station. *Talanta* **1993,** 40, (11), 1595-1600.

72. De Vries, W.; Van Wijck-Kapteijn, W. M. C.; Stouthamer, A. H., Influence of Oxygen on Growth, Cytochrome Synthesis and Fermentation Pattern in Propionic Acid Bacteria. *Journal of General Microbiology* **1972,** 71, (3), 515-524.

73. Van Voorhies, W. A.; Melvin, R. G.; Ballard, J. W. O.; Williams, J. B., Validation of manometric microrespirometers for measuring oxygen consumption in small arthropods. *Journal of Insect Physiology* **2008,** 54, (7), 1132-1137.

74. Roppola, K.; Kuokkanen, T.; Rämö, J.; Prokkola, H.; Ruotsalainen, J., Characterisation of organic fractions of pulp and paper mill wastewater with a manometric respirometric biochemical oxygen demand method and automatic chemical oxygen demand analyses. *Chemical Speciation and Bioavailability* **2009,** 21, (2), 121-130.

75. Vanderkooi, J. M.; Erecinska, M.; Silver, I. A., Oxygen in mammalian tissue: methods of measurement and affinities of various reactions. *American Journal of Physiology - Cell Physiology* **1991,** 260, (6), C1131-C1150.

76. Rensburg, M. J. v. Analysis of trace amounts of oxygen, carbon monoxide and carbon dioxide in nitrogen using gas chromatography. University of Pretoria, Pretoria, 2007.

77. Carpenter, J. H., The Accuracy of the Winkler Method for Dissolved Oxygen Analysis. *American Society of Limnology and Oceanography* **1965,** 10, (1), 135-140.

78. Pouvreau, L. A. M.; Strampraad, M. J. F.; Berloo, S. V.; Kattenberg, J. H.; de Vries, S.; Robert, K. P., NO, N2O, and O2 Reaction Kinetics: Scope and Limitations of the Clark Electrode. In *Methods in Enzymology*, Academic Press: 2008; Vol. Volume 436, pp 97-112.

79. Ahmad, R.; Kuppusamy, P., Theory, Instrumentation, and Applications of Electron Paramagnetic Resonance Oximetry. *Chemical Reviews* **2010,** 110, (5), 3212-3236.

80. Papkovsky, D. B.; Chandan, K. S.; Gregg, L. S., Methods in Optical Oxygen Sensing: Protocols and Critical Analyses. In *Methods in Enzymology*, Academic Press: 2004; Vol. Volume 381, pp 715-735.

81. Zenz, H.; Katinger, H., A gas-chromatographic method for the determination of oxygen uptake in aerated cultures. *Antonie van Leeuwenhoek* **1971,** 37, (1), 289-295.

82. Hirata, T.; Nishyama, T.; Sato, H.; Ishikawa, Y.; Shina, T.; Ishitani, T., A Fast Gas Chromatographic Method for the Separation of Nitrogen, Oxygen, Carbon dioxide and Argon and Its Application to In-package Modified Atmosphere. *J Pack. Sci. TechnoL* **1993,** 2, (1).

83. Driscoll, N. J.; Duffy, M.; Pappas, S., Determination of water and oxygen at low ppm levels by GC/far-FUV detection. *American Laboratory* **May 1988**, 68-71.

84. Culberson, C. H.; Huang, S., Automated amperometric oxygen titration. *Deep Sea Research Part A. Oceanographic Research Papers* **1987,** 34, (5-6), 875-880.

85. Granéli, W.; Granéli, E., Automatic potentiometric determination of dissolved oxygen. *Marine Biology* **1991,** 108, (2), 341-348.

86. Sahoo, P.; Ananthanarayanan, R.; Malathi, N.; Rajiniganth, M. P.; Murali, N.; Swaminathan, P., Pulsating potentiometric titration technique for assay of dissolved oxygen in water at trace level. *Analytica Chimica Acta* **2010,** 669, (12), 17-24.

87. Martz, T.; Takeshita, Y.; Rolph, R.; Bresnahan, P., Tracer Monitored Titrations: Measurement of Dissolved Oxygen. *Analytical Chemistry* **2012,** 84, (1), 290-296.

88. Labasque, T.; Chaumery, C.; Aminot, A.; Kergoat, G., Spectrophotometric Winkler determination of dissolved oxygen: re-examination of critical factors and reliability. *Marine Chemistry* **2004,** 88, (12), 53-60.

89. Horstkotte, B.; Alonso, J. C.; Miró, M.; Cerdá, V., A multisyringe flow injection Winkler-based spectrophotometric analyzer for in-line monitoring of dissolved oxygen in seawater. *Talanta* **2009,** 80, (3), 1341-1346.

90. Pai, S.-C.; Gong, G.-C.; Liu, K.-K., Determination of dissolved oxygen in seawater by direct spectrophotometry of total iodine. *Marine Chemistry* **1993,** 41, (4), 343-351.

91. Janata, J., *Principles of Chemical Sensors*. 2nd. Edition ed.; Springer: 2009.

92. Stetter, J. R.; Li, J., Amperometric Gas Sensors:A Review. *Chemical Reviews* **2008,** 108, (2), 352-366.

93. Skoog, D. A.; Leary, J. J., *Principles of Instrumental Analysis/Solution Manual*. Saunders: 1992.

94. Nei, L.; Compton, R. G., An improved Clark-type galvanic sensor for dissolved oxygen. *Sensors and Actuators B: Chemical* **1996,** 30, (2), 83-87.

95. Clark, L.; Wolf, R.; Granger, D.; Taylor, Z., Continuous Recording of Blood Oxygen Tensions by Polarography. *J. Appl. Physiol* **1953,** 6, 189-193.

96. Zhuiykov, S.; Kats, E.; Marney, D., Potentiometric sensor using sub-micron Cu2O-doped RuO2 sensing electrode with improved antifouling resistance. *Talanta* **2012,** 82, (2), 502-507.

97. Fouletier, J., Gas analysis with potentiometric sensors. a review. *Sensors and Actuators* **1982,** 3, (0), 295-314.

98. Toniolo, R.; Dossi, N.; Pizzariello, A.; Doherty, A. P.; Susmel, S.; Bontempelli, G., An oxygen amperometric gas sensor based on its electrocatalytic reduction in room temperature ionic liquids. *Journal of Electroanalytical Chemistry* **2012,** 670, (0), 23-29.

99. Rasmussen, H. N.; Rasmussen, U. F., Oxygen solubilities of media used in electrochemical respiration measurements. *Analytical Biochemistry* **2003,** 319, (1), 105-113.

100. Krishna, M. C.; English, S.; Yamada, K.; Yoo, J.; Murugesan, R.; Devasahayam, N.; Cook, J. A.; Golman, K.; Ardenkjaer-Larsen, J. H.; Subramanian, S.; Mitchell, J. B., Overhauser enhanced magnetic resonance imaging for tumor oximetry: Coregistration of tumor anatomy and tissue oxygen concentration. *Proceedings of the National Academy of Sciences* **2002,** 99, (4), 2216-2221.

101. http://www.yokogawa.com/iab/popup/vigilantplant/tdl/iab-vp-tdl-flash01-en.html TruePeak, VigilantPlant, Yokogawa Electric Corporation (5 mayo de 2012)

102. http://www.oxigraf.com/technology.html Laser Absorption Spectroscopy (22 Mayo de 2012)

103. Cummings, B.; Hamilton, M. L.; Ciaffoni, L.; Pragnell, T. R.; Peverall, R.; Ritchie, G. A. D.; Hancock, G.; Robbins, P. A., Laser-based absorption spectroscopy as a technique for rapid in-line analysis of respired gas concentrations of O 2 and CO 2. *Journal of Applied Physiology* **2011,** 111, (1), 303-307.

104. Lundin, P.; Svanberg, E. K.; Cocola, L.; Lewander, M.; Andersson-Engels, S.; Jahr, J.; Fellman, V.; Svanberg, K.; Svanberg, S. In *Non-invasive gas monitoring in newborn infants using diode laser absorption spectroscopy: a case study*, Optical Diagnostics and Sensing XII: Toward Point-of-Care Diagnostics; and Design and Performance Validation of Phantoms Used in Conjunction with Optical Measurement of Tissue IV, San Francisco, California, USA, 2012; SPIE: San Francisco, California, USA, 2012; pp 822903-11.

105. Rudolf Seitz, W., Chemical sensors based on fiber optics. *Analytical Chemistry* **1984,** 56, (A16).

106. Wolfbeis, O. S., *Fiber Optic Chemical Sensors and Biosensors*. CRC Press: 1991; Vol. 1.

107. Kautsky, H., Quenching of luminescence by oxygen. *Transactions of the Faraday Society* **1939,** 35, 216-219.

108. Bergman, I., Rapid-response Atmospheric Oxygen Monitor based on Fluorescence Quenching. *Nature* **1968,** 218, (5139), 396-396.

109. Costa Fernández, J. M.; Sanz Medel, A., *Fosforescencia molecular analítica: una aproximación práctica.* . Universidad de Granada: 2001.

110. Marazuela-Lamata, M. D. Diseño, caracterización y aplicación analítica de (bio)sensores de fibra óptica para la determinación de CO2, O2 y metabolitos de interés clínico. Universidad Complutense de Madrid, Madrid, 1997.

111. Schweitzer, C.; Schmidt, R., Physical Mechanisms of Generation and Deactivation of Singlet Oxygen. *Chemical Reviews* **2003,** 103, (5), 1685-1758.

112. Christian G. Hübner; Renn, A.; Renge, I.; Wild, U. P., Direct observation of the triplet lifetime quenching of single dye molecules by molecular oxygen *Journal of Chemical Physics* **2001,** 115, (21), 9619-9623.

113. DeRosa, M. C.; Crutchley, R. J., Photosensitized singlet oxygen and its applications. *Coordination Chemistry Reviews* **2002,** 233â€“234, (0), 351-371.

114. Wilkinson, F.; McGarvey, D. J.; Olea, A. F., Excited Triplet State Interactions with Molecular Oxygen: Influence of Charge Transfer on the Bimolecular Quenching Rate Constants and the Yields of Singlet Oxygen [O*2(1.DELTA.g)] for Substituted Naphthalenes in Various Solvents. *The Journal of Physical Chemistry* **1994,** 98, (14), 3762-3769.

115. Demas, J. N.; DeGraff, B. A., Applications of luminescent transition platinum group metal complexes to sensor technology and molecular probes. *Coordination Chemistry Reviews* **2001,** 211, (1), 317-351.

116. Lakowicz, J. R., *Principles of Fluorescence Spectroscopy*. 2nd ed.; Kluwer Academic: New York, 1999.

117. Wolfbeis, O. S., Materials for fluorescence-based optical chemical sensors. *Journal of Materials Chemistry* **2005,** 15, (27-28), 2657-2669.

118. Carraway, E. R.; Demas, J. N.; DeGraff, B. A., Luminescence quenching mechanism for microheterogeneous systems. *Analytical Chemistry* **1991,** 63, (4), 332-336.

119. Demas, J. N.; Degraff, B. A.; Xu, W., Modeling of Luminescence Quenching-Based Sensors: Comparison of Multisite and Nonlinear Gas Solubility Models. *Analytical Chemistry* **1995,** 67, (8), 1377-1380.

120. Lu, X.; Winnik, M. A., Luminescence Quenching in Polymer/Filler Nanocomposite Films Used in Oxygen Sensors. *Chemistry of Materials* **2001,** 13, (10), 3449-3463.

121. Amao, Y., Probes and Polymers for Optical Sensing of Oxygen. *Microchimica Acta* **2003,** 143, (1), 1-12.

122. Carraway, E. R.; Demas, J. N.; DeGraff, B. A.; Bacon, J. R., Photophysics and photochemistry of oxygen sensors based on luminescent transition-metal complexes. *Analytical Chemistry* **1991,** 63, (4), 337-342.

123. Mills, A., Response characteristics of optical sensors for oxygen: a model based on a distribution in tau and kq. *Analyst* **1999,** 124, (9), 1309-1314.

124. Roth, T. P. Diss. ETH No. 14001: Ruthenium(II) diimine complexes for luminescence-based oxygen sensors and Impedance spectroscopy of nitrogen dioxide-sensitive polymeric membranes. ETH Zurich, Zurich, 2001.

125. Mills, A., Controlling the sensitivity of optical oxygen sensors. *Sensors and Actuators B: Chemical* **1998,** 51, (13), 60-68.

126. Gijzeman, O. L. J.; Kaufman, F.; Porter, G., Oxygen quenching of aromatic triplet states in solution. Part 1. *Journal of the Chemical Society, Faraday Transactions 2: Molecular and Chemical Physics* **1973,** 69, 708-720.

127. Arik, M.; Celebi, N.; Onganer, Y., Fluorescence quenching of fluorescein with molecular oxygen in solution. *Journal of Photochemistry and Photobiology A: Chemistry* **2005,** 170, (2), 105-111.

128. Demas, J. N.; DeGraff, B. A., Luminescence-based sensors: microheterogeneous and temperature effects. *Sensors and Actuators B: Chemical* **1993,** 11, (1â€“3), 35-41.

129. Gewehr, P. M.; Delpy, D. T., Optical oxygen sensor based on phosphorescence lifetime quenching and employing a polymer immobilised metalloporphyrin probe: Part 2 - Sensor membranes and results. *Medical and Biological Engineering and Computing* **1993,** 31, (1), 11-21.

130. Hochreiner, H.; Sánchez-Barragán, I.; Costa-Fernández, J. M.; Sanz-Medel, A., Dual emission probe for luminescence oxygen sensing: a critical comparison between intensity, lifetime and ratiometric measurements. *Talanta* **2005,** 66, (3), 611-618.

131. Thompson, R. B.; Lakowicz, J. R., Fiber optic pH sensor based on phase fluorescence lifetimes. *Analytical Chemistry* **1993,** 65, (7), 853-856.

132. Kostov, Y.; Rao, G., Ratio measurements in oxygen determinations: wavelength ratiometry, lifetime discrimination, and polarization detection. *Sensors and Actuators B: Chemical* **2003,** 90, (13), 139-142.

133. Wang, X.-d.; Chen, H.-x.; Zhao, Y.; Chen, X.; Wang, X.-r., Optical oxygen sensors move towards colorimetric determination. *TrAC Trends in Analytical Chemistry* **2010,** 29, (4), 319-338.

134. Lippitsch, M. E.; Draxler, S., Luminescence decay-time-based optical sensors: principles and problems. *Sensors and Actuators B: Chemical* **1993,** 11, (13), 97-101.

135. Hartmann, P.; Leiner, M. J. P.; Lippitsch, M. E., Response characteristics of luminescent oxygen sensors. *Sensors and Actuators: B. Chemical* **1995,** 29, (1-3), 251-257.

136. Jenkins, D. M.; Zhu, C.; Su, W. W., A simple hybrid circuit for direct determination of fluorescence lifetimes. *Applied Engineering in Agriculture* **2008,** 24, (2), 259-263.

137. Chan, S. P.; Fuller, Z. J.; Demas, J. N.; DeGraff, B. A., Optimized Gating Scheme for Rapid Lifetime Determinations of Single-Exponential Luminescence Lifetimes. *Analytical Chemistry* **2001,** 73, (18), 4486-4490.

138. Schäferling, M., The Art of Fluorescence Imaging with Chemical Sensors. *Angewandte Chemie International Edition* **2012,** 51, (15), 3532-3554.

139. Lochmann, C.; Häupl, T.; Beuthan, J., Luminescence lifetime determination for oxygen imaging in human tissue. *Laser Physics Letters* **2008,** 5, (2), 151-155.

140. Becker, W.; Bergmann, A.; Hink, M. A.; König, K.; Benndorf, K.; Biskup, C., Fluorescence lifetime imaging by time-correlated single-photon counting. *Microscopy Research and Technique* **2004,** 63, (1), 58-66.

141. Trettnak, W.; Kolle, C.; Reininger, F.; Dolezal, C.; O'Leary, P., Miniaturized luminescence lifetime-based oxygen sensor instrumentation utilizing a phase modulation technique. *Sensors and Actuators, B: Chemical* **1996,** 36, (1-3), 506-512.

142. O'Keeffe, G.; MacCraith, B. D.; McEvoy, A. K.; McDonagh, C. M.; McGilp, J. F., Development of a LED-based phase fluorimetric oxygen sensor using evanescent wave excitation of a sol-gel immobilized dye. *Sensors and Actuators: B. Chemical* **1995,** 29, (1-3), 226-230.

143. Andrzejewski, D.; Klimant, I.; Podbielska, H., Method for lifetime-based chemical sensing using the demodulation of the luminescence signal. *Sensors and Actuators, B: Chemical* **2002,** 84, (2-3), 160-166.

144. Lippitsch, M. E.; Draxler, S., Luminescence decay-time-based optical sensors: principles and problems. *Sensors and Actuators: B. Chemical* **1993,** 11, (1-3), 97-101.

145. Ogurtsov, V. I.; Papkovsky, D. B., Selection of modulation frequency of excitation for luminescence lifetime-based oxygen sensors. *Sensors and Actuators, B: Chemical* **1998,** 51, (1-3), 377-381.

146. Hulanicki, A.; Geab, S.; Ingman, F., Chemical Sensors: Definition and Clasification. *Pure & Applied Chemistry* **1991,** 63, (9), 1247-1250.

147. Ziemer, L. S.; Lee, W. M. F.; Vinogradov, S. A.; Sehgal, C.; Wilson, D. F., Oxygen distribution in murine tumors: characterization using oxygen-dependent quenching of phosphorescence. *Journal of Applied Physiology* **2005,** 98, (4), 1503-1510.

148. Dmitriev, R.; Papkovsky, D., Optical probes and techniques for O2 measurement in live cells and tissue. *Cellular and Molecular Life Sciences* **2012,** 69, (12), 2025-2039.

149. Varcárcel Cases, M.; Luque de Castro, M. D., *Flow-through (bio)chemical Sensors*. Elsevier: 1994.

150. Ruzika, J.; Hansen, E. H., Optosensing at active surfaces: a new detection principle in flow injection analysis. *Analytica Chimica Acta* **1985,** 173, (0), 3-21.

151. Boisde, G., Les capteurs chimiques à fibres optiques. Réalités et perspectives. Chemical optical-fiber sensors: realities and prospects. *Entropie* **1990,** 26, (155), 28-42.

152. Optical Sensors, Optodes. In *Chemical Sensors and Biosensors for Medical and Biological Applications*, Spichiger-Keller, U. E., Ed. John Wiley & Sons: 2008.

153. Fischer, J. P.; Koop-Jakobsen, K., The multi fiber optode (MuFO): A novel system for simultaneous analysis of multiple fiber optic oxygen sensors. *Sensors and Actuators B: Chemical* **2012,** 168, (0), 354-359.

154. Tsukada, K.; Sakai, S.; Hase, K.; Minamitani, H., Development of catheter-type optical oxygen sensor and applications to bioinstrumentation. *Biosensors and Bioelectronics* **2003,** 18, (12), 1439-1445.

155. Pérez de Vargas-Sansalvador, I.; Martínez-Olmos, A.; Palma, A.; Fernández-Ramos, M.; Capitán-Vallvey, L., Compact optical instrument for simultaneous determination of oxygen and carbon dioxide. *Microchimica Acta* **2011,** 172, (3), 455-464.

156. Martinez-Olmos, A.; Pérez de Vargas-Sansalvador, I. M.; Palma, A. J.; Banqueri, J.; Fernández-Ramos, M. D.; Capitán-Vallvey, L. F., Multisensor probe for soil monitoring. *Sensors and Actuators B: Chemical* **2012,** 160, (1), 52-58.

157. Miró, M.; Hansen, E. H., Recent advances and future prospects of mesofluidic Lab-on-a-Valve platforms in analytical sciences: A critical review. *Analytica Chimica Acta* **2012**, (0).

158. Borchert, N.; Hempel, A.; Walsh, H.; Kerry, J. P.; Papkovsky, D. B., High throughput quality and safety assessment of packaged green produce using two optical oxygen sensor based systems. *Food Control* **2012,** 28, (1), 87-93.

159. Napp, J.; Behnke, T.; Fischer, L.; Würth, C.; Wottawa, M.; Katschinski, D. M.; Alves, F.; Resch-Genger, U.; Schäferling, M., Targeted Luminescent Near-Infrared Polymer-Nanoprobes for In Vivo Imaging of Tumor Hypoxia. *Analytical Chemistry* **2011,** 83, (23), 9039-9046.

160. López-Ruiz, N.; Martínez-Olmos, A.; Pérez de Vargas-Sansalvador, I. M.; Fernández-Ramos, M. D.; Carvajal, M. A.; Capitan-Vallvey, L. F.; Palma, A. J., Determination of O2 using colour sensing from image processing with mobile devices. *Sensors and Actuators B: Chemical* **2012**, (In press).

161. Wolfbeis, O. S.; Weidgans, B. M.; Baldini, F.; Chester, A. N.; Homola, J.; Martellucci, S., Fiber Optic Chemical Sensors and Biosensors: A View Back. In *Optical Chemical Sensors*, Springer Netherlands: 2006; Vol. 224, pp 17-44.

162. Fernández-Vallejo, M.; Lopez-Amo, M., Optical Fiber Networks for Remote Fiber Optic Sensors. *Sensors* **2012,** 12, (4), 3929-3951.

163. Wang, X.-d.; Gorris, H. H.; Stolwijk, J. A.; Meier, R. J.; Groegel, D. B. M.; Wegener, J.; Wolfbeis, O. S., Self-referenced RGB colour imaging of intracellular oxygen. *Chemical Science* **2012,** 2, (5), 901-906.

164. Shen, L.; Ratterman, M.; Klotzkin, D.; Papautsky, I., A CMOS optical detection system for point-of-use luminescent oxygen sensing. *Sensors and Actuators, B: Chemical* **2011,** 155, (1), 430-435.

165. Bhagwat, P.; Achanta, G. S.; Henthorn, D.; Kim, C.-S. In *Colorimetric phosphorescence measurements with a color camera for oxygen determination*, Smart Biomedical and Physiological Sensor Technology VIII, Orlando, Florida, USA, 2011; SPIE: Orlando, Florida, USA, 2011; pp 80250B-8.

166. Wolfbeis, O. S., Optical Technology until the Year 2000: An Historical Overview. In *Optical Sensors*, Narayanaswamy, R.; Wolfbeis, O. S., Eds. Springer: Verlag Berlin Heidelberg New York, 2004.

167. Medina-Castillo, A. L.; Fernandez-Sanchez, J. F.; Segura-Carretero, A.; Fernandez-Gutierrez, A., Design and synthesis by ATRP of novel, water-insoluble, lineal copolymers and their application in the development of fluorescent and pH-sensing nanofibres made by electrospinning. *Journal of Materials Chemistry* **2011,** 21, (18), 6742-6750.

168. Sharma, A.; Wolfbeis, O. S., Fiberoptic oxygen sensor based on fluorescence quenching and energy transfer. *Applied Spectroscopy* **1988,** 42, (6), 1009-1011.

169. Amao, Y.; Asai, K.; Okura, I., A Novel Optical Oxygen Sensing Based on Quenching of Photoexcited Triplet State of C70 in Polystyrene Film by Oxygen Using Time-resolved Spectroscopy. *Chemistry Letters* **1999,** 28, (2), 183-184.

170. Amao, Y.; Asai, K.; Okura, I., Fluorescence quenching oxygen sensor using an aluminum phthalocyanine-polystyrene film. *Analytica Chimica Acta* **2000,** 407, (1-2), 41-44.

171. Costa-Fernández, J. M.; Diaz-García, M. E.; Sanz-Medel, A., Sol-gel immobilized room-temperature phosphorescent metal-chelate as luminescent oxygen sensing material. *Analytica Chimica Acta* **1998,** 360, (1-3), 17-26.

172. Fleischauer, P. D.; Fleischauer, P., Photoluminescence of transition metal coordination compounds. *Chemical Reviews* **1970,** 70, (2), 199-230.

173. Sacksteder, L.; Demas, J. N.; DeGraff, B. A., Design of oxygen sensors based on quenching of luminescent metal complexes: Effect of ligand size on heterogeneity. *Analytical Chemistry* **1993,** 65, (23), 3480-3483.

174. Xu, W.; Kneas, K. A.; Demas, J. N.; DeGraff, B. A., Oxygen sensors based on luminescence quenching of metal complexes: Osmium complexes suitable for laser diode excitation. *Analytical Chemistry* **1996,** 68, (15), 2605-2609.

175. Demas, J. N.; Harris, E. W.; Flynn, C. M.; Diemente, D., Luminescent osmium(II) and iridium(III) complexes as photosensitizers. *Journal of the American Chemical Society* **1975,** 97, (13), 3838-3839.

176. Jianliang, S.; Ge, H.; Qing, S.; Zhaohong, Z.; Lei, G., Nanofibers doped with a novel red-emitting Europium complex: Synthesis, characterization, photophysical property and sensing activity toward molecular oxygen. *Spectrochimica Acta Part A: Molecular and Biomolecular Spectroscopy* **2012,** 91, (0), 192-197.

177. Vander Donckt, E.; Camerman, B.; Herne, R.; Vandeloise, R., Fibre-optic oxygen sensor based on luminescence quenching of a Pt(II) complex embedded in polymer matrices. *Sensors and Actuators B: Chemical* **1996,** 32, (2), 121-127.

178. Borisov, S. M.; Zenkl, G.; Klimant, I., Phosphorescent Platinum(II) and Palladium(II) Complexes with Azatetrabenzoporphyrins: A New Red Laser Diode-Compatible Indicators for Optical Oxygen Sensing. *ACS Applied Materials & Interfaces* **2010,** 2, (2), 366-374.

179. McMurray, H. N.; Douglas, P.; Busa, C.; Garley, M. S., Oxygen quenching of tris(2,2'-bipyridine) ruthenium(II) complexes in thin organic films. *Journal of Photochemistry and Photobiology A: Chemistry* **1994,** 80, (13), 283-288.

180. Mills, A.; Thomas, M. D., Effect of plasticizer viscosity on the sensitivity of an [Ru(bpy)32+(Ph4B-) 2]-based optical oxygen sensor. *Analyst* **1998,** 123, (5), 1135-1140.

181. Han, B.-H.; Manners, I.; Winnik, M. A., Oxygen Sensors Based on Mesoporous Silica Particles on Layer-by-Layer Self-assembled Films. *Chemistry of Materials* **2005,** 17, (12), 3160-3171.

182. Klimant, I.; Ruckruh, F.; Liebsch, G.; Stangelmayer, A.; Wolfbeis, O. S., Fast Response Oxygen Micro-Optodes Based on Novel Soluble Ormosil Glasses. *Microchimica Acta* **1999,** 131, (1), 35-46.

183. Hartmann, P.; Leiner, M. J. P.; Lippitsch, M. E., Luminescence quenching behavior of an oxygen sensor based on a Ru(II) complex dissolved in polystyrene. *Analytical Chemistry* **1995,** 67, (1), 88-93.

184. Amao, Y.; Ishikawa, Y.; Okura, I., Green luminescent iridium(III) complex immobilized in fluoropolymer film as optical oxygen-sensing material. *Analytica Chimica Acta* **2001,** 445, (2), 177-182.

185. Di Marco, G.; Lanza, M.; Pieruccini, M.; Campagna, S., A luminescent iridium(III) cyclometallated complex immobilized in a polymeric matrix as a solid-state oxygen sensor. *Advanced Materials* **1996,** 8, (7), 576-580.

186. Medina-Castillo, A. L.; Fernández-Sánchez, J. F.; Klein, C.; Nazeeruddin, M. K.; Segura-Carretero, A.; Fernández-Gutiérrez, A.; Graetzel, M.; Spichiger-Keller, U. E., Engineering of efficient phosphorescent iridium cationic complex for developing oxygen-sensitive polymeric and nanostructured films. *Analyst* **2007,** 132, (9), 929-936.

187. Lee, S. K.; Okura, I., Photoluminescent determination of oxygen using metalloporphyrin-polymer sensing systems. *Spectrochimica Acta - Part A: Molecular and Biomolecular Spectroscopy* **1998,** 54, (1), 91-100.

188. DiMarco, G.; Lanza, M., Optical solid-state oxygen sensors using metalloporphyrin complexes immobilized in suitable polymeric matrices. *Sensors and Actuators B: Chemical* **2000,** 63, (1), 42-48.

189. Borisov, S. M.; Lehner, P.; Klimant, I., Novel optical trace oxygen sensors based on platinum(II) and palladium(II) complexes with 5,10,15,20-meso-tetrakis-(2,3,4,5,6-pentafluorphenyl)-porphyrin covalently immobilized on silica-gel particles. *Analytica Chimica Acta* **2011,** 690, (1), 108-115.

190. Lee, S. K.; Okura, I., Photostable Optical Oxygen Sensing Material: Platinum Tetrakis(pentafluorophenyl)porphyrin Immobilized in Polystyrene. *Analytical Communications* **1997,** 34, (6), 185-188.

191. Papkovsky, D. B.; Ponomarev, G. V.; Trettnak, W.; O'Leary, P., Phosphorescent Complexes of Porphyrin Ketones: Optical Properties and Application to Oxygen Sensing. *Analytical Chemistry* **1995,** 67, (22), 4112-4117.

192. Hartmann, P.; Trettnak, W., Effects of Polymer Matrices on Calibration Functions of Luminescent Oxygen Sensors Based on Porphyrin Ketone Complexes. *Analytical Chemistry* **1996,** 68, (15), 2615-2620.

193. Borisov, S. M.; Klimant, I., Ultrabright oxygen optodes based on cyclometalated iridium(III) coumarin complexes. *Analytical Chemistry* **2007,** 79, (19), 7501-7509.

194. Juris, A.; Balzani, V.; Barigelletti, F.; Campagna, S.; Belser, P.; von Zelewsky, A., Ru(II) polypyridine complexes: photophysics, photochemistry, eletrochemistry, and chemiluminescence. *Coordination Chemistry Reviews* **1988,** 84, 85-277.

195. Lees, A. J., Luminescence properties of organometallic complexes. *Chemical Reviews* **1987,** 87, (4), 711-743.

196. McEvoy, A.; McDonagh, C.; Maccraith, B., Optimisation of sol-gel-derived silica films for optical oxygen sensing. *Journal of Sol-Gel Science and Technology* **1997,** 8, (1), 1121-1125.

197. Fernández-Sánchez, J. F.; Roth, T.; Cannas, R.; Nazeeruddin, M. K.; Spichiger, S.; Graetzel, M.; Spichiger-Keller, U. E., Novel oxygen sensitive complexes for optical oxygen sensing. *Talanta* **2007,** 71, (1), 242-250.

198. Medina-Castillo, A. L.; Fernández-Sánchez, J. F.; Klein, C.; Nazeeruddin, M. K.; Segura-Carretero, A.; Fernández-Gutiérrez, A.; Graetzel, M.; Spichiger-Keller, U. E., Engineering of efficient phosphorescent iridium cationic complex for developing oxygen-sensitive polymeric and nanostructured films. *The Analyst* **2007,** 132, (9), 929-936.

199. DeRosa, M. C.; Hodgson, D. J.; Enright, G. D.; Dawson, B.; Evans, C. E. B.; Crutchley, R. J., Iridium Luminophore Complexes for Unimolecular Oxygen Sensors. *Journal of the American Chemical Society* **2004,** 126, (24), 7619-7626.

200. Koren, K.; Borisov, S. M.; Saf, R.; Klimant, I., Strongly phosphorescent iridium(III)-porphyrins - New oxygen indicators with tuneable photophysical properties and functionalities. *European Journal of Inorganic Chemistry* **2011**, (10), 1531-1534.

201. Ruggi, A.; van Leeuwen, F. W. B.; Velders, A. H., Interaction of dioxygen with the electronic excited state of Ir(III) and Ru(II) complexes: Principles and biomedical applications. *Coordination Chemistry Reviews* **2011,** 255, (21-22), 2542-2554.

202. Flamigni, L.; Barbieri, A.; Sabatini, C.; Ventura, B.; Barigelletti, F., Photochemistry and photophysics of coordination compounds: Iridium. In *Topics in Current Chemistry*, 2007; Vol. 281, pp 143-203.

203. Clark, H. A.; Barker, S. L. R.; Brasuel, M.; Miller, M. T.; Monson, E.; Parus, S.; Shi, Z.-Y.; Song, A.; Thorsrud, B.; Kopelman, R.; Ade, A.; Meixner, W.; Athey, B.; Hoyer, M.; Hill, D.; Lightle, R.; Philbert, M. A., Subcellular optochemical nanobiosensors: probes encapsulated by biologically localised embedding (PEBBLEs). *Sensors and Actuators B: Chemical* **1998,** 51, (13), 12-16.

204. McDonagh, C.; MacCraith, B. D.; McEvoy, A. K., Tailoring of Sol-Gel Films for Optical Sensing of Oxygen in Gas and Aqueous Phase. *Analytical Chemistry* **1998,** 70, (1), 45-50.

205. McEvoy, A. K.; McDonagh, C. M.; MacCraith, B. D., Dissolved oxygen sensor based on fluorescence quenching of oxygen-sensitive ruthenium complexes immobilized in sol-gel-derived porous silica coatings. *Analyst* **1996,** 121, (6), 785-788.

206. Baleizao, C.; Nagl, S.; Schäferling, M.; Berberan-Santos, M. N.; Wolfbeis, O. S., Dual Fluorescence Sensor for Trace Oxygen and Temperature with Unmatched Range and Sensitivity. *Analytical Chemistry* **2008,** 80, (16), 6449-6457.

207. Mistlberger, G. n.; Borisov, S. M.; Klimant, I., Enhancing performance in optical sensing with magnetic nanoparticles. *Sensors and Actuators B: Chemical* **2009,** 139, (1), 174-180.

208. MacCraith, B. D.; McDonagh, C. M.; O'Keeffe, G.; McEvoy, A. K.; Butler, T.; Sheridan, F. R., Sol-gel coatings for optical chemical sensors and biosensors. *Sensors and Actuators B: Chemical* **1995,** 29, (13), 51-57.

209. Borisov, S. M.; Mayr, T.; Mistlberger, G. n.; Waich, K.; Koren, K.; Chojnacki, P.; Klimant, I., Precipitation as a simple and versatile method for preparation of optical nanochemosensors. *Talanta* **2009,** 79, (5), 1322-1330.

210. Chu, C.-S.; Lo, Y.-L., Optical fiber dissolved oxygen sensor based on Pt(II) complex and core-shell silica nanoparticles incorporated with sol-gel matrix. *Sensors and Actuators B: Chemical* **2010,** 151, (1), 83-89.

211. Mistlberger, G.; Medina-Castillo, A.; Borisov, S.; Mayr, T.; Fernández-Gutiérrez, A.; Fernández-Sánchez, J.; Klimant, I., Mini-emulsion solvent evaporation: a simple and versatile way to magnetic nanosensors. *Microchimica Acta* **2011,** 172, (3), 299-308.

212. Bonacchi, S.; Genovese, D.; Juris, R.; Montalti, M.; Prodi, L.; Rampazzo, E.; Zaccheroni, N., Luminescent Silica Nanoparticles: Extending the Frontiers of Brightness. *Angewandte Chemie International Edition* **2011,** 50, (18), 4056-4066.

213. Fernández-Sánchez, J. F.; Cannas, R.; Spichiger, S.; Steiger, R.; Spichiger-Keller, U. E., Novel nanostructured materials to develop oxygen-sensitive films for optical sensors. *Analytica Chimica Acta* **2006,** 566, (2), 271-282.

214. Borisov, S. M.; Mayr, T.; Klimant, I., Poly(styrene-block-vinylpyrrolidone) Beads as a Versatile Material for Simple Fabrication of Optical Nanosensors. *Analytical Chemistry* **2008,** 80, (3), 573-582.

215. Xu, W.; McDonough, R. C.; Langsdorf, B.; Demas, J. N.; DeGraff, B. A., Oxygen Sensors Based on Luminescence Quenching: Interactions of Metal Complexes with the Polymer Supports. *Analytical Chemistry* **1994,** 66, (23), 4133-4141.

216. Koren, K.; Borisov, S. M.; Klimant, I., Stable optical oxygen sensing materials based on click-coupling of fluorinated platinum(II) and palladium(II) porphyrins: A convenient way to eliminate dye migration and leaching. *Sensors and Actuators B: Chemical* **2012,** 169, 173-181.

217. Douglas, P.; Eaton, K., Response characteristics of thin film oxygen sensors, Pt and Pd octaethylporphyrins in polymer films. *Sensors and Actuators B: Chemical* **2002,** 82, (23), 200-208.

218. Apostolidis, A.; Klimant, I.; Andrzejewski, D.; Wolfbeis, O. S., A Combinatorial Approach for Development of Materials for Optical Sensing of Gases. *Journal of Combinatorial Chemistry* **2004,** 6, (3), 325-331.

219. Brandrup, J.; Immergut, E. H.; Grulke, E. A., *Polymer Handbook*. Wiley-Interscience: 2003.

220. Klimant, I.; Wolfbeis, O. S., Oxygen-Sensitive Luminescent Materials Based on Silicone-Soluble Ruthenium Diimine Complexes. *Analytical Chemistry* **1995,** 67, (18), 3160-3166.

221. Herman, S. D.; Christen, J. B. In *Fabrication and characterization of a silicone fluorescent oxygen sensor*, Biomedical Circuits and Systems Conference (BioCAS), 2010 IEEE, 3-5 Nov. 2010, 2010; 2010; pp 70-73.

222. Guillaume, F.; Greden, K.; Smyrl, W. H., Optical Sensors for Corrosion Systems: I. Oxygen Sensing. *Journal of The Electrochemical Society* **2008,** 155, (8), J213-J219.

223. Ichiraku, Y.; Stern, S. A.; Nakagawa, T., An investigation of the high gas permeability of poly (1-Trimethylsilyl-1-Propyne). *Journal of Membrane Science* **1987,** 34, (1), 5-18.

224. Amao, Y.; Asai, K.; Okura, I.; Shinohara, H.; Nishide, H., Platinum porphyrin embedded in poly(1-trimethylsilyl-1-propyne) film as an optical sensor for trace analysis of oxygen. *Analyst* **2000,** 125, (11), 1911-1914.

225. Tian, Y.; Shumway, B. R.; Meldrum, D. R., A New Cross-Linkable Oxygen Sensor Covalently Bonded into Poly(2-hydroxyethyl methacrylate)-co-Polyacrylamide Thin Film for Dissolved Oxygen Sensing. *Chemistry of Materials* **2010,** 22, (6), 2069-2078.

226. Mills, A.; Thomas, M., Fluorescence-based Thin Plastic Film Ion-pair Sensors for Oxygen. *Analyst* **1997,** 122, (1), 63-68.

227. Mills, A.; Lepre, A., Controlling the Response Characteristics of Luminescent Porphyrin Plastic Film Sensors for Oxygen. *Analytical Chemistry* **1997,** 69, (22), 4653-4659.

228. Cao, Y.; Lee Koo, Y.-E.; Kopelman, R., Poly(decyl methacrylate)-based fluorescent PEBBLE swarm nanosensors for measuring dissolved oxygen in biosamples. *Analyst* **2004,** 129, (8), 745-750.

229. Amao, Y.; Miyashita, T.; Okura, I., Platinum tetrakis(pentafluorophenyl)porphyrin immobilized in polytrifluoroethylmethacrylate film as a photostable optical oxygen detection material. *Journal of Fluorine Chemistry* **2001,** 107, (1), 101-106.

230. Borisov, S. M.; Krause, C.; Arain, S.; Wolfbeis, O. S., Composite Material for Simultaneous and Contactless Luminescent Sensing and Imaging of Oxygen and Carbon Dioxide. *Advanced Materials* **2006,** 18, (12), 1511-1516.

231. Lee, S.-K.; Okura, I., Photostable Optical Oxygen Sensing Material: Platinum Tetrakis(pentafluorophenyl)porphyrin Immobilized in Polystyrene. *Analytical Communications* **1997,** 34, (6), 185-188.

232. O'Riordan, T. s. C.; Voraberger, H.; Kerry, J. P.; Papkovsky, D. B., Study of migration of active components of phosphorescent oxygen sensors for food packaging applications. *Analytica Chimica Acta* **2005,** 530, (1), 135-141.

233. Stich, M. I. J.; Nagl, S.; Wolfbeis, O. S.; Henne, U.; Schaeferling, M., A Dual Luminescent Sensor Material for Simultaneous Imaging of Pressure and Temperature on Surfaces. *Advanced Functional Materials* **2008,** 18, (9), 1399-1406.

234. Borisov, S.; Seifner, R.; Klimant, I., A novel planar optical sensor for simultaneous monitoring of oxygen, carbon dioxide, pH and temperature. *Analytical and Bioanalytical Chemistry* **2011,** 400, (8), 2463-2474.

235. Voraberger, H. S.; Kreimaier, H.; Biebernik, K.; Kern, W., Novel oxygen optrode withstanding autoclavation: technical solutions and performance. *Sensors and Actuators B: Chemical* **2001,** 74, (13), 179-185.

236. Badocco, D.; Mondin, A.; Pastore, P.; Voltolina, S.; Gross, S., Dependence of calibration sensitivity of a polysulfone/Ru(II)-Tris(4,7-diphenyl-1,10-phenanthroline)-based oxygen optical sensor on its structural parameters. *Analytica Chimica Acta* **2008,** 627, (2), 239-246.

237. Mills, A.; Collé Williams, F., Chemical influences on the luminescence of ruthenium diimine complexes and its response to oxygen. *Thin Solid Films* **1997,** 306, (1), 163-170.

238. Nagai, K.; Masuda, T.; Nakagawa, T.; Freeman, B. D.; Pinnau, I., Poly[1-(trimethylsilyl)-1-propyne] and related polymers: synthesis, properties and functions. *Progress in Polymer Science* **2001,** 26, (5), 721-798.

239. Quinn, C. A. P.; Connor, R. E.; Heller, A., Biocompatible, glucose-permeable hydrogel for in situ coating of implantable biosensors. *Biomaterials* **1997,** 18, (24), 1665-1670.

240. O'Neal, D. P.; Meledeo, M. A.; Davis, J. R.; Ibey, B. L.; Gant, V. A.; Pishko, M. V.; Cote, G. L., Oxygen sensor based on the fluorescence quenching of a ruthenium complex immobilized in a biocompatible Poly(Ethylene glycol) hydrogel. *Sensors Journal, IEEE* **2004,** 4, (6), 728-734.

241. Onuki, Y.; Bhardwaj, U.; M.Pharm.; Fotios Papadimitrakopoulos; Burgess, D. J., A Review of the Biocompatibility of Implantable Devices: Current Challenges to Overcome Foreign Body Response. *Journal of Diabetes Science and Technology* **2008,** 2, (6), 1003-1015.

242. Wang, C.; Yu, B.; Knudsen, B.; Harmon, J.; Moussy, F.; Moussy, Y., Synthesis and Performance of Novel Hydrogels Coatings for Implantable Glucose Sensors. *Biomacromolecules* **2008,** 9, (2), 561-567.

243. Wang, X.-H.; Peng, H.-S.; Ding, H.; You, F.-T.; Huang, S.-H.; Teng, F.; Dong, B.; Song, H.-W., Biocompatible fluorescent core-shell nanoparticles for ratiometric oxygen sensing. *Journal of Materials Chemistry* **2012,** 22, (31), 16066-16071.

244. Houde, A. Y.; Stern, S. A., Permeability of ethyl cellulose to light gases. Effect of ethoxy content. *Journal of Membrane Science* **1994,** 92, (1), 95-101.

245. Papkovsky, D. B.; Mohr, G. J.; Wolfbeis, O. S., New polar plasticizers for luminescence-based sensors. *Analytica Chimica Acta* **1997,** 337, (2), 201-205.

246. Meier, B.; Werner, T.; Klimant, I.; Wolfbeis, O. S., Novel oxygen sensor material based on a ruthenium bipyridyl complex encapsulated in zeolite Y: dramatic differences in the efficiency of luminescence quenching by oxygen on going from surface-adsorbed to zeolite-encapsulated fluorophores. *Sensors and Actuators B: Chemical* **1995,** 29, (13), 240-245.

247. Lu, X.; Manners, I.; Winnik, M. A., Polymer/Silica Composite Films as Luminescent Oxygen Sensors. *Macromolecules* **2001,** 34, (6), 1917-1927.

248. Mackenzie, J. D.; Bescher, E. P., Structures, Properties and Potential Applications of Ormosils. *Journal of Sol-Gel Science and Technology* **1998,** 13, (1), 371-377.

249. Batzill, M.; Diebold, U., The surface and materials science of tin oxide. *Progress in Surface Science* **2005,** 79, (2-4), 47-154.

250. Chen, H. T.; Xiong, S. J.; Wu, X. L.; Zhu, J.; Shen, J. C.; Chu, P. K., Tin Oxide Nanoribbons with Vacancy Structures in Luminescence-Sensitive Oxygen Sensing. *Nano Letters* **2009,** 9, (5), 1926-1931.

251. Brugger, P. A.; Ketterer, J.; Steiger, R.; Zbinden, F. Recording sheets for ink jet printing. 2000.

252. Spichiger-Keller, U.; Spichiger, S.; Fernandez-Sanchez, J. F. Metal oxide membrane with a gas-selective compound. 2006.

253. Fernández-Sánchez, J. F.; Nezel, T.; Steiger, R.; Spichiger-Keller, U. E., Novel optical NO2-selective sensor based on phthalocyaninato-iron(II) incorporated into a nanostructured matrix. *Sensors and Actuators B: Chemical* **2006,** 113, (2), 630-638.

254. Koo, Y.-E. L.; Cao, Y.; Kopelman, R.; Koo, S. M.; Brasuel, M.; Philbert, M. A., Real-Time Measurements of Dissolved Oxygen Inside Live Cells by Organically Modified Silicate Fluorescent Nanosensors. *Analytical Chemistry* **2004,** 76, (9), 2498-2505.

255. Jiang, K.; Thomas, P. C.; Forry, S. P.; Devoe, D. L.; Raghavan, S. R., Microfluidic synthesis of monodisperse PDMS microbeads as discrete oxygen sensors. *Soft Matter* **2012,** 8, (4), 923-926.

256. Anker, J. N.; Koo, Y.-E.; Kopelman, R., Magnetically controlled sensor swarms. *Sensors and Actuators B: Chemical* **2007,** 121, (1), 83-92.

257. Chojnacki, P.; Mistlberger, G.; Klimant, I., Separable Magnetic Sensors for the Optical Determination of Oxygen. *Angewandte Chemie International Edition* **2007,** 46, (46), 8850-8853.

258. Medina-Castillo, A. L.; Mistlberger, G.; Fernández-Sánchez, J. F.; Segura-Carretero, A.; Klimant, I.; Fernández-Gutiérrez, A., Novel Strategy To Design Magnetic, Molecular Imprinted Polymers with Well-Controlled Structure for the Application in Optical Sensors. *Macromolecules* **2009,** 43, (1), 55-61.

259. Mistlberger, G.; Koren, K.; Scheucher, E.; Aigner, D.; Borisov, S. M.; Zankel, A.; Pölt, P.; Klimant, I., Multifunctional Magnetic Optical Sensor Particles with Tunable Sizes for Monitoring Metabolic Parameters and as a Basis for Nanotherapeutics. *Advanced Functional Materials* **2010,** 20, (11), 1842-1851.

260. Fernandez-Vallejo, M.; Lopez-Amo, M., Optical Fiber Networks for Remote Fiber Optic Sensors. *Sensors* **2012,** 12, (4), 3929-3951.

261. Shonat, R. D.; Kight, A. C., Oxygen Tension Imaging in the Mouse Retina. *Annals of Biomedical Engineering* **2003,** 31, (9), 1084-1096.

262. Dunphy, I.; Vinogradov, S. A.; Wilson, D. F., Oxyphor R2 and G2: phosphors for measuring oxygen by oxygen-dependent quenching of phosphorescence. *Analytical Biochemistry* **2002,** 310, (2), 191-198.

263. Lebedev, A. Y.; Cheprakov, A. V.; Sakadzic, S.; Boas, D. A.; Wilson, D. F.; Vinogradov, S. A., Dendritic Phosphorescent Probes for Oxygen Imaging in Biological Systems. *ACS Applied Materials & Interfaces* **2009,** 1, (6), 1292-1304.

264. Papkovsky, D. B.; Papkovskaia, N.; Smyth, A.; Kerry, J.; Ogurtsov, V. I., Phosphorescent Sensor Approach for Non-Destructive Measurement of Oxygen in Packaged Foods: Optimisation of Disposable Oxygen Sensors and their Characterization Over a Wide Temperature Range. *Analytical Letters* **2000,** 33, (9), 1755-1777.

265. Hempel, A. W.; Gillanders, R. N.; Papkovsky, D. B.; Kerry, J. P., Detection of cheese packaging containment failures using reversible optical oxygen sensors. *International Journal of Dairy Technology* **2012**.

266. Nur Hanani, Z. A.; Roos, Y. H.; Kerry, J. P., Use of beef, pork and fish gelatin sources in the manufacture of films and assessment of their composition and mechanical properties. *Food Hydrocolloids* **2012,** 29, (1), 144-151.

267. Heller, A.; Fischer, L. H.; Wolfbeis, O. S.; Goepferich, A., Long time monitoring of the respiratory activity of isolated mitochondria. *Experimental Cell Research* **2012,** 318, (14), 1667-1672.

268. Soley, A.; Fontova, A.; Gálvez, J.; Sarró, E.; Lecina, M.; Bragós, R.; Cairó, J. J.; Gòdia, F., Development of a simple disposable six minibioreactor system for suspension mammalian cell culture. *Process Biochemistry* **2012,** 47, (4), 597-605.

269. Komori, K.; Fujii, S.; Montagne, K.; Nakamura, H.; Kimura, H.; Otake, K.; Fujii, T.; Sakai, Y., Development of a well-of-the-well system-based embryo culture plate with an oxygen sensing photoluminescent probe. *Sensors and Actuators B: Chemical* **2012,** 162, (1), 278-283.

270. Dragu, A.; Taeger, C.; Buchholz, R.; Sommerfeld, B.; Hübner, H.; Birkholz, T.; Kleinmann, J.; Münch, F.; Horch, R.; Präbst, K., Online oxygen measurements in ex vivo perfused muscle tissue in a porcine model using dynamic quenching methods. *Archives of Orthopaedic and Trauma Surgery* **2012,** 132, (5), 655-661.

271. Haberer, C. M.; Rolle, M.; Liu, S.; Cirpka, O. A.; Grathwohl, P., A high-resolution non-invasive approach to quantify oxygen transport across the capillary fringe and within the underlying groundwater. *Journal of Contaminant Hydrology* **2012,** 122, (14), 26-39.

272. Gevaert, F.; Delebecq, G.; Menu, D.; Brutier, L., A fully automated system for measurements of photosynthetic oxygen exchange under immersed conditions: an example of its use in Laminaria digitata (Heterokontophyta: Phaeophyceae). *Limnology and Oceanography: Methods* **2011,** 9, 361–379.

273. Zhang, L. J.; Jaiswal, R. S., Turbine Nozzle Endwall film cooling study using pressure-sensitive paint. *Journal of Turbomachinery* **2001,** 123, (4), 730-738.

Experimental

Bloque I. Caracterización de nuevas fases sensoras ópticas basadas en complejos de Ir(III)

La sensibilidad de la fase sensora y las características espectrales de la misma son de gran importancia para resolver problemas analíticos, tal y como se ha comentado en la introducción.

La sensibilidad de la fase sensora viene impuesta por el tiempo de vida del luminóforo, por la compatibilidad con el soporte de inmovilización y por la permeabilidad a oxígeno. Es por tanto de vital importancia conocer la respuesta de un determinado indicador inmovilizado en matrices de diferente viscosidad y difusión a oxígeno para poder conseguir una buena fase sensora.

Por ello, el Capítulo 1 analiza la potencialidad de cuatro nuevos complejos de iridio de carácter catiónico y diferentes ligandos derivados la bipiridina inmovilizados en diversos soportes como fase sensora óptica luminiscentes para la determinación de oxígeno. En especial, se pretende evaluar su potencialidad como fases sensibles a oxígeno para bajas concentraciones cuando son depositados sobre una nanoestructura de óxido hidróxido de aluminio. Por otro lado, la mayoría de las fases sensoras desarrolladas hasta el momento emiten en la zona del rojo, ya que son los compuestos que mejor respuesta a oxígeno ofrecen. Sin embargo, para ciertas aplicaciones es necesario disponer de fases sensoras que emitan a otras longitudes de onda, siendo muy interesante disponer de fases sensoras que emitan en toda la región del espectro visible. Esto es importante en el campo de los sensores multiparamétricos para evitar solapamiento espectral de los indicadores, o en determinados casos puedes ser interesante para evitar interferencias de la matriz de medida.

Así, en el Capítulo 2 se evalúan tres nuevos complejos neutros de iridio que presentan emisión luminiscente en la región azul del espectro visible (en torno a los 470 nm), donde existen pocos o muy pocos complejos que presentan buenas propiedades analíticas para la determinación de oxígeno. Además se demuestra la compatibilidad de estos complejos neutros con soportes nanoestructurados de carácter polar por primera vez, mejorando su sensibilidad a oxígeno y ampliando la aplicabilidad de estos soportes en el desarrollo de fases sensoras ópticas.

Capítulo 1

Novel luminescent Ir (III) dyes for developing highly sensitive oxygen sensing films

M. Marin-SuarezdelToro[a], J.F. Fernandez-Sanchez[a,*], E. Baranoff[b], Md.K. Nazeeruddin[b], M. Graetzel[b], A. Fernandez-Gutierrez[a,*]

[a] *Department of Analytical Chemistry, Faculty of Sciences, University of Granada (UGR), C/Fuentenueva s/n, E-18071 Granada, Spain.*

[b] *Sciences and Engineering. Ecole Polytechnique Fédérale de Lausanne (EPFL). CH-1015 Lausanne, Switzerland.*

Abstract

New sensing films have been developed for the detection of molecular oxygen. These films are based on luminescent Ir(III) dyes incorporated either into polystyrene (with and without plasticizer) or metal oxide, nanostructured material. The preparation and characterization of each film have been investigated in detail. Due to their high sensitivity for low oxygen concentration, the parameters $p_{O_2}(s = {}^1/_2)$ and $\Delta I_{1\%}$ have been also evaluated in order to establish the most sensitive membrane for controlling concentrations between 0 and 10% and low oxygen concentrations (lower than 1%), respectively. The results show that the use of nanostructured material increased the sensitivity of the film; the most sensitive membrane for controlling O_2 between 0 and 10% is based on N-1001 immobilized in AP200/19 (k_{sv}= 2848 ± 101 bar^{-1} and $p_{O_2}(s = {}^1/_2)$ = 0.0006), and the complex N-969 incorporated into AP200/19 seems to be the most suitable for applications in oxygen trace sensing ($\Delta I_{1\%}$ = 93.13 ± 0.13 %).

Keywords: Luminescence; Sensor; Iridium complex; Oxygen; nanostructured material

* Corresponding author. Tel.: +34 958248409; fax: +34 958249510. *E-mail address:* jffernan@ugr.es (J.F. Fernández-Sánchez), albertof@ugr.es (A. Fernández-Gutiérrez).

1.1. Introduction

Developing methods for monitoring oxygen concentration in real time has become a priority due to the potential for improved medical diagnostics and management of conditions where oxygen imbalances are manifest;[1] oxygen, often acting as a key metabolite in aerobic systems with a multitude of biological functions, is of major importance in medical applications.[2] In addition, the determination of oxygen is important in other fields such as chemical analysis, packaging, process control, as well as in environmental monitoring.[3-6]

Furthermore, oxygen trace sensing has become crucial in microbiology, since a variety of microorganisms grow under special conditions, from atmosphere of residual oxygen to anaerobic conditions.[7] Therefore, oxygen trace sensing has special application in the control of modified atmosphere packaging (MAP) where an adequate oxygen concentration is required inside the package in order to maintain the microbiological stability of fresh-cut fruits and vegetables, by limiting aerobic respiration without inducing anaerobic processes.[8] In addition, oxygen trace control is important for avoiding browning, discoloration and softening, where usually concentration below 0.25-5 kPa of oxygen are needed.[9-12] For keeping the nutritional composition and antioxidant potential of fruits and vegetable, the required oxygen concentration varies from 2 to 10 kPa.[10, 13]

Optical techniques are attractive for frequent or continuous monitoring because they offer the advantages of high sensitivity and selectivity, insensitivity to electrical interferences, no need for a reference signal and the possibility of remote sensing for "in-situ" applications.[14] Optodes are also suitable for high-resolution imaging of solute distributions in complex environments such as aquatic sediments and there are also exciting possibilities for multi-parameter and multi-analyte sensing.[15, 16] Thus, optical oxygen sensing has attracted a lot of scientific effort and has received a great deal of attention in recent years as dynamic quenching of the luminescence emission by oxygen has proved to be very sensitive. [17]

Numerous probes and polymeric matrices have been reported.[18] Ideally, a matrix must be permeable to oxygen, should be structurally stable enough to withstand the mechanical stress and should increase photostability.[19] In addition, it has to prevent

leaching and the migration of chemical compounds by insulation and has to prevent the aggregation of the dye.[20-23]

Table 1. Summary of Iridium and Ruthenium dyes used as oxygen probes; 2006 to 2010, update of table 1 in Fernandez-Sanchez *et al.* [17].

Probe	Support for immobilization	$\lambda_{ex/em\ (nm)}$	ϕ_L	I_0/I_{100}	Ref.
$[Ru(dpp)_2bpy\text{-}OH](PF_6)_2$	Glass*	450/650	-	19	30
$[Ru(dpp)_2bpy\text{-}19](PF_6)_2$	Glass	450/625	-	8	30
$[Ru(bpy)_2phen]^{2+}$	Mesoporous silica MCM-41*	457/588	-	-	31
$[Ru(bpy)_3]^{2+}$	Molecular sieve MSU-3*	-/601	-	-	32
$[Ru(dpp)_3]^{2+}$ **	TEOS derived sol-gel matrix	480/590	-	-	33
$[Ru(phen)_2(Dppz\text{-}Si)]^{2+}$	ORMOSIL*	480/590	-	3.1	34
$[Ru(dpp)_2bpy]^{2+}$	Mesoporous silica MCM-41*	490/610	-	23.2	29
$[Ru(bpyPS_2)_3](PF_6)2$	Polystyrene*	450/600	-	-	35
$Ir(C_N)_2(acac)$	Polystyrene	477/566	-	-	28
$Ir(C_S)_2(acac)$	Polystyrene	455/544	-	-	28
$Ir(C_O)_2(acac)$	Polystyrene	472/544	-	-	28
$Ir(C_{S\text{-}Me})_2(acac)$	Polystyrene	475/566	-	-	28
$(C_S)2Ir(\mu\text{-}Cl)_2Ir(C_S)_2$	Polystyrene	484/588	-	-	28
$(C_N)2Ir(\mu\text{-}Cl)_2Ir(C_N)_2$	Polystyrene	463/567	-	-	28
N-948	Polystyrene	494/665	0.57	-	19
	ALOOH	494/665	0.20	-	19
L_1H_3	Coordination polymer	385/538	-	-	36
L_2H_3	Coordination polymer	400/565	-	-	36
$Ir(ppy\text{-}NPh_2)_3$	Ethyl cellulose	405/524	-	-	37
$Ir(mebtp)_3$	FIB	296/595	-	7.41	38
N-969	Polystyrene	385/585	0.86		This work
	ALOOH	350/490	0.86		This work
N-1001	Polystyrene	300/530	0.64		This work
	ALOOH	330/549	0.64		This work
N-1008	Polystyrene	305/510	0.92		This work
	ALOOH	340/512	0.92		This work
N-1010	Polystyrene	300/520	0.14		This work
	ALOOH	330/545	0.14		This work

* Covalent bound

** Linked with dendrons

Abbreviations: dpp=4,7-diphenyl-1,10-phenanthroline; bpy=2,2'-bipyridine; PF_6= Hexafluorophosphate; Dppz-Si=alkoxylane-modified dipyrido[3,2-a:2',3'-c]phenazine; phen = 1,10-phenanthroline; PS=polystyrene; C_N=3-(1-methylbenzoimidazol-2-yl)-7-(diethylamino)-coumarin; C_S=3-(benzothiazol-2-yl)-7-(diethylamino)-coumarin; C_O=3-(5-chlorobenzooxazol-2-yl)-7-(diethylamino)-coumarin; $C_{S\text{-}Me}$=3-(Benzothiazol-2-yl)-7-(dimethylamino)-coumarin; acac=acetylacetone; N-948=Ir(2-phenylpyridine)2(4,4-bis(2-(4-N,N-methylhexylaminophenyl)ethyl)-2-2-bipyridine)Cl]; L_1H_3=Ir(3-(2-pyridyl)benzoic acid)$_3$; L_2H_3=Ir(4-(2-pyridyl)benzoic acid)$_3$ ppy=2-phenylpyridine anion; NPh_2=diphenylamine; mebtp=2-Benzo[b]thiophene-2-yl-4-methyl-pyridine; MCM-41=Mobil Catalytic Material 41; TEOS=tetraethyl orthosilicate; ORMOSIL= Organically Modified Silicates;

ALOOH=aluminium oxide/hydroxide; FIB=poly(1,1,1,3,3,3-hexafluoroisoproplylmethacrylate-co-1H,1H-dihydroperfluorobutyl-methacrylate).

Most of the probes are based on the luminescence quenching of organometallic complexes by paramagnetic oxygen[24-26] immobilized into a solid matrix (Fernandez-Sanchez *et al.*[17], Sanchez-Barragan *et al.*[27] and Borisov *et al.*[28] have summarized the luminescence probes used for analyzing oxygen). However, it is likely the determination of trace oxygen concentrations by means of the quenching of the luminescence is still being developed. **Table 1** shows a summary about the most recent iridium and ruthenium dyes used for oxygen sensing, as a continuation of the previous table reported in of Fernandez-Sanchez *et al.*[17]

In this paper, we propose four novel Iridium(III) complexes: bis(2,4-difluorophenylpyridine)-4,4'-tert-butyl-2,2'bypyridine iridium(III) hexafluorophosphate (called N-969), 4,7-diphenyl-1,10-phenanthroline-bis(2phenylpyridine)iridium(III) hexafluorophosphate (called N-1001), [Ir(2,4-difluorophenylpyridine)$_2$(4,7-diphenyl-1,10-phenanthroline)](PF_6) (called N-1008) and [Ir(2-phenylpyridine)$_2$(4-bromo-2,2'-bipyridine)](PF_6) (called N-1010) as oxygen-sensitive probe when they are immobilized in polymeric films (polystyrene with and without plasticizers) and aluminum oxide-hydroxide nanostructured solid support. The synthesis of the complexes N-969 and N-1001 have been previously published[39, 40] but they have not been used as oxygen probe; this paper also shows the synthesis of complexes N-1008 and N-1010. These dyes were selected to cover a large variety of properties, such as a wide range of emission wavelengths which vary from 463 to 624 nm in solution, low to high quantum yield, and an expected high sensitivity to low oxygen concentrations, according to previous studies developed by our research group[17,19,21] which make them interesting not only for controlling residual oxygen or anaerobic conditions, but also in applications that requires different wavelengths and sensitivities.

1. 2. Materials and methods

1.2.1. Materials

For the synthesis of the Ir(III) complexes, the following chemicals were used: $IrCl_3$.x H_2O (Heraeus), 2-phenylpyridine (Sigma-Aldrich), 4,7-diphenylphenanthroline

(Sigma-Aldrich). 2-(2,4-difluorophenyl)pyridine was synthesized as reported in the literature.[41]

For the preparation of the membranes, synthesized dyes were used as well as chloroform (Fluka), quinine sulphate (Fluka), polystyrene (Scientific Polymers, USA) and *o*-cyanophenyl octyl ether (from Fluka, puriss.). The gas flow-system was supplied by 50 L gas bottles at 200 bars with nitrogen 60 and oxygen 55 (both from Air Liquid, Spain).

1.2.2. Synthesis of Ir complexes.

[Ir(2,4-difluorophenylpyridine)$_2$-(4,4'-dimethylamino-2,2'-bipyridine)](PF_6) (N-969)[39] and [Ir(2-phenylpyridine)$_2$(4,7-diphenyl-1,10-phenanthroline)](PF_6) (N-1001)[40] were synthesized as described in the literature.

Based on the similar procedures, [Ir(2,4-difluorophenylpyridine)$_2$(4,7-diphenyl-1,10-phenanthroline)](PF_6) (N-1008) and [Ir(2-phenylpyridine)$_2$(4-bromo-2,2'-bipyridine)](PF_6) (N-1010) have been synthesized in a low boiling solvent, dichloromethane, by reaction of the corresponding dichloro-bridged iridium(III) dimer with 2.5 equivalents of 4,7-diphenyl-1,10-phenanthroline or 4-bromo-2,2'-bipyridine ligand, respectively.

Fig. 1 shows the chemical structures of the Ir(III) complexes and Electronic Supporting Information (ESI) shows the aromatic part of ^{1}H NMR spectrum of N-1008 and N-1010 in $CDCl_3$.

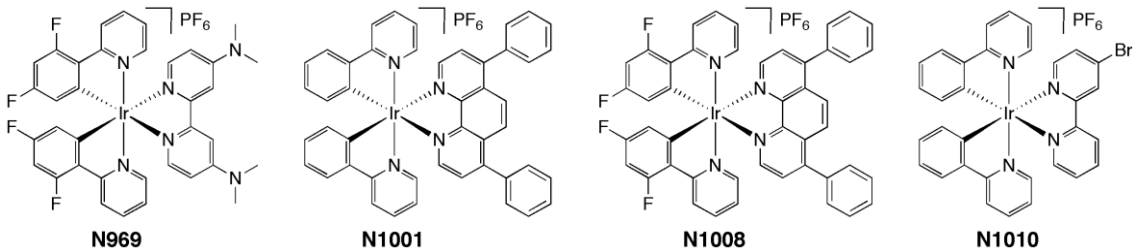

Fig. 1. Chemical structures of the Ir(III) complexes N-969, N-1001, N-1008 and N-1010

1.2.3. [Ir(2,4-difluorophenylpyridine)2(4,7-diphenyl-1,10-phenanthroline)](PF6) (N-1008).

Yield: 132 mg, 68%. Anal. Calcd for $C_{46}H_{28}F_{10}IrN_4P$: C, 52.62; H, 2.69; N, 5.34. Found: C, 52.84; H, 2.53; N, 5.37. ^{1}H NMR ($CDCl_3$): *d* 8.34-8.29 (4H, m), 8.18 (2H, s), 7.79 (2H, dt, *J* = 4.0, 0.8 Hz), 7.75 (2H, d, *J* = 5.2 Hz), 7.66-7.49 (12H, m), 7.10 (2H, dt, *J* = 7.6, 2.0 Hz), 6.62 (2H, ddd, *J* = 12.4, 9.2, 2.4 Hz), 5.81 (2H, dd, *J* = 8.4, 2.0 Hz). ES-MS *m/z* (calcd): 905.1668 (905.1879) $[M]^+$

1.2.4. [Ir(2-phenylpyridine)$_2$(4-bromo-2,2'-bipyridine)](PF$_6$) (N-1010).

Yield: 787 mg, 79%. Anal. Calcd for $C_{32}H_{23}BrF_6IrN_4P$: C, 43.64; H, 2.63; N, 6.36. Found: C, 43.79; H, 2.51; N, 6.37. ^{1}H NMR ($CDCl_3$): *d* 8.67 (1H, d, *J* = 1.6 Hz), 8.60 (1H, d, *J* = 8.4 Hz), 8.17 (1H, dt, *J* = 8.0, 1.6 Hz), 7.95-7.88 (3H, m), 7.77 (2H, dt, *J* = 8.4, 1.6 Hz), 7.73 (1H, d, *J* = 6.0 Hz), 7.68 (2H, ddd, *J* = 7.6, 2.8, 0.8 Hz), 7.59 (1H, d, *J* = 5.6 Hz), 7.53 (2H, m), 7.45 (1H, dt, *J* = 5.6, 1.2 Hz), 7.09 (2H, m), 7.03 (2H, tt, *J* = 7.6, 1.2 Hz), 6.91 (2H, dt, *J* = 7.6, 0.4 Hz), 6.27 (2H, ddd, *J* = 7.6, 4.4, 0.8 Hz). ES-MS *m/z* (calcd): 735.0544 (735.0735) $[M]^+$

1.2.5. Instrumentation

All luminescence measurements were carried out on a Varian Cary-Eclipse luminescence spectrometer equipped with a Xe flash lamp (peak power equivalent to 75 kW), Czerny-Turner monochromators, R-928 photomultiplier tube which is red sensitive (even 900 nm) with manual or automatic voltage.

For gas mixing, two mass flow controllers (MFC) of Type EL-FLOW® model F-201CV Bronkhorst High-Tech (Ruurlo, Netherlands) were used. After the MFCs, copper and stainless steel tubing was used to connect the MFC with the self-built flow-through cell.[19]

The system was controlled by Cary Eclipse software for Windows 95/98/NT which fully controls the luminescence spectrometer. The O_2-gas station was controlled by a self-written LabView 8.2 program connected to a Flow Bus interface (Bronkhosrt) that fully controls the Bronkhosrt mass-flow controllers via RS-232.

1.2.6. Preparation and characterization of oxygen sensing films

The nanostructured matrix was prepared by Ilford Imaging Switzerland following the procedure previously published.[17,19,20,21,22,23] The membrane used is called AP200/19 and it is based on aluminum oxide hydroxide coated by courting coating in PET, providing a positively charged nanostructured film with a pore diameter of 19 nm and a total pore volume of 20 mL/m^2.

The cocktails were prepared in sealable 4 mL flasks and then were filled up to 2 mL solution volume with chloroform (dye concentration of 1.5 mg mL^{-1}). **Table 2** shows the composition and the nomenclature of the different polystyrene cocktails, which were shaken on a Vortex-Genie® 2 (Scientific Industries, Bohemia, NY, USA) equipped with a home-made holder for multiple vials until all components were dissolved.

Table 2. Nomenclature and composition of the oxygen-sensitive membranes. PS, polystyrene; o-CPOE, o-cyanophenyl octyl ether

Name	wt. % PS	% Plasticizer	wt. % dye
PSOX	98.5	0	1.5
PS1X	90	8.5	1.5
PS2X	81	17.5	1.5

The membranes were obtained using a Laurell spin-coater model WS-400B-6NPP/LITE (North Wales, PA, USA). For polystyrene membranes, 200 µL of the cocktail was injected onto a rotating glass plate of a spinning device at 700 rpm. For the metal oxide, nanostructured membranes, 100 µL of the cocktail, containing only a solution of the dye, was injected onto the rotating metal oxide support fixed onto a spinning device at 300 rpm. Both, PS and AP200/19 membranes were transparent and allowed visible light to pass through. The resulting layers showed a thickness between 2 and 7 µm, depending on viscosity of the polymer mixture. Further optimization in thickness influence will have to be carried out for the corresponding application.

A standard protocol was used for characterizing the membranes. See **Table 3** for the standard settings. A time trace curve (see **Fig. 2**a) was used to recorder I_0 and I. To obtain the Stern-Volmer Plot (SVP), the oxygen partial pressures were calculated from the measured oxygen/nitrogen flows, assuming a constant environmental pressure of 1000 mbar. All the measurements were made at 10 different oxygen partial pressures between 0 and 0.1 bar and a room temperature of 21^o C (see Fig 2).

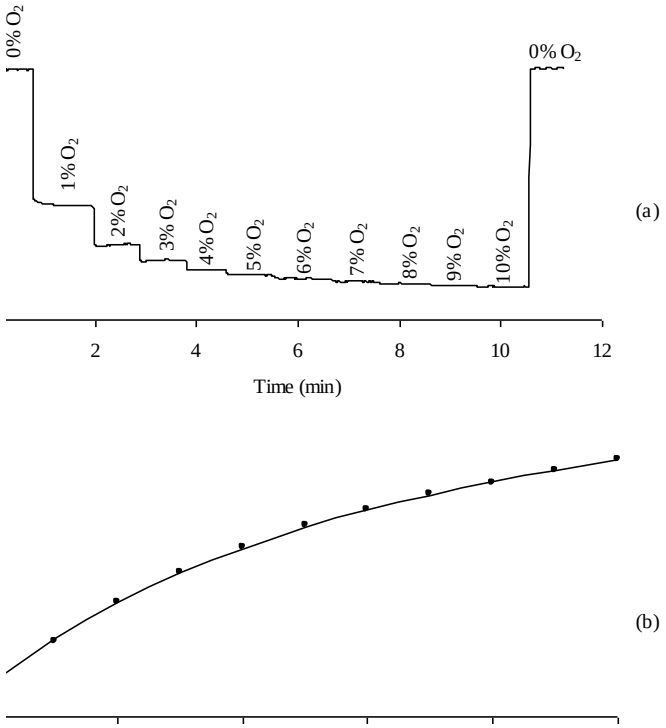

Fig. 2. a) Example of time trace curve for the PS0X membrane of N-1001. b) Stern-Volmer plot obtained for this membrane adjusting the data by Lehrer; [N-1001]=1.5 mg mL^{-1}; $\lambda_{exc/em}$=305/510 nm; slit $width_{exc/em}$=20/20 nm, t_d=120 μs and t_g=5 ms.

In addition, three replicas for each kind of membrane were prepared in order to evaluate the error. The experimental results were expressed as the average of 3 replicas ± error ($s \cdot t/\sqrt{n}$), where *s* is the standard deviation, *t* the student t and *n* the number of replicas.

1.3. Results and discussion

1.3.1. Spectroscopic behavior of the oxygen-sensitive material.

Full photophysical properties of the dyes N-969[39]and N-1001[40] have been previously described in the literature. UV-Visible absorption spectra for the four dyes in acetonitrile solution at 298 K display strong bands in the UV due to intraligand π-π* transitions and smaller bands in the visible due to metal-to-ligand charge-transfer (MLCT). When excited in acetonitrile solution within the MLCT absorption band, N-

1008 and N-1010 complexes show emission maxima at 538 and 624 nm respectively, with luminescence quantum yield of 0.73 and 0.05, respectively (see **Fig. 3**). The tuning of the emission maximum in the new dyes can be rationalized by taking into account the donor-acceptor character of the substituents and their impact on the HOMO and LUMO energy levels, as it is understood for other iridium complexes.[42] The blue shift of emission maximum observed in N1008 when compared to N1001 which has similar structure, is attributed to the addition of fluorine on the phenyl ring of the main ligand. Indeed, as in this type of complexes the HOMO orbital is mainly localized on this phenyl ring, the strong acceptor character of fluorine atoms stabilizes the HOMO energy level significantly more than the LUMO energy level, hence increasing the HOMO-LUMO gap. On the other hand, the red shift observed with N1010 when compared to the parent complex $Ir(2\text{-phenylpyridine})_2(bipyridine)^+$ which emits at 585 in acetonitrile[43] is attributed to the bromine substituent on the bipyridine ancillary ligand. As the LUMO orbital is mainly localized on the ancillary ligand in this type of complex, the acceptor character of the bromine stabilizes the LUMO energy level much more than the HOMO energy level, hence decreasing the HOMO-LUMO gap. The observed photoluminescence quantum yields in solution is tentatively explained by the energy gap law which states that the non-radiative decay rate increases exponentially as the emission energy decreases. An increase of the non-radiative decay rate induces a decrease of the photoluminescence quantum yield which is observed when going in order of decreasing emission energy from N969 to N1008 to N1001 to N1010 which emit at 463, 538, 605 and 634 with photoluminescence quantum yields of 0.85, 0.73, 0.53 and 0.05 respectively.

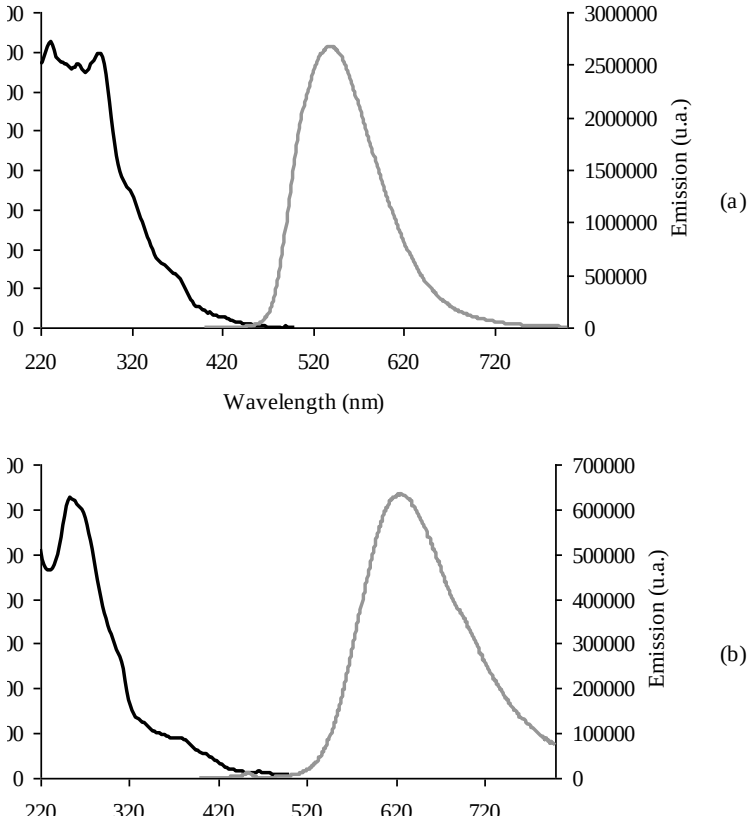

Fig.3. Absorption (black line) and emission (grey line) spectra in acetonitrile for the dye N-1008 (a) and the dye N-1010 (b)

Table 2 shows the composition and the terminology of the different sensing films studied, and **Table 3** shows the luminescence excitation and emission properties of the different sensing layers. In addition, **Table 3** also shows the luminescence quantum yield of the four Ir-complexes in solution and incorporated into the solid support. The luminescence quantum yields of the thin films were calculated according with reference [17] selecting 0.2 mg/L of quinine sulfate in sulfuric acid as reference, assuming a luminescence quantum yield of 0.54.[44]

Table 3.. Maximum luminescence excitation and emission wavelengths, $\lambda_{exc/em,}$ and luminescence quantum yield ($_{L,X}$) for the organometallic complexes dissolved in acetonitrile and incorporated into polystyrene (PS) and the metal oxide matrix AP200/19. ([dye]=1.5 mg mL^{-1}; monochromator slit $width_{exc/em}$=20/20 nm)

Dye	Solution		Membrane	$\lambda_{ex}/\lambda_{em}$ (nm)	Detector voltage (v)	$\Phi_{L,X}$[a]
	$\lambda_{ex}/\lambda_{em}$ (nm)	$\Phi_{L,X}$				
N969	380/463	0.85	PSOX PS1X PS2X	385/585	750	0.86±0.05
			AP200/19	350/490	590	
N1001	470/605	0.53	PSOX PS1X PS2X	300/530	800	0.64±0.05
			AP200/19	330/549	660	
N1008	400/538	0.73	PSOX PS1X PS2X	305/510	550	0.92±0.05
			AP200/19	340/512		
N1010	450/624	0.05	PSOX PS1X PS2X	300/520	770	0.14±0.05
			AP200/19	330/545		

[a] The luminescence quantum yields were calculated for the membrane PS0X according to reference 16 and the results are expressed as the average of three replicas ± st/√n (*n*=3, *t*=4.30 (2*P* = 0.05).

The incorporation of the dyes into a solid support generally increases the luminescence quantum yield compared to the solution. This is due to the more rigid environment in the solid support which decreases the non-radiative constant. A recent example shows this is very advantageous for iridium complexes used in light-emitting devices.[45]

For all the membranes, similar excitation and emission profiles were obtained (see Fig. 4a; Electronic Supporting Information (ESI) shows all the spectra for the four complexes immobilized in all the solid supports). For all of them, when molecular oxygen concentration is over 10%, the luminescence is completely quenched.

The different composition of the matrix has different impact on the aggregation behavior of the different dyes depending on their chemical structure. This hypothesis is further supported by the need of a two-site model most of the case (*vide infra*), which already requires dyes with at least two different environment, but not for N-1008 in the present work. Furthermore, the different emission maxima observed in matrices can be

in general explained by an expected difference in polarity of the medium. It is commonly known that emission maxima depends on polarity of the surrounding because in those complexes, emission is usually coming from Charge Transfer (CT) excited state[46] which energy level can be destabilized in non polar solvents (blue shift) and stabilized in polar solvents (red shift) in the case where the CT state has a higher dipole moment than the ground state. While it is expected that for the present complexes the emission is coming from a ^{3}MLCT state involving the ancillary bipyridine, further explanation requires quantitative knowledge about the type of CT state involved in the emission, implying the need for quantum chemical calculations which is out of the scope of the present paper. In all the cases the lifetime was lower than 50 μs; thus, it was not possible to measure the luminescence lifetime of the oxygen-sensitive membranes because the available instrumentation does not provide reliable data when the lifetime is lower than 50 μs.

1.3.2. Oxygen sensitive properties.

Luminescence quenching methods of analysis are based on the decrease in emission intensity in the presence of the quencher (oxygen), and are described by the Stern-Volmer equation (see equation 1)[14,17,19,21,25]

$$\frac{I_0}{I} = 1 + k_{SV}[O_2] \quad (1)$$

where I is the luminescence intensity, the subscript "0" refers to the value in the absence of quencher, k_{SV} is the Stern-Volmer constants and pO_2 is the partial pressure of oxygen. However, deviations have been observed, and these are often attributed to the heterogeneity of the media in which the dye is dispersed. In fact, only one of the dyes, N-1008, shows a linear SV plot when it is dissolved in PS with and without plasticizer.

The heterogeneity is attributed to different types of oxygen quenching sites within the matrix.[17,19,21] Therefore, this curvature of the Stern-Volmer plot needs a more complex model to be explained. In this case we obtained that the minimal model necessary to fit the experimental data was a two-site model. One of these models was proposed by Demas and co-workers, so called the Demas' model[47] (see equation 2):

$$\frac{I_0}{I} = \left[\frac{f_1}{1 + k_{SV1}[Q]} + \frac{f_2}{1 + k_{SV2}[Q]}\right]^{-1} \quad (2)$$

where f_i denotes the fractional contribution of the total luminescence emission from the luminophore located at site type i under unquenched conditions, which exhibit a discrete Stern-Volmer quenching constant given by k_{SVi}. Other two-site model was proposed by Lehrer[48] in which only one microenvironment is accessible to the quencher ($k_{SV,2}$=0; see equation 3)

$$\frac{I_0}{I} = \left[\frac{f}{1 + k_{SV}[Q]} + (1 - f)\right]^{-1} \quad (3)$$

where f_0 denotes the fraction of the total luminophore's population that is accessible to the quencher, and k_{SV} is the Stern-Volmer quenching constant which is associated with the accessible fraction of luminophores.

Practically in all the cases, except for the dye N-1008 incorporated into PS, the experimental results cannot be explained by a linear relationship, thus the two-site model has to be used to fit the experimental data (see **Fig. 2**). In addition, the fitting of the experimental data by using the Demas' model provides incorrect results; only Lehrer's model may be used to fit the experimental data. It means that the oxygen-sensitive nanostructured membranes are heterogenic which could explain the experimental results on AP200/19: the dye is located in two different environments, one which can be quenched by oxygen and another where oxygen is not able to quench it or has not access. Similar results with similar kind of complexes have been previously reported.[17,19,21] Another explanation could be based on dye aggregation effects which are more frequent on polymer films, providing similar results that when using nanostructured metal oxides. These hypotheses could explain why the Lehrer's model fits the experimental data.

Table 4 shows the k_{SV} for all the membranes. The analysis of the experimental results shows that the highest Stern-Volmer constant, k_{SV} equal to 2848 ± 101 bar^{-1}, corresponds to N-1001 incorporated into AP200/19. In general, the incorporation of the dyes into AP200/19 provides higher k_{SV} than within the PS-matrix. This effect of the AP200/19 matrix may rather be traced back to the capillary forces and the permeation of oxygen through the nanostructured matrix than to the chemical environment of the

pores. The metal oxide matrix is formed from agglomerated particles, where the nanopores are located inside while the macropores appear between agglomerated particles.[22] Since the capillary forces are high, the oxygen is quickly driven into the nanopores (pore diameter = 19 nm)[22] This structure was shown before to be responsible for the much higher sensitivity of different OMCs, Ru(II)- as well as a variety of iridium complexes (N-926, N-833 and N-837), to oxygen compared to the polystyrene matrix.[21]

Table 4. Oxygen sensitivity and $\Delta I_{1\%}$ of iridium(III) complexes incorporated into the AP200/19 and PS films ([dye]=1.5 mg mL^{-1}; slit width$_{exc/em}$=20/20 nm; t_d=120 µs; t_g=5 ms; for $\lambda_{exc/em}$ see Table 2).

Dye	Membrane	Lehrer's model [a]		$\Delta I_{1\%}$ [a] (%)	$p_{O_2}(S = ½)$
		K_{SV} (bar^{-1})	f_0		
N969	PSOX	358 ± 24	0.81 ± 0.02	79.66 ± 2.34	0.0045
	PS1X	87 ± 2	0.82 ± 0.01	52.32 ± 0.58	0.0180
	PS2X	53 ± 2[b]	1	41.63 ± 1.31	0.0189
	AP200/19	1231 ± 150	0.99 ± 0.00	93.13 ± 0.13	0.0008
N1001	PSOX	164 ± 11	0.92 ± 0.01	55.29 ± 2.40	0.0073
	PS1X	196 ± 32	0.95 ± 0.00	59.31 ± 8.34	0.0057
	PS2X	96 ± 11	0.97 ± 0.00	46.96 ± 2.62	0.0111
	AP200/19	2848 ± 101	0.78 ± 0.06	76.05 ± 5.73	0.0006
N1008	PSOX	72 ± 5[b]	1	40.96 ± 2.29	0.0139
	PS1X	34 ± 1[b]	1	27.48 ± 0.39	0.0294
	PS2X	28 ± 6[b]	1	25.46 ± 2.95	0.0357
	AP200/19	222 ± 8	0.96 ± 0.00	73.52 ± 2.54	0.0049
N1010	PSOX	313 ± 23	0.51 ± 0.03	38.97 ± 2.06	0.1597
	PS1X	103 ± 1	0.91± 0.00	54.35 ± 1.57	0.0118
	PS2X	113 ± 0	0.80 ± 0.10	48.05 ± 3.08	0.0147
	AP200/19	561 ± 112	0.21 ± 0.13	14.50 ± 2.82	-0.0031

[a] The experimental results have been expressed as the average of 3 replicas ± $s \cdot t / \sqrt{n}$ (n=3, t=4.30 (2P = 0.05)).
[b] Values obtained by a linear fitting

The results in **Table 4** also show that using the plasticizer (*o*-CPOE) decreases the k_{SV}. Medina-Castillo *et al*. have previously demonstrated that *o*-CPOE quenches the luminescence emission of the metal complex and thus reduces the fraction of the luminescent dye that is accessible for luminescence quenching by oxygen.[19]

Table 4 also shows the parameters $\Delta I_{1\%}$ and $p_{O_2}(S = ½)$ as rough guides to the sensitivity of the optical oxygen sensing films.

$p_{O_2}(S = ½)$ is defined as the value of the partial pressure of oxygen necessary to reduce the initial (oxygen free) luminescence exhibited by the film by 50%. From Equation 3 it follows that:

$$p_{O_2}(s = {}^1/_2) = \frac{1}{k_{SV}(2f_0 - 1)} \quad (4)$$

Table 4 shows that the incorporation of complexes into the nanostructured material provide lower $p_{O_2}(s = {}^1/_2)$ than when the same dyes are immobilized into PS (except for the dye N-1010); it means that the use of AP200/19 as solid support provide an increase on sensitivity. In addition, the lowest value of $p_{O_2}(s = {}^1/_2)$ is obtained by N-1001 immobilized in AP200/19 (0.0006). Therefore, it is possible to conclude that the most sensitive membrane consists on N-1001 immobilized on the metal oxide, nanostructured support, corroborating the conclusion carried out by analyzing the values of the Stern-Volmer constants.

$\Delta I_{1\%}$ is defined as the percentage of the luminescence quenched at 1% oxygen and it was calculated according to equation 5:

$$\Delta I_{1\%} = \frac{I_0 - I}{I_0} \times 100 \quad (5)$$

where $\Delta I_{1\%}$ is the percentage of luminescence quenched at 1% of oxygen, I_0 corresponds to the intensity of the film in absence of oxygen and I_1 is the intensity in the presence of a 0.01 bar (1%) of oxygen. Since the available instrumentation was not able to create flows below 1% O_2, the parameter $\Delta I_{1\%}$, were chosen to evaluate which membranes are expected to be more appropriate to be used for oxygen concentrations between 0 and 1%. This shows the ability of each sensing film to be used in applications that require the control of very low concentration of molecular oxygen, such as intelligent packaging or control of inert atmospheres, among others, although a deep study of sensitivity between 0 and 1% of oxygen should be carried out in further studies.

As can be seen in Table 4, the incorporation of complexes into the nanostructured material provide higher $\Delta I_{1\%}$ than when the same dyes are immobilized into PS (except for the dye N-1010); similar to $p_{O_2}(S = ½)$. In fact, the oxygen sensing film that show higher $\Delta I_{1\%}$, and therefore may be the most suitable for the uses mentioned above, is

prepared by the incorporation of the dye N-969 into AP200/19 (see **Fig. 4**). It shows a $\Delta I_{1\%}$ value of 93.13 ± 0.13 %. It can be also seen that, in general the addition of plasticizer to the cocktail composition decreases the $\Delta I_{1\%}$.

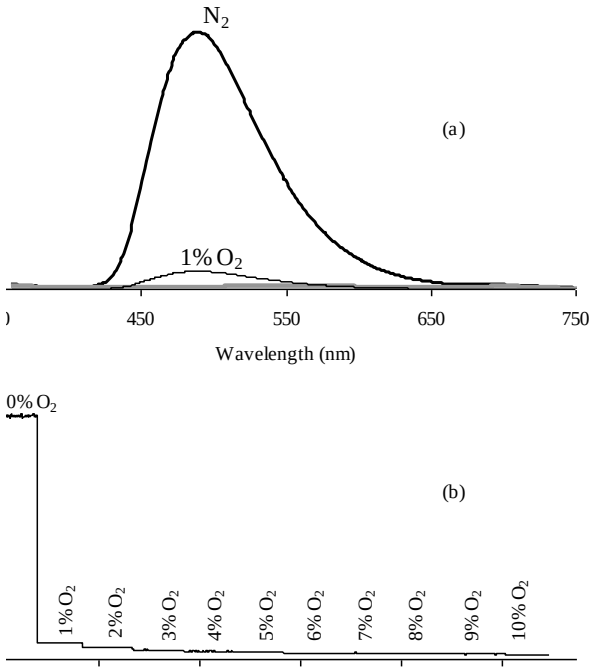

Fig. 4. . a) Emission spectra of N-969 incorporated into AP200/19 when in absence of oxygen (bold, black line), in presence of 1% oxygen (thin, black line) and with 10% of oxygen (grey line); b) Relative luminescence intensity of N-969 incorporated into AP200/19 at different concentration levels of O_2; [dye]=1.5 mg mL^{-1}; λ_{exc}=385 nm, monochromator slit width$_{exc/em}$=20/20 nm, t_d=120 µs; t_g=5 ms.

1.3.3. Reversibility, response time and long-term stability.

Fig. 2a shows the luminescence intensity of N-1001 membrane which varies with the partial pressure of oxygen. The complete reversibility of the luminescence emission of the oxygen-sensitive films allows to monitor an increasing and decreasing pO_2 continuously. The physico-chemical quenching reaction is a reversible process.

In addition, the oxygen-sensitive membranes show quick response times: the t_{95} response time for all of the studied sensing films were lower than 2 s when changing from 0 vol.% pO_2 to 1 vol.% pO_2, and lower than 4s when changing from 10 vol.% pO_2 to 0 vol.% pO_2.

Since their analytical performance (k_{SV}) did not change over 1 year storage under ambient conditions, the long-term stability of all the oxygen-sensitive membranes might be considered to be sufficiently good for measurements in the gas phase (see ESI). Furthermore, after excitation during 24 hours at the corresponding excitation wavelength, the sensitivity did not change, so the photochemical stability seems to be good for any further applications (see ESI).

1.4. Conclusions

The luminescent iridium-complexes N-969, N-1001, N-1008 and N-1010 were investigated in view of their application in oxygen-sensitive chemical sensors. The organometallic complexes were incorporated into a nanostructured metal oxide matrix as well as into a solvent polymeric polystyrene membrane and characterized in the gas phase for its response to oxygen. The films show one emission band which is quenched for oxygen concentrations over 10%.

The luminescence quantum yields were determined, resulting in a very high value for the dyes N-969 and N-1008. The most sensitive films is based on the dye N-1001 incorporated into AP200/19, showing a Stern-Volmer constant equal to 2848 ± 101 bar^{-1} and a $p_{O_2}(S = ½)$ equal to 0.0006. In addition, the parameter $\Delta I_{1\%}$ was evaluated in order to establish the most sensitive sensing films for controlling very low concentrations (lower than 1%) of molecular oxygen. In this case, the most sensitive film was the N-969 incorporated into AP200/19, with $\Delta I_{1\%}$ value of 93.13 ± 0.13 %, which is between 1.5 and 6 times higher than in other films.

An overview of luminescence probes used for analyzing oxygen shows that the dyes characterized in this work provide higher sensitivity, even for lower oxygen concentration, than the previously reported in the literature. When comparing these dyes with N-833, N-837, N-926[17] and N-948[19] supported into PS, it can be noticed than for similar quantum yields, in most of the membranes, the values of the Stern-Volmer constants are over 100 times higher; even when comparing these dyes into the nanostructured support[19,20] for a 10 times lower oxygen concentrations, values of K_{sv} are between 10 and 100 times higher. Unfortunately, no satisfying trend can be observed at the moment between sensing performances of the films and properties of the dyes in solution, which would be of great help for designing further improved sensing dyes. A

first reason is due to the different photophysical properties of dyes in solution compared to dyes in a solid matrix. Second, it is likely that the composition of the matrix has an impact on the aggregation behavior of the dyes. The observed oxygen sensing performances are the result of an interplay between intrinsic dyes performances, dyes aggregation behavior and film morphology. Conclusions can be made only on the films performances as a whole, not on a single factor.

Finally, the transparent oxygen-sensitive films show complete reversibility with short response times and very long-term stability, higher than 1 year.

Acknowledgment. The authors gratefully acknowledge the financial support of the Junta de Andalucía (Excellence Project FQM-02625 and Marín-SuárezdelToro's grant). Also, the authors are grateful to Ilford Imaging Switzerland GmbH (Switzerland) for supplying the metal oxide membranes and Dr. de la Torre-Vega and Ing. Rodriguez-Medina for automating the O_2-gas station.

Referencias

1. Stein, E. W.; Grant, P. S.; Zhu, H.; McShane, M. J., Microscale enzymatic optical biosensors using mass transport limiting nanofilms. 1. Fabrication and characterization using glucose as a model analyte. *Analytical Chemistry* **2007,** 79, (4), 1339-1348.
2. Park, E. J.; Reid, K. R.; Tang, W.; Kennedy, R. T.; Kopelman, R., Ratiometric fiber optic sensors for the detection of inter- and intra-cellular dissolved oxygen. *Journal of Materials Chemistry* **2005,** 15, (27-28), 2913-2919.
3. Rumsey, W. L.; Vanderkooi, J. M.; Wilson, D. F., Imaging of phosphorescence: A novel method for measuring oxygen distribution in perfused tissue. *Science* **1988,** 241, (4873), 1649-1651.
4. O'Mahony, F. C.; O'Riordan, T. C.; Papkovskaia, N.; Ogurtsov, V. I.; Kerry, J. P.; Popkovsky, D. B., Assessment of oxygen levels in convenience-style muscle-based sous vide products through optical means and impact on shelf-life stability. *Packaging Technology and Science* **2004,** 17, (4), 225-234.
5. Mills, A., Oxygen indicators and intelligent inks for packaging food. *Chemical Society Reviews* **2005,** 34, (12), 1003-1011.

6. O'Riordan, T. C.; Voraberger, H.; Kerry, J. P.; Papkovsky, D. B., Study of migration of active components of phosphorescent oxygen sensors for food packaging applications. *Analytica Chimica Acta* **2005,** 530, (1), 135-141.
7. F.A. Rainey, A. O., *Extremophiles* Academic Press: Amsterdam 2006.
8. Soliva-Fortuny, R. C.; Martín-Belloso, O., New advances in extending the shelf-life of fresh-cut fruits: a review. *Trends in Food Science & Technology* **2003,** 14, (9), 341-353.
9. K. Palmer-Wright, A. A. K., *Postharvest Biol. Technol.* **1997,** 10 89–97.
10. Fonseca, S. C.; Oliveira, F. A. R.; Brecht, J. K.; Chau, K. V., Influence of low oxygen and high carbon dioxide on shredded Galega kale quality for development of modified atmosphere packages. *Postharvest Biology and Technology* **2005,** 35, (3), 279-292.
11. Vilas-Boas, E. V. d. B.; Kader, A. A., Effect of atmospheric modification, 1-MCP and chemicals on quality of fresh-cut banana. *Postharvest Biology and Technology* **2006,** 39, (2), 155-162.
12. Gorny, J. R.; Hess-Pierce, B.; Cifuentes, R. A.; Kader, A. A., Quality changes in fresh-cut pear slices as affected by controlled atmospheres and chemical preservatives. *Postharvest Biology and Technology* **2002,** 24, (3), 271-278.
13. F. Carlin, C. N., Y. Chambroy, M. Reich, *Int. J. Food Sci. Technol.,* **1990,** 25, 110–119.
14. Orellana, G., Luminescent optical sensors. *Analytical and Bioanalytical Chemistry* **2004,** 379, (3), 344-346.
15. Kocincova, A. S.; Borisov, S. M.; Krause, C.; Wolfbeis, O. S., Fiber-optic microsensors for simultaneous sensing of oxygen and pH, and of oxygen and temperature. *Analytical Chemistry* **2007,** 79, (22), 8486-8493.
16. Hakonen, A.; Hulth, S., A high-precision ratiometric fluorosensor for pH: Implementing time-dependent non-linear calibration protocols for drift compensation. *Analytica Chimica Acta* **2008,** 606, (1), 63-71.
17. Fernandez-Sanchez, J. F.; Roth, T.; Cannas, R.; Nazeeruddin, M. K.; Spichiger, S.; Graetzel, M.; Spichiger-Keller, U. E., Novel oxygen sensitive complexes for optical oxygen sensing. *Talanta* **2007,** 71, (1), 242-250.
18. Wolfbeis, O. S., Materials for fluorescence-based optical chemical sensors. *Journal of Materials Chemistry* **2005,** 15, (27-28), 2657-2669.
19. Medina-Castillo, A. L.; FernÃ¡ndez-SÃ¡nchez, J. F.; Klein, C.; Nazeeruddin, M. K.; Segura-Carretero, A.; FernÃ¡ndez-GutiÃ©rrez, A.; Graetzel, M.; Spichiger-Keller, U. E., Engineering of efficient phosphorescent iridium cationic complex for developing oxygen-sensitive polymeric and nanostructured films. *Analyst* **2007,** 132, (9), 929-936.

20. Fernández-Sánchez, J. F.; Nezel, T.; Steiger, R.; Spichiger-Keller, U. E., Novel optical NO2-selective sensor based on phthalocyaninato-iron(II) incorporated into a nanostructured matrix. *Sensors and Actuators B: Chemical* **2006,** 113, (2), 630-638.
21. Fernández-Sánchez, J. F.; Cannas, R.; Spichiger, S.; Steiger, R.; Spichiger-Keller, U. E., Novel nanostructured materials to develop oxygen-sensitive films for optical sensors. *Analytica Chimica Acta* **2006,** 566, (2), 271-282.
22. R. Steiger, R. B., J.F. Fernandez-Sanchez, U.E. Spichiger-Keller, *Solid State Phenom.,* **2007,** 121–123, 1193–1197.
23. Fernández-Sánchez, J. F.; Fernández, I.; Steiger, R.; Beer, R.; Cannas, R.; Spichiger-Keller, U. E., Second-generation nanostructured metal oxide matrices to increase the thermal stability of CO and NO 2 sensing layers based on iron(II) phthalocyanine. *Advanced Functional Materials* **2007,** 17, (7), 1188-1198.
24. A. Gomez-Henz, M. P. A.-C., *Trends Anal. Chem.,* **2004,** 23, 127–136.
25. G. Orellana, D. G.-F., Springer: Berlin/Heidelberg, Germany, 2004.
26. Costa Fernández, J. M.; Sanz Medel, A., *Fosforescencia molecular analítica: una aproximación práctica.* . Universidad de Granada: 2001.
27. Sanchez-Barragan, I.; Costa-Fernandez, J. M.; Sanz-Medel, A.; Valledor, M.; Campo, J. C., Room-temperature phosphorescence (RTP) for optical sensing. *TrAC Trends in Analytical Chemistry* **2006,** 25, (10), 958-967.
28. Borisov, S. M.; Klimant, I., Ultrabright oxygen optodes based on cyclometalated iridium(III) coumarin complexes. *Analytical Chemistry* **2007,** 79, (19), 7501-7509.
29. Wu, X.; Song, L.; Li, B.; Liu, Y., Synthesis, characterization, and oxygen sensing properties of Ru(II) complex covalently grafted to mesoporous MCM-41. *Journal of Luminescence* **2010,** 130, (3), 374-379.
30. Chu, B. W. K.; Yam, V. W. W., Sensitive single-layered oxygen-sensing systems: Polypyridyl ruthenium(II) complexes covalently attached or deposited as langmuir-blodgett monolayer on glass surfaces. *Langmuir* **2006,** 22, (17), 7437-7443.
31. Lei, B.; Li, B.; Zhang, H.; Lu, S.; Zheng, Z.; Li, W.; Wang, Y., Mesostructured silica chemically doped with RuII as a superior optical oxygen sensor. *Advanced Functional Materials* **2006,** 16, (14), 1883-1891.
32. Zhang, H.; Li, B.; Lei, B.; Li, W., Oxygen-sensing materials based on [Ru(bpy)3]2+ covalently grafted MSU-3 mesoporous molecular sieves. *Journal of Luminescence* **2008,** 128, (8), 1331-1338.

33. Kim, H. J.; Jeong, Y. C.; Rhee, J. I., Encapsulation of tris(4,7-diphenyl-1,10-phenanthroline)ruthenium(II) complex linked with dendrons in sol-gels: Stable optical sensing membranes for dissolved oxygen. *Talanta* **2008,** 76, (5), 1070-1076.

34. Wu, X.; Cong, Y.; Liu, Y.; Ying, J.; Li, B., Luminescence and oxygen sensing properties of ORMOSILs covalently grafted with a novel ruthenium(II) complex. *Journal of Sol-Gel Science and Technology* **2009,** 49, (3), 355-363.

35. Payne, S. J.; Fiore, G. L.; Fraser, C. L.; Demas, J. N., Luminescence oxygen sensor based on a ruthenium(II) star polymer complex. *Analytical Chemistry* **2010,** 82, (3), 917-921.

36. Xie, Z.; Ma, L.; DeKrafft, K. E.; Jin, A.; Lin, W., Porous phosphorescent coordination polymers for oxygen sensing. *Journal of the American Chemical Society* **2009,** 132, (3), 922-923.

37. Mak, C. S. K.; Penflehner, D.; Stich, M.; Wolfbeis, O. S.; Chan, W. K.; Yersin, H., Exceptional oxygen sensing capabilities and triplet state properties of Ir(ppy-NPh2)3. *Chemistry of Materials* **2009,** 21, (11), 2173-2175.

38. Carlson, B.; Eichinger, B. E.; Kaminsky, W.; Phelan, G. D., Organometallic osmium and iridium complexes as phosphorescent dye in barometric sensitive coatings. *Sensors and Actuators B: Chemical* **2010,** 145, (1), 278-284.

39. De Angelis, F.; Fantacci, S.; Evans, N.; Klein, C.; Zakeeruddin, S. M.; Moser, J. E.; Kalyanasundaram, K.; Bolink, H. J.; GrÃ¤tzel, M.; Nazeeruddin, M. K., Controlling phosphorescence color and quantum yields in cationic iridium complexes: A combined experimental and theoretical study. *Inorganic Chemistry* **2007,** 46, (15), 5989-6001.

40. Bolink, H. J.; Cappelli, L.; Coronado, E.; GrÃ¤tzel, M.; OrtÃ-, E.; Costa, R. D.; Viruela, P. M.; Nazeeruddin, M. K., Stable single-layer light-emitting electrochemical cell using 4,7-diphenyl-1,10-phenanthroline-bis(2-phenylpyridine)iridium(III) hexafluorophosphate. *Journal of the American Chemical Society* **2006,** 128, (46), 14786-14787.

41. Lohse, O.; Thevenin, P.; Waldvogel, E., The palladium catalysed Suzuki coupling of 2- and 4-chloropyridines. *Synlett* **1999**, (1), 45-48.

42. Baranoff, E.; Yum, J.-H.; Graetzel, M.; Nazeeruddin, M. K., Cyclometallated iridium complexes for conversion of light into electricity and electricity into light. *Journal of Organometallic Chemistry* **2009,** 694, (17), 2661-2670.

43. Costa, R. D.; Orta, E.; Bolink, H. J.; Graber, S.; Schaffner, S.; Neuburger, M.; Housecroft, C. E.; Constable, E. C., Archetype cationic iridium complexes and their use in solid-state light-emitting electrochemical cells. *Advanced Functional Materials* **2009,** 19, (21), 3456-3463.

44. Melhuish, W. H., Quantum efficiencies of fluorescence of organic substan ces: Effect of solvent and concentration of the fluorescent solute. *Journal of Physical Chemistry* **1961,** 65, (2), 229-235.

45. Baranoff, E.; Suarez, S.; Bugnon, P.; Bolink, H. J.; Klein, C.; Scopelliti, R.; Zuppiroli, L.; GrÃ¤tzel, M.; Nazeeruddin, M. K., An ester-substituted iridium complex for efficient vacuum-processed organic light-emitting diodes. *ChemSusChem* **2009,** 2, (4), 305-308.

46. Flamigni, L.; Barbieri, A.; Sabatini, C.; Ventura, B.; Barigelletti, F., Photochemistry and photophysics of coordination compounds: Iridium. In *Topics in Current Chemistry*, 2007; Vol. 281, pp 143-203.

47. J.N. Demas, B. A. D., *Sens. Actuators B* **1991,** 11, 35–41.

48. Lehrer, S. S., Solute perturbation of protein fluorescence. The quenching of the tryptophyl fluorescence of model compounds and of lysozyme by iodide ion. *Biochemistry* **1971,** 10, (17), 3254-3263.

Supporting Information (SI)

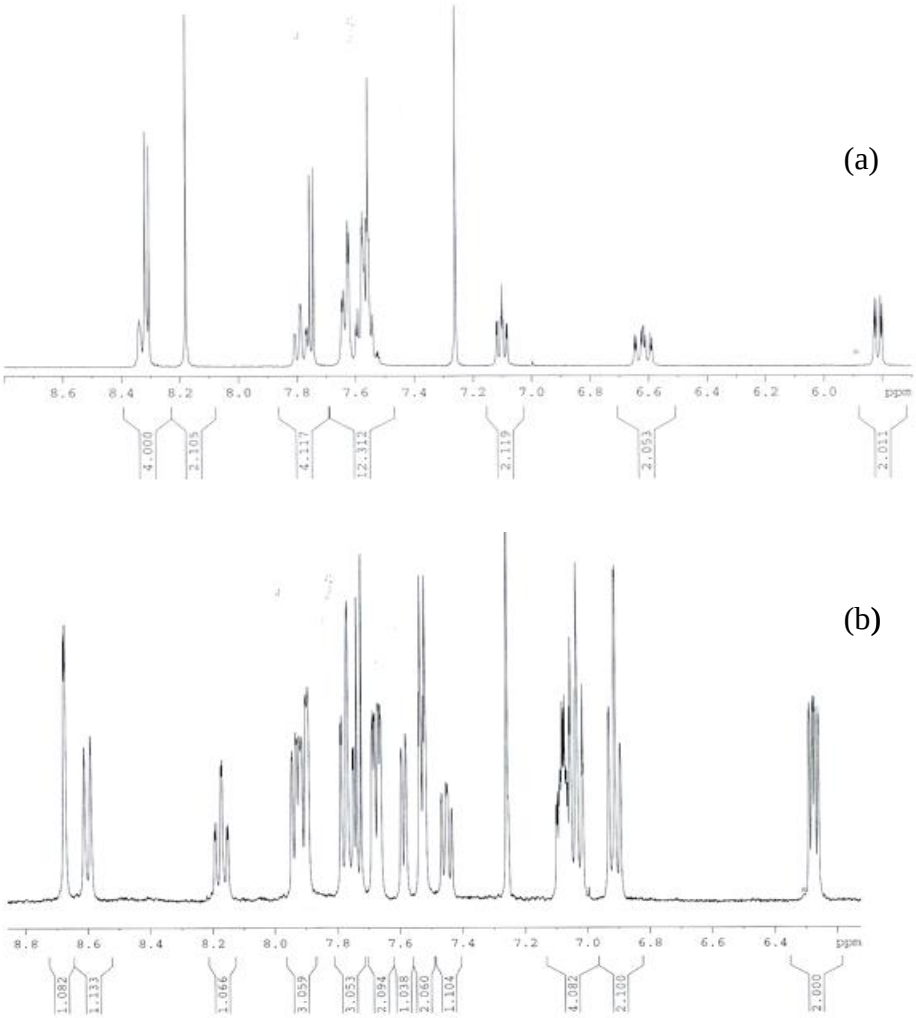

Fig. ESI-1. Aromatic part of the ^{1}H NMR spectrum of N-1008 (a) and N-1010 (b) in $CDCl_3$

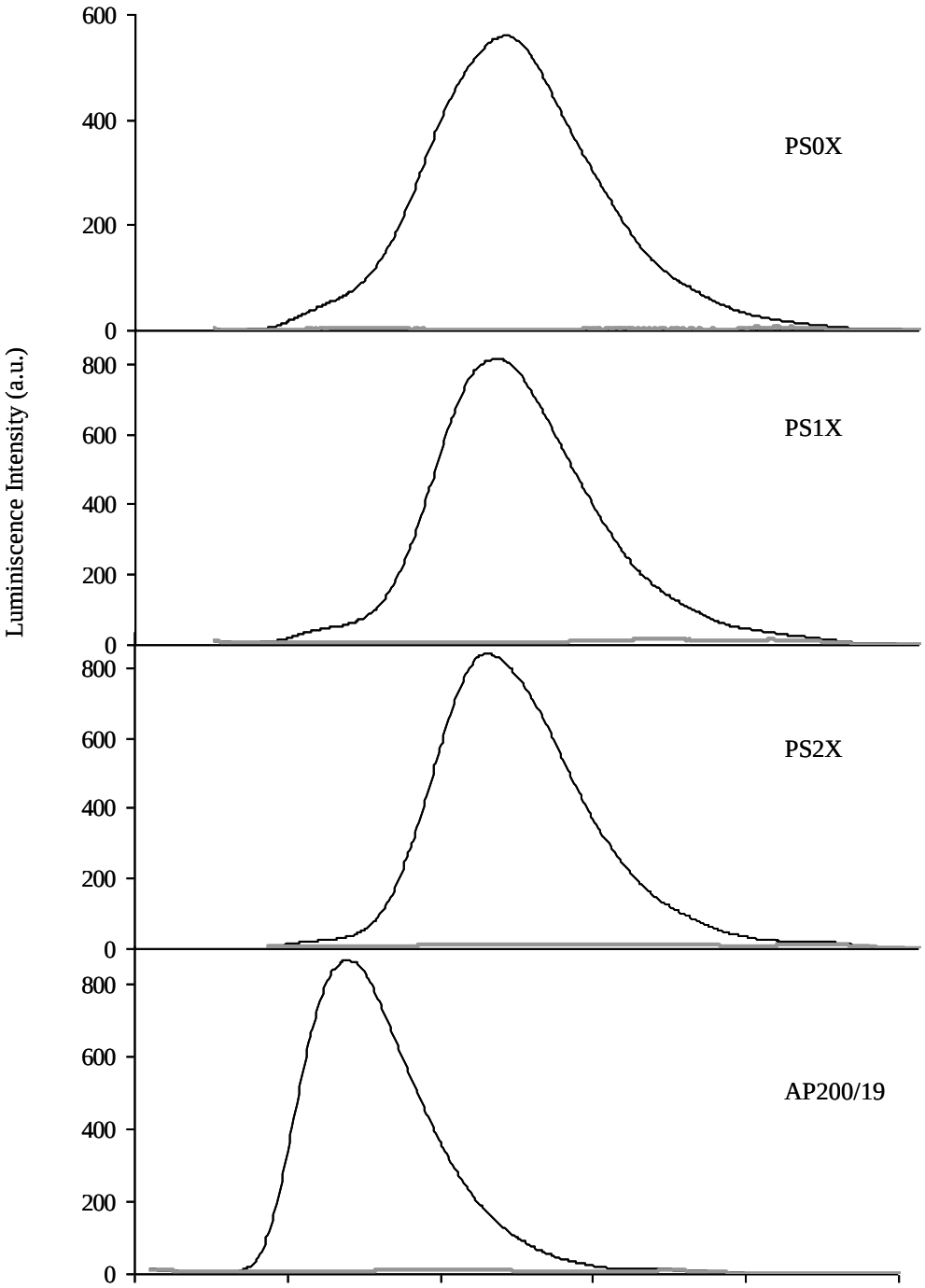

Fig. ESI-2. Emission spectra of N-969 incorporated into PS membranes (λ_{exc}=385 nm) and AP200/190 (λ_{exc}=350 nm) in absence of oxygen (black line) and with 10% of oxygen (grey line) ([dye]=1.5 mg mL^{-1}; monochromator slit $width_{exc/em}$=20/20 nm, t_d=120 µs; t_g=5 ms).

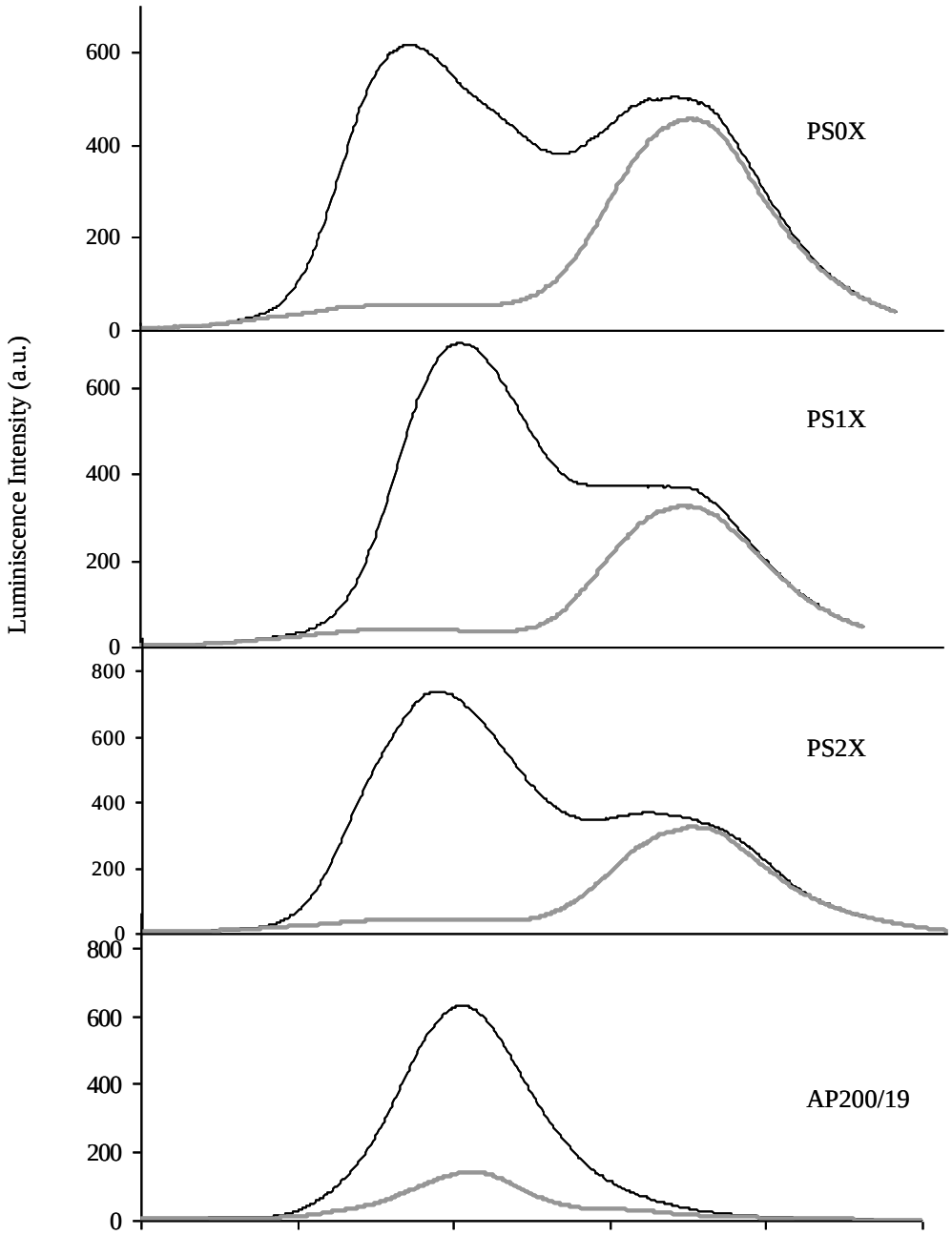

Fig. ESI-3. Emission spectra of N-1001 incorporated into PS membranes (λ_{exc}=300 nm) and AP200/190 (λ_{exc}=330 nm) in absence of oxygen (black line) and with 10% of oxygen (grey line) ([dye]=1.5 mg mL^{-1}; monochromator slit $width_{exc/em}$=20/20 nm, t_d=120 µs; t_g=5 ms).

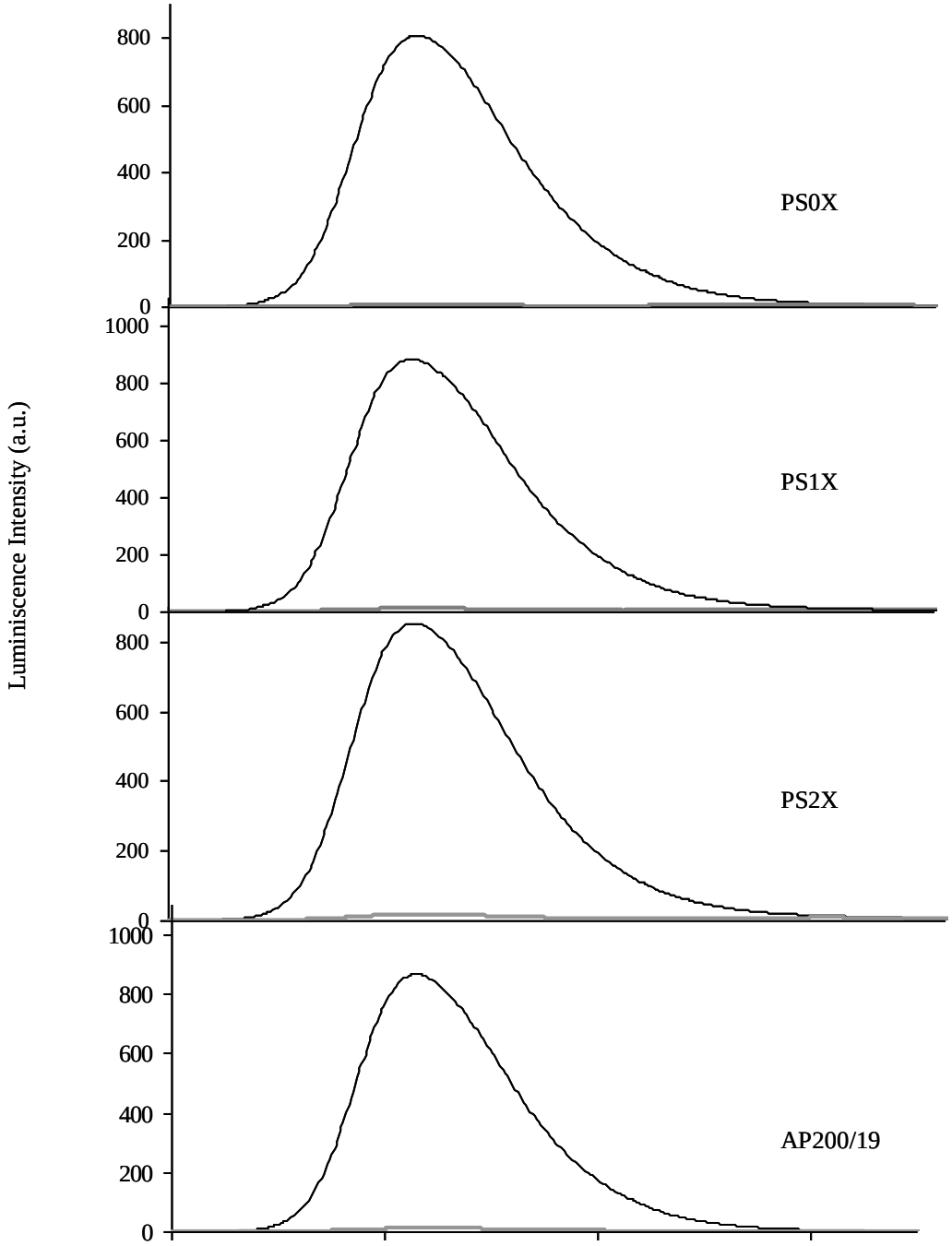

Fig. ESI-4. Emission spectra of N-1008 incorporated into PS membranes (λ_{exc}=305 nm) and AP200/190 (λ_{exc}=340 nm) in absence of oxygen (black line) and with 10% of oxygen (grey line) ([dye]=1.5 mg mL^{-1}; monochromator slit $width_{exc/em}$=20/20 nm, t_d=120 µs; t_g=5 ms).

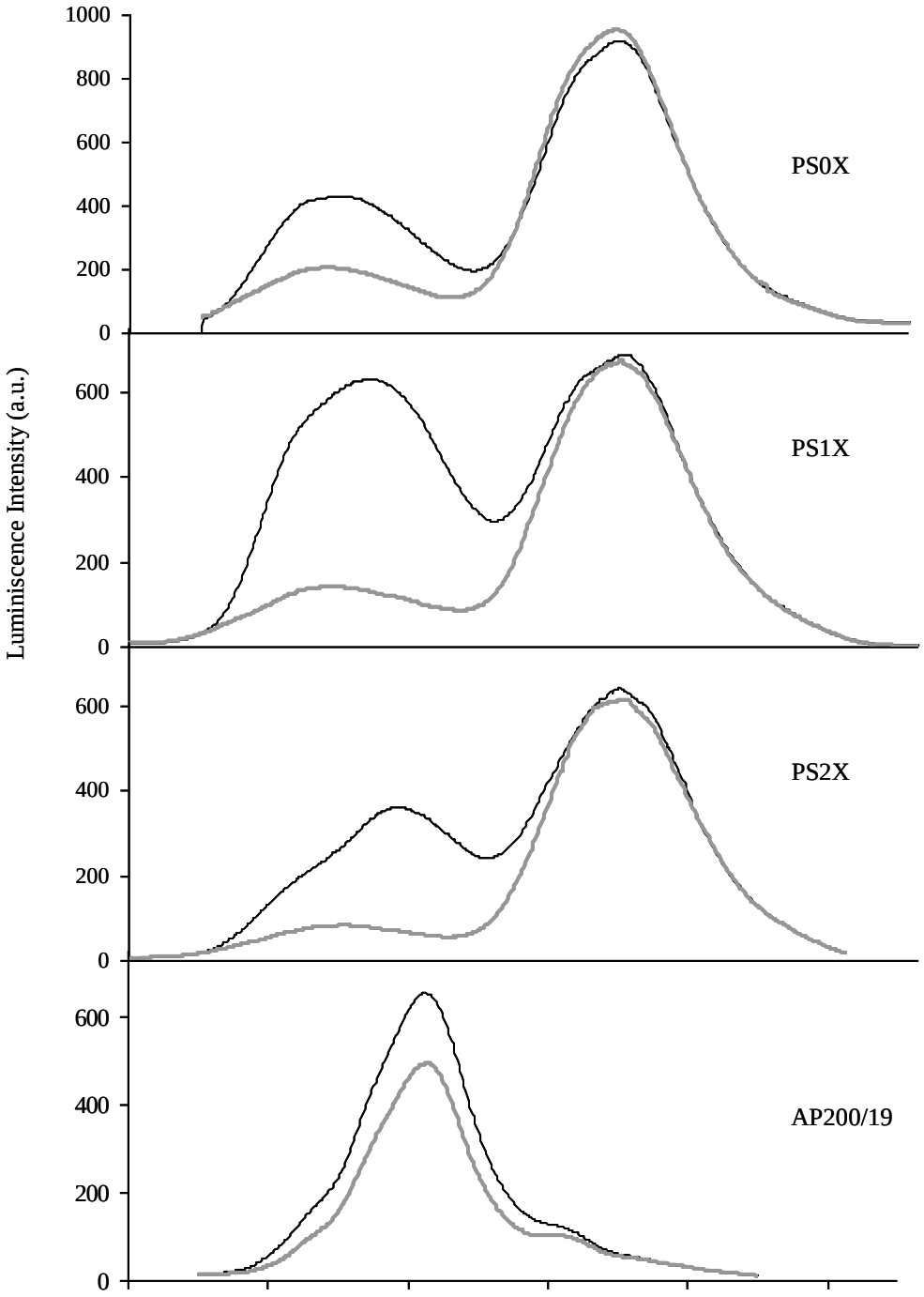

Fig. ESI-5. Emission spectra of N-1010 incorporated into PS membranes (λ_{exc}=300 nm) and AP200/190 (λ_{exc}=330 nm) in absence of oxygen (black line) and with 10% of oxygen (grey line) ([dye]=1.5 mg mL^{-1}; monochromator slit $width_{exc/em}$=20/20 nm, t_d=120 µs; t_g=5 ms).

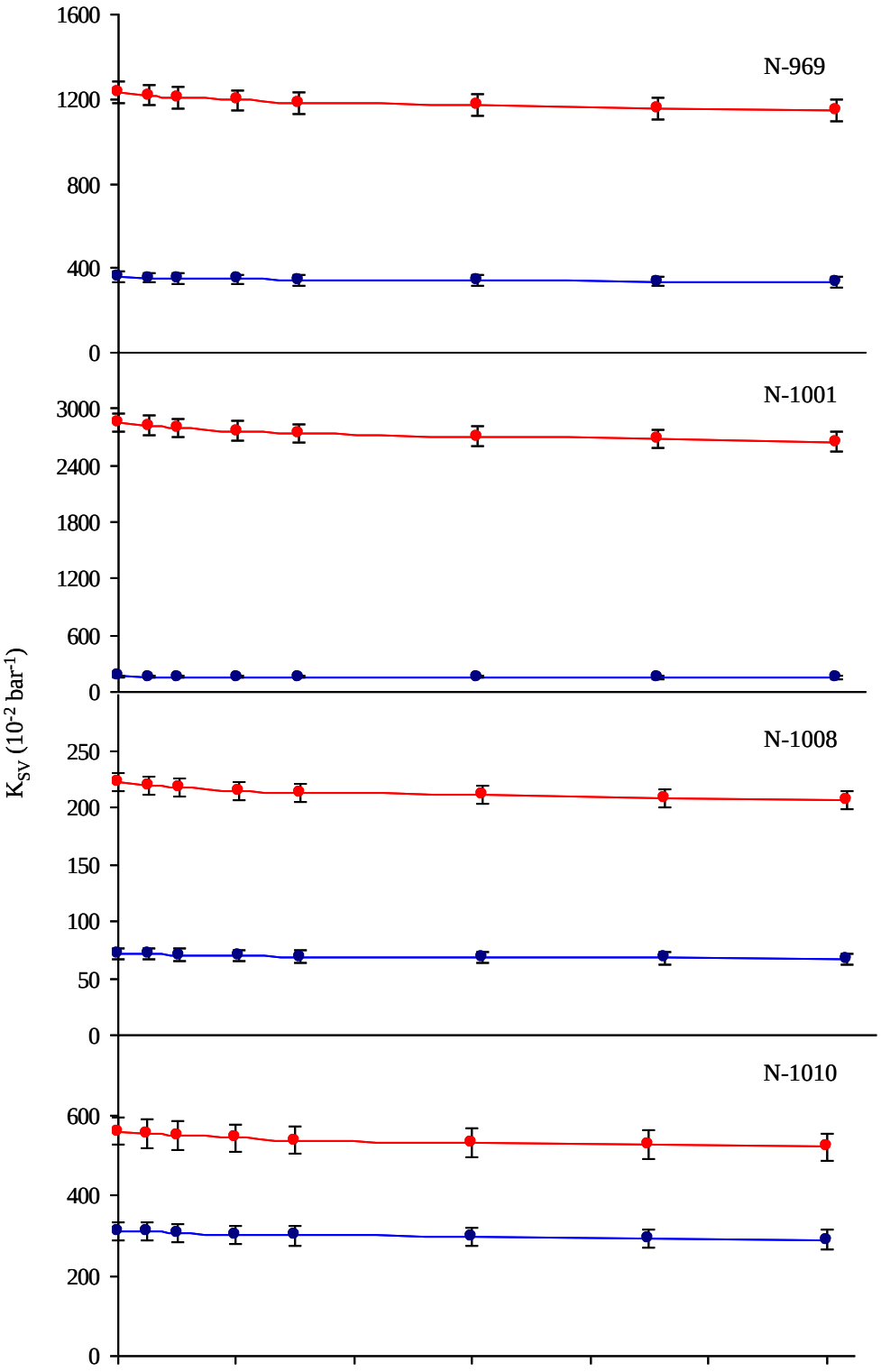

Fig. ESI-6. Variation of the Stern-Volmer constant versus time when the membranes (PS0X and AP200/19) were stored in absence of light at room temperature for one year.

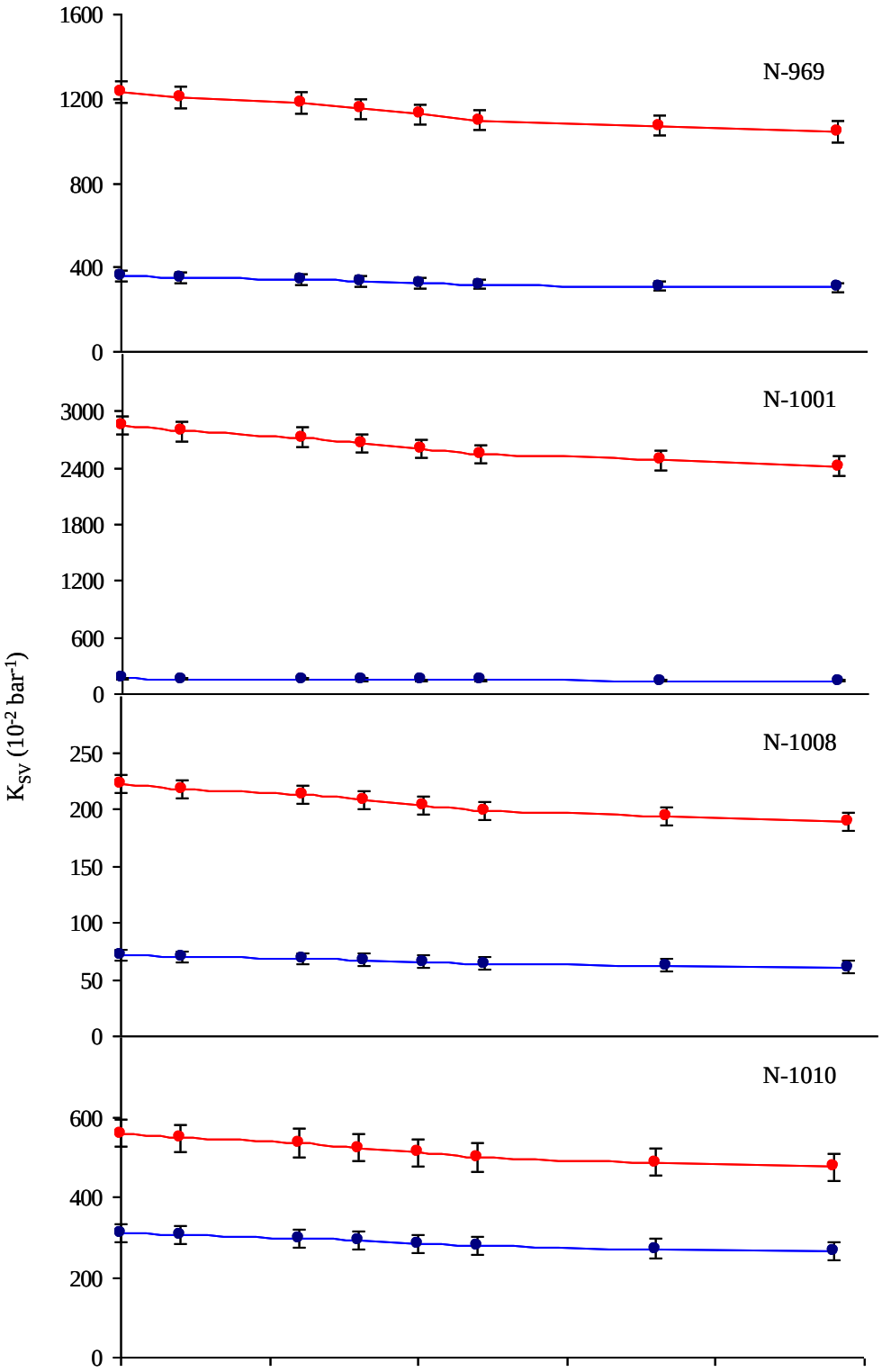

Fig. ESI-7. Variation of the Stern-Volmer constant versus time when the membranes (PS0X and AP200/19) were continuously excited during 24h with their excitation wavelength at room temperature, with a Xe lamp of 75 kW.

Capítulo 2

Nanocomposites containing neutral blue emitting cyclometalated iridium(III) emitters for oxygen sensing

Marta Marín-Suárez,[a] Basile F. E. Curchod,[b] Ivano Tavernelli,[b] Ursula Rothlisberger,[b] Rosario Scopelliti,[c] Jung Il,[c] Davide Di Censo,[c] Michael Grätzel,[c] Jorge Fernando Fernández-Sánchez,*[,a] Alberto Fernández-Gutiérrez,[a] Md. Khaja Nazeeruddin,[c] and Etienne Baranoff,*[,d,c]

[a] *Department of Analytical Chemistry, Faculty of Sciences, University of Granada, E-18071 Granada, Spain*

[b] *Laboratory of Computational Chemistry and Biochemistry, École Polytechnique Fédérale de Lausanne, CH-1015 Lausanne, Switzerland*

[c] *Laboratory of Photonics and Interfaces, École Polytechnique Fédérale de Lausanne, CH-1015 Lausanne, Switzerland*

[d] *School of Chemistry, University of Birmingham, Edgbaston, B15 2TT, England*

Abstract. The behavior towards oxygen sensing of nanocomposites made of the aluminum oxide-hydroxide nanostructured solid support (AP200/19) and neutral blue emitting cyclometalated iridium(III) complexes was studied. The results are compared with the same dyes immobilized in polystyrene films. Since the photo-luminescence of the complexes is totally quenched for oxygen concentrations just over 10%, these systems using the blue region of the visible spectrum are promising for oxygen detection at low concentration. In particular, dyes supported into the AP200/19 provide the best sensitivity to oxygen concentration, with the possibility to detect oxygen below 1% O_2 in gas (0.01 bar).

Keywords: cyclometalated iridium(III) complexes, phosphorescence, oxygen sensing, nanostructured films; **Corresponding authors*: jffernan@ugr.es, e.baranoff@bham.ac.uk

2.1. Introduction

Molecular oxygen plays an important role in life, since it is present in a variety of chemical reactions, not only as a reactant but also as a product. Although the detection of oxygen is well known, in recent years optical oxygen sensing has attracted a lot of scientific attention as the dynamic quenching of the luminescence emission by oxygen has proved to be a very sensitive technique.[1] Optical oxygen sensors are based on luminescent dyes whose fluorescence or phosphorescence is quenched by molecular oxygen. This process takes advantage of the excited state properties of the dyes, and therefore, the effects of quenchers on intensity and decay time are non-destructive and fully reversible, allowing the continuous monitoring of oxygen.[1] Since nowadays it is paramount to develop methods for monitoring oxygen concentration in real time, optical sensors have become very popular in many fields related to industry, medicine and environment.[2-9]

The quenching of an excited state by oxygen can occur through two mechanisms: electron transfer and energy transfer. In both cases, a long excited state lifetime will favor the process, enhancing the material oxygen sensing ability. In this respect, phosphorescent transition metal complexes are very appealing due to both their excited state lifetime on the microsecond time-scale and the triplet character of their emission, which increases the sensitivity to oxygen. Furthermore, cyclometalated iridium(III) complexes are attracting particular interest due to their generally high photoluminescence quantum yield and unique capability to have emission tuned over the entire visible spectrum.[10-12] Thus, in addition of their good chemical, photo- and electrochemical stability, cyclometalated iridium(III) complexes are an important class of dyes for oxygen sensing.[5, 13-18] To date, all cyclometalated iridium(III) dyes used for oxygen sensing are red or green emitters. However, the ability of these complexes to have emission color tuned over the entire visible spectrum is attractive for developing oxygen sensitive blue dyes, with enhanced sensitivity and quantum yield which improves the efficiency of the devices. In addition, having optical sensors in the entire region of the visible spectrum would increase the sensor performance when natural red emitters are present in the media or in order to perform dual optical measurements[9, 18, 19] and colorimetric sensing.[20]

An important component of an oxygen sensor is the matrix in which the emitting dyes are immobilized. The matrix materials impact the sensing ability mainly in two ways: first by the permeability to oxygen, which allows for fast diffusion of oxygen to the emitting molecules for quenching; second by their chemical nature leading to different aggregation of the dyes resulting in different accessibility of the dyes by oxygen. The aluminum oxide-hydroxide nanostructured solid support AP200/19 has recently shown very good performances for oxygen sensing using charged bis-cyclometalated iridium(III) complexes.[16, 17] Herein we report on the use of neutral blue phosphorescent iridium(III) complexes immobilized in AP200/19. In addition of providing oxygen sensing in the blue region of the visible spectrum, it is the first evaluation of neutral dyes with the AP200/19 matrix.

First, we briefly describe the synthesis, characterization, and theoretical calculation rationalizing the properties of the new dyes. To obtain emission in the blue region, we developed new phosphorescent emitters using ester and trifluoromethyl ketone groups. The trifluoromethyl ketone was expected to lead to deeper blue and high solubility while the ester would be an interesting group for future grafting of the dyes onto specific substrates through carboxylic acid attachment to an inorganic material. Secondly, we evaluated the oxygen sensing properties of the dyes by their physical immobilization in a matrix. For this evaluation, two types of matrices were selected: a classical polystyrene membrane and the novel aluminum oxide-hydroxide nanostructured matrix, AP200/19. Polystyrene films show different compatibility with dyes depending on their polarity and they provide good permeability to oxygen while preventing other quenchers to interacts with the dye.[13] The metal oxide matrix is expected to provide a better sensitivity by driving the oxygen into the nanopores and isolating the dyes from each other.[15] The influence of plasticizer on the sensing ability of the polymeric film was analyzed and compared to the positively charged nanostructure which has been never used in combination with non-charged complexes.

Scheme 1. Synthetic path for blue emitting dyes.

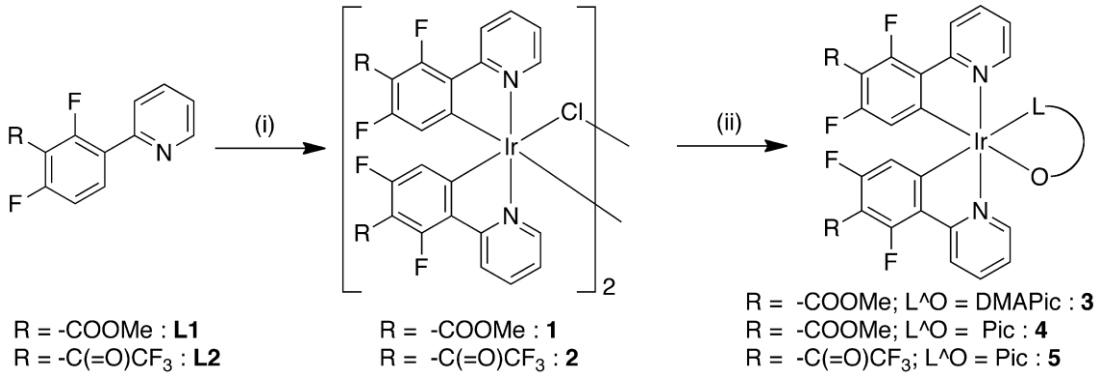

(i) **L1:** $IrCl_3$, x·H_2O, 2-ethoxyethanol/H_2O, 125 °C, 18 hrs; **L2**: $IrCl_3$, x·H_2O, 2-ethoxyethanol, 125 °C, 18 hrs;
(ii) DMAPic = 4-N,N-dimethylaminopicolinic acid or Pic = picolinic acid, TBAOH, CH_2Cl_2, 40 °C, 12 hrs.

2.2. Experimental section

2.2.1. Materials and methods

Iridium trichloride hydrate was purchased from Heraeus. Tetrabutyl ammonium hydroxide (TBAOH) was used as the hydrate (30 water molecules per TBAOH molecule). 2,6-difluoro-3-(pyridine-2-yl)benzoic acid was prepared as reported in the literature.[21] All materials and solvents were of reagent quality and used as received. ^{1}H and ^{13}C NMR spectra were recorded using a Bruker AV 400 MHz spectrometer. Chemical shifts δ (in ppm) are referenced to residual solvent peaks. For ^{1}H NMR: $CDCl_3$, 7.24 ppm; for ^{13}C NMR: $CDCl_3$, 77.0 ppm. High-resolution mass spectra (HRMS) were obtained with a Waters Q-TOF-MS instrument using electrospray ionisation (ESI). UV-visible spectra were recorded in a 1 cm path length quartz cell on a Cary 100 spectrophotometer. Emission spectra were recorded on a Fluorolog 3-22 using a 90° optical geometry. The photoluminescence quantum yields were determined using fluorescein (10^{-5} M in 0.1 M NaOH; air equilibrated; QY = 0.93) as standard.[22] Excited-state lifetimes were measured using a FL-1061PC TCSPC and 406 nm Nanoled as excitation source. Voltammetric measurements employed a PC controlled AutoLab PSTAT10 electrochemical workstation and were carried out in an Ar-filled glove box, oxygen and water < 1 ppm. Cyclic Voltammetry (CV) and Differential Pulse Voltammetry (DPV) techniques were used to estimate the redox potentials. DPV was used in support to the CV to have a better estimate of the electrochemical potentials when the systems show behavior next to the irreversibility, i.e. one of the two peaks in

the CV is not well defined. DPVs were carried out sweeping from negative to positive potentials and mean values are calculated. CVs were obtained at a scan rate of 1 and 0.1 $V.s^{-1}$. DPVs were obtained at a Modulation Potential of 50 mV, a Step Potential of 10 mV, a Modulation Time of 50 ms and an Interval Time of 100 ms. Measurements were carried out using 0.1 M $TBAPF_6$ as supporting electrolyte in acetonitrile (MeCN). Glassy carbon, platinum plate and platinum wire were used as working, counter and quasi-reference electrodes, respectively. At the end of each measurement, ferrocene was added as internal reference. Data collections for X-ray crystal structures were performed at low temperature [100(2) K] using Mo K_a radiation on a Bruker APEX II CCD diffractometer equipped with a kappa geometry goniometer. All datasets were reduced by EvalCCD[23] and then corrected for absorption.[24] The solutions and refinements were performed by SHELX.[25] The crystal structures were refined using full-matrix least-squares based on F^2 with all non hydrogen atoms anisotropically defined. Hydrogen atoms were placed in calculated positions by means of the "riding" model. In both structures disordered solvent molecules (CH_2Cl_2) were treated by SQUEEZE[26] and additional twinning problems were carefully analyzed by TWINROTMAT[26] (in the case of **3** a new dataset was created and then used for refinement, obtaining 4 BASF parameters: 0.0107(13), 0.0040(7), 0.0054(7), 0.0045(8); in the case of **5** a TWIN matrix [1 0 0 0 -1 0 0 0 -1] was directly applied to the original dataset with a final BASF parameter of 0.0040(2)). Disorder problems dealing with one $-COCF_3$ moiety were found during the last stages of refinement of **5** and treated by the split model combined with some restraints (SIMU card).

Tetrakis-(L1)-μ-(dichloro)-diiridium(III) **(1).** A mixture of $IrCl_3$, x $\cdot H_2O$ with 2.3 eq. of **L1** in a 3:1 mixture of 2-methoxyethanol and water was heated to 125 °C for 18 h. After cooling, the complex was precipitated with H_2O. The precipitate was isolated by vacuum filtration through a fritted glass and washed copiously with water and hexanes. The yellow solid was vacuum-dried to yield **1** (average yield about 80% on gram-scale). ^{1}H-NMR ($CDCl_3$, 400 MHz): 9.07 (d, 4H, J = 5.6 Hz); 8.37 (d, 4H, J = 8.8 Hz); 7.89 (t, 4H, J = 7.2 Hz); 6.89 (t, 4H, J = 7.2 Hz); 5.29 (d, 4H, J = 10.4 Hz); 3.83 (s, 12 H).

Tetrakis-(L2)-μ-(dichloro)-diiridium(III) **(2).** $IrCl_3 \cdot n$H2O (1.72 g, 4.88 mmol) was dissolved in 2-ethoxyethanol (150 mL) and degassed with argon at 75 °C for 30 min. Then 2.2 equiv of **L2** (3.11 g, 10.8 mmol) were added directly and about 10 mL 2-

ethoxy-ethanol were used for rinsing. The mixture was heated to 125 °C for 18 h under argon and protected from light with an aluminum foil. After cooling to about 50 °C, solvent was reduced to half volume under vacuum. After cooling to room temperature, the mixture was poured into Erlenmeyer containing 600 mL of deionized water and additional 100 mL of deionized water was used for rinsing the reaction flask. Those steps were performed in air and without full protection from light. The flask was stored in the fridge (about 6 °C) for 4 hours. The precipitate was isolated by vacuum filtration through a fritted glass and washed copiously with water. The yellow solid was vaccuum-dried at room temperature overnight, protected from light with an aluminum foil, to yield **2** as a yellow solid (3.59 g, 2.24 mmol, yield= 92 %). ^{1}H-NMR ($CDCl_3$, 400 MHz): 9.07 (dd, 4H, *J* = 6.4, 0.8 Hz); 8.42 (d, 4H, *J* = 8.4 Hz); 7.99 (t, 4H, *J* = 9.2 Hz); 6.89 (t, 4H, *J* = 9.2 Hz); 5.42 (d, 4H, *J* = 10.4 Hz).

[Ir(L1)$_2$(4-(N,N-dimethylamino)picolinate)] **(3).** A mixture of 4-dimethylamino-picolinic acid (91 mg, 4 eq.) and TBAOH (330 mg, 3 eq.) in dichloromethane was refluxed at 40 °C for half an hour and cooled down to 30°C. **1** (198 mg, 1 eq.) was added to the TBA 4-DMA-picolinate mixture. The mixture was heated at 40 °C for 12 hours under argon protected from light with an aluminum foil. The mixture was cooled to room temperature and deposited on top of a silica column (SiO_2/CH_2Cl_2). The product was eluted using CH_2Cl_2/MeOH 0 to 5% to yield **3** as a yellow powder (177 mg, 76%). ^{1}H-NMR ($CDCl_3$, 400 MHz): 8.77 (dd, 1H, *J* = 5.2, 1.2 Hz); 8.33 (d, 1H, *J* = 8.8 Hz); 8.26 (d, 1H, *J* = 8.4 Hz); 7.81 (m, 2H); 7.60 (dd, 1H, *J* = 5.6, 1.6 Hz); 7.52 (d, 1H, *J* = 3.2 Hz); 7.23 (t, 1H, *J* = 7.6, 1.6 Hz); 7.21 (d, 1H, *J* = 6.4 Hz); 7.04 (t, 1H, *J* = 7.6, 1.6 Hz); 6.45 (dd, 1H, *J* = 6.4, 3.2 Hz); 5.88 (d, 1H, *J* = 10.0 Hz); 5.68 (d, 1H, *J* = 10.0 Hz); 3.91 (s, 3H); 3.87 (s, 3H); 3.09 (s, 6H). TOF MS ES: MH^+ *m/z*: calc. 855.1420 found: 855.1389.

[Ir(L1)$_2$(picolinate)] **(4).** A mixture of picolinic acid (136 mg, 4 eq.) and TBAOH (665 mg, 3 eq.) in dichloromethane was refluxed at 40 °C for half an hour and cooled down to 30°C. **1** (400 mg, 1 eq.) was added to the TBA picolinate mixture. The mixture was heated at 40 °C for 12 hours under argon protected from light with an aluminum foil. The mixture was cooled to room temperature and deposited on top of a silica column (SiO_2/CH_2Cl_2). The product was eluted using CH_2Cl_2/MeOH 0 to 5% to yield **4** as a yellow powder (327 mg, 73%). ^{1}H-NMR ($CDCl_3$, 400 MHz): 8.74 (ddd, 1H, *J* = 5.6, 1.6, 0.8 Hz); 8.37 (m, 2H); 8.30 (d, 1H, *J* = 8.4 Hz); 7.98 (td, 1H, *J* = 8.0, 1.6 Hz); 7.84 (m, 2H); 7.75 (ddd, 1H, *J* = 7.2, 1.6, 0.8 Hz); 7.46 (ddd, 1H, *J* = 7.6, 5.6, 1.6 Hz); 7.41 (ddd, 1H, *J* =

5.6, 1.6, 0.8 Hz); 7.27 (dt, 1H, *J* = 7.2, 1.6 Hz); 7.04 (dt, 1H, *J* = 7.2, 1.6 Hz); 5.89 (d, 1H, *J* = 10.0 Hz); 5.63 (d, 1H, *J* = 10.0 Hz); 3.92 (s, 3H); 3.88 (s, 3H). TOF MS ES: MH^+ *m/z*: calc. 812.0997 found: 812.0978.

[Ir(L2)$_2$(picolinate)] **(5).** A mixture of picolinic acid (500 mg, 4 eq.) and TBAOH (2.4 g, 3 eq.) in dichloromethane (100 mL) was refluxed at 40 °C for half an hour and cooled down to 30°C. **2** (1.6 g, 1 mmol, 1 eq.) was dissolved in dichloromethane (20 mL) and added to the TBA picolinate mixture. Additional 10 mL of dichloromethane were used for rinsing. The mixture was heated at 30 °C for 12 hours under argon protected from light with an aluminum foil. The mixture was cooled to room temperature and deposited on top of a silica column (SiO_2/CH_2Cl_2). The product was eluted using CH_2Cl_2/acetone 0 to 25% to yield **5** as a yellow powder (1.42 g, 80%). ^{1}H-NMR ($CDCl_3$, 400 MHz): 8.78 (dd, 1H, *J* = 5.6, 0.4 Hz); 8.40-8.32 (m, 3H); 8.04 (td, 1H, *J* = 7.6, 1.2 Hz); 7.92 (m, 2H); 7.76 (ddd, 1H, *J* = 5.2, 1.6, 0.8 Hz); 7.53 (ddd, 1H, *J* = 7.6, 5.2, 1.6 Hz); 7.46 (dd, 1H, *J* = 5.6, 0.8 Hz); 7.35 (ddd, 1H, *J* = 7.6, 6.0, 1.6 Hz); 7.13 (ddd, 1H, *J* = 7.6, 6.0, 1.6 Hz); 6.02 (d, 1H, *J* = 10.0 Hz); 5.72 (d, 1H, *J* = 10.0 Hz). TOF MS ES: MH^+ *m/z*: calc. 888.0534 found: 888.0547.

Theoretical calculations.

Full geometry optimizations of the iridium compounds in their singlet ground state were performed with DFT using the M06 functional[27] with the relativistic effective core potential and basis set LANL2DZ[28] for the iridium, the TZVP[29, 30] basis set for the remaining atoms, an ultrafine integration grid, and tight geometrical convergence criteria with the Gaussian 09 package.[31] At each ground state (singlet) geometry, LR-TDDFT calculations were performed using the same basis sets and *xc*-functional for the first 50 singlet states. Condensed-phase effects were taken into account using a self-consistent reaction-field (SCRF) model in which the solvent is implicitly represented by a dielectric continuum characterized by its relative static dielectric permittivity ε. Within the different approaches that can be followed to calculate the electrostatic potential created by the polarized continuum in the cavity, we have employed the integral equation formalism of the polarizable continuum model (IEFPCM).[32] A relative permittivity of 35.688 was employed to simulate acetonitrile,[31] the solvent used in the experimental work. To gain insights into the phosphorescence behavior of the different iridium compounds, we optimized the geometry of the first triplet state using

unrestricted DFT (U-DFT) with the same basis set as described before. As suggested by a recent work,[33] we used the *xc*-functional M05-2X[34] for this task, due to its excellent performance for the emission spectra for a series of iridium-based compounds. At the minimum energy structure, we computed the difference in energy between the triplet (T_1) and singlet (S_0) state (ΔSCF method) with the inclusion of implicit solvent and obtained an estimation of the first phosphorescence band. See Supporting Information for additional details on the calculations.

Oxygen sensing.

To obtain the polymeric films, different cocktails were prepared in sealable 4 mL flasks, filled up to 2 mL volume with chloroform (dye concentration of 1.5 mg mL^{-1}) and shaken on a Vortex-Genie® 2 (Scientific Industries, Bohemia, NY, USA) equipped with a home-made holder. A nanostructure prepared by Ilford Imaging Switzerland following the procedure previously published[15-17] was also used as supporting matrix. This nanostructure is called AP200/19 and it is based on a polyethylene terephthalate (PET) thin plate coated by courting coating with aluminum oxide hydroxide, which provides a positively charged nanostructured film with a pore diameter of 19 nm and a total pore volume of 20 mL/m^2.

Once all the components were dissolved in chloroform, a Laurell spin-coater model WS-400B-6NPP/LITE (North Wales, PA, USA) was used to spin-coat the respective cocktail on the supports. For polystyrene membranes, 200 μL of the cocktail was injected onto a rotating glass plate of a spinning device at 700 rpm, while for the metal oxide nanostructured membranes, 100 μL of the cocktail was injected onto the rotating metal oxide support fixed onto a spinning device at 300 rpm. Both, PS and AP200/19 membranes were transparent and showed a thickness between 2 and 7 μm. Three replicas for each kind of membrane were prepared in order to evaluate the error. All the experimental results are expressed as the average of 3 replicas ± error ($s \cdot t/\sqrt{n}$), where *s* is the standard deviation, *t* the Student's t and *n* the number of replicas.

The luminescence measurements were obtained by means of a Varian Cary-Eclipse luminescence spectrometer equipped with a Xe flash lamp (peak power equivalent to 75 kW), Czerny-Turner monochromators, R-928 photomultiplier tube which is red sensitive (even 900 nm) with manual or automatic voltage. For gas mixing, two mass

flow controllers (MFC) of Type EL-FLOW® model F-201CV Bronkhorst High-Tech (Ruurlo, Netherlands) were connected to copper and stainless steel tubing. These tubes connect the MFCs and a flow-through cell specially designed for the spectrometer. The system was controlled by Cary Eclipse software for Windows 95/98/NT which fully controls the luminescence spectrometer. The O_2-gas station was controlled by a self-written LabView 8.2 program connected to a Flow Bus interface (Bronkhosrt) that fully controls the Bronkhosrt mass-flow controllers via RS-232. A time trace curve was used to recorder I_0 and the intensity I at different oxygen partial pressures, which were calculated from the measured oxygen/nitrogen flows, assuming a constant environmental pressure of 1000 mbar. To obtain the Stern-Volmer Plot (SVP), all the measurements were made at 10 different oxygen partial pressures between 0 and 0.1 bar and a room temperature of 21 ^{o}C.

2.3. Results and discussion

2.3.1. Synthesis and characterization

Scheme 1 represents the route for the synthesis of the blue emitting dyes. The preparation of the ligands started with 2-(2,4-difluorophenyl)pyridine. The proton between the two fluorine atoms is significantly acidic due to the strong acceptor character of the neighboring halogens. Therefore deprotonation by *n*-butyl lithium (n-BuLi) or lithium diisopropyl amine (LDA) followed by quenching of the intermediate anion with the required electrophile leads to the desired substitution. Ligand **L1** is obtained quenching with CO_2 followed by esterification with methanol. In the case of ligand **L2** quenching by ethyl trifluoroacetic acid leads to a mixture of ligand **L2** and its reduced form, 2-(2,4-difluoro-3-(2,2,2-trifluoroethanol)phenyl)pyridine (**L2b**). The two products **L2** and **L2b** can be separated by silica gel column chromatography. **L2b** can be oxidized to **L2** using a procedure based on copper chloride (see details for the ligands in ESI). The chloro-bridged iridium dimer **1** has been synthesized following the classical procedure based on iridium tris-chloride heated in a mixture 2-ethoxyethanol/water in presence of a slight excess of the ester substituted ligand **L1**. On the other hand, we found that in those conditions **L2** leads to mixtures of complexes with the trifluoromethyl ketone group reduced to the alcohol and/or hydrated. We could isolate the pure iridium dimer by performing the reaction in pure 2-ethoxyethanol. To synthesize the final dyes it was necessary to avoid saponification

for **3** and **4** and hydrolysis in the case of **5**. Therefore the ancillary ligand (DMAPic or Pic) was refluxed with a default of tetrabutyl ammonium hydroxide (TBAOH) prior to the addition of the chloro-bridged dimer. Following this procedure the reactions proceed smoothly and the blue emitting dyes are obtained with good yields, >70%.

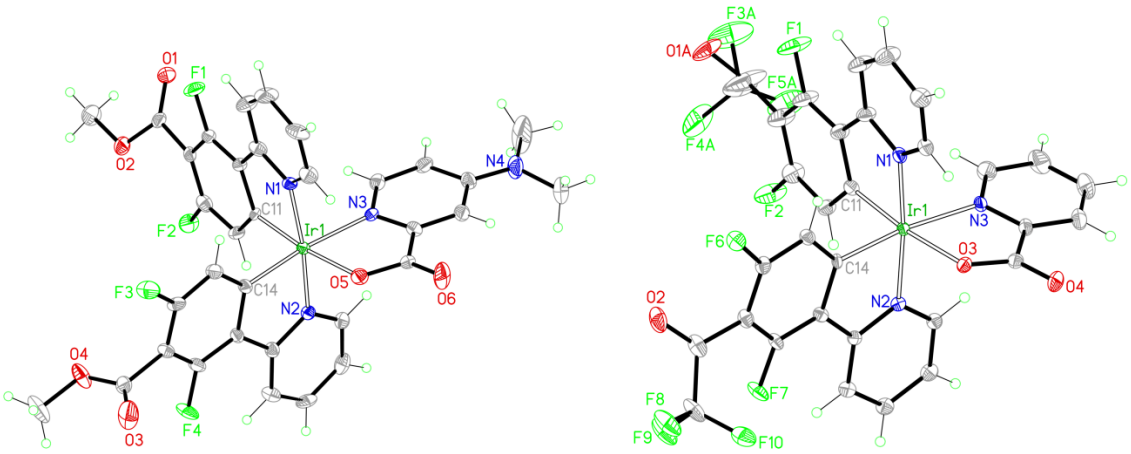

Figure 1. Ortep drawings of 3 (left) and 5 (right).

Single crystals of **3** and **5** suitable for X-ray diffraction analysis have been grown by slow diffusion of hexane into a dichloromethane solution of the complexes. ORTEP drawings of the structures are shown in Figure 1 and selected crystallographic data are provided in Table S1 and Table S2. The two complexes have the expected octahedral coordination geometry around the iridium center with the cis-C,C trans-N,N chelate configuration. It should be noted that the ester and trifluoroethanone groups are out of the plane of the cyclometalated ligands while the *N,N*-dimethyl-amino group of **3** is in the same plane as the pyridine of the ancillary ligand.

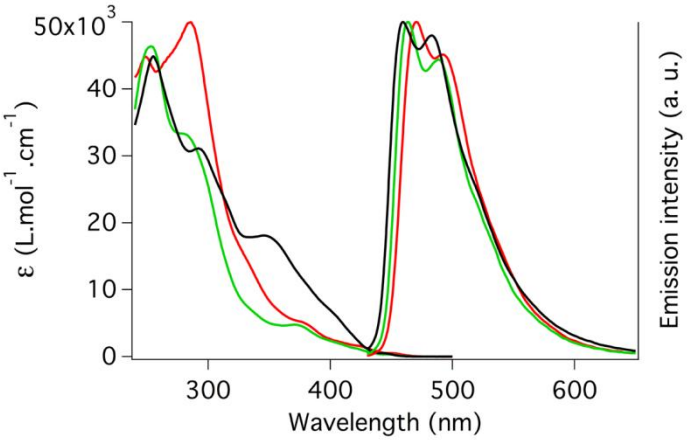

Figure 2. Absorption (left) and emission (right) spectra in acetonitrile at room-temperature of 3 (red), 4 (green) and 5 (black).

Table 1. Photophysical and electrochemical data of the dyes in acetonitrile.

	Absorption[a]		Emission in solution[b]				Redox[c]		DFT/M06	
	λ_{abs} / nm (ε, 10^3 L mol^{-1} cm^{-1})	λ_{max} (nm)	Φ_{em}	τ (µs)	k_r [d] (10^5 s^{-1})	k_{nr} [d] (10^5 s^{-1})	E_{ox} (V)	E_{red} (V)	IE[e] (eV)	EA[f] (eV)
3	248 (44.7), 284 (49.9) 380 (4.9), 452 (0.5)	470	0.39	1.78	2.19	3.43	1.04	-2.36	5.90	-2.18
4	252 (46.3),282 (33.2), 372 (4.8), 450 (0.3)	463	0.44	1.94	2.27	2.89	1.07	-2.28	5.99	-2.23
5	255 (44.9), 291 (31.1) 346 (18.1), 445 (0.5)	459	0.08	2.29	0.35	4.02	1.22	-1.85 -2.36	6.21	-2.59

[a] Acetonitrile at room temperature. [b] Degassed acetonitrile at room temperature. [c] 0.1 M $TBAPF_6$, in acetonitrile, potentials *vs* ferrocenium/ferrocene. [d] Calculated using the relations $k_r = \Phi_{em} / \tau$ and $k_{nr} = 1/\tau - k_r$. [e] Theoretical vertical ionization energies computed at the DFT/M06 level of theory. [f] Theoretical vertical electron affinity energies computed at the DFT/M06 level of theory. [g] τ : lifetime of excited state; [h] Φ_{em}: photoluminescence quantum yield in solution

2.3.2. Electrochemistry

Electrochemical potentials are reported vs ferrocenium/ferrocene in **Table 1**. The complexes **3**, **4** and **5** show reversible oxidation processes at 1.04, 1.07 and 1.22 V *vs* Fc^+/Fc, respectively. The higher oxidation potential for **5** compared to **4** reflects the significantly stronger acceptor character of the trifluoroethanone than the methyl-ester group (Hammett parameters: $COCF_3$: σm = 0.63, σp = 0.80; COOMe: σm = 0.37, σp = 0.45).[35] Results from theoretical calculations present the same trend for the vertical ionization potentials (IE) of the three compounds. A difference of 0.09 eV is found between the computed IEs of **3** and **4**. Complex **5** exhibits a lower IE, lying at 0.31 eV and 0.22 eV from **3** and **4**, respectively.

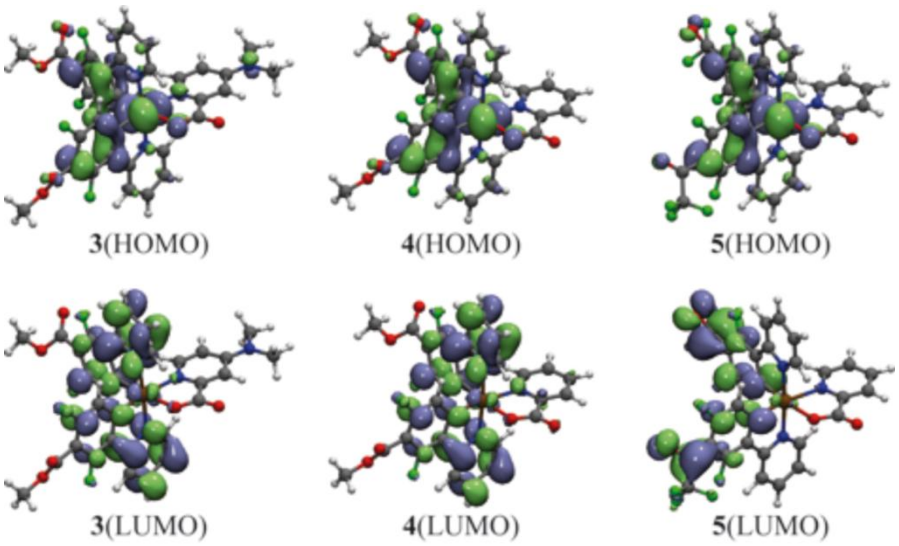

Figure 3. Kohn-Sham HOMO and LUMO for compounds **3**, **4**, and **5** computed for the ground state geometry at the DFT/M06 level of theory. Isosurfaces are set to 0.03 a.u.

Based on both σ m and σ p Hammett parameters, the reduction potentials are in the range expected[36] but for **5** which is much lower than anticipated (-1.85 V *vs* Fc^+/Fc). By analogy with the reduction potential of α, α, α -trifluoroacetophenones (-1.42 *vs* SCE[37] in acetonitrile that is ≈ -1.8 *vs* Fc^+/Fc) we attribute the first reduction of **5** to the reduction of the trifluoroethanone group instead of the cyclometalated ligand as usually found in such complexes. This finding correlates well with the LUMO localization of **5**, which is found to be mostly on the $-COCF_3$ moieties (**Figure 3**), in contrast with the other two compounds. As a result, the electron affinity (EA) of **5** is computed to be 0.36 eV (0.41 eV) lower than the one of **4** (**3**), which reflects the same trend than the experimental values for E_{red}.

2.3.3. Photophysical properties

UV-visible absorption spectra have been measured in acetonitrile solution at room temperature (**Figure 2** and **Table 1**). They display strong bands in the UV up to 300 nm attributed to intraligand (π-π*) transitions. Lower-energy absorption bands correspond to metal-to-ligand charge transfer (MLCT) transitions. Finally, weak bands with ε ~ 400 $M^{-1}cm^{-1}$ are ascribed to spin-forbidden transitions directly to triplet states. Overall, the three spectra have similar band positions however significant differences in absorption coefficient are observed. A first band around 250 nm is similar for the three complexes with absorption coefficient about 45,000 M^{-1} cm^{-1}. The second band around 385 nm has similar intensity (about 32,000 M^{-1} cm^{-1}) for **4** and **5** while **3** is stronger (50,000 M^{-1} cm^{-1});

it is therefore attributed to a π-π* transition involving the ancillary ligand. MLCT transitions from about 350 nm for all complexes are similar for **3** and **4** (about 5,000 M^{-1} cm^{-1}) while **5** has significantly more intense transitions (18,000 M^{-1} cm^{-1} at 348 nm and 7,000 M^{-1} cm^{-1} at 400 nm). This points to a higher MLCT character for **5**. LR-TDDFT calculations confirm that the first singlet vertical excitation of **5** possesses the largest oscillator strength among the three complexes, due to the enhanced delocalization of the excited electron over the -$COCF_3$ moieties and the ppy ligands (**3**: 390 nm, oscillator strength = 0.0363; **4**: 385 nm, oscillator strength = 0.0430; **5**: 385 nm, oscillator strength = 0.1365).

When **3**, **4** and **5** in solution in acetonitrile are excited in the MLCT bands, they show sky-blue emission with photoluminescence quantum yield Φ_{em} of 0.39, 0.44 and 0.08, respectively (**Figure 2** and **Table 1**). As expected from the presence of additional strong acceptor groups on the cyclometalated phenyl, the emission maxima are blue-shifted for the three complexes when compared to the classical sky-blue emitter FIrPic (λ_{max} = 470 nm in acetonitrile), [Ir(2-(2,4-difluorophenyl)pyridine)$_2$(picolinate)]. The ester group results in a 7 nm blue shift similar to our previous report with charged complexes based on carbene ancillary ligands[38] and the trifluorethanone group further blue shift the emission to 459 nm. The donor effect of DMAPic is seen as red shifting the emission compared to non-substituted pic.[39]

For complexes **3**, **4** and **5** the excited state lifetimes are 1.78, 1.94 and 2.29 μs, respectively. Assuming unitary intersystem crossing quantum yield, radiative (k_r) and non-radiative (k_{nr}) decay rates can be calculated from phosphorescence quantum yields and lifetimes. This leads to a radiative lifetime τ_{rad} (respectively k_r) of 4.56 μs (2.19 x10^5 s^{-1}), 4.40 μs (2.27 x10^5 s^{-1}) and 28.6 μs (0.35 x10^5 s^{-1}) for **3**, **4** and **5**, respectively. **3** and **4** are very similar as the non-chromophoric ancillary ligands are closely related.[40] On the other hand, **5** has very different radiative properties, attributed to the lower lying LUMO introduced by the $COCF_3$ group, as supported by theoretical calculations.

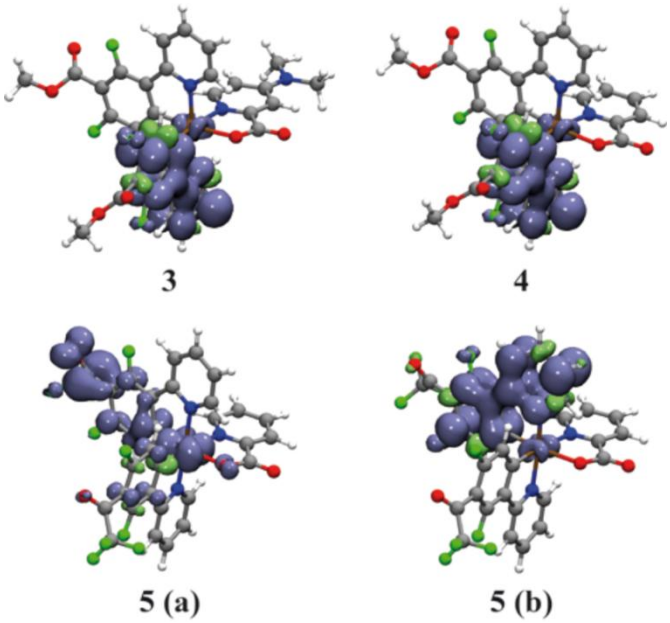

Figure 4. Spin density for each computed compound resulting from the unrestricted DFT calculations of triplet states (isovalue set to 0.003 a.u.).

SCF calculations on T_1 of **3** and **4** provide energy differences between the first triplet state and the ground state in agreement with the measured emission, 2.63 eV (exp.: 2.64 eV) and 2.63 eV (exp.: 2.68 eV), respectively. The character of T_1 can in both cases be defined as a MLCT-LC (see spin density plot in Figure 4). For **5**, the direct optimization of T_1 provides an electronic state where the excited electron occupies a π* orbital mostly localized on the -$COCF_3$ group, as expected from the calculated LUMO for the ground state (**Figure 3**). This triplet state lies at 2.22 eV above the ground state (see spin density plot in Figure 4, 5(a)). Another triplet state can be formed by populating the first unoccupied π* orbital located on the ppy ligand. After geometry optimization of this state, the transition energy (2.65 eV) obtained from ΔSCF matches well the experiment value 2.70 eV. This triplet state is similar to the first one of compound **3** and **4** and therefore possesses the expected MLCT-LC character (see spin density plot in Figure 4, 5(b)). Even though a complete discussion of the nonradiative paths and radiative properties of **5** is outside the scope of this article and would necessitate the inclusion of spin-orbit coupling, the presence of low-lying triplet states could help explaining the weaker quantum yield and the long radiative lifetime of **5**.

2.3.4. Oxygen sensing.

To evaluate the oxygen sensing properties of the dyes, both a nanostructured metal oxide matrix, AP200/19, and a polymeric polystyrene membrane were used to

physically immobilize the dyes. **Table 2** shows the composition and the nomenclature of the different polystyrene (PS) cocktails, with and without the plasticizer *o*-cyanophenyl octyl ether (*o*-CPOE) as well as the one for the nanostructured matrix.

Table 2. Nomenclature and composition of the oxygen-sensitive membranes. PS, polystyrene; *o*-CPOE, *o*-cyanophenyl octyl ether; AP200/19, aluminum oxide hydroxide nanostructured matrix.

Name	wt. % PS	wt. % o-CPOE	wt. % dye
PS0X	98.5	0	1.5
PS1X	90	8.5	1.5
PS2X	81	17.5	1.5
AP200/19	-	-	1.5

Table 3. Maxima luminescence excitation and emission wavelengths, $\lambda_{exc/em,}$ for the dyes incorporated into polystyrene (PS) and metal oxide matrix AP200/19. ([dye]=1.5 mg mL^{-1}; monochromator slit $width_{exc/em}$=20/20 nm)

	3	4	5
Membrane	$\lambda_{ex/em}$ (nm)	$\lambda_{ex/em}$ (nm)	$\lambda_{ex/em}$ (nm)
PS0X	303/470	300/470	300/465
PS1X	303/470	300/470	300/465
PS2X	303/470	300/470	300/465
AP200/19	335/470	335/467	340/465

Table 3 shows the luminescence excitation and emission properties of the different sensing layers. As can be seen compared to **Table 1**, where the spectrum is recorded in solution, the incorporation of the dyes into a solid support slightly changes the emission properties of the dyes, which is attributed to the change of environment.

For all the membranes, similar emission profiles were obtained and the luminescence was completely quenched when molecular oxygen concentration is over 10% (see ESI). Since in all the cases the lifetime was lower than 50 µs, it was not possible to measure the luminescence lifetime with our available instrumentation, which does not provide reliable data with lifetimes below 50 µs. Therefore, the oxygen sensing properties were evaluated by the reduction in emission intensity when different quencher (oxygen) concentrations are present. This reduction in intensity is described by the Stern-Volmer equation (see eq 1)

$$\frac{I_0}{I} = 1 + k_{SV}\, pO_2 \qquad (1)$$

where I is the luminescence intensity, the subscript "0" refers to the value in the absence of quencher, k_{SV} is the Stern-Volmer constants and pO_2 is the partial pressure of oxygen.

The heterogeneity of the medium where the dyes are immobilized often causes a deviation in the linearity of the response in the Stern-Volmer equation. The downward deviation is usually explained by the presence of sites within the matrix with different accessibility to oxygen. Consequently, the dyes are quenched differently depending on their accessibility by oxygen, which results in different Stern-Volmer constants for each site.[15-17] In this case, a multi-site model, each having a linear behavior, is necessary to describe the response of the films to the presence of oxygen. Generally, the two-site model proposed by Demas and co-workers, so called Demas' model,[41] is applied (see eq 2)

$$\frac{I_0}{I} = \left[\frac{f_1}{1 + k_{SV1} pO_2} + \frac{f_2}{1 + k_{SV2} pO_2} \right]^{-1} \quad (2)$$

where f_i denotes the fractional contribution of the total luminescence emission from the luminophore located at site type i under unquenched conditions, which exhibit a discrete Stern-Volmer quenching constant given by k_{SVi}.

Another two-site model was proposed by Lehrer.[42] In this model, only one microenvironment is accessible to the quencher (therefore k_{SV2}=0; see eq 3)

$$\frac{I_0}{I} = \left[\frac{f_0}{1 + k_{SV} pO_2} + (1 - f_0) \right]^{-1} \quad (3)$$

where f_0 denotes the fraction of the total luminophore's population that the quencher is able to access, and k_{SV} is the Stern-Volmer quenching constant associated with the accessible fraction of luminophores.

Table 4. Oxygen sensitivity, $\Delta I_{1\%}$ and $pO_2(S=1/2)$, of the dyes incorporated into PS films and the AP200/19 nanostructure).[a]

		Demas' Model					Lehrer's Model			$\Delta I_{1\%}$ (%)[a,d]	$pO_2(S=½)$ (mbar)[a,e]
		k_{SV1} (bar^{-1})	f_1	k_{SV2} (bar^{-1})	f_2	r[c]	k_{SV} (bar^{-1})	f_0	r[c]		
3	PS0X	134.65 ± 27.53	0.71 ± 0.02	2.02 ± 0.27	0.28 ± 0.02	0.9999	106.47 ± 13.17	0.78 ± 0.01	0.9984	43.49	16.77
	PS1X	42.48 ± 0.51[b]	1.00 ± 0.00	-	-	0.9992	42.48 ± 0.51[b]	1.00 ± 0.00	0.9992	36.70	23.54
	PS2X	198.60 ± 62.67	0.67 ±0.07	21.10 ± 4.10	0.33 ± 0.08	0.9998	89.82 ± 0.26	0.96 ± 0.00	0.9988	51.40	12.22
	AP200/19	780.77 ± 18.28	0.91 ± 0.00	8.68 ± 1.05	0.05 ± 0.01	0.9913	568.62 ± 49.44	0.98 ± 0.01	0.9901	86.47	1.83
4	PS0X	150.30 ± 63.30	0.64 ± 0.09	2.14 ± 0.1	0.35 ± 0.10	0.9849	106.25 ± 28.60	0.72 ± 0.1	0.9938	39.79	21.57
	PS1X	48.56 ± 1.84[b]	1.00 ± 0.00	-	-	0.9989	48.56 ± 1.84[b]	1.00 ± 0.00	0.9989	40.18	20.60
	PS2X	168.23 ± 21.61	0.71 ± 0.06	17.21 ± 0.07	0.28 ± 0.07	0.9999	89.55 ± 4.72	0.95 ± 0.01	0.9989	51.15	12.41
	AP200/19	667.06 ± 185.41	0.89 ± 0.01	11.84 ± 0.01	0.08 ± 0.01	0.9937	392.98 ± 63.47	0.97 ± 0.00	0.9913	81.58	2.70
5	PS0X	178.41 ± 8.55	0.74 ± 0.03	3.38 ± 1.13	0.25 ± 0.03	0.9869	125.40 ± 9.77	0.83 ± 0.04	0.9855	50.83	12.17
	PS1X	57.30 ± 2.54[b]	1.00 ± 0.00	-	-	0.9996	57.30 ± 2.54[b]	1.00 ± 0.00	0.9996	44.06	17.46
	PS2X	355.40 ± 8.55	0.50 ± 0.02	32.56 ± 1.14	0.50 ± 0.02	0.9988	83.44 ± 1.07	0.97 ± 0.01	0.9978	49.65	12.82
	AP200/19	748.66 ± 56.84	0.90 ± 0.02	16.04 ± 7.73	0.06 ± 0.01	0.9974	485.25 ± 15.03	0.99 ± 0.00	0.9962	85.11	2.12

[a] [dye]=1.5 mg mL^{-1}; slit width$_{exc/em}$=20/20 nm; t_d=120 µs; t_g=5 ms; for $\lambda_{exc/em}$ see Table 3, the experimental results have been expressed as the average of 3 replicas $\pm\ s \cdot t/\sqrt{n}$ (n=3, t=4.30 (2P = 0.05)); [b] Values obtained by a linear fitting; [c] Regression coefficient of the model fit; [d] $\Delta I_{1\%}$ is the percentage of quenching reached when the oxygen concentration in the media is 1% (v/v), compared with the total available quenching; [e] pO_2(S=1/2) is the partial pressure of oxygen necessary to reduce 50% of the initial (oxygen free) luminescence exhibited by the film.

Table 4 shows the Stern-Volmer constants for each film according to Demas' and Lehrer's Models. In most cases the dye is located in two different environments, except for the polymeric sensing films containing 8.5 wt% of plasticizer (named PS1X), where the quenching follows linearly the standard Stern-Volmer equation. In all other cases the relationship between oxygen concentration and I_0/I does not follow a linear relationship (see ESI), and Demas' and Lehrer's models were used to adjust the experimental data. Similar results have been found using similar dyes and supports.[14-17]

The fact that the non-linear results can be adjusted using both models may be explained by looking at the results for the membranes PS0X reported in **Table 4**. For Demas' model, k_{SV1} is much higher than k_{SV2}, and the fractional contribution of the sites

possessing k_{SV2} (expressed with f_2) is lower than the contribution of the sites having k_{SV1}. Therefore, the sensitivity to oxygen associated to the second group of sites can be neglected, which leads to the Lehrer's model, where only one of the sites is quenched by oxygen. However, by using Lehrer fitting, the quenching capacity associated to this second site is not taken into account, which produces a decrease in the k_{SV} of PS2X compared to PS0X for Lehrer model, when it possesses, in fact, a better sensitivity (as can be seen in in **Table 4** and Fig.5).

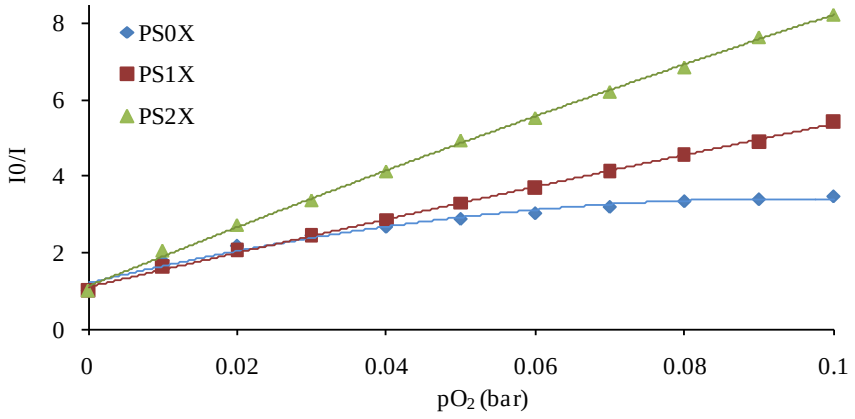

Figure 5. Stern-Volmer plot obtained for plasticizer free (PS0X) and non-free (8.5 wt.% for PS1X and 17.5 wt% for PS2X) polymeric membranes of dye 3. Dye concentration=1.5 mg mL^{-1}; $\lambda_{exc/em}$=303/470 nm; slit $width_{exc/em}$=20/20 nm, t_d=120 µs and t_g=5 ms.

The results found in the polymeric films when comparing both models can be explained by the heterogeneity of the media and the aggregation of the dye, which are frequent on polymeric films.[14, 16, 17] The addition of the right amount of plasticizer appears important to control the homogeneity of the media, leading to a linear response to oxygen, always an advantage in terms of calibration for further implementation as oxygen sensors. As can be seen in Figure 5 for the polymeric membranes of the dye **3**, the presence of plasticizer increases the sensitivity to oxygen of the film in the site possessing k_{SV2} (in the high O_2 concentration of the range studied), whose value goes from 2.02 bar^{-1} for the plasticizer-free membrane (PS0X) to 21.10 bar^{-1} for PS2X, improving the sensing capability of the membrane. Similar behaviors were found for dyes **4** and **5**.

Generally, plasticizers improve the mechanical properties of the matrix, the solubility of the components in the membrane, and increase the diffusion of oxygen.[43-45]These aspects may be responsible of the linearity and improvement in oxygen sensitivity of PS1X and PS2X. Although an increase in the viscosity often decrease the sensitivity of the membranes, the compatibility between the plasticizer and the polymer seems to be the most important factor which determines the sensitivity of the membranes.[44, 45] In addition, the use of plasticizer improves the efficiency of the luminescence. Indeed, the voltage of the photomultiplier was decreased while keeping the level of the emission peak, when increasing the amount of plasticizer (see ESI), in contrast to previous reports using charged iridium complexes where plasticizers can act as a quencher of the luminescence.[16, 17] Here, the improved solubility of the dye and permeability to oxygen of the film seems to thwart these issues, resulting in an enhancement of the sensitivity for the membranes containing high plasticizer concentration, as can be noticed in Figure 5 and confirmed with the data showed in **Table 4** for Demas' model.

The incorporation of the dyes into AP200/19 provides higher k_{SV} than the immobilization into the PS-matrix. For all dyes, the sensitivity to oxygen (concentration between 0 and 10% in volume) of the metal oxide hydroxide nanocomposite is about 4 times higher than with the polymeric matrix. The metal oxide matrix is formed from agglomerated nanoparticles, where the nanopores are located inside while the macropores appear between agglomerated particles.[46] Therefore, the heterogeneity of the nanostructured oxide hydroxide membranes is responsible of the non-linearity response to oxygen, in which one of the sites is highly sensitive to oxygen, as previously demonstrated by Fernandez-Sanchez et al..[46] The capillary forces are responsible of this high sensitivity since they drive the oxygen quickly into the nanopores,[14] in line with previous reports using this nanostructure in combination with charged Ru(II) and Ir(III) dyes.[14, 16, 17] The AP200/19 matrix is positively charged and its compatibility with charged complexes has proved to improve the sensitivity to oxygen in different degree depending on the properties of the dyes.[14, 16, 17] However, this is the first time that this metal oxide nanostructure is used in combination with non-charged complexes. The results confirm and generalize its suitability to enhance the oxygen sensing ability for low oxygen concentration.

Overall, dye **3** supported in the oxide hydroxide nanostructure is the most sensitive film according to both Lehrer and Demas' models from 0 to 10 % O_2 (k_{SV1}= 780.77 ±

18.28 bar^{-1}). Nevertheless, dye **5** immobilized into the nanostructured matrix posses a similar sensitivity to oxygen (k_{SV1}= 748.66 ± 56.84 bar^{-1}). Furthermore, for classic polymeric membranes, dye **5** provides a better sensitivity to oxygen than **3** and **4**. This behavior is attributed to the higher radiative lifetime of dye **5**, which usually provides a better sensitivity to oxygen.

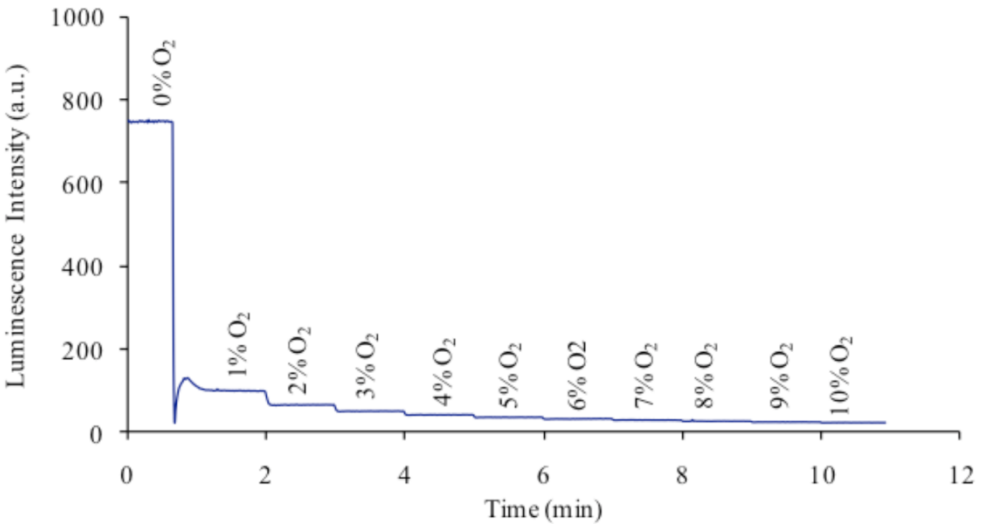

Figure 6. Example of time trace curve for the AP200/19 membrane of dye 3. dye concentration=1.5 mg mL^{-1}; $\lambda_{exc/em}$=335/470 nm; slit width$_{exc/em}$=20/20 nm, t_d=120 µs and t_g=5 ms.

Figure 6 gives an example of the high sensitivity to low oxygen concentration. Already for 1% of oxygen, the intensity of luminescence is practically totally quenched. This intensity drop can be compared with the parameters $\Delta I_{1\%}$ and $pO_2(S=1/2)$ as rough guides of the sensitivity of the optical oxygen sensing films to low oxygen concentrations (**Table 4**).[16] $pO_2(S=1/2)$ is defined as the partial pressure of oxygen necessary to reduce 50% of the initial (oxygen free) luminescence exhibited by the film. Similarly, $\Delta I_{1\%}$ is defined as the percentage of quenching reached when the oxygen concentration in the media is 1% (v/v), compared with the total available quenching. The practical pressure necessary to quench the luminescence by 50% is higher for the polymeric films than for the metal oxide hydroxide matrix, whose intensity is quenched by 50% with less than 0.003 bars. Furthermore, when the oxygen concentration is 1%, the nanostructure leads to more than 80% of luminescence quenching, while only 50% is reached with the polymeric films. This clearly shows the

high potential of this metal oxides hydroxide nanostructure to serve as matrices for oxygen trace sensors.

2.4. Conclusion

Three new neutral blue emitting cyclometalated iridium(III) complexes have been synthesized and characterized by means of spectroscopic and electrochemical methods and X-ray crystal structure. In addition to fluorine, the dyes use methyl ester (–COOMe) and trifluoroethanone (–COCF3) groups as strong acceptor to blue shift the emission compare to FIrPic. Interestingly the –COCF3 group changes the LUMO localization, which is found to be mostly on the -$COCF_3$ moieties, in contrast to usual complexes based on 2-phenylpyridine skeleton.

All three dyes were investigated in order to evaluate their potential as oxygen-sensitive chemical sensors in the blue region of the visible spectrum. The dyes were physically immobilized into a nanostructured metal oxide matrix, AP200/19, and a classical polymeric polystyrene membrane, showing in both cases a single emission band, which is totally quenched for oxygen concentrations over 10%.

The sensitivity to oxygen was evaluated according to Demas and Lehrer's models and shows that the oxygen sensing properties are the result of interplay between the performance and aggregation of the dye and the film morphology. The use of different amount of plasticizer has an impact on the aggregation behavior of the dyes and oxygen diffusion, overall improving the oxygen sensing ability.

On the other hand, the most sensitive films are based on the AP200/19, which shows in all the cases a Stern-Volmer constant 4 times higher than the polystyrene classic membrane. In addition $p_{O_2}(S = ½)$ and the parameter $\Delta I_{1\%}$ were evaluated in order to establish the ability of the membranes to be sensitive to low oxygen concentrations. In all the cases the metal oxide hydroxide nanostructure provides the best results, probably due first to the more rigid environment and more homogeneous distribution of the dye in the mesoporous structure, avoiding the energy transfer between the molecules, and second to the nanostructure of the matrix improving oxygen diffusion. These results confirm the suitability of this type of nanostructure to improve the oxygen sensitive properties of non-charged complexes. Nevertheless, further studies about the stability, the dye migration, and the sensitivity below 1% oxygen will be

necessary for the implementation as oxygen trace sensors in intelligent food packages[47] or chambers with electrical equipment where oxygen leakages can be harmful.[48]

Acknowledgment. We acknowledge financial support for this work by the Regional Government of Andalusia (Excellence projects P07-FQM-2625 and P07-FQM-2738), the Spanish Ministry of Science and Innovation (CTQ2008-01394), Solvay S.A. and the Swiss National Science Foundation (NCCR-MUST interdisciplinary research program). MMS thanks the Regional Government of Andalusia for supporting her doctoral grant.

Referencias

1. Wolfbeis, O. S., Materials for fluorescence-based optical chemical sensors. *Journal of Materials Chemistry* **2005,** 15, (27-28), 2657-2669.
2. Amao, Y., Probes and Polymers for Optical Sensing of Oxygen. *Microchimica Acta* **2003,** 143, (1), 1-12.
3. Loloee, R.; Askeland, P. A.; Ghosh, R. N. In *Dissolved Oxygen Sensing in a Flow Stream using Molybdenum Chloride Optical Indicators*, Sensors, 2007 IEEE, 28-31 Oct. 2007, 2007; 2007; pp 1404-1407.
4. Baleizao, C.; Nagl, S.; Schäferling, M.; Berberan-Santos, M. N.; Wolfbeis, O. S., Dual Fluorescence Sensor for Trace Oxygen and Temperature with Unmatched Range and Sensitivity. *Analytical Chemistry* **2008,** 80, (16), 6449-6457.
5. Achatz, D. E.; Meier, R. J.; Fischer, L. H.; Wolfbeis, O. S., Luminescent Sensing of Oxygen Using a Quenchable Probe and Upconverting Nanoparticles. *Angewandte Chemie, International Edition* **2011,** 50, (1), 260-263.
6. Lange, C. A. K.; Stavrakas, P.; Luhmann, U. F. O.; de Silva, D. J.; Ali, R. R.; Gregor, Z. J.; Bainbridge, J. W. B., Intraocular Oxygen Distribution in Advanced Proliferative Diabetic Retinopathy. *Am. J. Ophthalmol.* **2011,** 152, (3), 406-412.e3.
7. Song, D. H.; Kim, H. D.; Kim, K. C., Dissolved oxygen concentration field measurement in micro-scale water flows using PtOEP/PS film sensor. *Optics and Lasers in Engineering* **2011**, (0).
8. Xie, K.; Zhang, X.-W.; Huang, L.; Wang, Y.-T.; Lei, Y.; Rong, J.; Qian, C.-W.; Xie, Q.-L.; Wang, Y.-F.; Hong, A.; Xiong, S., On-line monitoring of oxygen in Tubespin, a novel, small-scale disposable bioreactor. *Cytotechnology* **2011,** 63, (4), 345-350.

9. Medina-Castillo, A. L.; Fernández-Sánchez, J. F.; Fernández-Gutiérrez, A., One-Step Fabrication of Multifunctional Core-Shell Fibres by Co-Electrospinning. *Advanced Functional Materials* **2011,** 21, (18), 3488-3495.

10. Liu, Z.; Bian, Z.; Huang, C.; Bozec, H.; Guerchais, V., Luminescent Iridium Complexes and Their Applications Molecular Organometallic Materials for Optics. In Springer Berlin / Heidelberg: 2010; Vol. 28, pp 113-142.

11. Ruggi, A.; van Leeuwen, F. W. B.; Velders, A. H., Interaction of dioxygen with the electronic excited state of Ir(III) and Ru(II) complexes: Principles and biomedical applications. *Coordination Chemistry Reviews* **2011,** 255, (21-22), 2542-2554.

12. Koren, K.; Borisov, S. M.; Saf, R.; Klimant, I., Strongly Phosphorescent Iridium(III)–Porphyrins – New Oxygen Indicators with Tuneable Photophysical Properties and Functionalities. *European Journal of Inorganic Chemistry* **2011,** 2011, (10), 1531-1534.

13. Amao, Y.; Ishikawa, Y.; Okura, I., Green luminescent iridium(III) complex immobilized in fluoropolymer film as optical oxygen-sensing material. *Analytica Chimica Acta* **2001,** 445, (2), 177-182.

14. Spichiger-Keller, U.; Spichiger, S.; Fernandez-Sanchez, J. F. Metal oxide membrane with a gas-selective compound. 2006.

15. Fernández-Sánchez, J. F.; Roth, T.; Cannas, R.; Nazeeruddin, M. K.; Spichiger, S.; Graetzel, M.; Spichiger-Keller, U. E., Novel oxygen sensitive complexes for optical oxygen sensing. *Talanta* **2007,** 71, (1), 242-250.

16. Marin-Suarez del Toro, M.; Fernandez-Sanchez, J. F.; Baranoff, E.; Nazeeruddin, M. K.; Graetzel, M.; Fernandez-Gutierrez, A., Novel luminescent Ir(III) dyes for developing highly sensitive oxygen sensing films. *Talanta* **2010,** 82, (2), 620-626.

17. Medina-Castillo, A. L.; Fernandez-Sanchez, J. F.; Klein, C.; Nazeeruddin, M. K.; Segura-Carretero, A.; Fernandez-Gutierrez, A.; Graetzel, M.; Spichiger-Keller, U. E., Engineering of efficient phosphorescent iridium cationic complex for developing oxygen-sensitive polymeric and nanostructured films. *Analyst* **2007,** 132, (9), 929-936.

18. Borisov, S.; Seifner, R.; Klimant, I., A novel planar optical sensor for simultaneous monitoring of oxygen, carbon dioxide, pH and temperature. *Analytical and Bioanalytical Chemistry* **2011,** 400, (8), 2463-2474.

19. Lu, H.; Jin, Y.; Tian, Y.; Zhang, W.; Holl, M. R.; Meldrum, D. R., New ratiometric optical oxygen and pH dual sensors with three emission colors for measuring photosynthetic activity in cyanobacteria. *Journal of Materials Chemistry* **2011,** 21, (48), 19293-19301.

20. Evans, R. C.; Douglas, P., Optical oxygen sensors move towards colorimetric determination. *Anal. Chem.* **2006,** 78, 5645-5652.

21. Kimyonok, A.; Domercq, B.; Haldi, A.; Cho, J.-Y.; Carlise, J. R.; Wang, X.-Y.; Hayden, L. E.; Jones, S. C.; Barlow, S.; Marder, S. R.; Kippelen, B.; Weck, M., Norbornene-based copolymers with iridium complexes and bis(carbazolyl)fluorene groups in their side-chains and their use in light-emitting diodes. *Chem. Mater.* **2007,** 19, 5602-5608.
22. Shen, J.; Snook, R. D., *Chem. Phys. Lett.* **1989,** 155, 585.
23. Duisenberg, A. J. M.; Kroon-Batenburg, L. M. J.; Schreurs, A. M. M., *J. Appl. Crystallogr.* **2003,** 36, 220-229.
24. Blessing, R. H., *Acta Crystallogr., Sect. A* **1995,** 51, 33-38.
25. Sheldrick, G. M., SHELX. *Acta Crystallogr., Sect. A* **2008,** 64, 112-122.
26. Spek, A. L., PLATON. *Acta Cryst. Sect D* **2009,** 65, 148-155.
27. Zhao, Y.; Truhlar, D. G., *Theor. Chem. Acc.* **2008,** 120, 215-241.
28. Hay, P. J.; Wadt, W. R., *J. Chem. Phys.* **1985,** 82, 299-310.
29. Schaefer, A.; Horn, H.; Ahlrichs, R., *J. Chem. Phys.* **1992,** 97, 2571-2577.
30. Schaefer, A.; Huber, C.; Ahlrichs, R., *J. Chem. Phys.* **1994,** 100, 5829-5835.
31. Frisch, M. J.; Trucks, G. W.; Schlegel, H. B.; Scuseria, G. E.; Robb, M. A.; Cheeseman, J. R.; Scalmani, G.; Barone, V.; Mennucci, B.; Petersson, G. A.; Nakatsuji, H.; Caricato, M.; Li, X.; Hratchian, H. P.; Izmaylov, A. F.; Bloino, J.; Zheng, G.; Sonnenberg, J. L.; Hada, M.; Ehara, M.; Toyota, K.; Fukuda, R.; Hasegawa, J.; Ishida, M.; Nakajima, T.; Honda, Y.; Kitao, O.; Nakai, H.; Vreven, T.; Montgomery, J., J. A.; Peralta, J. E.; Ogliaro, F.; Bearpark, M.; Heyd, J. J.; Brothers, E.; Kudin, K. N.; Staroverov, V. N.; Kobayashi, R.; Normand, J.; Raghavachari, K.; Rendell, A.; Burant, J. C.; Iyengar, S. S.; Tomasi, J.; Cossi, M.; Rega, N.; Millam, J. M.; Klene, M.; Knox, J. E.; Cross, J. B.; Bakken, V.; Adamo, C.; Jaramillo, J.; Gomperts, R.; Stratmann, R. E.; Yazyev, O.; Austin, A. J.; Cammi, R.; Pomelli, C.; Ochterski, J. W.; Martin, R. L.; Morokuma, K.; Zakrzewski, V. G.; Voth, G. A.; Salvador, P.; Dannenberg, J. J.; Dapprich, S.; Daniels, A. D.; Farkas, Ö.; Foresman, J. B.; Ortiz, J. V.; Cioslowski, J.; Fox, D. J., *Gaussian 09, Revision A.02*. Gaussian, Inc.: Wallingford CT, 2009.
32. Tomasi, J.; Mennucci, B.; Cammi, R., *Chem. Rev.* **2005,** 105, 2999-3093.
33. Swiderek, K.; Paneth, P., *J. Phys. Org. Chem.* **2009,** 22, 845.
34. Zhao, Y.; Schultz, N. E.; Truhlar, D. G., *J. Chem. Theory and Comput.* **2006,** 2, 364.
35. Hansch, C.; Leo, A.; Taft, R. W., A Survey of Hammett Substituted Constants and Resonance and Field Parameters. *Chem. Rev.* **1991,** 91, 165-195.
36. Baranoff, E.; Curchod, B. F. E.; Monti, F.; Steimer, F.; Accorsi, G.; Tavernelli, I.; Rothlisberger, U.; Scopelliti, R.; Grätzel, M.; Nazeeruddin, M. K., *Inorganic Chemistry* **2012,** 51, 799-811.

37. Yang, J.-S.; Liu, K.-T.; Su, Y. O., *Journal of Physical Organic Chemistry* **1990,** 3, 723-731.

38. Kessler, F.; Costa, R. D.; Di Censo, D.; Scopelliti, R.; Ortì, E.; Bolink, H. J.; Meier, S.; Sarfert, W.; Grätzel, M.; Nazeeruddin, M. K.; Baranoff, E., *Dalton Transactions* **2012,** 41, 180.

39. Baranoff, E.; Jung, I.; Scopelliti, R.; Solari, E.; Grätzel, M.; Nazeeruddin, M. K., *Dalton Transactions* **2011,** 40, 6860.

40. Li, J.; Djurovich, P. I.; Alleyne, B. D.; Yousufuddin, M.; Ho, N. N.; Thomas, J. C.; Peters, J. C.; Bau, R.; Thompson, M. E., Synthetic control of excited-state properties in cyclometalated Ir(III) complexes using ancillary ligands. *Inorganic Chemistry* **2005,** 44, (6), 1713-1727.

41. Demas, J. N.; DeGraff, B. A., Luminescence-based sensors: microheterogeneous and temperature effects. *Sensors and Actuators B: Chemical* **1993,** 11, (1-3), 35-41.

42. Lehrer, S., Solute perturbation of protein fluorescence. Quenching of the tryptophyl fluorescence of model compounds and of lysozyme by iodide ion. *Biochemistry* **1971,** 10, (17), 3254-3263.

43. Papkovsky, D. B.; Mohr, G. J.; Wolfbeis, O. S., New polar plasticizers for luminescence-based sensors. *Analytica Chimica Acta* **1997,** 337, (2), 201-205.

44. Di Marco, G.; Lanza, M., Optical solid-state oxygen sensors using metalloporphyrin complexes immobilized in suitable polymeric matrices. *Sensors and Actuators, B: Chemical* **2000,** 63, (12), 42-48.

45. Mills, A., Effect of plasticizer viscosity on the sensitivity of an [Ru(bpy)32+(Ph4B-)2]-based optical oxygen sensor. *Analyst* **1998,** 123, (5), 1135-1140.

46. Fernández-Sánchez, J. F.; Nezel, T.; Steiger, R.; Spichiger-Keller, U. E., Novel optical NO2-selective sensor based on phthalocyaninato-iron(II) incorporated into a nanostructured matrix. *Sensors and Actuators, B: Chemical* **2006,** 113, (2), 630-638.

47. Rojas-Graü, M. A.; Oms-Oliu, G.; Soliva-Fortuny, R.; Martín-Belloso, O., The use of packaging techniques to maintain freshness in fresh-cut fruits and vegetables: A review. *International Journal of Food Science and Technology* **2009,** 44, (5), 875-889.

48. Denison, D. M.; Ernsting, J.; Tonkins, W. J.; Cresswell, A. W., Problem of Fire in Oxygen-rich Surroundings. *Nature* **1968,** 218, (5147), 1110-1113.

Anexo

Supporting Information

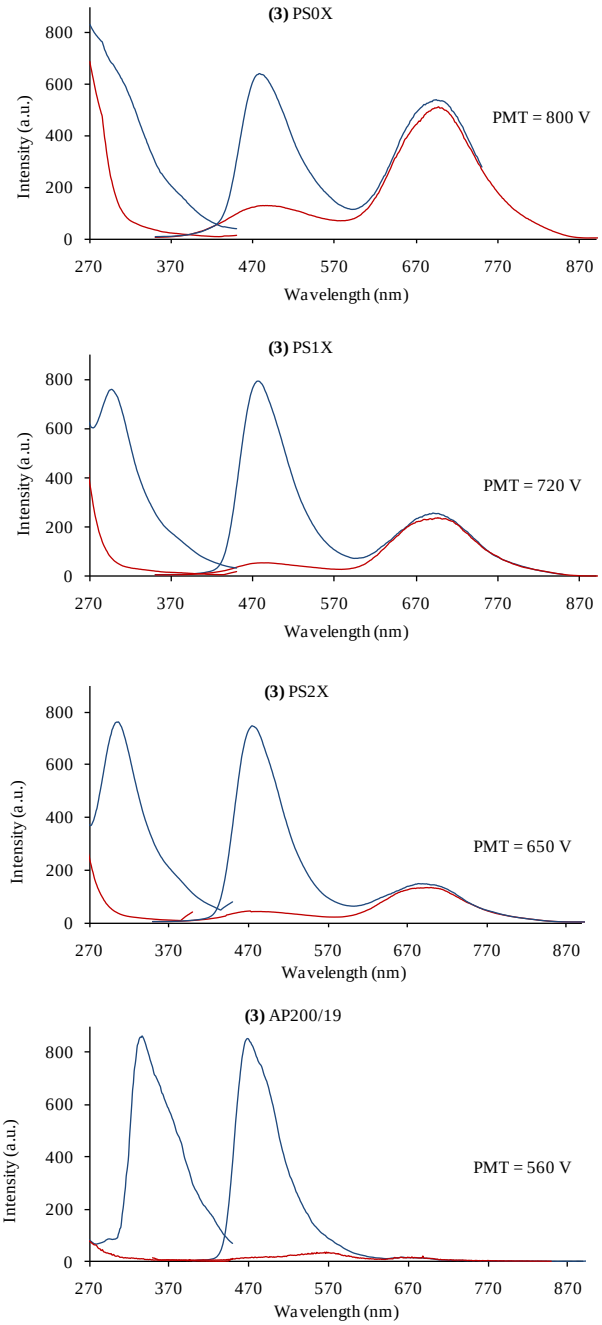

Figure S1. Excitation and emission spectra of **3** incorporated into PS membranes ($\lambda_{ex/em}$=303/470 nm) and AP200/190 ($\lambda_{ex/em}$=335/470 nm) in absence of oxygen (blue line) and with 10% of oxygen (red line) ([dye]=1.5 mg mL^{-1}; monochromator slit $width_{exc/em}$=20/20 nm, t_d=120 µs; t_g=5 ms, photomultiplier voltage is indicated for each graphic as PMT).

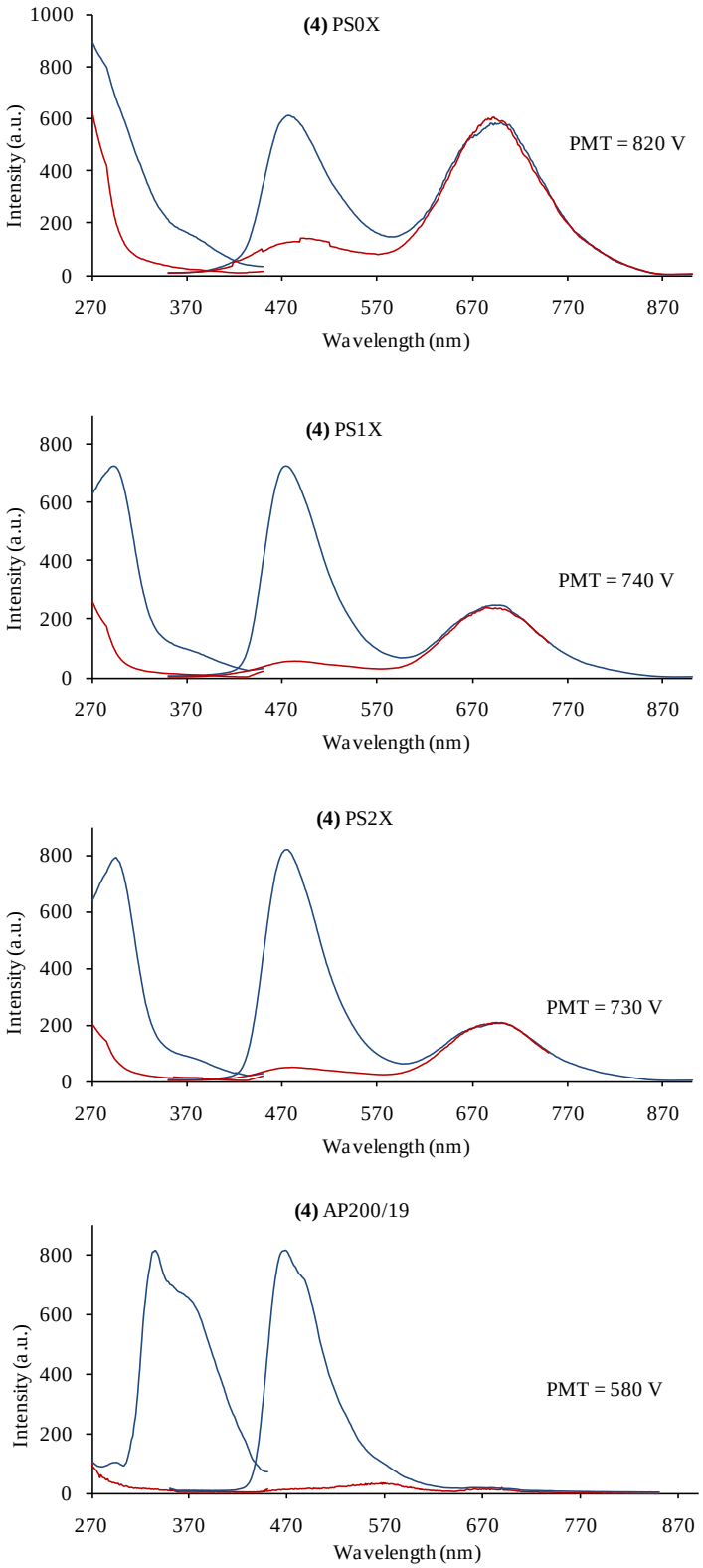

Figure S2. Excitation and emission spectra of **4** incorporated into PS membranes ($\lambda_{ex/em}$=300/470 nm) and AP200/190 ($\lambda_{ex/em}$=335/467 nm) in absence of oxygen (blue line) and with 10% of oxygen (red line) ([dye]=1.5 mg mL^{-1}; monochromator slit $width_{exc/em}$=20/20 nm, t_d=120 µs; t_g=5 ms, photomultiplier voltage is indicated for each graphic as PMT).

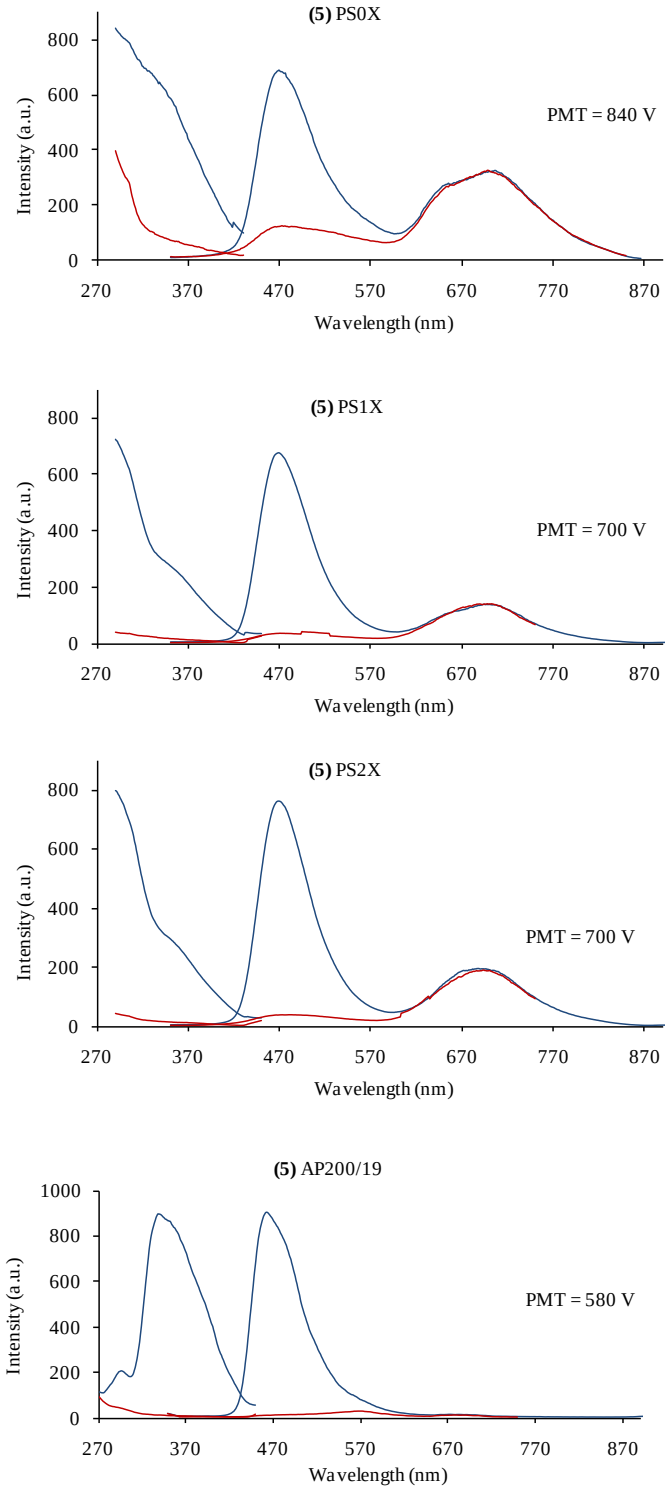

Figure S3. Excitation and emission spectra of **5** incorporated into PS membranes ($\lambda_{ex(em}$=300/465 nm) and AP200/190 ($\lambda_{ex/em}$=340/465 nm) in absence of oxygen (black line) and with 10% of oxygen (grey line) ([dye]=1.5 mg mL^{-1}; monochromator slit $width_{exc/em}$=20/20 nm, t_d=120 µs; t_g=5 ms, photomultiplier voltage is indicated for each graphic as PMT).

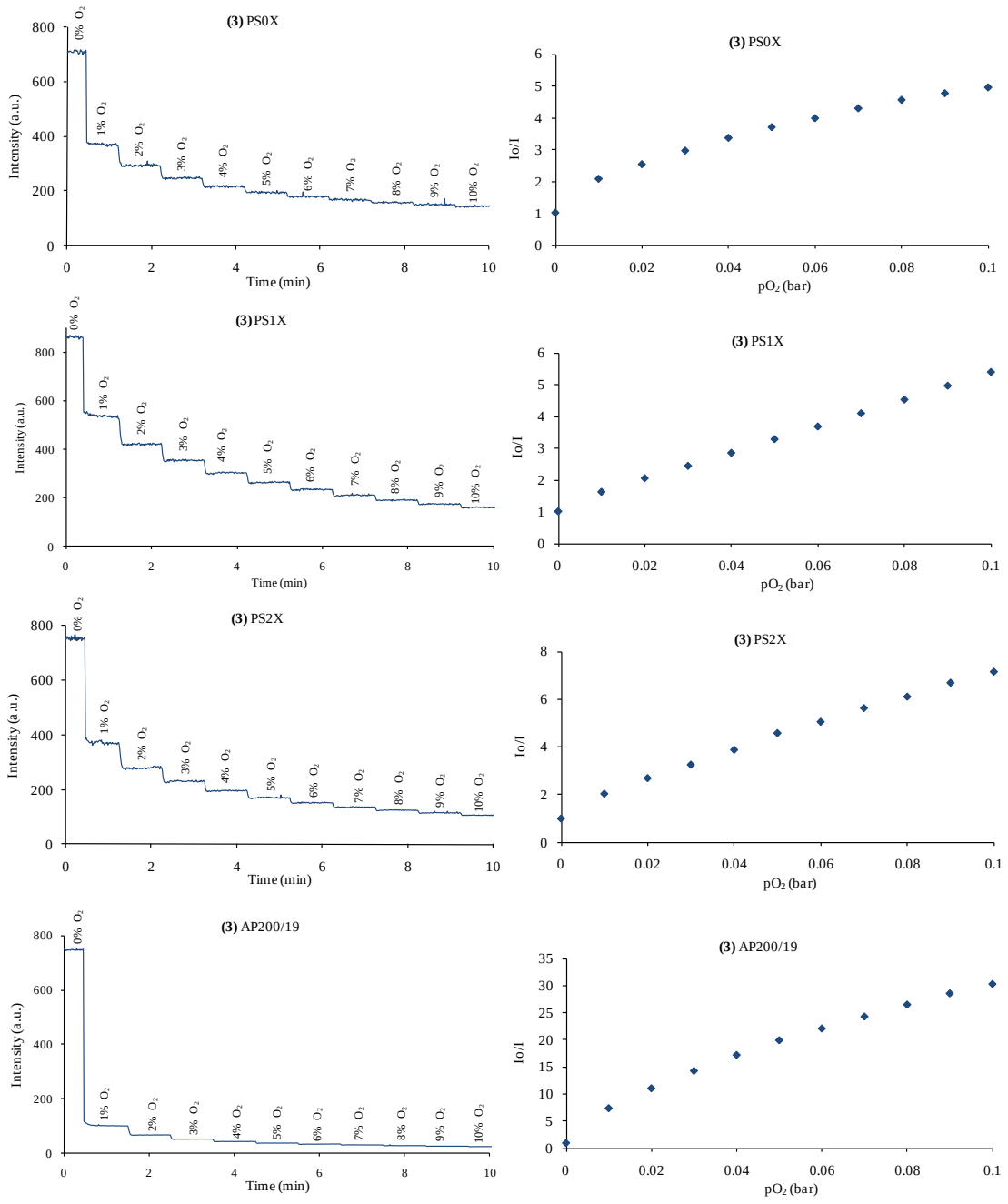

Figure S4. Luminescence intensity of **3** recorded versus time (left) for different oxygen concentration and the corresponding Stern-Volmer plot (right) for the PS membranes ($\lambda_{ex/em}$=303/470 nm) and the AP200/190 ($\lambda_{ex/em}$=335/470 nm) ([dye]=1.5 mg mL^{-1}; monochromator slit $width_{exc/em}$=20/20 nm, t_d=120 µs; t_g=5 ms).

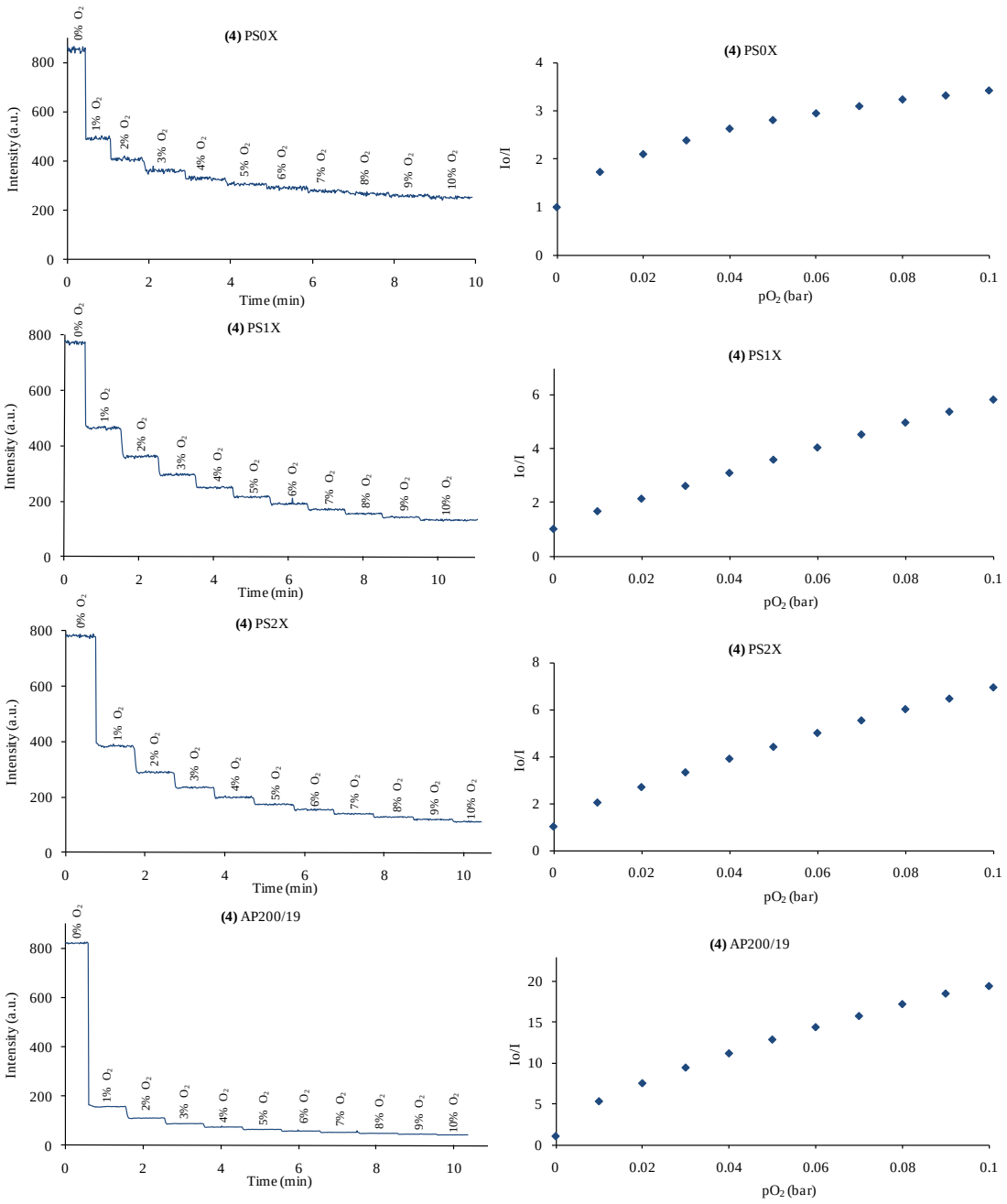

Figure S5. Luminescence intensity of **4** recorded versus time (left) for different oxygen concentration and the corresponding Stern-Volmer plot (right) for the PS membranes ($\lambda_{ex/em}$=300/470 nm) and the AP200/190 ($\lambda_{ex/em}$=335/467nm) ([dye]=1.5 mg mL^{-1}; monochromator slit $width_{exc/em}$=20/20 nm, t_d=120 µs; t_g=5 ms).

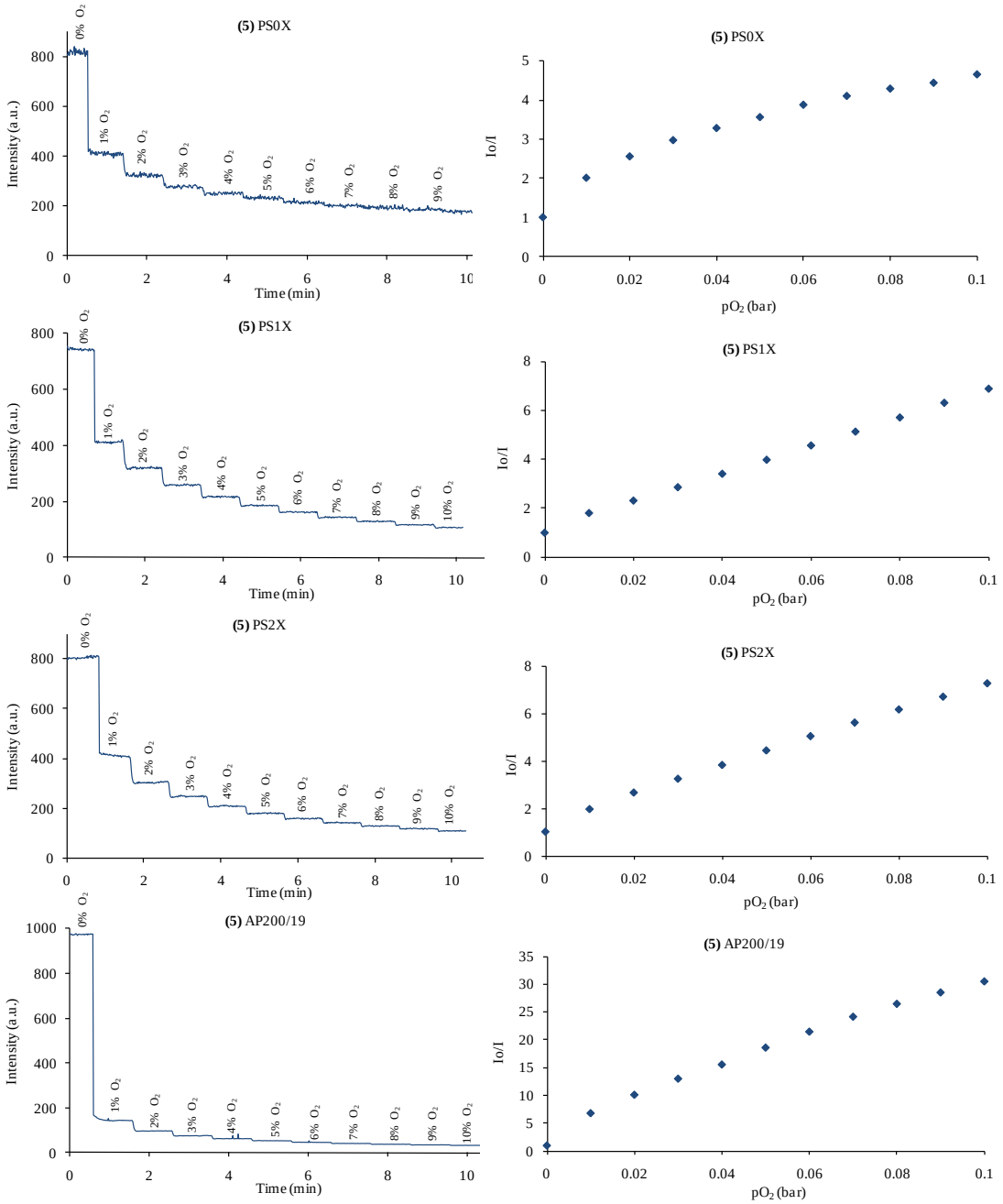

Figure S6. Luminescence intensity of **5** recorded versus time (left) for different oxygen concentration and the corresponding Stern-Volmer plot (right) for the PS membranes ($\lambda_{ex/em}$=300/465 nm) and the AP200/190 ($\lambda_{ex/em}$=340/465 nm) ([dye]=1.5 mg mL^{-1}; monochromator slit $width_{exc/em}$=20/20 nm, t_d=120 µs; t_g=5 ms).

Scheme S1. Synthetic path for the ligands **L1** and **L2**.

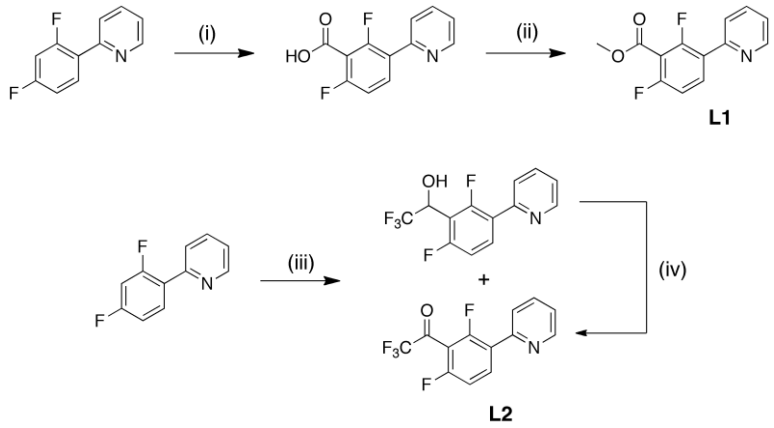

(i) a) LDA b) CO_2; (ii) H_2SO_4, MeOH; (iii) a) n-BuLi b) ethyl trifluoroacetic acid; (iv) a) CuCl, 1,10-phenanthroline b) Dicarbethoxyhydrazine, K_2CO_3.

Methyl 2,6-difluoro-3-(pyridin-2-yl)benzoate (L1). Sulfuric acid (98%, 0.2 ml) was added to 2,6-difluoro-3-(pyridine-2-yl)benzoic acid (0.5 g, 2.12 mmol) in methanol (20 ml) and the mixture was heated to 120 °C for 2.5 h. After cooling to room temperature, water (40 mL) was added and the mixture was neutralized with $NaHCO_3$. Water (50 ml) was added and extracted with ethylacetate. The organic phase was washed by brine (50 ml), dried over $MgSO_4$, and the volatiles removed under vacuum. The crude was purified by column chromatography on silica gel with a 1:1 mixture of ethylacetate/hexane as the eluent to yield **L1** as a white powder (R_f = 0.4, 0.21 g, yield: 40 %.) ^{1}H NMR (400 MHz, $CDCl_3$): 8.71 (d, 1H), 8.12 (m, 1H), 7.76 (d, 2H), 7.28 (t, 1H), 7.08 (td, 1H), 3.98 (s, 3H).

2-(2,4-Difluoro-3-(2,2,2-Trifluoroethanone)phenyl)pyridine (L2). n-BuLi in hexane (6.12 ml, 9.78 mmol, 1.1 eq.) was added dropwise over 15 min. to a stirred solution of 2-(2,4-difluorophenyl)pyridine (1.7 g, 8.89 mmol, 1 eq.) in THF (30 ml) at -78 °C. The mixture was stirred for 1 hr at -78 °C, and ethyl trifluoroacetic acid (1.17 ml, 9.78 mmol, 1.1 eq) added dropwise over 10 min. The mixture was warmed to room temperature overnight while stirring. Water (50 ml) was added and the mixture extracted with dichloromethane. The organic phase was washed by brine (50 ml), dried over $MgSO_4$, and the volatiles removed under vacuum. The crude was purified by column chromatography on silica gel with a 1:2 mixture of ethylacetate/hexane as the eluent to yield **L2** (R_f = 0.4, 0.53 g, yield: 21%) and 2-(2,4-difluoro-3-(2,2,2-Trifluoroethanol)phenyl)pyridine, **L2b**, (R_f = 0.1, 0.61 g, yield: 24%) as a pale yellow oils which crystallized upon standing. (**L2b**) ^{1}H NMR (400 MHz, $CDCl_3$): 8.73 (d, 1H), 8.04 (dd, 1H), 7.79 (t, 1H), 7.73 (d, 1H), 7.30 (t, 1H), 7.11 (t, 1H), 5.47 (bs, 1H), 3.51 (bs, 1H). (**L2**) ^{1}H NMR (400 MHz, $CDCl_3$): 8.73 (d, 1H), 8.31 (dd, 1H), 7.80 (t, 1H), 7.78 (s, 1H), 7.32 (t, 1H), 7.18 (t, 1H).

2-(2,4-Difluoro-3-(2,2,2-Trifluoroethanone)phenyl)pyridine (L2) from 2-(2,4-difluoro-3-(2,2,2-Trifluoroethanol)phenyl)pyridine (L2b). To a 25 mL two-necked flask fitted with a reflux condenser and an oxygen inlet were added toluene (15 ml) followed sequentially by CuCl (0.010 g, 0.10 mmol, 5 % eq.) and 1.10-phenanthroline (0.019 g, 0.10 mmol, 5 % eq.). The mixture was stirred at room temperature until the color darkened (about 20 min). 1,2-Dicarbethoxyhydrazine (0.09 g, 0.52 mmol, 25 % eq.) was

added followed by solid K_2CO_3 (0.56 g, 4.15 mmol, 2 eq) and the stirring continued for another 10 min. **L2b** (0.6 g, 2.07 mmol, 1 eq.) was added as a solid, and the solution heated to reflux with oxygen bubbling. After 2 hr, the reaction was found to be complete by TLC, the mixture was cooled to room temperature and the solvent was evaporated in *vacuo*. The crude product was purified by chromatography on silica gel with CH_2Cl_2 as the eluent to yield **L2** as colorless oil (0.52 g, 87 %). Sometimes the hydrated ligand was obtained. In that case it is subjected to vacuum distillation at 85 to 90 °C (65 °C / 0.08 torr) followed by alumina column chromatography eluted with a 1:2 mixture of ethylacetate/hexane followed by then pure ethylacetate to yield colorless oil.

Table S1. Selected distances (Å) and angles (deg.) for **3** and **5**

	3	5		3	5
Bond distance			Bond angle		
Ir-N(1)	2.042(6)	2.038(3)	C(11)-Ir-C(14)	89.4(3)	88.69(15)
Ir-N(2)	2.037(6)	2.057(3)	C(11)-Ir-N(1)	80.9(3)	80.98(14)
Ir-N(3)	2.146(6)	2.150(3)	C(14)-Ir-N(1)	94.4(3)	93.82(13)
Ir-C(11)	1.991(7)	1.984(4)	C(11)-Ir-N(3)	97.8(3)	98.53(14)
Ir-C(14)	2.003(7)	2.008(3)	C(14)-Ir-O(5/3)[a]	95.8(2)	95.82(12)
Ir-O(5/3)[a]	2.150(5)	2.140(3)	N(1)-Ir-N(2)	173.6(2)	174.06(12)

[a] O(5) for complex **3** and O(3) for complex **5**.

Table S2. Crystallographic data for **3** and **5**

	3	**5**
empirical formula	$C_{34}H_{25}F_4IrN_4O_6$	$C_{32}H_{14}F_{10}IrN_3O_4$
formula weight	853.78	886.66
temperature, K	100(2)	100(2)
wavelength (Å)	0.71073	0.71073
crystal system	Monoclinic	Monoclinic
space group	$P2_1/c$	$P2_1/c$
unit cell dimensions		
a (Å)	22.152(4)	20.248(3)
b (Å)	9.7488(14)	12.5782(14)
c (Å)	17.9625(18)	15.3528(10)
□ (deg)	90	90
□ (deg)	97.127(11)	91.222(9)
□ (deg)	90	90
volume (Å^3)	3849.1(10)	3909.3(8)
Z	4	4
density, calc d (g/cm^3)	1.473	1.507
absorption coefficient (mm^{-1})	3.532	3.497
F(000)	1672	1704
crystal size (mm^3)	0.42 x 0.32 x 0.26	0.41 x 0.32 x 0.27
□ range for data collection (deg)	3.31 to 27.55	3.37 to 27.51
reflections collected	8179	80870
independent reflections	8179 [R(int) = 0.0000]	8930 [R(int) = 0.0498]
Absorption correction	Semi-empirical from equivalents	Semi-empirical from equivalents
refinement method	Full-matrix least-squares on F^2	Full-matrix least-squares on F^2
data/restraints/parameters	8179 / 6 / 447	8930 / 72 / 497
goodness-of-fit on F^2	1.186	1.158
final *R* indices [*I* > 2□(*I*)]	R_1 = 0.0555	R_1 = 0.0310
	wR_2 = 0.1321	wR_2 = 0.0687
R indices (all data)	R_1 = 0.0596	R_1 = 0.0380
	wR_2 = 0.1344	wR_2 = 0.0714

Cartesian coordinates of the computed species

Complex **3** - GS

Ir	0.425772	-0.669517	0.197565
F	0.088518	4.330671	1.684970
F	-0.950792	3.542788	-2.800258
F	-4.318539	-0.743451	2.711598
F	-4.154899	-2.441974	-1.633984
O	0.097308	6.308729	-0.237135
O	-1.707098	5.762541	-1.443650
O	-6.248233	-2.434452	1.622309
O	-6.428611	-1.616552	-0.453174
O	1.107370	-2.677406	0.749483
O	2.888778	-4.004553	0.881616
N	0.742178	0.169670	2.049628
N	-0.043056	-1.439692	-1.661304
N	2.575084	-0.615562	-0.100754
N	6.692443	-0.936202	-0.586857
C	1.089119	-0.548971	3.121632
H	1.194443	-1.615447	2.957864
C	1.290027	0.029254	4.354915
H	1.566818	-0.586115	5.199942
C	1.122436	1.398905	4.472610
H	1.270026	1.890147	5.426468
C	0.765101	2.143762	3.366425
H	0.631143	3.210216	3.452127
C	0.569708	1.514101	2.140422
C	0.171974	2.126808	0.877224
C	-0.048148	3.481127	0.667689
C	-0.446344	4.012275	-0.555365
C	-0.608452	3.095286	-1.594015
C	-0.388364	1.746588	-1.444629
H	-0.521274	1.107916	-2.310943
C	0.007772	1.233755	-0.212812
C	-0.629773	5.475328	-0.714273
C	-1.941972	7.148857	-1.693378
H	-1.096213	7.593619	-2.218984
H	-2.104793	7.685516	-0.758110
H	-2.833953	7.195352	-2.311726
C	-1.542053	-0.994835	0.435519
C	-2.291828	-0.723888	1.575633
H	-1.850410	-0.265318	2.454016
C	-3.629737	-1.033615	1.609744
C	-4.307871	-1.600694	0.531157
C	-3.544560	-1.856036	-0.603160
C	-2.186584	-1.572525	-0.685527
C	-1.337699	-1.809988	-1.849728
C	-1.723845	-2.337799	-3.079015
H	-2.748063	-2.633034	-3.239663
C	-0.797993	-2.476521	-4.093066
H	-1.103168	-2.884939	-5.048573
C	0.514759	-2.093301	-3.878752
H	1.269539	-2.183612	-4.647851
C	0.849420	-1.577447	-2.647280
H	1.859736	-1.255733	-2.424738
C	-5.747134	-1.940600	0.644748
C	-7.818186	-1.946080	-0.445566
H	-7.958088	-3.019003	-0.309040
H	-8.204997	-1.637575	-1.412714
H	-8.335003	-1.413137	0.353241
C	2.356350	-2.929676	0.633822
C	3.215639	-1.770152	0.158894
C	4.570582	-1.914738	0.012797
H	4.996920	-2.880598	0.245055
C	5.357132	-0.830350	-0.427522
C	4.664456	0.370389	-0.687965
H	5.179826	1.257336	-1.027707
C	3.305630	0.425777	-0.514317
H	2.762293	1.343640	-0.716153
C	7.363608	-2.190205	-0.306265
H	7.240351	-2.487823	0.739497
H	8.426533	-2.074637	-0.500595
H	6.989057	-2.998230	-0.941846
C	7.464451	0.203723	-1.039630
H	7.147276	0.535924	-2.033046
H	8.512706	-0.077113	-1.097413
H	7.377900	1.048135	-0.348938

Complex **3** – T1

Ir	0.455102	-0.677952	0.202863
F	-0.024842	4.299331	1.707932
F	-1.011723	3.506854	-2.797562
F	-4.287393	-0.876815	2.742499
F	-4.167157	-2.427017	-1.674933
O	-0.061306	6.281802	-0.240789
O	-1.877195	5.678503	-1.395459
O	-6.163900	-2.665342	1.533598
O	-6.429550	-1.537811	-0.379422
O	1.181837	-2.666784	0.751972
O	3.000065	-3.951314	0.852693
N	0.760053	0.156670	2.063851
N	0.022620	-1.425819	-1.649343
N	2.592496	-0.571053	-0.123661
N	6.709351	-0.789279	-0.626206
C	1.139042	-0.550729	3.129071
H	1.268383	-1.609352	2.964271
C	1.341072	0.036547	4.361476
H	1.644686	-0.566728	5.201478
C	1.137833	1.402138	4.477324
H	1.283915	1.898668	5.424603
C	0.744915	2.136700	3.372180
H	0.585353	3.195390	3.457551
C	0.554818	1.491723	2.153294
C	0.134778	2.097206	0.881470
C	-0.128036	3.442271	0.679210
C	-0.534271	3.965499	-0.541393
C	-0.658441	3.053148	-1.583991
C	-0.398334	1.709988	-1.445702

H	-0.503364	1.071452	-2.309841
C	0.002313	1.205962	-0.211296
C	-0.775629	5.425035	-0.698329
C	-2.158288	7.071268	-1.637969
H	-1.335842	7.522700	-2.183618
H	-2.304885	7.586509	-0.694246
H	-3.064826	7.081543	-2.228096
C	-1.477782	-1.040980	0.477338
C	-2.227038	-0.826121	1.610648
H	-1.787602	-0.407657	2.504313
C	-3.579547	-1.129329	1.631150
C	-4.267320	-1.653186	0.514341
C	-3.550032	-1.868315	-0.620628
C	-2.138264	-1.582197	-0.726976
C	-1.357009	-1.756053	-1.844081
C	-1.762414	-2.230677	-3.152774
H	-2.801757	-2.433941	-3.334020
C	-0.847656	-2.415370	-4.134477
H	-1.152822	-2.769605	-5.106580
C	0.517500	-2.135100	-3.874324
H	1.278477	-2.276004	-4.622498
C	0.878303	-1.630303	-2.618159
H	1.907182	-1.375721	-2.410902
C	-5.711172	-2.017513	0.625138
C	-7.831105	-1.880266	-0.366039
H	-7.944533	-2.959032	-0.397692
H	-8.245589	-1.421279	-1.253363
H	-8.296310	-1.482633	0.529941
C	2.434068	-2.889199	0.616531
C	3.263999	-1.705927	0.131812
C	4.620820	-1.825562	-0.017369
H	5.067489	-2.777345	0.212498
C	5.378974	-0.716563	-0.460887
C	4.654790	0.470531	-0.715712
H	5.143274	1.369210	-1.050946
C	3.293751	0.489922	-0.536281
H	2.726986	1.389018	-0.730759
C	7.413055	-2.029921	-0.337812
H	7.292749	-2.314921	0.707159
H	8.467653	-1.883804	-0.535467
H	7.051723	-2.840508	-0.969925
C	7.450904	0.377896	-1.077612
H	7.103517	0.706532	-2.056870
H	8.498477	0.114984	-1.155479
H	7.352041	1.202486	-0.371652

Complex **4** - GS

Ir	0.566969	-1.005283	0.069630
F	2.092302	3.732383	1.671912
F	0.565564	3.548141	-2.737887
F	-3.711346	0.466836	2.953007
F	-4.452190	-0.935790	-1.437339
O	2.675797	5.661962	-0.212134
O	0.721671	5.831315	-1.290383
O	-6.190772	-0.352000	1.970265
O	-6.188564	0.590949	-0.059571
O	0.535105	-3.148883	0.522976
O	1.756567	-5.011611	0.496130
N	1.271802	-0.409226	1.910701
N	-0.267314	-1.476672	-1.761716
N	2.588939	-1.684961	-0.376477
H	6.047755	-3.216036	-1.030043
C	1.406356	-1.248498	2.941987
H	1.123009	-2.277394	2.751316
C	1.865231	-0.828375	4.170106
H	1.957095	-1.536519	4.982128
C	2.191865	0.508325	4.326026
H	2.554712	0.877396	5.277369
C	2.054306	1.377320	3.261951
H	2.304273	2.419717	3.378116
C	1.582658	0.907035	2.039864
C	1.347909	1.673636	0.820497
C	1.603414	3.027850	0.652731
C	1.341187	3.715495	-0.528182
C	0.804143	2.958370	-1.568936
C	0.546669	1.611989	-1.460879
H	0.143829	1.097090	-2.326043
C	0.814722	0.942350	-0.271303
C	1.673394	5.156318	-0.647872
C	0.972954	7.221932	-1.497766
H	1.885013	7.365478	-2.078269
H	1.070122	7.740933	-0.543621
H	0.115941	7.603042	-2.045834
C	-1.366817	-0.629849	0.454779
C	-1.891907	-0.172607	1.658452
H	-1.259961	0.050736	2.511108
C	-3.246941	0.012261	1.791518
C	-4.151598	-0.214931	0.755295
C	-3.606970	-0.664927	-0.442660
C	-2.246422	-0.881919	-0.625257
C	-1.617847	-1.352040	-1.856090
C	-2.248565	-1.653951	-3.060070
H	-3.318761	-1.557146	-3.145514
C	-1.503939	-2.071131	-4.144506
H	-1.998073	-2.302812	-5.079928
C	-0.130083	-2.191494	-4.025935
H	0.489220	-2.512687	-4.852066
C	0.448230	-1.881892	-2.815970
H	1.519271	-1.952460	-2.670598
C	-5.606210	-0.018526	0.971607
C	-7.598863	0.789476	0.047331
H	-8.113864	-0.165138	0.160750
H	-7.904525	1.273087	-0.876157
H	-7.833172	1.426670	0.900725
C	1.610314	-3.809264	0.318838
C	2.793494	-2.995710	-0.174033
C	4.027347	-3.574899	-0.399724
H	4.141602	-4.636344	-0.223510
C	5.072108	-2.784148	-0.844489
C	4.852877	-1.432334	-1.044775
H	5.641899	-0.777850	-1.390345
C	3.594481	-0.917383	-0.800355
H	3.371629	0.134156	-0.947198

Complex **4** – T1

Ir	0.591460	-0.998155	0.072080
F	2.019238	3.757159	1.690749
F	0.520716	3.557744	-2.738021
F	-3.728884	0.399309	2.955966
F	-4.468420	-0.989121	-1.454458
O	2.572736	5.699000	-0.219248
O	0.593713	5.834546	-1.248468
O	-6.183414	-0.629429	1.901340
O	-6.198552	0.572812	0.015460
O	0.592681	-3.137570	0.527395
O	1.846010	-4.981807	0.467336
N	1.285065	-0.403927	1.921657
N	-0.199031	-1.466916	-1.755271
N	2.615965	-1.638742	-0.396218
H	6.090555	-3.112690	-1.078992
C	1.444347	-1.242758	2.946412
H	1.175778	-2.270370	2.755482
C	1.911556	-0.816333	4.172800
H	2.025252	-1.521750	4.979714
C	2.216936	0.526281	4.326250
H	2.583714	0.899360	5.270428
C	2.051154	1.397245	3.263494
H	2.284628	2.439237	3.378780
C	1.574856	0.912494	2.048786
C	1.322607	1.679944	0.820656
C	1.547799	3.037601	0.659991
C	1.278152	3.721101	-0.518430
C	0.767001	2.957819	-1.562653
C	0.537368	1.605192	-1.465849
H	0.154511	1.082721	-2.329446
C	0.811361	0.941207	-0.273918
C	1.570135	5.175291	-0.636178
C	0.820505	7.243935	-1.449013
H	1.713116	7.391008	-2.048692
H	0.932226	7.738246	-0.489482
H	-0.057353	7.603699	-1.968702
C	-1.320709	-0.666436	0.485431
C	-1.865172	-0.236194	1.671746
H	-1.246717	-0.020836	2.530640
C	-3.234617	-0.053596	1.794639
C	-4.139709	-0.282613	0.734879
C	-3.623711	-0.698286	-0.452104
C	-2.210007	-0.905712	-0.667894
C	-1.617426	-1.294197	-1.844521
C	-2.252978	-1.545197	-3.123286
H	-3.308487	-1.371021	-3.222896
C	-1.529750	-1.989839	-4.178779
H	-2.005791	-2.176120	-5.128589
C	-0.137422	-2.204653	-4.025399
H	0.473925	-2.565107	-4.834672
C	0.462542	-1.909112	-2.794222
H	1.528152	-2.032801	-2.670732
C	-5.609636	-0.145283	0.959958
C	-7.629214	0.715352	0.138106
H	-8.097509	-0.263272	0.113232
H	-7.930702	1.310493	-0.713183
H	-7.868515	1.219660	1.068560
C	1.674145	-3.779653	0.302163
C	2.843595	-2.944128	-0.202021
C	4.081791	-3.510230	-0.437910
H	4.211839	-4.566604	-0.268030
C	5.112872	-2.698322	-0.885520
C	4.871705	-1.347670	-1.076886
H	5.645885	-0.680961	-1.421480
C	3.604475	-0.852428	-0.821302
H	3.362564	0.190942	-0.958454

Complex **5** - GS

Ir	-0.096763	1.305028	0.054224
F	-3.486605	-1.972360	2.293041
F	-2.404371	-2.995413	-2.131271
F	3.251012	-1.751020	2.908884
F	4.187134	-1.194631	-1.629099
F	7.318449	-2.331544	0.875382
F	6.425729	-2.775584	-1.023399
F	6.409694	-0.756714	-0.258392
O	4.988792	-3.327483	1.535476
O	0.957276	3.208494	0.235344
O	0.738483	5.414328	0.016951
N	-0.817917	1.282915	1.983267
N	0.685386	1.175753	-1.856026
N	-1.614283	2.803639	-0.388242
C	-0.454640	2.182436	2.902109
H	0.250053	2.936353	2.570375
C	-0.939185	2.144658	4.190354
H	-0.619793	2.888066	4.907663
C	-1.825246	1.136476	4.529021
H	-2.225597	1.071629	5.533114
C	-2.201719	0.205821	3.580593
H	-2.888074	-0.583450	3.841045
C	-1.684726	0.283980	2.291807
C	-1.938768	-0.619223	1.171530
C	-2.794190	-1.708499	1.191710
C	-3.015280	-2.530648	0.080696
C	-2.286845	-2.204237	-1.067754
C	-1.419264	-1.145835	-1.135990
H	-0.883795	-0.979969	-2.063685
C	-1.238414	-0.321811	-0.027511
C	-3.923382	-3.681835	0.183437
C	1.481508	0.121183	0.402873
C	1.827622	-0.451795	1.623045
H	1.236214	-0.291366	2.517591
C	2.944144	-1.242092	1.723222
C	3.797822	-1.492744	0.640305
C	3.424784	-0.912083	-0.572478
C	2.295848	-0.126867	-0.730465
C	1.835850	0.464288	-1.984774
C	2.437114	0.355486	-3.234453
H	3.352457	-0.202682	-3.346374
C	1.858078	0.958933	-4.332793
H	2.326843	0.870804	-5.304960

C	0.682754	1.673139	-4.180743
H	0.195803	2.157093	-5.016086
C	0.128641	1.756789	-2.923347
H	-0.791528	2.300965	-2.749154
C	4.966730	-2.367939	0.811507
C	6.302151	-2.036199	0.076554
C	0.294167	4.275268	-0.009023
C	-1.172127	4.069869	-0.342226
C	-2.016904	5.136418	-0.580804
H	-1.611888	6.138706	-0.533446
C	-3.346786	4.890479	-0.873406
H	-4.028135	5.710137	-1.065015
C	-3.794326	3.581571	-0.914361
H	-4.825765	3.344459	-1.138356
C	-2.896479	2.561350	-0.666928
H	-3.199063	1.519966	-0.692872
O	-4.061582	-4.355784	1.169339
C	-4.825085	-4.058092	-1.033146
F	-6.002973	-4.470917	-0.585784
F	-4.282595	-5.057421	-1.724603
F	-5.039490	-3.039945	-1.857686

Complex **5** - Ta

Ir	-0.001499	1.180823	0.039599
F	-3.691718	-1.644058	2.354791
F	-2.792758	-2.827530	-2.107224
F	3.452681	-1.694451	2.937066
F	4.204005	-1.401488	-1.659842
F	7.420303	-2.354797	0.820791
F	6.495848	-2.788590	-1.077128
F	6.435634	-0.776722	-0.271877
O	5.095155	-3.386508	1.516271
O	1.069513	3.017866	0.141818
O	0.974868	5.233353	-0.087341
N	-0.665346	1.262320	1.984903
N	0.706101	0.992727	-1.893077
N	-1.500235	2.737293	-0.400962
C	-0.190881	2.127071	2.881644
H	0.595457	2.781605	2.538715
C	-0.676086	2.165735	4.173212
H	-0.269886	2.873757	4.876647
C	-1.675761	1.275291	4.525516
H	-2.077454	1.273957	5.527157
C	-2.166678	0.378175	3.590845
H	-2.940992	-0.315413	3.859961
C	-1.645263	0.382011	2.303302
C	-2.022527	-0.490675	1.182774
C	-2.984955	-1.478047	1.225738
C	-3.333033	-2.295892	0.126900
C	-2.591804	-2.027632	-1.040943
C	-1.641091	-1.046337	-1.150398
H	-1.129946	-0.924946	-2.093233
C	-1.334440	-0.263215	-0.038575
C	-4.307210	-3.356738	0.263924
C	1.586043	0.032778	0.399304
C	1.964768	-0.453578	1.642427
H	1.406683	-0.239069	2.540054
C	3.088575	-1.242648	1.737253
C	3.876157	-1.559496	0.633494
C	3.469238	-1.053394	-0.596097
C	2.343413	-0.267691	-0.753558
C	1.849704	0.280019	-2.025024
C	2.432746	0.130549	-3.275215
H	3.341335	-0.430541	-3.389918
C	1.830367	0.711744	-4.379128
H	2.278516	0.597959	-5.354100
C	0.661914	1.435418	-4.223244
H	0.163672	1.900134	-5.058027
C	0.127915	1.552964	-2.955756
H	-0.783165	2.100843	-2.776877
C	5.066377	-2.432611	0.795266
C	6.378838	-2.071723	0.042655
C	0.462905	4.130217	-0.096323
C	-1.016205	3.985677	-0.392371
C	-1.816046	5.083897	-0.629169
H	-1.372239	6.066101	-0.611648
C	-3.164871	4.880458	-0.880488
H	-3.817982	5.718322	-1.069998
C	-3.661516	3.588025	-0.881649
H	-4.703337	3.385634	-1.070873
C	-2.797161	2.534718	-0.637500
H	-3.136479	1.510399	-0.634981
O	-4.464485	-4.031133	1.330380
C	-5.212133	-3.690789	-0.885386
F	-6.446947	-4.011628	-0.442477
F	-4.817035	-4.767450	-1.621686
F	-5.374527	-2.678038	-1.763262

Complex **5** - Tb

Ir	-0.082897	1.300792	0.063367
F	-3.437994	-2.089323	2.296790
F	-2.407429	-2.992199	-2.175952
F	3.291319	-1.722786	2.927607
F	4.173530	-1.224828	-1.635824
F	7.339091	-2.343740	0.776522
F	6.364712	-2.706219	-1.109950
F	6.383273	-0.712098	-0.256379
O	5.032701	-3.295669	1.546361
O	0.935901	3.208861	0.290088
O	0.681395	5.414775	0.085023
N	-0.775693	1.270905	1.981398
N	0.697434	1.193105	-1.851738
N	-1.624621	2.773734	-0.377068
C	-0.479249	2.137525	2.910443
H	0.198457	2.928928	2.623470
C	-0.984429	2.062388	4.220541
H	-0.698811	2.812235	4.937646
C	-1.840286	0.985447	4.564754
H	-2.221501	0.898914	5.570007
C	-2.172376	0.068766	3.625974
H	-2.815423	-0.755353	3.873752

C	-1.659435	0.181280	2.269766
C	-1.895214	-0.640512	1.195274
C	-2.758907	-1.795097	1.183783
C	-2.963847	-2.561181	0.068806
C	-2.263892	-2.200077	-1.101297
C	-1.407264	-1.114700	-1.169714
H	-0.900541	-0.924100	-2.104009
C	-1.209593	-0.311772	-0.069889
C	-3.892742	-3.713935	0.129819
C	1.491461	0.131521	0.415749
C	1.848591	-0.426244	1.640799
H	1.267663	-0.253584	2.533869
C	2.964945	-1.219245	1.731986
C	3.798165	-1.489402	0.643233
C	3.414361	-0.922720	-0.569498
C	2.292811	-0.131182	-0.721505
C	1.835052	0.470081	-1.983127
C	2.445492	0.358748	-3.228151
H	3.348988	-0.210440	-3.342011
C	1.880294	0.986688	-4.324065
H	2.350895	0.901464	-5.291637
C	0.717174	1.721389	-4.169263
H	0.245784	2.223802	-4.998076
C	0.156577	1.798027	-2.910795
H	-0.750597	2.352433	-2.731779
C	4.980764	-2.353233	0.804813
C	6.286866	-2.012169	0.029576
C	0.258447	4.266620	0.045387
C	-1.205902	4.043710	-0.306991
C	-2.060025	5.105528	-0.534828
H	-1.672482	6.109162	-0.469584
C	-3.386535	4.840908	-0.840075
H	-4.077350	5.649735	-1.023152
C	-3.813595	3.524546	-0.903832
H	-4.836656	3.275566	-1.136212
C	-2.898778	2.513036	-0.666627
H	-3.177004	1.470458	-0.712300
O	-3.969070	-4.474837	1.051081
C	-4.886215	-3.931791	-1.047031
F	-6.056621	-4.342767	-0.561947
F	-4.436469	-4.872011	-1.881458
F	-5.098072	-2.812604	-1.741842

Bloque II: Estrategias para el control de las propiedades ópticas y morfológicas de fases sensores

Las propiedades de las fases sensoras son muy importantes para lograr unas características necesarias para la resolución de problemas analíticos. Los enfoques que se pueden seguir para controlar sus propiedades atienden tanto a factores químicos (composición, polaridad, etc.) como a características morfológicas (espesor de la fase sensora, porosidad, homogeneidad, etc.).

Dentro de las estrategias para controlar estas propiedades está el uso de reacciones de polimerización radical controlada por transferencia de átomo (*Atom Transfer Radical Polymerization*, ATRP), que permite desarrollar materiales a la carta, ya sean orgánicos o híbridos, con propiedades y morfología adecuadas para el desarrollo de fases sensoras.

La ATRP es un tipo de polimerización radical controlada (CRP). El desarrollo de técnicas CRP ha sufrido un gran avance en los últimos años debido a la necesidad de crear estructuras complejas de polímeros para diferentes aplicaciones, donde el control la estructura polimérica se consigue controlando adecuadamente el crecimiento de las cadenas durante la polimerización. De esta forma se pueden crear copolímeros que contengan segmentos rígidos y flexibles, o que combinen propiedades hidrofílicas e hidrofóbicas, con una dispersión mínima de los pesos moleculares de las cadenas poliméricas.

Todos esos métodos de CRP se basan en el establecimiento de un equilibrio químico rápido y dinámico entre una poca cantidad de macrorradicales en crecimiento y una gran cantidad de especies inactivas, que en el caso de la ATRP son haluros de alquilo. El equilibrio formado hace que las etapas de terminación características en la polimerización convencional (responsable de la diferencia en composición química y de la distribución de pesos moleculares de las cadenas) sean prácticamente nulas. Así todas las cadenas poliméricas crecen al mismo tiempo, adicionando monómero, durante todo el tiempo que dura la polimerización.

Por el interés creciente de esta técnica de CRP, en este capítulo se ha realizado una revisión bibliográfica de las fases sensoras ópticas desarrollados mediante ATRP, haciendo un especial énfasis en cómo cada uno de los elementos de la polimerización puede influir sobre las características finales que se desean conseguir en la fase sensora.

Por otro lado, conseguir unas características morfológicas adecuadas de la fase sensora requiere en la mayoría de los casos planear una serie de experimentos y optimizar la fase sensora mediante ensayo-error. En este sentido, el uso de diseño de experimentos puede ser muy útil para modelizar la respuesta de parámetros morfológicos en función de las condiciones de preparación de la fase sensora con un número mínimo de experimentos. Los modelos de diseño de experimentos son modelos estadísticos clásicos cuyo objetivo es averiguar si unos determinados factores influyen en una variable de interés y obtener un modelo estadístico-matemático que permita hacer predicciones de respuestas futuras.

Así, en el Capítulo 4 se recoge la modelización del tamaño y polidipsersidad de nanopartículas poliméricas sensibles a oxígeno haciendo uso de metodologías de superficie de respuesta, las cuales permiten crear un "catálogo" de condiciones de síntesis y propiedades con el objetivo de producir nanopartículas con propiedades *a la carta*.

Capítulo 3

Atom transfer radical polymerization (ATRP) as a tool for the development of optical sensing phases

M. Marin-Suarez[a], A.L. Medina-Castillo[a,b,*], J.F. Fernandez-Sanchez[a], A. Fernandez-Gutierrez[a]

[a] *Department of Analytical Chemistry, Faculty of Sciences, University of Granada (UGR), C/Fuentenueva s/n, E-18071 Granada, Spain.*

[b] *NanoMyP, Nanomateriales y Polimeros S.L., Spin-Off company of the UGR, BIC building, Avd. Innovacion 1, 18100, Granada, Spain*

Abstract

The advantages of atom transfer radical polymerization (ATRP) for synthesizing well-defined polymers have made this technique very popular in the last few years for the synthesis of new polymers and copolymers with optical properties. The components involved in ATRP and their relations with the composition, functionalities and topology have been reviewed according to the optical properties of the obtained (co)polymers. Since in ATRP several functionalities and architectures can be combined, this technique has resulted to be a useful tool for the synthesis of new (co)polymers specially designed to meet the requirements of the sensor setup.

*Keywords:*ATRP, nanostructures, polymers, optical sensors, sensing phase;
*Corresponding author. *E-mail address:* antonioluismedina@ugr.es

3. 1. Introduction

A chemical sensor is defined by the IUPAC as a device that transforms chemical information into an analytically useful signal.[1] This chemical information may originate from a chemical reaction involving the analyte or from a physical property of the system investigated. Although the first developed sensors were electrochemical,

recent advances in spectroscopic techniques have attracted a crescent interest in optical sensing due to its advantages.[2-4]

In an optical sensor the interaction between an analyte and its receptor produces a change in the optical phenomena, which can be easily measured. Thus, it is essential for all optical sensors to possess a receptor that has the ability to interact with the target analyte. The receptor needs to be supported into a matrix, forming the so-called sensing phase.

Absorbance/luminescence optical sensors are based either on the inherent luminescence properties of the sensing phase, or on the presence of a chemical indicator physically or chemically immobilized in this phase. Furthermore, the advances in nanoplasmonic in recent years have demonstrated that surface plasmon resonance (SPR) is one of the most powerful optical recognition mechanism for the identification of molecular species, with the potential of reaching single-molecule detection under ambient conditions.[5-7]

Furthermore, optical techniques are very useful in the evaluation of molecularly imprinted polymers (MIPs). MIPs are tailor-made polymers which possess defined cavities that are able to selectively recognize a target molecule or a group of related compounds.[8] Such specific recognition can be caused by either covalent or non-covalent interactions and it results in changes in the optical properties of the MIP.[9]

The sensing phases can be based on different materials such as, polymers, metal-oxide, sol-gel nanostructures, or hybrid organic-inorganic phases.[10-15] These materials are then deposited on a solid support such as a waveguide, an optical fibre or a microchip, which will provide the support for the optical measurement.[16] Traditionally, polymer matrices have been widely used in optical sensing due to their advantages:transparency to visible light, mechanical stability and facility to obtain different shapes, thickness and compositions. However, polymers can suffer for thermal o photodegradation, long diffusion times of the analyte, strong intrinsic fluorescence or aggregation of the chemical species.[16-18] These disadvantages make it necessary to develop new polymeric materials possessing well defined composition and functionalities, therefore giving the opportunity to design new sensing phases according to the needs of the sensor setup and the chemical species involved in the recognition reaction.

Among all kind of polymerization reactions, radical polymerization is the most widely used method for polymer synthesis, as a radical process is more tolerant to functional groups and impurities.[19] In recent years, there has been a fast growth in the development and understanding of controlled/living radical polymerization (CPR).[20] All CPR methods are base on activation and deactivation steps that establish a rapid dynamic equilibrium between a small amount of growing radicals and a large amount of dormant species. In the so-called transition metal catalyzed atom transfer radical polymerization (ATRP), the radicals, or the active species, are generated through a reversible redox process catalyzed by a transition metal complex (M_t^n) which undergoes a one electron oxidation with concomitant abstraction of a (pseudo)halogen atom, X, from a dormant species, R-X. This process is characterized by a rate constant of activation (k_{act}) and deactivation (k_{deact}), as it is represented in **Fig. 1**

Figure 1. Atom transfer radical polymerization mechanism

The polymerization proceed in a similar manner as a conventional radical polymerization: by subsequent addition of the intermediate radicals to the monomers, and it is characterized by a rate constant of propagation (k_p). Termination reactions (k_t) also occur in ATRP, mainly through radical coupling and disproportion; however, in the well-controlled ATRP, no more than a few percent of the polymer chains undergo termination. This is one on the reasons why transition metal catalyzed ATRP is becoming very popular as it allows the synthesis of a variety of well-defined polymers and copolymers, which are very useful in the development of new optical sensing materials. Nevertheless, ATRP cannot only be used as a tool to develop new (co)polymer as matrices for optical sensing, but also for the assisted-detection of biomolecules.[21-26]

This review will pay special attention to those transition metal catalyzed ATRP reactions used to develop new polymers and copolymers with adequate optical properties for the preparation of advanced optical sensing phases. The reviewed sensing phases are principally based on organic polymeric thin films (optodes),

polymer brushes grown from a surface and hybrid organic-inorganic materials such as high functionalized nanoparticles, nanofibers, polymer-grafted composites, etc. These matrices contain inherent optical properties, or an indicator physically or chemically entrapped, resulting in optical sensing phases mainly based on absorbance, luminescence and surface plasmon resonance.

3. 2. Discussion

3. 2.1. Types of sensing phases developed by ATRP

In order to organize the information that will be described along the different sections of this work, **Table 1** shows a summary of the reviewed sensing phases taking into account the specific applications. In this table, for each optical principle (OP) that is applied, the type of target molecule with the corresponding references are shown.

Table 1. Summary of the main optical principles applied in the sensing phases developed by ATRP.

OP[i]	Target molecule	Sensing phase	References
SPR	Proteins	Copolymer brush	21, 27-32
SPR	Pathogen	Copolymer brush	33
SPR	DNA	Copolymer brush	26
EL	DNA	Copolymer brush	25
EL	Proteins	Copolymer brush	22
XPS	Proteins	Copolymer brush	34
A	DNA	Copolymer brush	23, 24
AS	Metal ions	Copolymer brush	35, 36
AS	Metal ions	Copolymer	37
FQ	Oxygen	Star copolymers	38-40
FQ	pH	Copolymers	41, 42
FQ	pH	Hybrid material	43
FQ	Temperature	Hybrid material	44
FQ	Temperature	Copolymer	45
FRET	pH	Polymer	46
FI	Theophyiline	MIP	47
FI	Bisphenol A	MIP	48-50

[i]OP = Optical Principle; SPR = Surface Plasmon Resonance; EL = Ellipsometry; XPS = X-ray photoelectron spectroscopy; A = Absorbance; AS = Absorbance Shift; FQ = Fluoresncence Quenching; FRET = Fluorescence Resonance Energy Transfer; FI = Fluorescence Intensity.

As it can be seen, many of the applications of (co)polymers synthesized by ATRP are linked to the development of biosensors. In most of the examples found in the literature, the ATRP was initiated from a gold surface, which allows the detection by SPR of several types of protein that adsorb in the polymer brushes. As it will be show in section 2.2 and 2.3, non-fouling properties can be obtained with the different

functionalities and topologies easily reachable by ATRP, allowing the selective adsorption of proteins.

This work also analyzed chemical sensor based on linear or branched copolymers obtained by ATRP can be further mechanized as films or nanofibres. Therefore, (co)polymers with an adequate chemical composition can be applied to develop oxygen, pH or temperature probes. In these cases the fluorescence quenching, produced by the changes of these properties, is responsible for the optical sensing capability. Besides, fluorescence resonance energy transfer (FRET) has been also useful to develop pH-sensitive polymers, where the fluorescence spectra changes under the presence of different pH.

Furthermore, other (co)polymers possessing complexation properties can produce a colorimetric change that is measured by absorbance, allowing the selective detection of metal ions. In this case, due to versatility of the ATRP, the polymer can grow from a surface, resulting in a polymer brush, or from a macroinitiator, resulting in a copolymer that can be spin-coated onto a glass surface in order to allow the absorption measurement.

The different topologies and functionalities obtained by ATRP can be also exploited in the synthesis of new copolymers with free crosslinkable groups that can be used to develop molecularly imprinted polymers.

Next sections will describe the sensing phases according to the different ATRP components, taking into account how the different catalysts and ligands, monomers and functionalities, solvents, and topology have been applied to obtain adequate optical performance.

3.2.2. ATRP components involved in the development of (co)polymers with application in optical sensors.

ATRP is a multicomponent reaction, in which the main components are: the monomers, an initiator with a transferable (pseudo)halogen, and a catalyst (composed of a transition metal species with any suitable ligand). Some other factors, such as additives, solvent and temperature must be taken into account in order to obtain a successful ATRP.[51, 52] In recent years there has been a great advance in understanding the mechanism of ATRP. These advances have allowed the development of different

modes of initiation/activation/deactivation of ATRP such as: simultaneous reverse and normal initiation ATRP (SR&SI),[53] activators generated by electron transfer ATRP (AGET),[54] hybrid catalyst systems and bimetallic ATRP.[55] All the advances in ATRP mentioned above, have been used to design and synthesize novel functional (co)polymer with selected properties such as: monomer distributions, functionalities and/or architectures, which allow the design of optical sensing phases with desired characteristics.

3.2.2.1. Catalyst system

One of the most important components of ATRP is the catalyst, since it determines the position of the atom transfer equilibrium and the exchange between dormant and active species. [51, 55-57]

Different transition metals, such as molybdenum, chromium, rhenium, ruthenium, iron, rhodium, nickel, palladium and copper may be used in catalysis for ATRP.[57] Complexes of late and middle transition metals are usually more efficient, however, copper catalysts have been superior for ATRP in terms of versatility and cost and they have been applied in the different polymerization systems.[51, 58-61] In fact the majority of the ATRP catalysts found in the literature which were used to develop new (co)polymers for optical sensing are copper-based systems.

On the other hand, the catalytic activity and selectivity is strongly dependant on the ligand.[51, 57] Its role is to solubilize the transition-metal salt and adjust the redox potential of the metal centre for appropriate reactivity.[62-64] **Fig. 2** shows the most common ligands used in transition metal catalyzed ATRP for the development of (co)polymers with optical sensing applications.

The first ATRP system based on copper catalyst was reported in 1995.[56, 65] Initially cuprous halides complexed by three molecules of 2,2′-bipyridine (bpy) were used as catalyst.[51] In fact, CuR/bpy systems where R= Cl or Br, is one of the most utilized catalyst in ATRP for the synthesis of (co)polymers with application in optical sensing.[21, 25, 27-31, 33-35, 66] Since nitrogen-based ligands work particularly well for copper-mediated ATRP,[51, 62-64] other bidentate ligands derived from bpy, such as 4,4′-Dinonyl-2,2′-dipyridyl[38] or 4,4′-di(5-nonyl)-2,2′-bipyridine (dNbpy)[41] have also been used.

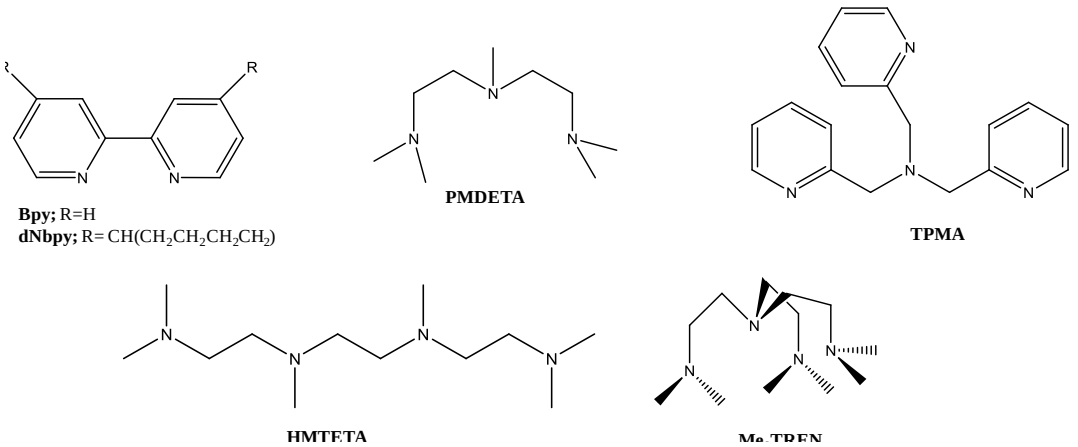

Figure 2. Most common ligands used in ATRP. bpy = biprydine; dNbpy = 4,4′-di(5-nonyl)-2,2′-bipyridine; PMDETA = N,N,N',N',N''-Pentamethyldiethylenetriamine; TPMA = tris[(2-pyridyl)methyl]amine; HMTETA = 1,1,4,7,10,10-hexamethyltriethylenetetraamine; Me_6TREN = tris[2-(dimethylamino)ethyl]amine

Another interesting type of α-diimine ligands are *N*-alkyl-2-pyridinemethanimines, since they are able to reach a higher control over polymerization compared to bipyridyl. [67, 68] Furthermore, by increasing the length of the alkyl chain of the ligand, the solubility of the catalyst complex can be tuned resulting in a better control over the polimerization.[68] This has been shown in the synthesis of fluorescent star polymers via ATRP using a porphyrin initiator and different monomers, solvents and ligands, demonstrating the efficacy and versatility of ATRP when using appropriate reaction components.[40]

In fact the use of multidentate aliphatic amines as ligands, either linear or branched, reduces the cost of catalyst while increasing the rate of polymerization, with a good overall reaction control.[51, 62-64, 69] In this aspect, cuprous halides complexed by the linear tetradentate ligand 1,1,4,7,10,10-hexamethyltriethylenetetraamine (HMTETA) have been also used as catalyst in ATRP to develop a new oxygen sensitive star-shaped polymer[39] and water-soluble conjugated polymers (WSCPs) used as thermoresponsive fluorescent sensors.[45] ATRP catalyzed with copper and the tridentate ligand N,N,N',N',N''-Pentamethyldiethylenetriamine (PMDETA) has allowed the development of new (co)polymers which can be used in different areas such as: brushes for biosensing,[32, 70, 71] thin film for colorimetric ion-sensing,[36, 37] or nanofibres for fluorescent pH-sensing.[42] PMDETA has also been applied in the synthesis of molecularly imprinted polymers with both crosslinkable and specific functionalities.[47]

Nevertheless, branched tetradentate amine ligands such as tris[2-(dimethylamino)ethyl]amine (Me_6TREN) and tris[(2-pyridyl)methyl]amine (TPMA), provide the most efficient ATRP catalysis.[72, 73] TPMA has been only used in polymer synthesis by AGET ATRP for the detection of protein binding.[22] Me_6TREN is found in the synthesis of poly(acrylic acid) brushes for biosensing applications, where the use of a more active ligand such as Me_6TREN instead of PMDETA, allows the polymerization to proceed without thermal treatment.[32] Me_6TREN has also resulted very successful in ATRP of *N*-isopropopylacrylamida (NIPAM)[74] and thus it was used in its polymerization with pyrene (Pyr) acting as initiator. This polymer was subsequently conjugate to fullerene (C60), for thedevelopment of an hybrid polymeric temperature sensor.[44] Me_6TREN has also been used in the synthesis of two sulphonamide-based pH sensitive polymers, where the use of a stronger ligand is necessary for a successful ATRP. [46] These pH sensitive polymers are based on fluorescence resonance energy transfer (FRET) from a Pyr donor to a coumarin acceptor[46] or on the fluorescence quenching of Pyr produced by carbon nanotubes (CNT)[43] where the polymer aggregates as a function of the pH.

3.2.2.2 ATRP monomers

Functionalities will provide the final material with different properties such as charge, hydrophilicity, polarity, metal complexation, etc. and they are normally added to the polymer directly by the monomer or by chemical modification of its moieties.[51, 52, 75] These functionalities play an important role in optical sensing, since they may provide inherent optical properties to the sensing phase, may be involved in the selective binding of the analyte, and/or may be necessaries to covalently/physically immobilize an optical indicator, enhancing the performance of the sensor in any case.

Most important the different types of functionalities found in literature which can provide the polymer with useful properties for its application in optical sensing, have been introduced by using different types of monomers and functionalities such as: epoxy, carboxyl, hydroxyl and amino groups, active esters, charged monomers, sugar moieties, fluorescent monomers and photo-switchable monomers.

The importance of epoxy groups in polymer brushes can be noticed in the synthesis of poly[oligo(ethyleneglycol) methacrylate) (POEGMA) bearing epoxy groups.[29] After the copolymerization of POEGMA with glycidyl methacrylate (GMA) via surface

initiated ATRP (SI-ATRP),[76] the new POEGMA-co-GMA polymer can be used a 3D scaffold. This scaffold allows protein penetration and its subsequent attachment to the film through the available epoxy group of the polymer. It should be taken into account, that the hydrophobicity provided by GMA could result in a higher non-specific adsorption of proteins. However, the fact that reaction between epoxy and amine groups can only take place when the protein is pre-adsorbed on the surface,[77] makes ATRP a interesting tool to develop new matrices for surface plasmon resonance.[29] In fact, POEGMA-co-GMA brushes allow the simultaneous detection through SPR technique of three biomarkers (α-fetoprotein, carcinoembryonic antigen and hepatitis B surface antigen) present in human serum.[29]

In materials for sensing applications, carboxyl groups may serve as a versatile platform to carry out many chemical modifications. Normally carboxyl groups are attached, through activation with zero-length crosslinking agents,[78] to any molecule carrying an amino group, such as bioactive species that can act as sensing probes, developing sensing biopolymers.

One example are the poly(acrylic acid) brushes obtained after acid hydrolysis of poly(tert-butyl acrylate) brushes synthesized by SI-ARTP.[32] Its carboxyl groups were subsequently activated by the water soluble 1-ethyl-3-(3-dimethylaminopropyl)carbodiimide hydrochloride (EDC) and *N*-hydroxysuccinimide (NHS) and coupled with biotin through its amide-bond. Therefore, it was possible to evaluate the binding capacity of biotin as function of the different carboxyl density obtained by controlling the molecular weight of the brushes polymerized by ATRP. Biospecific recognition between the biotin attached and streptavidin (SA) was evaluated: the biotin/SA binding capacity increases with molecular weight of the polymer. The presence of an higher amount of carboxyl groups also prevents the adsorption of non-specific components with a similar isoelectric point to SA, such as bovine serum albumin (BSA) and fibrinogen (FIB).[32]

Hydroxyl groups are also susceptible of crosslinking with biomolecules. Poly[oligo(ethyele glycol)methyl ether methacrylate] (Poly(MeOEGMA)), poly[oligo(ethyele glycol) methacrylate] (Poly(HOEGMA)) and poly(2-hydroxyethyl methacrylate) (Poly(HEMA)) brushes were polymerized by SI-ATRP in order to obtain a suitable platform for the SPR detection of the food pathogen *Cronobacter* in milk

samples.[33] However, between all the copolymer, only PolyHEMA showed resistance to fouling from all types of milk samples, probably due to a higher hydrophilicity that decreases the hydrophobic interactions between the lipidic components of milk. Therefore, the hydroxyl groups of polyHEMA were activated by *N,N'*-Disuccinimidyl carbonate in anhydrous DMF, and antibody against *Cronobacter* (antiCB) was subsequently covalently immobilized.[33] The well-controlled polymerization achieved by ATRP allows the optimization of the surface thickness of poly(HEMA) brushes down to 19 nm; therefore the antigens can be captured much closer to the gold surface and generate a stronger optical response compared to the conventional method in which the proteins are covalently attached on a thiol-modified gold surface.[33]

The ATRP of polymer with active ester pendant groups can also serve as platform for the chemical attachment of molecules that contain primary amines in their structures. For example, the aminolysis of the *N*-Hydroxysuccinimide (NHS) present in the *N*-hydroxysuccinimide 4-vinyl benzoate (NHS4VB) monomer allows the reaction with 1-aminomethylpyrene (Pyr-N) or octadecylamine (ODA).[70] Furthermore, due to the retention of the bromine end group after ATRP, PolyNHS4VB was also used to synthesize block copolymers with different monomers, such as 2-hydroxylethylacrylate (HEA), *tert*-butyl acrylate (*t*BA) or styrene.[70] These different functionalities together with the well-controlled characteristics of ATRP result in tuneable microenvironments, with different surface architectures that can easily conjugated with amino-containing molecules while improving the sensor's performance.

In fact, active ester can easily allow the attachment of proteins through amide-coupling.[27] It is possible to modify the surface of a sulfobetaine polymer (PSPB) synthesized by ATRP via a second ATRP to introduce *N*-methacryloyloxysuccinimide (MAOSu). This succinimide-containing moiety allows the amide-coupling with concanavalin A (ConA), a sugar-binding protein.[27] In the opposite way, this sugar binding capacity was used to bind ConA with sugar residues present in mannose-carrying polymer brushes synthesized via ATRP, allowing the detection of this protein by SPR.[31]

One can also notice the importance of functionalities in physical adsorption. In order to obtain a successful immobilization of an optical indicator for cadmium ions (5,10,15,20-Tetrakis (1-methyl-4-pyridinio) porphyrin tetra (p-toluenesulfonate),

TMPyP), negatively charged polymer brushes were synthesized onto a chitosan/cellulose (CS/CA) membrane via SI-ATRP. The selected monomer (3-sulfopropyl methacrylate potassium salt, SMP) provides the polymer surface with $-SO_3^-$ groups that interact with TMPyP through a strong ion-par electrostatic interaction. This physical immobilization of the indicator onto the CS/CA membrane allows the interaction with cadmium ions present in an aqueous solution. This interaction produces a ligand-to-metal charge-transfer (LMCT) transition between the indicator and the Cd ions, resulting in colour changes that can be measured by absorbance. It should be noticed that functionalities of the polymer brushes not only allow the electrostatic interaction with the indicator but also take part in the adsorption of cadmium ions , as it was demonstrated by Freundlich and Langmuir adsorption isotherms.[35]

Functionalities play also an important role in water-solubility properties, as it can be seen in the synthesis of novel water-insoluble linear copolymers for the design of pH-sensitive nanostructured films.[42] In this case, the hydrophobicity of the copolymer poly(methyl methacrylate)-co-fluorescein *o*-acrylate (poly(MMA-co-FOA)), prepared by reverse-ATRP, was tuned with the incorporation of hydroxyethyl methacrylate (HEMA), which provides the new material with the enough hydrophilicity for the water ions (OH^- and H_3O^+) to penetrate and thus, protonate and deprotonate the pH-sensitive probe (FOA). Furthermore, as it can be seen in **Fig. 3** it was also possible to adjust the pK_a of the resulting copolymer, either by incorporatin a positively charged monomer (such as 3-methacryloylaminopropyl-trimethylammonium chloride, MAPTAC) in order to decrease the pK_a, or a negatively charged monomer (such as 2-acrylamido-2-methylpropane sulfonic acid, AAMPS) to increase the pK_a.[42] The solubility of these copolymers in different organic media makes them easily exploited as sensing matrices for different techniques such as electrospinning, spin-coating, deep-coating, spray-dry, etc.[42, 79]

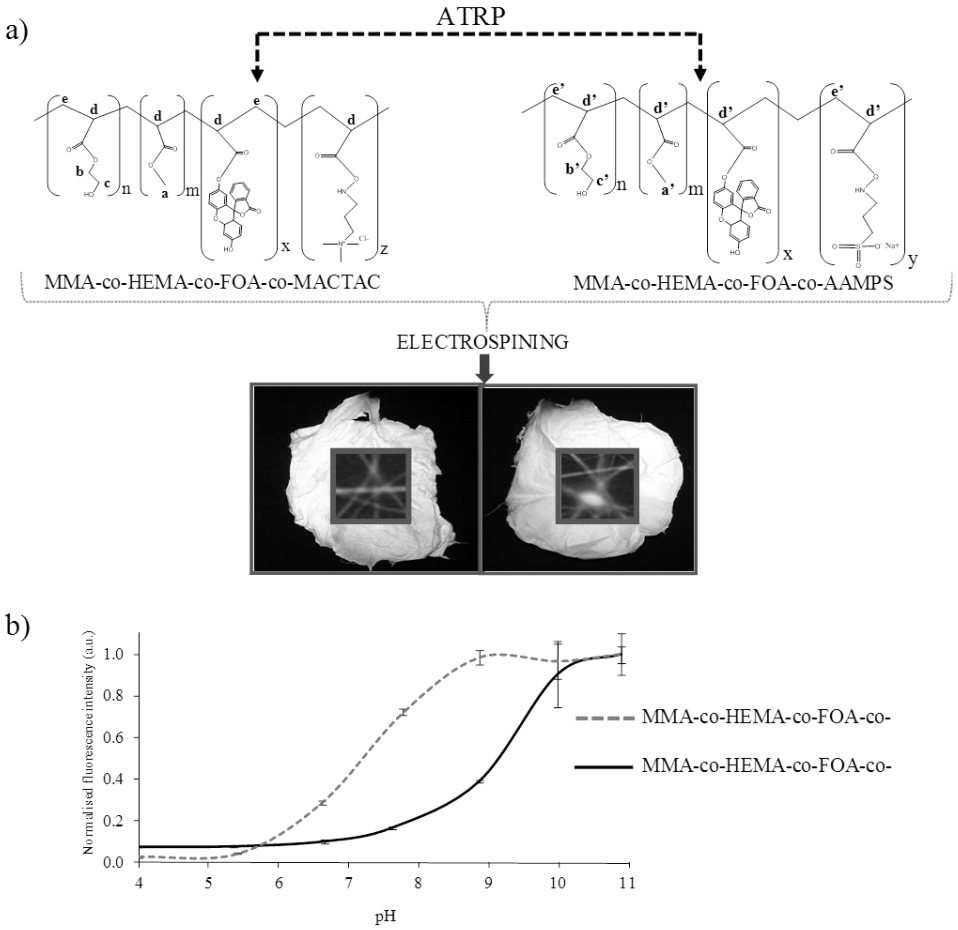

Figure 3. a) Structure of the pH-sensitive copolymers synthesized via ATRP. These copolymer were used to produce nanofibres via electrospinning showing no modification on the luminescent properties. b) Luminescent properties of the nanofibres produced with both polymers at different pH values, where it can be noticed the pK_a tuning

The relevance of electrostatic properties for water solubility can also be noticed in the synthesis via ATRP of water-soluble diblock copolymers (WSCPs) containing conjugated amino-terminal polyfluorene (PF) block and coil-like poly-NIPAM.[45] It is important to highlight that, prior to ATRP, the amine residues of the PF-macroinitiator were postquaternized in order to make the corresponding cationic polymer macroinitiator soluble in water.[45] Furthermore, the low thermal phase behaviour of PNIPAM induces a thermo-micellization of the copolymer when it is heated above 40ºC. The resulting structure, possessing a core of PNIPAM and a corona of hydrophilic PF, also possess fluorescence quenching capabilities even when the analyte is present only in traces.[45]

The thermal properties of NIPAM have been also used for the synthesis of polymeric temperature sensors based on pyrene (Pyr) and fullerene (C60) attached to a PolyNIPAM backbone. The conformational change in the copolymer due to temperature and the following quenching of Pyr produced by C60 are responsible for its thermosensitivity.[44] It should be noticed that to allow the conjugation of copolymer with C60 it is necessary either to modify the C60 with carboxyl groups, or to take advantage of the fact that having a halide end in the polymer is inherent to ATRP.[51] In the first case, the carboxilated C60 is conjugated with hydroxyl groups present on HEMA moiety of a Pyr-HEMA-PNIPAM copolymer. In the second option (see **Fig. 4a**), an azide group that easily conjugate to C60 is included at the end of the PNIPAM backbone via nucleophilic substitution (S_N reactions) of the bromide-end,[44] which reveals the importance of functionalitation in these kind of applications.

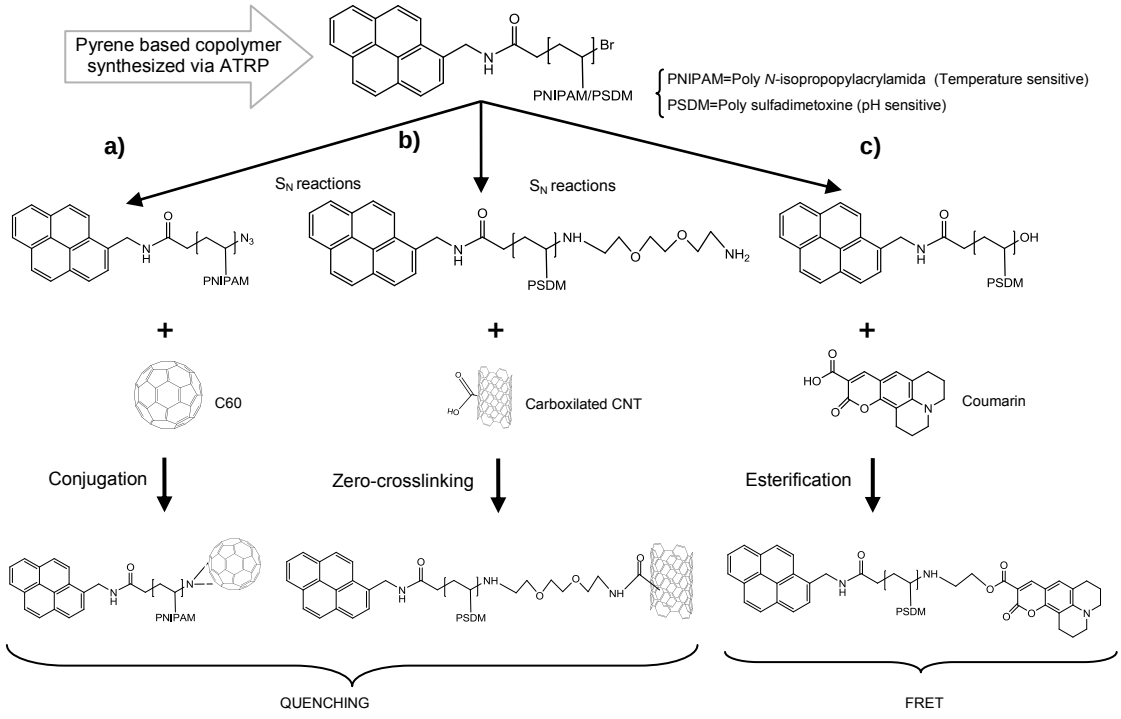

Figure 4. Different routes followed after the nucleophilic sustitution or the bromide-end of pyrene-containing polymers having temperature or pH-sensitive moieties in its structure, a) azide conjugation with fullerene b) zero crosslinkend with a carboxilated nanotube c) esterification with coumarine.

The ability of these alkyl halide groups to yield different functional groups has also been applied in the synthesis of a pH-sensitive material based on quenching produced by CNT and the capacity of some weak acid groups such as carboxylate or sulphate to introduce pH-induced conformational transition.[80, 81] Therefore, sulfadimetoxine

monomer (PSDM) can react with pyrene previously modified to behave as an ATRP initiator, leading to a pH-sensitive copolymer. The *tert*-alkyl halide present at the end of Pyr-PSDM polymer yields an amine group, which can produce a strong conjugation with the carboxylic acid group present in a premodified CNT (see **Fig. 4b**), developing a pH-sensitive hybrid materal.[43]

In a similar manner, this PSDM can be used to develop pH-sensitive polymers based on FRET. The fluorescent pH-sensitive Pyr-PSDM polymer acts as FRET donor in the pyrene end-side, while the other end of the backbone, where a hydroxyl group generated via S_N can link to a coumarin, plays the FRET acceptor role (see **Fig. 4c**).[46] Since FRET efficiency is inversely proportional to the distance between the donor and the acceptor, the conformational change induced in the polymer by PSDM at different pH is responsible for the variation in fluorescence intensity.[46]

Functionalization in conjugation with photoisomerization of a monomer can also be useful for the synthesis of new polymers via SI-ATRP, which can induce the reversible adsorption of proteins. This is the case of azopolymer brushes based on 4-[(4-((6(Methacryloyloxy)hexyl)oxy)phenyl)diazenyl]benzoic acid grafted onto an Au substrate. The carboxyl groups present in the polymer film surface are responsible of the adsorption of bovine serum albumin (BSA). On the other hand, with the photoisomerization of the azobenzene moiety from *trans* to *cis* under UV light, these carboxyl groups move to an inner part of the film decreasing the surface density. Such photoisomerization results in the reduction of the interactions with BSA, which can be measured by SPR.[28]

Another interesting moiety is based on the capability of merocyanine to bind some metal ions through complexation with the phenolate anion. Therefore, spiropyran containing polymer can be polymerized via SI-ATRP in order to get a reversible switching between a colourless closed form of spiropyran (SP) and a coloured merocyanine open form (MC).[36] In this case, the absorbance of the polymer decreases along with a metal-dependant blue shift upon complexation with different metal ions. In order to explore the influence that the steric bulk of SP has on the colorimetric response of the copolymer, various poly(methyl methacrylate-co-spiropyran methyl methacrylate) (poly(MMA-co-PSMA) with different monomer concentrations were synthesized. The results show that an increase in the concentration of SPMA in the

polymer leads to a smaller variation in the response, both in absorbance and blue shift, probably because the chromophore has difficulties to accommodate the ions due to the steric impediment of SP.[37]

Functionalities play an even more significant role in the synthesis of molecularly imprinted polymers, as the functional groups of the growing polymer have to interact with the complementary functional groups of the template. This interaction is responsible of the formation of adequate cavities that recognize and bind selectively the target analyte.[8, 9, 82-84] Therefore, copolymers having HEMA and *tert*-butyl methacrylate in their structure have been synthesized via ATRP for the preparation of MIPs. In this case, the methacryloylation of the hydroxyl groups were carried out in order to obtain a crosslinkable copolymer. Then, this copolymer in presence of a template was used to synthesize MIPs that allowed the selective detection of theophylline towards molecules with similar structure such as caffeine and theobromine.[47]

3.2.2.3. Solvent

Although ATRP can be carried out in bulk, the use of a solvent it is normally necessary in order to solve solubility incompatibilities in the resulting polymeric mixture.[51, 52, 84] These solubility issues can be seen in the synthesis of star polymers from a porphyrin initiator core via ATRP, where no polymerization of styrene (St) in toluene is observed; however, when using anisole as polar co-solvent, the polymerization is slow but successful. Furhtermore, the use of MMA as monomer in toluene also proceed effectively, as in this case MMA may be acting as co-solvent of the porphyrin initiating cores.[40]

In order to increase the solubility of the catalytic system $CuBr_2$/PMDETA and adequately solvate the polymeric chains, a mixture of *m*-xylene and DMSO (50/50, v/v) has been chosen to develop a pH-sensitive polymer.[42] In this case, the authors also felt the importance to control the volume of solvent used during the synthesis, because if the growing polymeric chains are very closed to each other it could produce the gelification of the polymer due to the crosslinking between the acid groups of FOA and the alcohol groups of HEMA.[42] In addition, the choice of the solvent may affect the ATRP efficiency, since it can interact with the catalytic system.[85-87] It is well known that solvent polarity and temperature affect the structure features of copper catalyzed

systems,[88] thus, the choice of an adequate solvent and temperature in order to develop new (co)polymers via ATRP for application in optical sensing should be taken into account.

Several types of solvents have been used for the synthesis of polymers with application in optical sensing. Aprotic polar solvents such as dimethylformamide (DMF) or tetrahydrofurane (THF) have been selected for the synthesis of polymer for temperature,[44] pH,[43, 46] oxygen[39] or ion sensing.[36, 37] Synthesis of polymer brushes for biosensing applications seems to prefer dimethylsulfoxide (DMSO),[70] aniosole,[28, 71] acetone[32] or even polar solvent such as methanol,[66] water[33] or water/methanol mixtures.[30, 89] As should be expected, ATRP-assisted detection of biomolecules takes place in aqueous media.[21-26]

ARTP can also be carried out in heterogeneous media, such as miniemulsion. It is the case of the polymerization of polyacrylate from CdS quantum dots previously modified to act as the initiator.[90] The versatility of using ATRP in different heterogenus media is shown in the synthesis of molecularly imprinted polymer for bisphenol A, which has been performed in bulk polymerization,[50] via precipitation[49] and through miniemulsion.[48]

3.2.3. Topology of the (co)polymers obtained by ATRP with application in optical sensing phases

Different methodologies, such as normal ATRP, reverse ATRP and activator generated by electron transfer ATRP can be selected for polymer synthesis.[55] These strategies may lead to different relatively monomer position into the copolymer chains. Furthermore, the use of different kind of initiators and functionalities may lead to the polymerization of either linear or branched (co)polymers. In any case, the number of branches, their composition and relative placement in the macromolecule may provide different properties to the materials prepared with these copolymers.[51, 52]

In normal ATRP[55], the initiating radicals are generated from an alkyl halide in the presence of a transition metal in its lower oxidation state. Most of the sensing phases developed using (co)polymers synthesized via ATRP employ normal ATRP with a bromide-initiator. Bifunctional alkyl bromide can be also attached to a backbone or surfaces in order to develop polymer brushes, hyperbranched polymers and hybrid

materials. When the initiator is anchored to small multifunctional molecules, these molecules can act as initiator for the formation of star-polymers via ATRP. Different polymer compositions and topologies are represented in **Fig. 5**

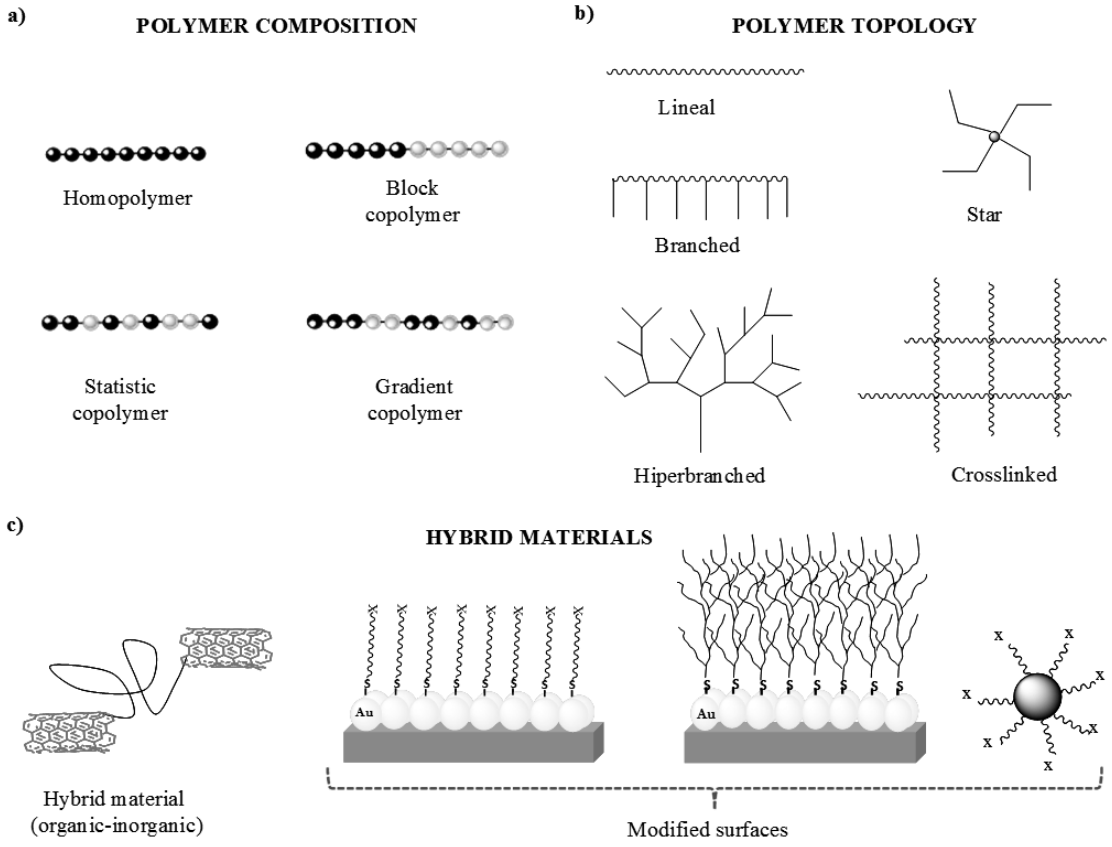

Figure 5. Polymers obtained by ATRP can be classified according to a) copolymer composition, b) topology and c) hybrid materials

2.3.1 Linear (co)polymers

As it can be seen in **Fig. 5a**, combinations of monomers arranged in a linear polymer lead to the formation of statistical, gradient or block (co)polymers. For example, an alkyl bromide, ethyl-2-bromoisobutyrate, can be used as initiator to copolymerize a statistical copolymer of MMA and SPMA with different percentages. The copolymer is then spin-coated on a glass surface to serve as colorimetric sensors for divalent metal ions.[37]

Other monomers arranged in linear shape have been used for the development of fluorescent pH-sensitive systems[44, 46]. For instance, the ATRP of a pH-sensitive monomer (sulfodimetoxine, SDM) from a pyrene-based bromo-initator gives the fluorescent properties to the polymer. By attaching this linear polymer to a FRET

acceptor, such as coumarine, the sensing properties can be exploited.[46] Hybrid sensitive materials can be also developed by combining linear sensitive polymeric chains with inorganic moieties. This PolySDM can also be anchored to one or several molecules of fullerene that act as quencher, therefore acting as a pH-sensitive hybrid material.[44]

On the other hand, it is also possible to use a conventional radical initiator, such a azobisisobutyronitrile (AIBN), to generate *in situ* the lower oxidation state of the catalyst.[51] Therefore, although in the so-called reverse ATRP it is not possible to generate block copolymer, it allows the formation of statistical or gradient linear copolymers when the monomers used in the copolymerization have similar reactivity ratios.[55] This type of copolymerization has been applied in the synthesis of pH-sensitive copolymers.[42]

3.2.3.2. Graft copolymers

Graft copolymers are branched copolymers consisting of a linear backbone and different branches arbitrarily distributed. Normally, the polymer grows from a macroinitiator, which normally is a backbone with pendant functionalities that can be modified to work as initiating sites for ATRP. Therefore, grafting can be accomplished from organic or inorganic backbones, but while inorganic interface can only be synthesized by other method than ATRP, an organic backbone can be synthesized via ATRP or any other polymerization mechanism.[51, 52]

For example, an organic backbone consisting on trimethylsilyl-protected 2-hydroxyethyl methacrylate was prepared by ATRP.[91] The subsequent esterification with 2-bromoisobutyryl bromide yields poly[2-(2-bromoisobutyryloxy)ethyl methacrylate]. Bromide groups present in this backbone act as a initiating sites to graft a fluorescent pH-sensitive monomer, fluorescein *O*-methacrylate (FMA), through a second ATRP in order to develop fluorescent pH-responsive bottlebrushes.[41]

On the other hand, in the synthesis of WSCPs, an organic backbone containing bromo-initiating sites was synthesized via esterification of a hydroxi-functionalized polyfluorene, previously synthesized via several non-ATRP reactions. The water soluble fluorescent macroinitiator was used for an efficient ATRP initiation of NIPAM, leading to the formation of self-assembly diblock copolymers.[45]

Other organic chains may have available functionalities for the anchoring of the ATRP initiator. For example, hydroxyl groups present in a ethyl cellulose backbone can be esterified with 2-bromoisobutyril bromide to yield a 2-bromoisobutyryloxy initiator that allows the growing of a photoresponsive polymer.[71]

3.2.3.3. Polymer grafted from surface

When the polymer is not growing from an organic/inorganic backbone, but the interface is either spherical or planar, the ATRP is normally called surfaced initiated atom transfer radical polymerization (SI-ATRP). Growing of linear/branched (co)polymer from a surface leads to the formation of polymer brushes, resulting in a polymer layer that can be tuned.[76]

Therefore, although the importance of functionalities in the polymeric properties has been highly stressed, surface packing density and film thickness are also very important characteristic in platforms for biosensing. For this reason, ATRP can offer one of the best synthetic tools to design surface initiated polymer brushes for SPR of biomolecules, since it allows the optimization of the interactions between inter and intra chains in order to achieve resistance to non-specific protein adsorption. Furthermore, by controlling film thickness it is possible to enhance the surface plasmon signal.[27-30, 32-34, 70, 71]

This type of polymerization needs a suitable initiator to be immobilized on the surface for the ATRP to proceed. However, not many materials include, in their structure, sites where it is possible to anchor the initiating groups for ATRP. Therefore, surfaces have to be modified either via successive chemical reactions or by attaching a previously formed functional initiator for ATRP.[76] In fact, SI-ATRP of (co)polymers with application in optical sensing materials are grown from different surfaces types, normally by attaching an initiator with a 2-bromoisobutyryl group, which is responsible for the ATRP initiation.

For SPR in biomolecules, Au surfaces are normally modified using the gold affinity to thiols. Some authors used a two-step method (**Fig. 6a**) which entails the self-assembly of an hydroxythiol, for example 11-mercapto-1-undecanol. In this way it is possible to obtain a hydroxyl-terminated gold surface that further reacts with an ATRP bifunctional initiator, such as 2-bromoiso-butyryl bromide.[30] The same two-step

method can be used to obtain amine-terminated gold substrates by the self-assembly of cysteamine, allowing the subsequent attachment of a suitable initiator.[29] On the other hand, it is also possible to use a single step method (**Fig. 6b**) to modify the gold surface by self-assembly of a previously synthesized initiator. Such initiator needs to have a mercapto group at one of its ends. Examples can be found in the immobilization of mercaptomethyl 2-bromo-2-methylpropanoate, that further allow the ATRP of AZO4 to produce photosensitive azopolymers brushes, [28] or in the ATRP of poly(acrylic acid) brushes from ω-mercaptoundecyl bromoisobutyrate for biosensing applications.[32]

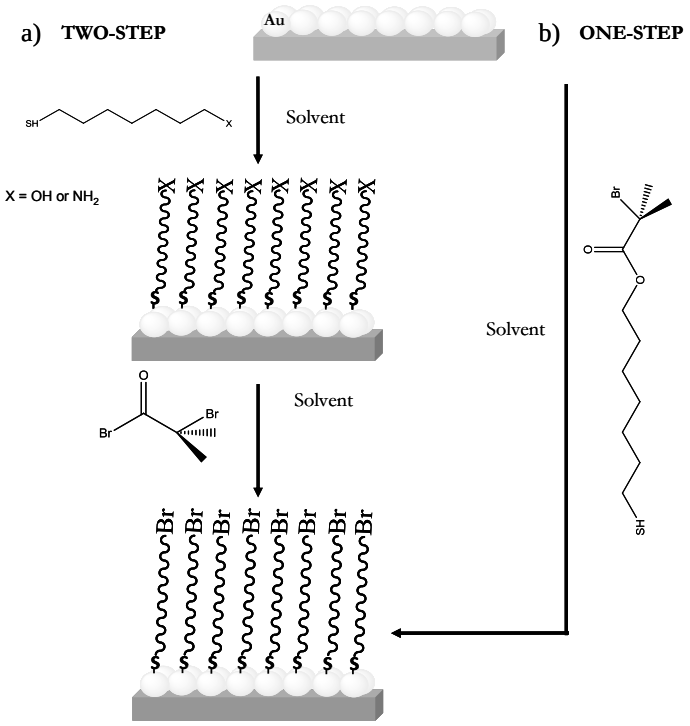

Figure 6. Different routes followed to obtain Au surfaces having initiating groups for ATRP, a) Two-step method, b) One-step method

Other modifications are based on silane-coupling. For example, gold surface modified with silicon oxide further reacts with the initiator 11-(2-bromo-2-methyl)propionyloxyundecenyl, which allows the growing of polymer brushes with different monomer and functionalities.[70] Other silicone surfaces have been modified via silane-coupling of 2-bromo-2-methylpropionic acid 3-(ethoxydimethylsilanyl)propyl ester.[32]

Inorganic substrates can be also modified, for instance, taking advantages of silane groups present in the initiator. In this aspect, it is possible to couple 11-[2-bromo-2-

methyl)propionyloxy]undecyltrichlorosilane to a glass substrate for molecular recognition.[27]

Ultracrystalline diamond surfaces can also be modified via electro-grafted aryldiazonium salts that contain a bromo-initiator for the ATRP of styrene and MMA. The polymer brushes obtained were used as adsorbents for human serum albumin (HSA).[34] In fact, aryldiazonium salts are becoming very popular to provide grafted initiators for various polymerization routes, including ATRP[92]

Spherical surface, such as Quantum Dots (QDs), are also susceptible of SI-ATRP In this case, in order to avoid the degradation of QDs it is necessary to use an initiator with lower reactivity than bromide. Therefore, tris(3-hydroxypropyl)phospine (THP) is reacted with 2-chloropropionyl chloride to obtain a chloro-initiator that is subsequently attached to the QDs spherical surface by a ligand exchange, allowing the ATRP to take place from its surface.[90]

Organic substrates that already incorporate the anchoring groups for the ATRP initiator can be used. In order to produce a membrane for the adsorption of metal ions, membrane containing cellulose acetate and chitosan allows the attachment of an α-bromoisobutyryl bromide initiator through the hydroxyl and amine groups presents on the surface.[35]

Some other surface modifications are based on the fact that detection of biomolecules may also be achieved by attaching a chemical moiety to the target biomolecule that once immobilized on a substrate, acts as initiator for ATRP. Thus, the growing of the polymer film over this biomolecule can be measured via SPR using ellipsometry[22, 25] or absorbance.[24, 26] Furthermore, following a "graft-on-a-graft" strategy,[93] it is possible to further polymerize the brushes via a second ATRP, resulting in the formation of hyperbranched structures, whose growth can amplify the detection of biomolecules plus shortening the detection time.[21, 23]

2.3.4. Star-polymers

Multifunctional small molecules can be used as initiator to synthesize star polymers. In this aspect, star-shaped polymers containing luminescent cores have been synthesized, showing effective luminescence properties.

Following a "core-first" approach, it is possible to use iridium(III) complex as both the initiator and the luminescent core to synthesize one three-arm star polymer based on 2-(carbazol-9-yl) ethyl methacrylate as the polymeric arm repeating unit. The first step consists of the modification of Ir(III) complex through successive reactions to yield bromoisobutyryl-decorated complex; this demonstrate that metal ions can serve as template for polymerization initiator compatible with ATRP. [38] Results show that the polymer may be a good candidate as luminescent material in optical sensing, since the UV/vis absorption spectrum in dichloromethane displays a broad band from 270 to 500 nm.[38]

In the same way, different star polymers of styrene and alkyl methacrylates can be synthesized from a porphyrin initiator.[40] In this case, a free-base tetraporphyrin initiator is modified by the esterification with 2-bromo-2-methylpropanoyl bromide, and subsequently metalated with Zn, Cu or Pd. The different metal tetrabromoporphyrins were used by the authors as initiator for ATRP of different monomer and catalyst systems, resulting in the inhibition of polymerization when using Cu and Pt. Since porphyrins containing Pd and Pt have resulted very effective for sensitive pressure paints, these atoms were introduced by direct replacement of Zn(II) in the core of the polymer. The thin films obtained by air-brush of the resulting Pd and Pt star-polymers showed good luminescent properties.[40]

A novel quenchometric oxygen sensor based on a star polymer combining six-arm ruthenium complex and polystyrene, $[Ru(bpyPS_2)_3](PF_6)$ was developed using ATRP.[39] Although this six-arm star polymer has narrow molecular weight distribution, there is a clear indication of heterogeneous environments around the Ru centre, since lifetime data of the polymeric film shows multi-exponential decays. This could be explained by the side reactions involved in ATRP, even though it is a well-controlled polymerization technique.[55] However, this kind of polymers, not only solve the leaching problem of the luminophore associated to physical doped polymers, but also allow the use of higher metal ion concentrations without exceeding the solubility of the complex, which results in good signals for optical sensing.[39]

3.3. Summary and outlook

In this review it has been shown the importance of ATRP to develop new polymers and copolymers with application as optical sensing phases. The components involved

in the reaction have been analyzed, showing that in most of the cases the catalyst involved in the polymerization is a copper-based catalyst with different amine-based ligands.

Functionalities present in the polymer have been analyzed, since they provide the material with different properties such as charge, hydrophobicity, complexation, protein binding ability, etc. These properties can be useful for the development of different types of optical sensing phases depending on the property that is exploited. Protein binding capability can therefore be useful to obtain biosensors, which are normally measure via SPR. Hydrophobicity and hydrophilicity can be easily tuned by ATRP, providing the polymer with properties that will enhance the sensor performance. Moreover, the use of fluorescent pH or temperature sensitive monomers in conjugation with a tuneable microenvironment makes it possible to design sensing phases for specific applications. Since having a bromide-end is inherent to polymers synthesized by ATRP, the possibility of this group to yield different functionalities via nucleophilic substitution is useful to add special properties to the polymer, which allow its use as a sensing platform.

Furthermore, versatility of ATRP has been shown since it can be carried out in different media, from bulk to minuemulsion polymerization. Although different organic solvents are normally selected, aqueous ATRP is often applied for assisted-detection of biomolecules.

Several polymer topologies can be reached via ATRP. Although functionalities are very important for the sensor performance, architecture of the polymer should also be taken into account. In many applications, the initiator of ATRP is attached to a gold surface and the polymerization leads to the formation of polymer brushes with application in SPR. Attachment of the initiator can also be done on the polymer backbone, synthesized or not by ATRP, which allows the development of a variety of grafted (co)polymers. The use of small multifunctional fluorescent molecules as macroinitiators it is also becoming very popular, in order to develop star-shaped polymers with application in oxygen sensing.

Therefore in this review we have shown the utility of this polymerization technique for the development of new (co)polymers having inherent optical properties or the ability to immobilize different indicators, which are responsible of the optical signal.

These (co)polymers can also be very effective in providing a matrix where the analyte can be entrapped, enhancing the performance of the sensor. However, effort should be focus in the development of an even more efficient ATRP, that simplify the synthesis of (co)polymers with adequate optical sensing properties while controlling weight distribution and topology.

Referencias

1. Hulanicki, A.; Geab, S.; Ingman, F., Chemical Sensors: Definition and Clasification. *Pure & Applied Chemistry* **1991,** 63, (9), 1247-1250.
2. Rogers, K. R.; Lin, J. N., Biosensors for environmental monitoring. *Biosensors and Bioelectronics* **1992,** 7, (5), 317-321.
3. Seitz, W. R., Chemical sensors based on fiber optics. *Analytical Chemistry* **1984,** 56, (1), 16A-34A.
4. Wolfbeis, O. S., Fiber-Optic Chemical Sensors and Biosensors. *Analytical Chemistry* **2002,** 74, (12), 2663-2678.
5. Angelome, P. C.; Liz-Marzan, L. M., Monitoring Solvent Evaporation from Thin Films by Localized Surface Plasmon Resonance Shifts. *The Journal of Physical Chemistry C* **2010,** 114, (43), 18379-18383.
6. Abalde-Cela, S.; Hermida-Ramón, J. M.; Contreras-Carballada, P.; De Cola, L.; Guerrero-Martínez, A.; Alvarez-Puebla, R. A.; Liz-Marzán, L. M., SERS Chiral Recognition and Quantification of Enantiomers through Cyclodextrin Supramolecular Complexation. *ChemPhysChem* **2011,** 12, (8), 1529-1535.
7. Contreras-Cáceres, R.; Abalde-Cela, S.; Guardia-Girós, P.; Fernández-Barbero, A.; Párez-Juste, J.; Alvarez-Puebla, R. A.; Liz-Marzán, L. M., Multifunctional Microgel Magnetic/Optical Traps for SERS Ultradetection. *Langmuir* **2011,** 27, (8), 4520-4525.
8. Whitcombe, M. J.; Vulfson, E. N., Imprinted Polymers. *Advanced Materials* **2001,** 13, (7), 467-478.
9. Henry, O. Y. F.; Cullen, D. C.; Piletsky, S. A., Optical interrogation of molecularly imprinted polymers and development of MIP sensors: a review. *Analytical and Bioanalytical Chemistry* **2005,** 382, (4), 947-956.
10. Fernández-Sánchez, J. F.; Cannas, R.; Spichiger, S.; Steiger, R.; Spichiger-Keller, U. E., Novel nanostructured materials to develop oxygen-sensitive films for optical sensors. *Analytica Chimica Acta* **2006,** 566, (2), 271-282.

11. Borisov, S. M.; Mayr, T.; Mistlberger, G.; Waich, K.; Koren, K.; Chojnacki, P.; Klimant, I., Precipitation as a simple and versatile method for preparation of optical nanochemosensors. *Talanta* **2009,** 79, (5), 1322-1330.

12. Pelfrey, S.; Cantu, T.; Papantonakis, M. R.; Simonson, D. L.; McGill, R. A.; Macossay, J., Microscopic and spectroscopic studies of thermally enhanced electrospun PMMA micro- and nanofibers. *Polymer Chemistry* **2010,** 1, (6), 866-869.

13. Marín Suárez del Toro, M.; Fernandez-Sanchez, J. F.; Baranoff, E.; Nazeeruddin, M. K.; Graetzel, M.; Fernandez-Gutierrez, A., Novel luminescent Ir(III) dyes for developing highly sensitive oxygen sensing films. *Talanta* **2010,** 82, (2), 620-626.

14. Kim, H. J.; Jeong, Y. C.; Rhee, J. I., Encapsulation of tris(4,7-diphenyl-1,10-phenanthroline)ruthenium(II) complex linked with dendrons in sol-gels: Stable optical sensing membranes for dissolved oxygen. *Talanta* **2008,** 76, (5), 1070-1076.

15. Fernández-Sánchez, J. F.; Cannas, R.; Spichiger, S.; Steiger, R.; Spichiger-Keller, U. E., Optical CO2-sensing layers for clinical application based on pH-sensitive indicators incorporated into nanoscopic metal-oxide supports. *Sensors and Actuators B: Chemical* **2007,** 128, (1), 145-153.

16. Wolfbeis, O. S., Materials for fluorescence-based optical chemical sensors. *Journal of Materials Chemistry* **2005,** 15, (27-28), 2657-2669.

17. Amao, Y., Probes and Polymers for Optical Sensing of Oxygen. *Microchimica Acta* **2003,** 143, (1), 1-12.

18. Fernández-Sánchez, J. F.; Fernández, I.; Steiger, R.; Beer, R.; Cannas, R.; Spichiger-Keller, U. E., Second Generation Nanostructured Metal Oxide Matrices to Increase the Thermal Stability of CO and NO2 Sensing Layers Based on Iron(II) Phthalocyanine. *Advanced Functional Materials* **2007,** 17, (7), 1188-1198.

19. Matyjaszewski, K.; Gaynor, S. G.; Clara, D. C.; Charles, E. C.; Jr, Free radical polymerization. In *Applied Polymer Science: 21st Century*, Pergamon: Oxford, 2000; pp 929-977.

20. Matyjaszewski, K., Controlled radical polymerization. *Current Opinion in Solid State and Materials Science* **1996,** 1, (6), 769-776.

21. Liu, Y.; Dong, Y.; Jauw, J.; Linman, M. J.; Cheng, Q., Highly Sensitive Detection of Protein Toxins by Surface Plasmon Resonance with Biotinylation-Based Inline Atom Transfer Radical Polymerization Amplification. *Analytical Chemistry* **2010,** 82, (9), 3679-3685.

22. Qian, H.; He, L., Detection of Protein Binding Using Activator Generated by Electron Transfer for Atom Transfer Radical Polymerization. *Analytical Chemistry* **2009,** 81, (23), 9824-9827.

23. Lou, X.; Lewis, M. S.; Gorman, C. B.; He, L., Detection of DNA Point Mutation by Atom Transfer Radical Polymerization. *Analytical Chemistry* **2005,** 77, (15), 4698-4705.

24. Lou, X.; Wang, C.; He, L., Core-Shell Au Nanoparticle Formation with DNA-Polymer Hybrid Coatings Using Aqueous ATRP. *Biomacromolecules* **2007,** 8, (5), 1385-1390.

25. Okelo, G. O.; He, L., Cu(0) as the reaction additive in purge-free ATRP-assisted DNA detection. *Biosensors and Bioelectronics* **2007,** 23, (4), 588-592.

26. Lou, X.; He, L., Surface passivation using oligo(ethylene glycol) in ATRP-assisted DNA detection. *Sensors and Actuators B: Chemical* **2008,** 129, (1), 225-230.

27. Kitano, H.; Suzuki, H.; Matsuura, K.; Ohno, K., Molecular Recognition at the Exterior Surface of a Zwitterionic Telomer Brush. *Langmuir* **2009,** 26, (9), 6767-6774.

28. Zhang, Z.; Wang, Y.; Yan, F.; Peng, D.; Ma, Z., Photosensitive Azopolymer Brushes via Atom Transfer Radical Polymerization for Protein Sensing. *Chinese Journal of Chemistry* **2011,** 29, (1), 153-158.

29. Hu, W.; Liu, Y.; Lu, Z.; Li, C. M., Poly[oligo(ethylene glycol) methacrylate-co-glycidyl methacrylate] Brush Substrate for Sensitive Surface Plasmon Resonance Imaging Protein Arrays. *Advanced Functional Materials* **2010,** 20, (20), 3497-3503.

30. Zhao, C.; Li, L.; Zheng, J., Achieving Highly Effective Nonfouling Performance for Surface-Grafted Poly(HPMA) via Atom-Transfer Radical Polymerization. *Langmuir* **2010,** 26, (22), 17375-17382.

31. Anraku, Y.; Takahashi, Y.; Kitano, H.; Hakari, M., Recognition of sugars on surface-bound cap-shaped gold particles modified with a polymer brush. *Colloids and Surfaces B: Biointerfaces* **2007,** 57, (1), 61-68.

32. Akkahat, P.; Hoven, V. P., Introducing surface-tethered poly(acrylic acid) brushes as 3D functional thin film for biosensing applications. *Colloids and Surfaces B: Biointerfaces* **2011,** 86, (1), 198-205.

33. Rodriguez-Emmenegger, C.; Avramenko, O. A.; Brynda, E.; Skvor, J.; Alles, A. B., Poly(HEMA) brushes emerging as a new platform for direct detection of food pathogen in milk samples. *Biosensors and Bioelectronics* **2011,** 26, (11), 4545-4551.

34. Matrab, T.; Chehimi, M. M.; Boudou, J. P.; Benedic, F.; Wang, J.; Naguib, N. N.; Carlisle, J. A., Surface functionalization of ultrananocrystalline diamond using atom transfer radical polymerization (ATRP) initiated by electro-grafted aryldiazonium salts. *Diamond and Related Materials* **2006,** 15, (4-8), 639-644.

35. Zhang, L.; Zhao, Y.-H.; Bai, R., Development of a multifunctional membrane for chromatic warning and enhanced adsorptive removal of heavy metal ions: Application to cadmium. *Journal of Membrane Science* **2011,** 379, (1-2), 69-79.

36. Fries, K.; Samanta, S.; Orski, S.; Locklin, J., Reversible colorimetric ion sensors based on surface initiated polymerization of photochromic polymers. *Chemical Communications* **2008**, (47), 6288-6290.

37. Fries, K. H.; Driskell, J. D.; Samanta, S.; Locklin, J., Spectroscopic analysis of metal ion binding in spiropyran containing copolymer thin films. *Analytical Chemistry* **2010,** 82, (8), 3306-3314.

38. Deng, Y.; Liu, S.-J.; Zhao, B.-M.; Wang, P.; Fan, Q.-L.; Huang, W.; Wang, L.-H., Synthesis and characterization of one star-shaped polymer with charged iridium complex as luminescent core. *Journal of Luminescence* **2010,** 131, (10), 2166-2173.

39. Payne, S. J.; Fiore, G. L.; Fraser, C. L.; Demas, J. N., Luminescence Oxygen Sensor Based on a Ruthenium(II) Star Polymer Complex. *Analytical Chemistry* **2010,** 82, (3), 917-921.

40. High, L. R. H.; Holder, S. J.; Penfold, H. V., Synthesis of Star Polymers of Styrene and Alkyl (Meth)acrylates from a Porphyrin Initiator Core via ATRP. *Macromolecules* **2007,** 40, (20), 7157-7165.

41. Nese, A.; Lebedeva, N. V.; Sherwood, G.; Averick, S.; Li, Y.; Gao, H.; Peteanu, L.; Sheiko, S. S.; Matyjaszewski, K., pH-Responsive Fluorescent Molecular Bottlebrushes Prepared by Atom Transfer Radical Polymerization. *Macromolecules* **2011,** 44, (15), 5905-5910.

42. Medina-Castillo, A. L.; Fernandez-Sanchez, J. F.; Segura-Carretero, A.; Fernandez-Gutierrez, A., Design and synthesis by ATRP of novel, water-insoluble, lineal copolymers and their application in the development of fluorescent and pH-sensing nanofibres made by electrospinning. *Journal of Materials Chemistry* **2011,** 21, (18), 6742-6750.

43. Cho, E. S.; Hong, S. W.; Jo, W. H., A New pH Sensor Using the Fluorescence Quenching of Carbon Nanotubes. *Macromolecular Rapid Communications* **2008,** 29, (22), 1798-1803.

44. Hong, S. W.; Kim, D. Y.; Lee, J. U.; Jo, W. H., Synthesis of Polymeric Temperature Sensor Based on Photophysical Property of Fullerene and Thermal Sensitivity of Poly(N-isopropylacrylamide). *Macromolecules* **2009,** 42, (7), 2756-2761.

45. Wang, W.; Wang, R.; Zhang, C.; Lu, S.; Liu, T., Synthesis, characterization and self-assembly behavior in water as fluorescent sensors of cationic water-soluble conjugated polyfluorene-b-poly(N-isopropylacrylamide) diblock copolymers. *Polymer* **2009,** 50, (5), 1236-1245.

46. Hong, S. W.; Kim, K. H.; Huh, J.; Ahn, C.-H.; Jo, W. H., Design and Synthesis of a New pH Sensitive Polymeric Sensor Using Fluorescence Resonance Energy Transfer. *Chemistry of Materials* **2005,** 17, (25), 6213-6215.

47. Li, Z.; Day, M.; Ding, J.; Faid, K., Synthesis and Characterization of Functional Methacrylate Copolymers and Their Application in Molecular Imprinting. *Macromolecules* **2005,** 38, (7), 2620-2625.

48. Liu, J.; Wang, W.; Xie, Y.; Huang, Y.; Liu, Y.; Liu, X.; Zhao, R.; Liu, G.; Chen, Y., A novel polychloromethylstyrene coated superparamagnetic surface molecularly imprinted core-shell nanoparticle for bisphenol A. *Journal of Materials Chemistry* **2011,** 21, (25), 9232-9238.

49. Zu, B.; Pan, G.; Guo, X.; Zhang, Y.; Zhang, H., Preparation of molecularly imprinted polymer microspheres via atom transfer radical precipitation polymerization. *Journal of Polymer Science Part A: Polymer Chemistry* **2009,** 47, (13), 3257-3270.

50. Zu, B.; Zhang, Y.; Guo, X.; Zhang, H., Preparation of molecularly imprinted polymers via atom transfer radical “bulk” polymerization. *Journal of Polymer Science Part A: Polymer Chemistry* **2009,** 48, (3), 532-541.

51. Matyjaszewski, K.; Xia, J., Atom Transfer Radical Polymerization. *Chemical Reviews* **2001,** 101, (9), 2921-2990.

52. Ouchi, M.; Terashima, T.; Sawamoto, M., Transition metal-catalyzed living radical polymerization: Toward perfection in catalysis and precision polymer synthesis. *Chemical Reviews* **2009,** 109, (11), 4963-5050.

53. Gromada, J. r. m.; Matyjaszewski, K., Simultaneous Reverse and Normal Initiation in Atom Transfer Radical Polymerization. *Macromolecules* **2001,** 34, (22), 7664-7671.

54. Jakubowski, W.; Matyjaszewski, K., Activator generated by electron transfer for atom transfer radical polymerization. *Macromolecules* **2005,** 38, (10), 4139-4146.

55. Braunecker, W. A.; Matyjaszewski, K., Recent mechanistic developments in atom transfer radical polymerization. *Journal of Molecular Catalysis A: Chemical* **2006,** 254, (1-2), 155-164.

56. Wang, J.-S.; Matyjaszewski, K., Controlled/"living" radical polymerization. atom transfer radical polymerization in the presence of transition-metal complexes. *Journal of the American Chemical Society* **1995,** 117, (20), 5614-5615.

57. di Lena, F.; Matyjaszewski, K., Transition metal catalysts for controlled radical polymerization. *Progress in Polymer Science* **2010,** 35, (8), 959-1021.

58. Matyjaszewski, K.; Tsarevsky, N. V.; Braunecker, W. A.; Dong, H.; Huang, J.; Jakubowski, W.; Kwak, Y.; Nicolay, R.; Tang, W.; Yoon, J. A., Role of Cu0 in Controlled/"Living" Radical Polymerization. *Macromolecules* **2007,** 40, (22), 7795-7806.

59. Matyjaszewski, K., Radical Nature of Cu-Catalyzed Controlled Radical Polymerizations (Atom Transfer Radical Polymerization). *Macromolecules* **1998,** 31, (15), 4710-4717.

60. Patten, T. E.; Matyjaszewski, K., Copper(I)-Catalyzed Atom Transfer Radical Polymerization. *Accounts of Chemical Research* **1999,** 32, (10), 895-903.

61. Wang, J.-S.; Matyjaszewski, K., "Living"/Controlled Radical Polymerization. Transition-Metal-Catalyzed Atom Transfer Radical Polymerization in the Presence of a Conventional Radical Initiator. *Macromolecules* **1995,** 28, (22), 7572-7573.

62. Xia, J.; Zhang, X.; Matyjaszewski, K., The Effect of Ligands on Copper-Mediated Atom Transfer Radical Polymerization. In *Transition Metal Catalysis in Macromolecular Design*, American Chemical Society: 2000; Vol. 760, pp 207-223.

63. Tang, W.; Tsarevsky, N. V.; Matyjaszewski, K., Determination of Equilibrium Constants for Atom Transfer Radical Polymerization. *Journal of the American Chemical Society* **2006,** 128, (5), 1598-1604.

64. Tang, W.; Kwak, Y.; Braunecker, W.; Tsarevsky, N. V.; Coote, M. L.; Matyjaszewski, K., Understanding Atom Transfer Radical Polymerization: Effect of Ligand and Initiator Structures on the Equilibrium Constants. *Journal of the American Chemical Society* **2008,** 130, (32), 10702-10713.

65. Wang, J.-S.; Matyjaszewski, K., Controlled/"Living" Radical Polymerization. Halogen Atom Transfer Radical Polymerization Promoted by a Cu(I)/Cu(II) Redox Process. *Macromolecules* **1995,** 28, (23), 7901-7910.

66. Yang, Q.; Wang, L.; Huo, J.; Ding, J.; Xiang, W., Novel comb-structured-polymer-grafted carbon black by surface-initiated atom transfer radical polymerization and ring-opening polymerization. *Journal of Applied Polymer Science* **2009,** 117, (2), 824-827.

67. Clark, A. J.; Duncalf, D. J.; Filik, R. P.; Haddleton, D. M.; Thomas, G. H.; Wongtap, H., N-alkyl-2-pyridylmethanimines as tuneable alternatives to bipyridine ligands in copper mediated atom transfer radical cyclisation. *Tetrahedron Letters* **1999,** 40, (19), 3807-3810.

68. Amass, A. J.; Wyres, C. A.; Colclough, E.; Marcia Hohn, I., N-alkyl-2-pyridinemethanimine mediated atom transfer radical polymerisation of styrene: the transition from heterogeneous to homogeneous catalysis. *Polymer* **2000,** 41, (5), 1697-1702.

69. Xia, J.; Matyjaszewski, K., Controlled/"Living" Radical Polymerization. Atom Transfer Radical Polymerization Using Multidentate Amine Ligands. *Macromolecules* **1997,** 30, (25), 7697-7700.

70. Orski, S. V.; Fries, K. H.; Sheppard, G. R.; Locklin, J., High Density Scaffolding of Functional Polymer Brushes: Surface Initiated Atom Transfer Radical Polymerization of Active Esters. *Langmuir* **2009,** 26, (3), 2136-2143.

71. Tang, X.; Gao, L.; Fan, X.; Zhou, Q., Controlled grafting of ethyl cellulose with azobenzene-containing polymethacrylates via atom transfer radical polymerization. *Journal of Polymer Science Part A: Polymer Chemistry* **2007,** 45, (9), 1653-1660.

72. Xia, J.; Matyjaszewski, K., Controlled/"Living" Radical Polymerization. Atom Transfer Radical Polymerization Catalyzed by Copper(I) and Picolylamine Complexes. *Macromolecules* **1999,** 32, (8), 2434-2437.

73. Xia, J.; Gaynor, S. G.; Matyjaszewski, K., Controlled/"Living" Radical Polymerization. Atom Transfer Radical Polymerization of Acrylates at Ambient Temperature. *Macromolecules* **1998,** 31, (17), 5958-5959.

74. Masci, G.; Giacomelli, L.; Crescenzi, V., Atom transfer radical polymerization of N-isopropylacrylamide. *Macromolecular Rapid Communications* **2004,** 25, (4), 559-564.

75. Coessens, V.; Pintauer, T.; Matyjaszewski, K., Functional polymers by atom transfer radical polymerization. *Progress in Polymer Science* **2001,** 26, (3), 337-377.

76. Fristrup, C. J.; Jankova, K.; Hvilsted, S., Surface-initiated atom transfer radical polymerization-a technique to develop biofunctional coatings. *Soft Matter* **2009,** 5, (23), 4623-4634.

77. Mateo, C.; Fernández-Lorente, G.; Abian, O.; Fernández-Lafuente, R.; Guisán, J. M., Multifunctional epoxy supports: A new tool to improve the covalent immobilization of proteins. The promotion of physical adsorptions of proteins on the supports before their covalent linkage. *Biomacromolecules* **2000,** 1, (4), 739-745.

78. Greg T, H., Chapter 2 - The Chemistry of Reactive Groups. In *Bioconjugate Techniques (Second Edition)*, Academic Press: New York, 2008; pp 169-212.

79. Medina-Castillo, A. L.; Fernández-Sánchez, J. F.; Fernández-Gutiérrez, A., One-Step Fabrication of Multifunctional Core-Shell Fibres by Co-Electrospinning. *Advanced Functional Materials* **2011,** 21, (18), 3488-3495.

80. Kathmann, E. E. L.; White, L. A.; McCormick, C. L., Water-Soluble Polymers. 73. Electrolyte- and pH-Responsive Zwitterionic Copolymers of 4-[(2-Acrylamido-2-methylpropyl)- dimethylammonio]butanoate with 3-[(2-Acrylamido-2-methyl-

propyl)dimethylammonio]propanesulfonate. *Macromolecules* **1997,** 30, (18), 5297-5304.

81. Benrebouh, A.; Avoce, D.; Zhu, X. X., Thermo- and pH-sensitive polymers containing cholic acid derivatives. *Polymer* **2001,** 42, (9), 4031-4038.
82. Valero-Navarro, A.; Medina-Castillo, A. L.; Fernandez-Sanchez, J. F.; Fernández-Gutiérrez, A., Synthesis of a novel polyurethane-based-magnetic imprinted polymer for the selective optical detection of 1-naphthylamine in drinking water. *Biosensors and Bioelectronics* **2011,** 26, (11), 4520-4525.
83. Valero-Navarro, A.; Gómez-Romero, M.; Fernández-Sánchez, J. F.; Cormack, P. A. G.; Segura-Carretero, A.; Fernández-Gutiérrez, A., Synthesis of caffeic acid molecularly imprinted polymer microspheres and high-performance liquid chromatography evaluation of their sorption properties. *Journal of Chromatography A* **2011,** 1218, (41), 7289-7296.
84. Medina-Castillo, A. L.; Fernandez-Sanchez, J. F.; Segura-Carretero, A.; Fernandez-Gutierrez, A., Micrometer and Submicrometer Particles Prepared by Precipitation Polymerization: Thermodynamic Model and Experimental Evidence of the Relation between Flory's Parameter and Particle Size. *Macromolecules* **2010,** 43, (13), 5804-5813.
85. Matyjaszewski, K.; Patten, T. E.; Xia, J., Controlled/"Living" Radical Polymerization. Kinetics of the Homogeneous Atom Transfer Radical Polymerization of Styrene. *Journal of the American Chemical Society* **1997,** 119, (4), 674-680.
86. Matyjaszewski, K.; Davis, K.; Patten, T. E.; Wei, M., Observation and analysis of a slow termination process in the atom transfer radical polymerization of styrene. *Tetrahedron* **1997,** 53, (45), 15321-15329.
87. Matyjaszewski, K.; Nakagawa, Y.; Jasieczek, C. B., Polymerization of n-Butyl Acrylate by Atom Transfer Radical Polymerization. Remarkable Effect of Ethylene Carbonate and Other Solvents. *Macromolecules* **1998,** 31, (5), 1535-1541.
88. Pintauer, T.; Matyjaszewski, K., Structural aspects of copper catalyzed atom transfer radical polymerization. *Coordination Chemistry Reviews* **2005,** 249, (11-12), 1155-1184.
89. Gao, C.; Li, G.; Xue, H.; Yang, W.; Zhang, F.; Jiang, S., Functionalizable and ultra-low fouling zwitterionic surfaces via adhesive mussel mimetic linkages. *Biomaterials* **2010,** 31, (7), 1486-1492.
90. Esteves, A. C. C.; Bombalski, L.; Trindade, T.; Matyjaszewski, K.; Barros-Timmons, A., Polymer Grafting from CdS Quantum Dots via AGET ATRP in Miniemulsion. *Small* **2007,** 3, (7), 1230-1236.

91. Beers, K. L.; Gaynor, S. G.; Matyjaszewski, K.; Sheiko, S. S.; MÃ¶ller, M., The Synthesis of Densely Grafted Copolymers by Atom Transfer Radical Polymerization. *Macromolecules* **1998,** 31, (26), 9413-9415.

92. Mahouche-Chergui, S.; Gam-Derouich, S.; Mangeney, C.; Chehimi, M. M., Aryl diazonium salts: a new class of coupling agents for bonding polymers, biomacromolecules and nanoparticles to surfaces. *Chemical Society Reviews* **2011,** 40, (7), 4143-4166.

93. Bergbreiter, D.; Kippenberger, A.; Jordan, R., Hyperbranched Surface Graft Polymerizations Surface-Initiated Polymerization II. In Springer Berlin / Heidelberg: 2006; Vol. 198, pp 1-49.

Capítulo 4

Modelization of size and polydispersity of magnetic hybrid oxygen-sensitive nanoparticles for dissolved oxygen measurements

M. Marín-Suárez[1*], M.C. Arias-Martos[1], J.F. Fernández-Sánchez[1*], T. Galeano-Díaz[2], A. Fernández-Gutiérrez[1]

[1] *Department of Analytical Chemistry, University of Granada, Avda. Fuentenueva s/n, 18071 Granada (Spain)*

[2] *Department of Analytical Chemistry, University of Extremadura, Avda. de Elvas s/n, 06071 Badajoz (Spain)*

Abstract

An experimental design has been applied in order to model both size and polydispersity of poly(styrene-co-maleic anhydride) nanoparticles. The design has been applied to predict the synthesis conditions for targeting size and homogeneity of magnetic hybrid, oxygen-sensitive nanoparticles. A screening test was firstly done in order to determine the influence of the different parameters involved in the process and a central composite design was subsequent realized to obtain various response surfaces which model the preparation of oxygen-sensitive nanoparticles with different sizes and polydispersities by miniemulsion evaporation. This method has been corroborated by producing polymeric nanoparticles with different sizes (100, 200 and 300 nm) and magnetic hybrid oxygen-sensitive nanoparticles of 200 nm. The resulting oxygen sensing nanoparticles have sizes between 180 and 210 nm, can be easily collected with a magnet and show enhanced sensitivity towards dissolved oxygen (Stern-Volmer constants ranging from 34.62 ± 1.05 to 50.28 ± 1.04 bar^{-1} depending on the polymer) compared to a classical polystyrene membrane.

Keywords: RSM (Response Surface Methodology); experimental design; nanoparticles; oxygen sensing; polymeric nanoparticles. *E-mail addresses*: mmarinst@ugr.es (M. Marín-Suárez); jffernan@ugr.es (J.F. Fernández-Sánchez)

4.1 Introduction

Optical oxygen sensing has become the most popular method for monitoring oxygen in real time[1-5], due to the importance of molecular oxygen in many areas such as medicine, industry or environment[6-10] and the advantages of optical sensors[11]. Optical oxygen sensors are usually composed of organic dyes, whose luminescence is quenched by paramagnetic oxygen, immobilised into oxygen-permeable organic matrices[12]. These types of matrices provide the mechanical support to the sensing phase and must be transparent to visible light and permeable to oxygen[11-13]. Polymeric materials can provide this selectively permeable barrier to oxygen which prevents other quenchers to interact with the dye. However, the quenching behavior of polymeric sensing films is a diffusion-controlled reaction[14]. When the measurement is carried out in aqueous phase, the sensitivity is usually decreased compared to gas phase, mainly due to the low diffusion of oxygen in water and the number density of oxygen molecules in solution[15]. Several efforts have been done in order to improve the sensitivity to dissolved oxygen (DO) of these sensing phases, many of them base on the use of organically modified silicates (*ormosil*) [16-19]. The use of nanoparticles has also shown improved dissolved oxygen sensitivity compared to planar films[20-22], since they combine the flexibility of dissolved indicators with the robustness of conventional optical sensors[23]. When magnetic properties are incorporated into such particles, a sensing spot can be easily isolated from the sample by means of a magnetic field and be read out from outside with a fibre optic[24-26]. In addition, polymeric nanoparticles are also attractive for many fields, from biomedical applications [27-29] to a widely variety of materials[30, 31], including smart nanoparticles that can act as chemical or biological probes[23, 26, 32-34].

Beyond the different possible methods to develop polymeric nanoparticles, miniemulsion-evaporation is a simple and versatile technique that offers some advantages towards others, such a precipitation-evaporation or spray-drying[35]. In miniemulsion evaporation method, a water-immiscible cocktail containing a linear polymer or copolymer and an indicator dye is emulsified in water with the help of a sonicator and surfactant. This technique possesses flexibility regarding to polymers and solvents and it is able to produce sub-micron sensing particles with moderate polydispersity, although size and size distribution are not easily tuneable due to the

factors involved in the production. In fact, size control is still a challenge in different areas where it is necessary to address appropriate size-dependant properties[32, 36-38].

In this way, statistical design offers a tool to find out, by using a minimum number of experiments, the influence of the parameters involved in the process, allowing to better control the synthesis conditions that determine size and size distribution of formed nanoparticles. The use of response surface methodology (RSM) is a good alternative to the classical one-variable-at-a-time optimization[39], since it is able to generate large amounts of information from a small number of experiments. In addition, RSM allows to evaluate the effect on the response of interaction between the variables and to determine the critical point. For this objective, second-order symmetrical design should be applied, being the central composite design (CCD) the most utilized for the development of analytical procedures[40].

In this work, a preliminary screening test has been carried out to choose which are the most influencing variables, regarding to either the process (time and amplitude of sonication) or the raw materials (polymer, surfactant and solvent), involved in the production of nanoparticles by miniemulsion solvent evaporation, using poly(styrene-co-maleic anhydride) of three different molecular weights. In addition, central composite design (CCD) was subsequently applied to evaluate the interaction between the variables selected from the screening test. The evaluation of the results was done according to the size and size distribution of the nanoparticles, specifically, nanoparticles of diameter below 200 nm with a small size distribution are pursued in order to facilitate the magnetic collection and enhance the contact with the oxygen present in the media. The possibility of producing nanoparticles upon request and/or predicting the polydispersity and size associated to certain experimental conditions, which is of great interest for to the variety of application mentioned above. Therefore, the ability of statistical experimental design to obtain a catalogue of size and polydispersity is also tested in the synthesis of magnetic oxygen sensing nanoparticles targeting 200 nm, which are expected to show enhanced oxygen sensitivity to DO.

4.2. Materials and Methods

4.2.1. Reagents

Polymer nanoparticles were prepared by the emulsification of a water insoluble cocktail and the consequent evaporation of the solvent. Poly(styrene-co-maleic anhydride) polymers of three different molecular weights and maleic contents were used. Polymer 1 (7% maleic anhydride, Mw =224000 g mol^{-1}), chloroform and sodium dodecyl sulphate (SDS) were purchased to Sigma Aldrich. Polymer 2 (8.3% maleic anhydride, Mw=180000 g mol^{-1}) and polymer 3 (11% maleic anhydride, Mw=14400 g mol^{-1}) were kindly provided by Polyscope (www.polyscope.eu) and Sartomer Inc. (www.sartomereurope.com) respectively. Magnetic nanoparticles consisting of magnetite (Fe_3O_4) covered with oleic acid were synthesized following the procedure described elsewhere[41]. Oxygen indicator Pt(II) meso-Tetra(pentafluorophenyl)porphine (PtTFPP) was purchased from Frontier Scientific Services. The oxygen indicator was selected due to its good oxygen sensing capability and stability[42].

A high energy probe sonicator from Branson S-450 Digital was used to develop the nanoparticles. The parameters utilized to characterize them were size (*d*, in nanometres) and polydispersion index (PdI), both measured with a Zetananosizer (Malvern Instrument).

4.2.2. Preparation of the nanoparticles

In a first step of the work, simple non-sensing nanoparticles were produced by adding a cocktail containing the polymer in chloroform into a solution of SDS in 40 mL of deionised water. The biphasic mixture was cooled and sonicated with a high-energy probe sonicator and the solvent was evaporated by blowing air for 2 hours. The resulting particles formed stable dispersions. In a second step, magnetite and the oxygen indicator PtTFPP were added into the chloroform cocktail prior to mixture, in order to produce magnetic optical sensing particles. Magnetite and oxygen indicator concentrations were 10% (w/w) and 1.5% (w/w), both respect to the total polymer amount.

4.2.3. *Experimental design*

The software package THE UNSCRAMBLER 6.11b from CAMO (Trondheim, Norway), running under Windows XP, was used for the application of chemometrics.

Prior to response surface methodology (RSM), a screening test was carried out to identify which independent variables present more significant effects. After the evaluation of the variables, those with largest influence on the results were selected for new studies. The new experiments were designed according to a central composite design (CCD), a class of experimental designs for response surface modelling and optimization, based on adding star and centre samples to the samples resulting from a two-level factorial design. This provides the intermediate levels necessary for fitting a quadratic model, that is to say, data obtained from the experiments can be fitted by the following second-order polynomial equation, in order to be able to determine an optimum[39]:

$$y = \beta_0 + \sum_{i=1}^{k} \beta_i \cdot x_i + \sum_{i=1}^{k} \beta_{ii} \cdot x_i^{\,2} + \sum_{1 \le i \le j}^{k} \beta_{ij} \cdot x_i \cdot x_j \qquad (1)$$

where y is the response variable under study, either size (d), polydispersity (PdI), or any other response function, x_i are the predictors or independent variables and (β_i), (β_{ii}) and (β_{ij}) are the corresponding linear, quadratic and interactive regression coefficients that express the link between variation in the predictors and variation in the response.

The regression coefficients were determined using The Unscrambler software (THE UNSCRAMBLER® 6.11b. CAMO ASA) and further utilized by a self-made program developed with MATLAB 7.7 to calculate the synthesis conditions necessary to evaluate the prediction capability of the surfaces.

4.2.4. *Evaluation of the fitted model*

The best approach to evaluate the significance of the variables on the response and the quality of the fitted model is the analysis of variance (ANOVA). ANOVA compares the variance of the response accounted for a given effect to the residual variance which summarizes experimental error. The response variance associated to a specific source is measured by the *mean square* (MS) which is the *sum of squares* (SS) divided by the number of degrees of freedom. Therefore, it is possible to evaluate the significance of

the regression by *f-ratios* associated to every tested effect. *F-ratios* are computed as the ratio of MS of regression (effect) to MS of the residuals (error), which have a statistical distribution[43]. Thus, by comparing the F-*ratio* with its theoretical distribution (Fisher distribution), we obtain the significance level (given by a *p-value*) of the effect. The smaller the *p-value*, the more likely it is that the observed effect is not due to chance. Usually, an effect is declared significant if p-value<0.05 (significance at the 5% level).

Essentially, a model is well fitted to the experimental data when there is a significant regression, but also, a non-significant *lack of fit,* which is directly related to the model quality. Whenever possible, the error part is divided into two sources of variation, pure error (estimated from replicated samples) and *lack of fit*, what remains of the residual sum of squares once pure error has been removed. The significance of the lack of fit of the model can be tested comparing the MS due to the pure error and the MS due to the *lack of fit* of the model. A significant *lack of fit* means that the shape of the model does not adequately describe the data. For instance, this can be the case if a linear model is used when there is an important curvature. Therefore, in a good model most of the variations in the residuals are attributed to the pure error rather than to the *lack of fit*, which leads to a value of *lack of fit* below the tabulated value of the Fisher distribution parameter (F test), from which we obtained the significante level (*p-value*)[39, 43]. Furthermore, R^2 can be also used to establish the goodness-of-fit and it is computed as the square of the correlation coefficient between predicted and measured values. Its value is always between 0 and 1, being the closer to 1 the better.

Therefore, for any of the terms in the models, a small p-value indicates more significance, which allows the selection of the most influencing variables on the respective response variables, and the evaluation of the model fit.

4.2.5. Evaluation of the oxygen sensitivity

The oxygen sensitivity was evaluated by measuring the luminescence intensity at different oxygen concentration with a Varian Cary-Eclipse luminescence spectrometer equipped with a Xe flash lamp (peak power equivalent to 75 kW), Czerny-Turner monochromators, R-928 photomultiplier tube which is red sensitive (even 900 nm), with manual voltage set at 600 V and monochromator slit $width_{exc/em}$=5/5 nm.

The excitation was set at 395 nm and the intensity of luminescence was collected at 650 nm by means of a fibre optic specially designed with a magnet in its tip[44]. For gas mixing, two mass flow controllers (MFC) of Type EL-FLOW® model F-201CV Bronkhorst High-Tech (Ruurlo, Netherlands) were connected to copper and stainless steel tubing, and the gas was bubbled to the samples.

A time-trace curve was used to record I_0 and I by bubbling 5 different oxygen partial pressures between 0 and 0.4 bar into the dispersion of nanoparticles in water, at a room temperature of 21º C. A solubility constant of oxygen in water of 0.0023 mol L^{-1} atm^{-1} was calculated by means of a Clark electrode. Therefore, the Stern-Volmer Plot (SVP) was obtained by plotting the ratios I_0/I obtained from the time-trace curve versus dissolved oxygen (DO).

4.3. Results and discussion

4.3.1. Screening test

The first stage in response surface methodology requires the selection of the independent variables with major effects and the delimitation of the experimental range to be examined, according to the aim of the study[39]. In the production of nanoparticles via miniemulsion-evaporation, it is very difficult to identify and control the contribution of each of the variables affecting the system.

Therefore a screening test was first carried out to determine which of the variables present more significant effects over size and size distribution, since the aim is to study the synthesis conditions leading to particles whose size and polydispersity can be controlled. Furthermore, because one of the challenges is to produce nanoparticles with size below 200 nm and low *PdI* (below 0.2) it was necessary to search for an overall criterion that combine the magnitude of both properties into a single variable. This is normally done by a mathematical relationship, the so-called response function, which contains the specifications that each response should fulfil. Based on this methodology and bearing in mind the objective of the study, response functions (*RF*) have to be designed to penalize the values of *PdI* over 0.2 and the increasing of the size up to 200 nm.Due to the high subjectivity of response functions[45], diverse and similar functions were assayed to construct screening and optimization models, being the best results obtained with the following one:

$$RF = (200 - d)\left(\frac{0.2}{PdI}\right) \quad (2)$$

For the screening test, a Plackett-Burman design was followed for the variables and ranges shown in **Table 1**, which are the main variables affecting the production of nanoparticles by miniemulsion-solvent evaporation.[35] This type of design gives information about the main effects of the design variables with the smallest possible number of experiments. The model matrix for the screening test is shown in **Table 2,** where the values of the factors are given by − (minus) for low level and + (plus) for high level.

Table 1 Codes for the different variables and their corresponding ranges, low (-) and high (+) levels, the effects and p-values obtained from the screening test.

Code	Variable	Level		*d* (nm)		*PdI*		*FR*	
		-	+	Effect	p-value	Effect	p-value	Effect	p-value
W	Molecular Weight ($g \cdot mol^{-1}$)	14400	240000	157.155	0.0018	0.0450	0.0406	0.8040	0.0423
C_p	Polymer concentration ($mg\ mL^{-1}$)	10	160	217.845	0.0009	0.1030	0.0082	-0.4830	0.1056
V	Volume of organic phase (mL)	0.4	8	-335.400	0.0004	-0.348	0.0007	1.2200	0.0190
C_{SDS}	SDS concentration ($mg\ mL^{-1}$)	0.14	2.88	75.715	0.0076	0.0385	0.0543	-0.0025	0.9897
A	Amplitude of sonication (%)	20	90	-87.155	0.0057	-0.0340	0.0681	0.1060	0.5982
t	Time of sonication (min)	5	10	-121.645	0.003	0.0065	0.559	0.4260	0.1304
Error[a]				± 23.3		± 0.033		± 0.60	

[a] Experimental error from replicate reference samples

After an analysis of variance (ANOVA) it was found that all the examined variables (see Table 1) have a significant effect (*p-value* lower than 0.05) over *d*, whereas only two of them do it over *PdI* (*Cp* and *V*) and over *RF* (*W* and *V*). This is in concordance with the results obtained considering significant those variables whose effect exceeds the experimental error estimated from replicated reference samples, as can be also

compared in Table 1. From these results, type and concentration of polymer, and volume of organic phase, were selected as the most significant variables.

Table 2 Plackett-Burman design model matrix for the screening test, where the values of the factors are given by – (minus) for low level and + (plus) for high level.

Exp.	*W* (g·mol^{-1})	C_p (mg mL^{-1})	*V* (mL)	C_{SDS} (mg mL^{-1})	*A* (%)	*t* (min)	*d* (nm)	*PdI*
T1	–	+	+	–	–	+	78.72	0.185
T2	+	–	–	–	+	–	173.9	0.202
T3	+	+	+	–	+	+	302.3	0.473
T4	–	–	–	+	+	+	469.1	0.563
T5	+	–	+	+	–	+	196.2	0.223
T6	–	+	–	–	–	–	886.1	0.648
T7	–	–	+	+	+	–	170.0	0.125
T8	+	–	–	+	–	–	302.9	0.443

4.3.2. Analysis of response surfaces

The second step in RSM is the choice of the experimental design for optimization purposes, followed by the statistical treatment of the results[39]. CCD was chosen as the experimental design in order to construct the experimental matrix. This methodology was presented by Box and Wilson[40] and consists of the following parts: (1) a full or fractional factorial design; (2) an additional design, often a star design with experimental points at a certain distance from its centre; and (3) a central point. Samples from factorial design and star samples will have the same leverage, i.e. the information they carry will have equal weight on the analysis. This property, called rotatability, is important if you want to achieve uniform quality of prediction in all directions from the center[46].

Regarding to the results obtained in the screening test, the response surface methodology was used to study the effect of polymer concentration in the discontinuous phase (C_p), the oil/water ratio (V) and the molecular weight of the polymer (W) on the responses *d*, *PdI* and *RF*. It should be highlighted that, in order to evaluate the influence of molecular weight, each set of experiment had to be repeated for each kind of polymer, with different molecular weight and maleic acid content, since the type of polymer acts as a discrete variable (only three kinds of polymers were available).

The experiments designed using a CCD, consisting of 2^2 factorial design and star samples with three central points, are shown in **Table 3**. It also shows the results for

particle size and polydispersity of the nanoparticles obtained in all experiments for each kind of polymer. Individual experiments were carried out in random order. The response surface methodology was applied to these responses, size and polydispersity, individually, as well as to *RF* values calculated from them. The resulting second-order polynomial equations reduced from Eq. 1 follows the next structure for each response variable and type of polymer:

$$y = \beta_0 + \beta_1 \cdot V + \beta_2 \cdot c_p + \beta_{11} \cdot V^2 + \beta_{22} \cdot c_p^2 + \beta_{12} \cdot V \cdot c_p \quad (3)$$

where y is the response variable of study, either size (d), polydispersity (PdI), or RF. **Table 4** shows the values of the β coefficients for the different response variables associated to each type of polymer. The values of the coefficients are calculated from the previously centered variable values.

Table 3 Central composite design (CCD) for the variables selected (V and C_p) and their corresponding particle size and polydispersity index obtained for each kind of polymer (1, 2 and 3).

Exp. No.	V (mL)	C_p (mg mL^{-1})	Polymer 1		Polymer 2		Polymer 3	
			***d* (nm)**	***PdI***	***d* (nm)**	***PdI***	***d* (nm)**	***PdI***
D1	6.90	32.00	213.9	0.145	189	0.145	159.1	0.11
D2	4.25	85.25	251.4	0.216	220.6	0.199	146.5	0.111
D3	7.99	85.25	323.7	0.295	270.3	0.239	195.4	0.108
D4	1.60	32.00	138.8	0.100	135.9	0.115	101.9	0.12
D5	6.90	138.50	289.8	0.287	256.1	0.253	194.6	0.162
D6	4.25	85.25	258.5	0.245	259.7	0.223	142.9	0.090
D7	1.60	13.50	211.9	0.242	197.9	0.199	120.7	0.110
D8	4.25	10.17	138.4	0.109	123.8	0.126	104.8	0.118
D9	4.25	85.25	258.4	0.250	241.7	0.224	142.8	0.089
D10	0.51	85.25	241.4	0.342	174.9	0.193	133.1	0.141
D11	4.25	160.33	210.8	0.228	230.0	0.255	181.0	0.136

Table 4 β coefficient of the second-order polynomial equations obtained from the RSM for each type of polymer and response.

	Polymer 1			Polymer 2			Polymer 3		
	d	***PdI***	***RF***	***d***	***PdI***	***RF***	***d***	***PdI***	***RF***
β_0	256.16	2.37e-01	-47.39	240.69	0.215	-37.18	144.10	$9.63 \cdot 10^{-02}$	117.47
β_1	12.73	1.12e-03	-13.17	11.63	$7.04 \cdot 10^{-03}$	-12.41	10.36	$-2.14 \cdot 10^{-04}$	-16.49
β_2	0.59	1.06e-03	-0.82	0.66	$8.80 \cdot 10^{-04}$	-0.88	0.38	$1.59 \cdot 10^{-04}$	-0.65
β_{11}	$4.96 \cdot 10^{-03}$	$-3.07 \cdot 10^{-10}$	17.71	$9.04 \cdot 10^{-03}$	$4.25 \cdot 10^{-05}$	9.94	$2.96 \cdot 10^{-02}$	$1.10 \cdot 10^{-04}$	-9.65
β_{22}	1.36	$4.03 \cdot 10^{-03}$	-0.95	-1.47	$-8.61 \cdot 10^{-04}$	9.26	1.10	$2.00 \cdot 10^{-03}$	-21.52
β_{12}	$-1.58 \cdot 10^{-02}$	$-1.66 \cdot 10^{-05}$	41.50	$-1.17 \cdot 10^{-02}$	$-6.66 \cdot 10^{-06}$	35.39	$-1.06 \cdot 10^{-03}$	$5.40 \cdot 10^{-06}$	-4.29

To visualise the effect of the solvent volume and polymer concentration on the particle size, polydispersity and FR, response surface and contour plots of the quadric polynomial models were generated for each kind of polymer (**Fig. 1**). The models were

evaluated in terms of quality and accuracy, resulting in good surface parameters but not with a well-defined maximum, as can be seen in Fig. 1. Analysis of variance (ANOVA) was used to evaluate the significance of each model and its lack of fit, as well as R^2 (see **Table 5**). In general, all the models showed good fitting properties, with small p-value for the model fit but large for the lack of fit, with R^2 close to 1, except for the response of *PdI* in polymer 3 that possesses a p-value of 0.1562 and a R^2 of 0.724.

Table 5 Significance of the quadratic polynomial models and lack of fit obtained for *d*, *PdI* and *RF* for each polymer.

Polymer		*d*(nm)		*PdI*		*FR*	
		p-value[a]	$R^{2\,b}$	p-value[a]	$R^{2\,b}$	p-value[a]	$R^{2\,b}$
1	Model	0.0007	0.972	0.0569	0.825	0.0013	0.964
	Lack of Fit	0.0547		0.0959		0.0006	
2	Model	0.0015	0.962	0.0067	0.929	0.0003	0.979
	Lack of Fit	0.9197		0.3291		0.8092	
3	Model	0.0073	0.927	0.1562	0.724	0.0293	0.869
	Lack of Fit	0.0171		0.3062		0.2015	

[a] p-value < 0.05 indicates a major significance
[b] R^2 close to 1 indicates the goodness of the fit.

As shown in **Fig. 1**, similar behaviours were found for any of the responses, except for polymer 3. As expected, both size and polydispersity increased with an increase in either solvent volume or polymer concentration, this is, an increase in polymer total amount produces an increase in size and size distribution.

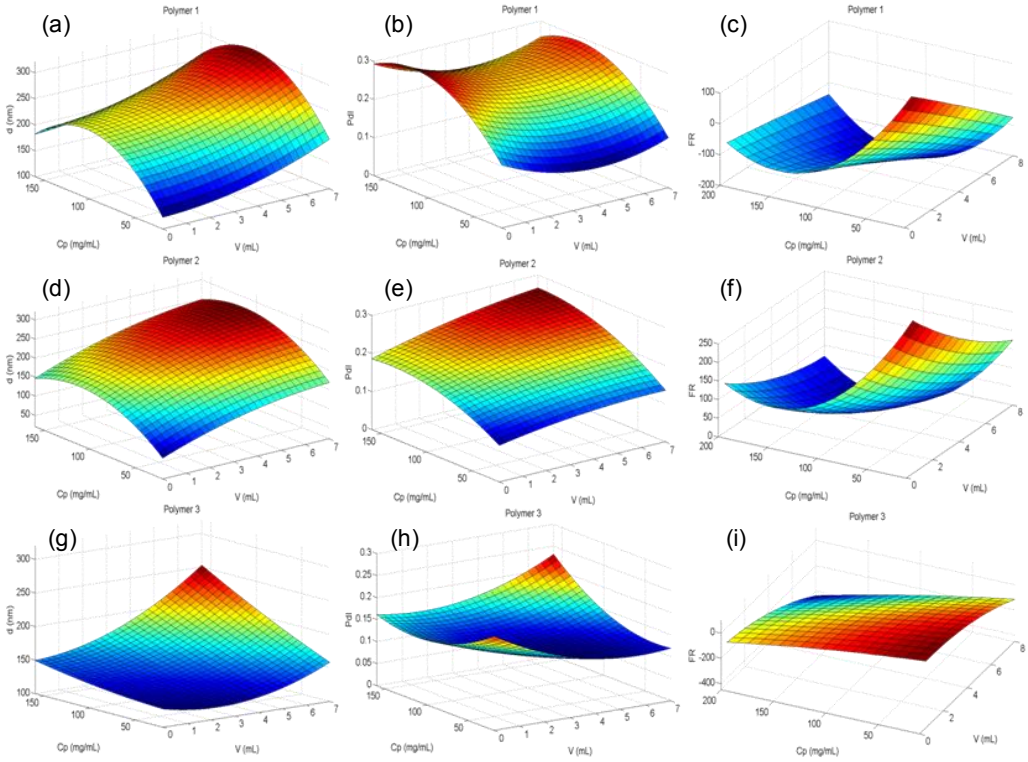

Fig. 1 Response surface corresponding to: (a) size for polymer 1, (b) polydispersity index for polymer 1, (c) FR for polymer 1; (d) size for polymer 2, (e) polydispersity index for polymer 2, (f) FR for polymer 2; (g) size for polymer 3, (h) polydispersity index for polymer 3, (i) FR for polymer 3.

From the results, it can also be observed that for the polymer having a higher molecular weight the particle size is also increased, when comparing with the results provided by the other two, in the same synthesis conditions.

The morphology of the nanoparticles was analyzed by scanning electron microscope (SEM), revealing that the particles are spherical, with a smooth surface and confirming the average size obtained from the Zetasizer analyzer, as can be seen in **Fig. 2** (a) (b) and (c) for polymers 1, 2 and 3, respectively.

4.3.3. Prediction of the surface

From the response surface obtained for the *RF* (**Fig. 1**), it can be determined the range of synthesis conditions in which it is possible to achieve both minimum size and polydispersity However, sometimes it may be necessary to choose among the synthesis conditions leading to a particular particle size and polydispersity. In order to determine the influence of the synthesis conditions over these two parameters, it would be necessary to overlap the corresponding surfaces to find the region that satisfy

both responses, which entails that the objective regions for both responses coincide. In these cases, a multicriteria methodology can be applied in order to find a compromise between size and polydispersity[45], in our case to obtain a particle size upon request with the smallest *PdI* achievable.

Therefore the prediction capability of the response surface methodology was used to design a new set of experiments bearing in mind that the aim of these experiments was to produce nanoparticles of 100, 200 and 300 nm with the lowest polydispersity index achievable according to the conditions of the design. However, it should be noticed that as size is function of molecular weight, for the polymer of highest molecular weight (polymer 1) it was not possible to obtain particles of 100 nm in the studied range, while for the polymers of lower molecular weight (polymer 2 and 3) no particles of 300 nm were obtained.

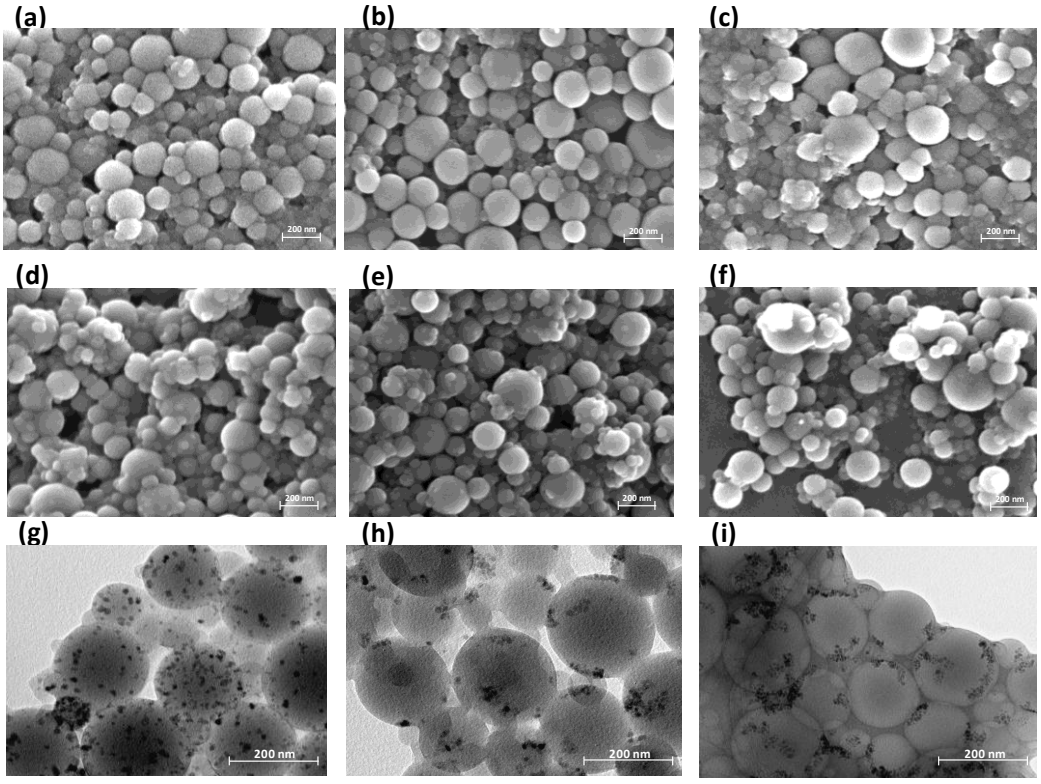

Fig. 2 SEM and TEM photographs of the samples. Pictures (a), (b) and (c) correspond to SEM photographs for polymer 1, 2 and 3 respectively, all with the target size of 200 nm (see Table 6). Nanoparticles containing magnetite and the oxygen indicator PtTFPP are shown in the SEM photographs (d), (e) and (f) and in the TEM photographs (g), (h) and (i) for polymer 1, 2 and 3 respectively.

The procedure to select the synthesis conditions is as follows: **Fig. 3** (a) shows the size response surface of polymer 1 and the region to achieve 200 ± 10 nm nanoparticles; this region contains several pairs of solvent volume and polymer concentration which can be selected to achieve this size. Subsequently, it was possible to choose among all these pairs of values, those leading to the minimum polydispersity index according to the response surface for *PdI*, as it is shown in **Fig. 3** (b).

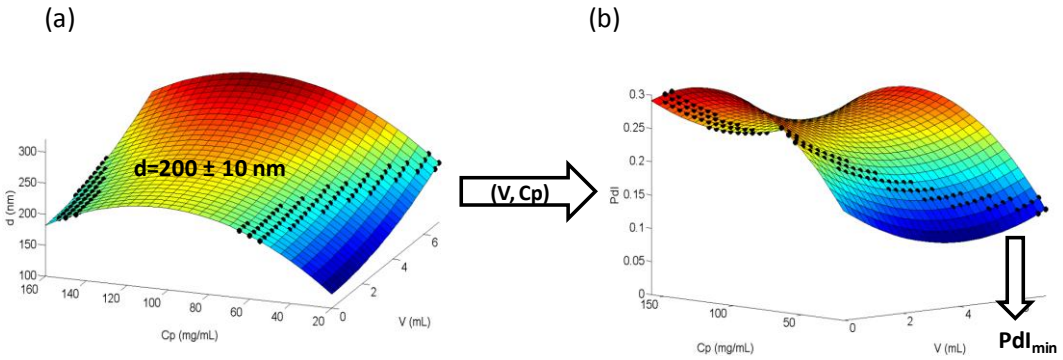

Fig. 3 (a) Size response surface for polymer 1, where the black dots indicates the pairs of (V, c_p) that fulfill a size of 200 ± 10 nm. (b) *PdI* response surface for polymer 1, where the black dots correspond to the values of *PdI* associated to a size of 200 ± 10 nm. The optimal synthesis conditions for a minimum *PdI* and the target size can be found.

The calculation of the values for volume of solvent and polymer concentration necessary to obtain the required size, d_{theo}, was done using a self-made program developed with MATLAB, according to the quadratic polynomial equation for d supplied by Unscrambler for each polymer. In the same way, MATLAB was used to predict the values of *PdI* that would result from the application of the previous conditions of solvent and polymer concentration. From all the possible values of *PdI* obtained, the lower value, PdI_{min}, was taken in order to select the final synthesis conditions. A summary of the synthesis conditions and predicted values for each polymer is shown in **Table 6**.

Table 6 Prediction capability of the surface where for each type of polymer it is shown: target size, synthesis conditions (V and C_p), theoretical size (d_{theo}) and minimum *PdI* (PdI_{min}) achievable obtained from the surfaces responses, and experimental values of d (d_{exp}) and *PdI* (PdI_{exp}) obtained from the aforesaid synthesis conditions.

Pol.	Target size (nm)	V (ml)	C_p (mg mL^{-1})	d_{theo} (nm)	PdI_{min}	d_{exp} (nm)	PdI_{exp}
1	200 ± 10	6.8	20.0	190.8 ± 24.5	0.106 ± 0.098	168.0 ± 13.2	0.100 ± 0.030
	300 ± 10	7.0	73.3	293.8 ± 25.3	0.262 ± 0.090	319.3 ± 21.8	0.311 ± 0.045
2	100 ± 10	0.8	20.0	111.8 ± 28.7	0.109 ± 0.039	119.93 ± 2.7	0.121 ± 0.032
	200 ± 10	6.2	33.3	189.7 ± 24.9	0.166 ± 0.034	183.93 ± 8.5	0.163 ± 0.027
3	100 ± 10	3.3	23.3	106.6 ± 24.4	0.115 ± 0.033	95.5 ± 4.2	0.133 ± 0.018
	200 ± 10	7.0	106.7	193.7 ± 24.9	0.125 ± 0.033	195.7 ± 26.4	0.125 ± 0.043

Therefore, experiments were carried out to evaluate this predictive capability of the response surfaces generated for the different polymers andnanoparticles were synthesized in the selected conditions. The size and polydispersity were experimentally measured (d_{exp} and PdI_{exp}) and compared with the intended values (d_{theo} and PdI_{min}), as it is shown in **Table 6**. All the experiments were carried out in triplicate in order to evaluate the error. As can be seen in Table 6 the range of d and *PdI* predicted from the RSM models, for selected synthesis conditions, are in concordance with the experimental values. This indicates that the quadratic polynomial equations obtained by fitting the data acquired from the CCD design are adequate to describe the influence of the independent variables (volume of solvent and polymer's concentration) on the particle size and polydispersion index. Therefore, it is possible the application of RSM to obtain a catalogue of d and *PdI* achievable inside the range of synthesis, and/or the synthesis of nanoparticles with size and *PdI* upon request.

4.3.4. *Magnetic oxygen sensing nanoparticles*

Once the synthesis conditions were selected for the desired objective, magnetite and oxygen indicator were added to the cocktail in order to evaluate its influence in d and *PdI* when developing magnetic oxygen sensing nanoparticles, targeting a size of 200 nm. As can be seen in **Table 7**, the presence of magnetite and/or PtTFPP seems to

increase both size and polydispersity compared to the blank nanoparticles synthesized in the same conditions, but always within the range of experimental error.

Furthermore, the oxygen sensitivity was evaluated in order to confirm the sensing capability of the particles. Oxygen properties can be evaluated by the quenching in emission intensity when different quencher (oxygen) concentrations are present. This decrease in intensity is described by the Stern-Volmer equation [47] (see Eq. 4).

$$\frac{I_0}{I} = 1 + k_{SV} pO_2 \quad (4)$$

where I is the luminescence intensity, the subscript "0" refers to the value in the absence of quencher, k_{SV} is the Stern-Volmer constants representing the sensitivity to oxygen and pO_2 is the partial pressure of oxygen.

Table 7 Size and polydispersity of the particles containing the magnetite and the oxygen indicator for the same synthesis conditions targeting 200 nm (see Table 6).

Polymer	Oxygen sensitive-magnetic nanoparticles		
	***d* (nm)**	***PdI***	**k_{SV} (bar^{-1})**
1	180.33 ± 7.49	0.139 ± 0.01	36.16 ± 1.53
2	207.33 ± 25.88	0.164 ± 0.05	50.28 ± 1.04
3	193.16 ± 2.72	0.175 ± 0.03	34.62 ± 1.05
PS[a] (aqueos)	-	-	1.63 ± 0.05
PS[a] (gas)	-	-	79.95 ± 1.34

[a] Reference polystyrene membrane prepared as in reference 4

From the Stern-Volmer plots, the sensitivity to oxygen was calculated, showing good response to oxygen. Table 7 also shows the k_{SV} of the oxygen sensitive nanoparticles targeting 200 nm, and a polystyrene classical membrane taken as a reference. The polystyrene membrane was prepared as in previous works[4] and measured in the same conditions than the nanoparticles. The Stern-Volmer constant of the hybrid nanoparticles reached the 45% and 62 % of the reference value in gas phase (k_{SVgas} = 79.95 bar^{-1}). Nevertheless, the sensitivity to oxygen of the films increased more than 20 times compared to the reference membrane in aqueous phase (k_{SV}=1.63 bar^{-1}), confirming the enhancement of the oxygen sensitivity when magnetic nanoparticles are used.

Fig. 2 shows the SEM photographs of the nanoparticle targeting 200 nm, both blank and oxygen sensitive. It can be noticed the increase in polydispersity of the nanoparticles containing magnetite and the oxygen sensitive dye (see Fig. 2 (d), (e) and (f) for polymer 1, 2 and 3) compared to the blank nanoparticles (see Fig. 2 (a), (b) and (c)). Transmission electron microscopy (TEM) was also used to investigate the distribution of magnetite inside the nanoparticle, as can be seen in Fig. 2 (g), (h) and (i). Magnetite seems to be better distributed in the polymer of high molecular weight (Fig. 2 (g)), probably due to the higher molecular weight of this polymer, which allows the better entrapping of the magnetite.

4.4. Conclusions

A method has been developed to model both size and polydispersity of polymeric nanoparticles and it has been used for synthesising magnetic hybrid, oxygen-sensitive nanoparticles targeting a diameter of 200 nm by miniemulsion evaporation technique. This method allows to select the synthesis conditions for a targeted size and to predict the polydispersity associated to a certain experimental conditions with a minimum number of experiments.

Size, polydispersity and a response function specially designed with the objective of obtaining nanoparticles not bigger than 200 nm with *PdI* lower than 0.2, were the parameters of study. Thus, a central composite design was applied, and response surface methodology was used to correlate the response of *d*, *PdI* and *RF* of the nanoparticles with the synthesis conditions. The results showed good fitting parameters, except for *PdI* of polymer 3, which showed a model with a p-value higher than 0.05 and a R^2 of 0.724.

Response surface methodology was also used to obtain nanoparticles upon request, with a targeted size and/or polydispersity. Experiments were performed from the synthesis conditions (*V* and *Cp*) obtained from the combination of the response surface of size and polydispersity, targeting a size of 100, 200 and 300 nm for each polymer with the lower *PdI* achievable. These experimental values for the targeted nanoparticles agreed with the theoretical values of *d* and *PdI* obtained from the surface, demonstrating that this methodology also allows us to easily obtain a catalogue of size and polydispersity while exploring all synthesis conditions and associated responses with a small number of experiments.

Finally, size controllable, magnetic oxygen sensitive nanoparticles were produced by using the proposed methodology. In this case, an oxygen sensitive probe (PtTFPP) and magnetite were also added to the cocktail. The resulted particles did not show relevant changes in size or polydispersity when comparing to the blank nanoparticles in the same synthesis conditions. Therefore, 200 ± 10 nm oxygen sensing nanoparticles easily collectable with a magnet were obtained upon request. The nanoparticles showed improved response to oxygen concentration in aqueous phase, with a Stern-Volmer constant more than 20 times higher than in a conventional polystyrene liquid membrane.

Acknowledgments

The authors gratefully acknowledge the financial support of the Junta de Andalucía (Excellence Project P07-FQM-2625, P07-FQM-2738 and Marín-Suárez's grant). The authors are also grateful to Santiago Rodriguez-Medina for his advice using MATLAB.

Referencias

1. Medina-Castillo, A. L.; Fernández-Sánchez, J. F.; Fernández-Gutiérrez, A., One-Step Fabrication of Multifunctional Core-Shell Fibres by Co-Electrospinning. *Advanced Functional Materials* **2011,** 21, (18), 3488-3495.
2. Mistlberger, G.; Koren, K.; Borisov, S. M.; Klimant, I., Magnetically Remote-Controlled Optical Sensor Spheres for Monitoring Oxygen or pH. *Analytical Chemistry* **2010,** 82, (5), 2124-2128.
3. Fitzgerald, M.; Papkovsky, D. B.; Smiddy, M.; Kerry, J. P.; O'Sullivan, C. K.; Buckley, D. J.; Guilbault, G. G., Nondestructive Monitoring of Oxygen Profiles in Packaged Foods Using Phase-Fluorimetric Oxygen Sensor. *Journal of Food Science* **2001,** 66, (1), 105-110.
4. Marín-SuárezdelToro, M.; Fernández-Sánchez, J. F.; Baranoff, E.; Nazeeruddin, M. K.; Graetzel, M.; Fernández-Gutierrez, A., Novel luminescent Ir(III) dyes for developing highly sensitive oxygen sensing films. *Talanta* **2010,** 82, (2), 620-626.

5. Fernández-Sánchez, J. F.; Cannas, R.; Spichiger, S.; Steiger, R.; Spichiger-Keller, U. E., Novel nanostructured materials to develop oxygen-sensitive films for optical sensors. *Analytica Chimica Acta* **2006,** 566, (2), 271-282.
6. Jamnik, P.; Raspor, P., Methods for monitoring oxidative stress response in yeasts. *Journal of Biochemical and Molecular Toxicology* **2005,** 19, (4), 195-203.
7. Yun, Y.-S.; Park, J. I.; Park, J. M., High-rate slurry-phase decomposition of food wastes: indirect performance estimation from dissolved oxygen. *Process Biochemistry* **2005,** 40, (3-4), 1301-1306.
8. Gao, F. G.; Fay, J. M.; Mathew, G.; Jeevarajan, A. S.; Anderson, M. M., Optical sensor based on fluorescent quenching and pulsed blue LED excitation for long-term monitoring of dissolved oxygen in NASA space bioreactors. *Journal of Biomedical Optics* **2005,** 10, (5), 054005-6.
9. Lange, C. A. K.; Stavrakas, P.; Luhmann, U. F. O.; de Silva, D. J.; Ali, R. R.; Gregor, Z. J.; Bainbridge, J. W. B., Intraocular Oxygen Distribution in Advanced Proliferative Diabetic Retinopathy. *American Journal of Ophthalmology* **2011,** 152, (3), 406-412.e3.
10. Song, D. H.; Kim, H. D.; Kim, K. C., Dissolved oxygen concentration field measurement in micro-scale water flows using PtOEP/PS film sensor. *Optics and Lasers in Engineering* **2011**, (0).
11. Wolfbeis, O. S., Materials for fluorescence-based optical chemical sensors. *Journal of Materials Chemistry* **2005,** 15, (27-28), 2657-2669.
12. Amao, Y., Probes and Polymers for Optical Sensing of Oxygen. *Microchimica Acta* **2003,** 143, (1), 1-12.
13. Fernádez-Sánchez, J. F.; Cannas, R.; Spichiger, S.; Steiger, R.; Spichiger-Keller, U. E., Novel nanostructured materials to develop oxygen-sensitive films for optical sensors. *Analytica Chimica Acta* **2006,** 566, (2), 271-282.
14. Ware, W. R., Oxygen quenching of fluorescence in solution: An experimental study of the diffusion process. *The Journal of Physical Chemistry* **1962,** 66, (3), 455-458.
15. Lavin, P.; McDonagh, C. M.; MacCraith, B. D., Optimization of Ormosil Films for Optical Sensor Applications. *Journal of Sol-Gel Science and Technology* **1998,** 13, (1), 641-645.
16. Chen, X.; Zhong, Z.; Li, Z.; Jiang, Y.; Wang, X.; Wong, K., Characterization of ormosil film for dissolved oxygen-sensing. *Sensors and Actuators B: Chemical* **2002,** 87, (2), 233-238.
17. Chu, C.-S.; Lo, Y.-L., Optical fiber dissolved oxygen sensor based on Pt(II) complex and core-shell silica nanoparticles incorporated with sol-gel matrix. *Sensors and Actuators B: Chemical* **2010,** 151, (1), 83-89.

18. Koo, Y.-E. L.; Cao, Y.; Kopelman, R.; Koo, S. M.; Brasuel, M.; Philbert, M. A., Real-Time Measurements of Dissolved Oxygen Inside Live Cells by Organically Modified Silicate Fluorescent Nanosensors. *Analytical Chemistry* **2004,** 76, (9), 2498-2505.
19. McDonagh, C.; MacCraith, B. D.; McEvoy, A. K., Tailoring of Sol-Gel Films for Optical Sensing of Oxygen in Gas and Aqueous Phase. *Analytical Chemistry* **1998,** 70, (1), 45-50.
20. Buck, S. M.; Koo, Y.-E. L.; Park, E.; Xu, H.; Philbert, M. A.; Brasuel, M. A.; Kopelman, R., Optochemical nanosensor PEBBLEs: photonic explorers for bioanalysis with biologically localized embedding. *Current Opinion in Chemical Biology* **2004,** 8, (5), 540-546.
21. Xu, H.; Aylott, J. W.; Kopelman, R.; Miller, T. J.; Philbert, M. A., A Real-Time Ratiometric Method for the Determination of Molecular Oxygen Inside Living Cells Using Sol-Gel-Based Spherical Optical Nanosensors with Applications to Rat C6 Glioma. *Analytical Chemistry* **2001,** 73, (17), 4124-4133.
22. Borisov, S. M.; Mayr, T.; Klimant, I., Poly(styrene-block-vinylpyrrolidone) Beads as a Versatile Material for Simple Fabrication of Optical Nanosensors. *Analytical Chemistry* **2008,** 80, (3), 573-582.
23. Borisov, S. M.; Klimant, I., Optical nanosensors-smart tools in bioanalytics. *Analyst* **2008,** 133, (10), 1302-1307.
24. Chojnacki, P.; Mistlberger, G.; Klimant, I., Separable Magnetic Sensors for the Optical Determination of Oxygen. *Angewandte Chemie International Edition* **2007,** 46, (46), 8850-8853.
25. Mistlberger, G. n.; Borisov, S. M.; Klimant, I., Enhancing performance in optical sensing with magnetic nanoparticles. *Sensors and Actuators B: Chemical* **2009,** 139, (1), 174-180.
26. Medina-Castillo, A. L.; Mistlberger, G.; Fernández-Sánchez, J. F.; Segura-Carretero, A.; Klimant, I.; Fernández-Gutiérrez, A., Novel Strategy To Design Magnetic, Molecular Imprinted Polymers with Well-Controlled Structure for the Application in Optical Sensors. *Macromolecules* **2009,** 43, (1), 55-61.
27. Nasongkla, N.; Bey, E.; Ren, J.; Ai, H.; Khemtong, C.; Guthi, J. S.; Chin, S.-F.; Sherry, A. D.; Boothman, D. A.; Gao, J., Multifunctional Polymeric Micelles as Cancer-Targeted, MRI-Ultrasensitive Drug Delivery Systems. *Nano Letters* **2006,** 6, (11), 2427-2430.
28. Kim, J.; Lee, J. E.; Lee, S. H.; Yu, J. H.; Lee, J. H.; Park, T. G.; Hyeon, T., Designed Fabrication of a Multifunctional Polymer Nanomedical Platform for Simultaneous Cancer- Targeted Imaging and Magnetically Guided Drug Delivery. *Advanced Materials* **2008,** 20, (3), 478-483.

29. Kopelman, R.; Lee Koo, Y.-E.; Philbert, M.; Moffat, B. A.; Ramachandra Reddy, G.; McConville, P.; Hall, D. E.; Chenevert, T. L.; Bhojani, M. S.; Buck, S. M.; Rehemtulla, A.; Ross, B. D., Multifunctional nanoparticle platforms for in vivo MRI enhancement and photodynamic therapy of a rat brain cancer. *Journal of Magnetism and Magnetic Materials* **2005,** 293, (1), 404-410.

30. Kim, S.-H.; Cho, Y.-S.; Jeon, S.-J.; Eun, T. H.; Yi, G.-R.; Yang, S.-M., Microspheres with Tunable Refractive Index by Controlled Assembly of Nanoparticles. *Advanced Materials* **2008,** 20, (17), 3268-3273.

31. Hatzigrigoriou, N. B.; Papaspyrides, C. D., Nanotechnology in plastic food-contact materials. *Journal of Applied Polymer Science* **2011,** 122, (6), 3719-3738.

32. Mistlberger, G.; Koren, K.; Scheucher, E.; Aigner, D.; Borisov, S. M.; Zankel, A.; Pölt, P.; Klimant, I., Multifunctional Magnetic Optical Sensor Particles with Tunable Sizes for Monitoring Metabolic Parameters and as a Basis for Nanotherapeutics. *Advanced Functional Materials* **2010,** 20, (11), 1842-1851.

33. Valero-Navarro, Á.; Gómez-Romero, M.; Fernández-Sánchez, J. F.; Cormack, P. A. G.; Segura-Carretero, A.; Fernández-Gutiérrez, A., Synthesis of caffeic acid molecularly imprinted polymer microspheres and high-performance liquid chromatography evaluation of their sorption properties. *Journal of Chromatography A* **2011,** 1218, (41), 7289-7296.

34. Steiner, M.-S.; Duerkop, A.; Wolfbeis, O. S., Optical methods for sensing glucose. *Chemical Society Reviews* **2011,** 40, (9), 4805-4839.

35. Mistlberger, G.; Medina-Castillo, A.; Borisov, S.; Mayr, T.; Fernández-Gutiérrez, A.; Fernández-Sánchez, J.; Klimant, I., Mini-emulsion solvent evaporation: a simple and versatile way to magnetic nanosensors. *Microchimica Acta* **2010,** 172, (3), 299-308.

36. Lee, M.; Cho, Y.; Park, J.; Chung, H.; Jeong, S.; Choi, K.; Moon, D.; Kim, S.; Kim, I.-S.; Kwon, I., Size control of self-assembled nanoparticles by an emulsion/solvent evaporation method. *Colloid & Polymer Science* **2006,** 284, (5), 506-512.

37. Medina-Castillo, A. L.; Fernández-Sánchez, J. F.; Segura-Carretero, A.; Fernández-Gutiérrez, A., Micrometer and Submicrometer Particles Prepared by Precipitation Polymerization: Thermodynamic Model and Experimental Evidence of the Relation between Flory's Parameter and Particle Size. *Macromolecules* **2010,** 43, (13), 5804-5813.

38. Chiewpattanakul, P.; Covis, R.; Vanderesse, R.; Thanomsub, B.; Marie, E.; Durand, A., Design of polymeric nanoparticles for the encapsulation of monoacylglycerol. *Colloid & Polymer Science* **2010,** 288, (9), 959-967.

39. Bezerra, M. A.; Santelli, R. E.; Oliveira, E. P.; Villar, L. S.; Escaleira, L. A., Response surface methodology (RSM) as a tool for optimization in analytical chemistry. *Talanta* **2008,** 76, (5), 965-977.

40. Box, G. E. P.; Wilson, K. B., On the Experimental Attainment of Optimum Conditions. *Journal of the Royal Statistical Society. Series B (Methodological)* **1951,** 13, (1), 1-45.

41. Ramírez, L. P.; Landfester, K., Magnetic Polystyrene Nanoparticles with a High Magnetite Content Obtained by Miniemulsion Processes. *Macromolecular Chemistry and Physics* **2003,** 204, (1), 22-31.

42. Amao, Y.; Miyashita, T.; Okura, I., Platinum tetrakis(pentafluorophenyl)porphyrin immobilized in polytrifluoroethylmethacrylate film as a photostable optical oxygen detection material. *Journal of Fluorine Chemistry* **2001,** 107, (1), 101-106.

43. Montgomery, D. C., *Design and Analysis of Experiments*. John Wiley and Sons: New York 2005.

44. Mistlberger, G.; Chojnacki, P.; Klimant, I., Magnetic sensor particles: an optimized magnetic separator with an optical window. *Journal of Physics D: Applied Physics* **2008,** 41, (8), 085003.

45. Hendriks, M. M. W. B.; de Boer, J. H.; Smilde, A. K.; Doornbos, D. A., Multicriteria decision making. *Chemometrics and Intelligent Laboratory Systems* **1992,** 16, (3), 175-191.

46. Khuri, A. I.; Mukhopadhyay, S., Response surface methodology. *Wiley Interdisciplinary Reviews: Computational Statistics* **2010,** 2, (2), 128-149.

47. Lakowicz, J. R., *Principles of fluorescence spectroscopy*. 3rd ed.; Springer: 2006; Vol. 1.

Bloque III. Diseño de fases sensoras ópticas adaptables a un microrrobot inalámbrico para medidas in vivo de oxígeno ocular.

Las situaciones de hipoxia en el líquido ocular están relacionadas con enfermedades oculares como la retinopatía diabética, la retinopatía del prematuro o el glaucoma, entre otras. Sin embargo, su relación con la concentración de oxígeno no se entiende por completo, lo cual hace necesario el control de oxígeno dentro del líquido ocular.

Uno de los enfoques que se puede seguir para la determinación de oxígeno *in vivo* en el líquido ocular es el uso de un microrrobot inalámbrico. Éste puede atender a varios prototipos, todos ellos controlados por una plataforma magnética externa, tal como se observa en la Figura III.a, que le permite navegar en el interior del líquido ocular. De este modo, recubriendo el microrrobot con una fase sensora a oxígeno se puede determinar la concentración de éste en el líquido ocular mediante excitación y recolección externa (véase la Figura III.b).

a)

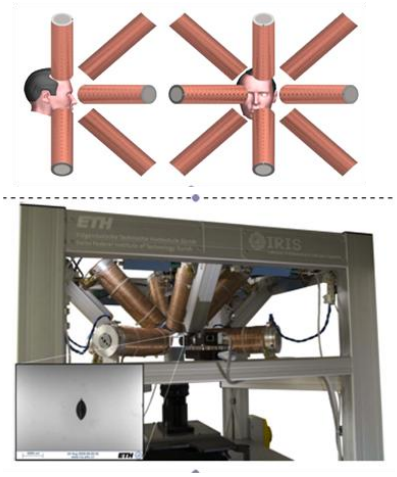

b)

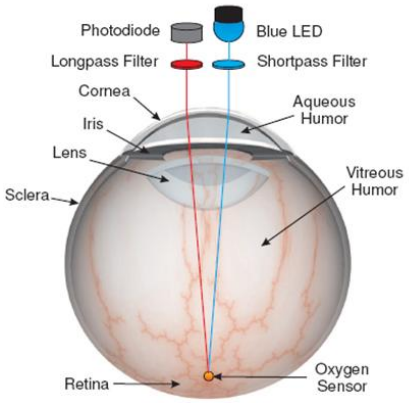

Fig. III. a)Sistema electromagnético para el control inalámbrico del microrrobot; b)Esquema de la realización de las medidas luminiscentes en el interior del ojo.

Diseñar una fase sensora implementable en este tipo de dispositivos de medida requiere cumplir con una serie de requisitos ya que los mismos poseen una morfología tridimensional, un tamaño micrométrico y se van a usar en el interior del ojo. Estos requisitos se pueden resumir en:

- Alta intensidad de emisión lumínica. Este requisito es necesario puesto que al tratarse de un sensor inalámbrico diseñado para moverse dentro del ojo es necesario que la emisión posea intensidad suficiente para ser detectada por el fotodetector, situado a una cierta distancia de la fase sensora y fuera del ojo, lo que también dependerá de la sensibilidad de éste.
- Biocompatibilidad de la matriz: el material de soporte debe ser cuidadosamente seleccionado, en relación tanto a su biocompatibilidad como a su capacidad de retener al indicador evitando que lixivie.
- Tiempo de respuesta corto, lo cual es esencial para aplicaciones biomédicas.
- Deposición homogénea. Es necesario que toda la superficie del robot este cubierta homogéneamente para que la intensidad lumínica que llega al detector sea la misma cualquiera sea la posición del robot dentro del ojo, y que además no influya en la navegación.

Con el objetivo de cumplir con el máximo de estos requisitos, resulta necesario elegir complejos con tiempo de vida largo y longitud de onda en torno a los 650 nm, que es donde los detectores poseen su máxima sensibilidad. Como matriz, el poliestireno ha demostrado biocompatibilidad y buenas propiedades para aislar al indicador y evitar que lixivie. Por estos motivos se eligió el complejo PtOEP en poliestireno como componentes de la fase sensora, y se estudiaron sus propiedades analíticas bajo diferentes condiciones. Estos resultados componen el Capitulo 5 de este bloque.

Una vez seleccionados los materiales componentes de la fase sensora y su morfología, el método de deposición elegido debe ser capaz de suministrar una espesor pequeño (para acortar el tiempo de respuesta) y una distribución homogénea de la fase sensora en toda la estructura 3D del dispositivo inalámbrico, que además posee dimensiones micrométricas. Por este motivo, se decidió evaluar una método de deposición basado en la movilidad electroforética de nanopartículas de poli(estireno-co-anhídrido maleico) con indicador PtTFPP para el desarrollo de fases sensora ópticas, resultados que se recogen en el Capitulo 6.

Capítulo 5

In Vitro Oxygen Sensing using Intraocular Microrobots

O. Ergeneman[a*], George Chatzipirpiridis[a], M. Marín-Suárez[b*], S. Medina-Rodríguez[b], S. Pané[a], J.F. Fernández-Sánchez[b], B. J. Nelson[a], A. Fernández-Gutiérrez[b]

[a]*Institute of Robotics and Intelligent Systems, ETH Zurich, Tannenstrasse 3, CH-8092, Zurich, Switzerland*

[b]*Department of Analytical Chemistry, Faculty of Sciences, University of Granada, Avda. Fuentenueva s/n, E-18071 Granada, Spain*

Abstract

We present a luminescence oxygen sensor incorporated in a wireless intraocular microrobot for minimally-invasive diagnosis. This microrobot can be accurately controlled in the intraocular cavity by applying magnetic fields. The microrobot consists of a magnetic body susceptible to magnetic fields and a sensor coating. This coating embodies Pt(II) octaethylporphine (PtOEP) dyes as the luminescence material and polystyrene asa supporting matrix, and it can be wirelessly excited and read out by optical means. The sensor works based on quenching of luminescence in the presence of oxygen. The excitation and emission spectrum, response time, and oxygen sensitivity of the sensor were characterized using a spectrometer. A custom device was designed and built to use this sensor for intraocular measurements with the microrobot. Due to the intrinsic nature of luminescence lifetimes, a frequency-domain lifetime measurement approach was employed. An alternative design with increased performance was demonstrated by using poly(styrene-co-maleic anhydride) (PS-MA) and PtOEP nanospheres.

5.1. Introduction

Detecting selective reactions at confined spaces is one of the major trends in biomedical nanotechnology. Methods of monitoring localized changes in concentrations of specific analytes such as oligoelements, biomolecules or protons could have a great impact on the field of targeted diagnosis platforms (TDP). The interdisciplinary nature of chemical sensing (i.e.: materials science, electronics, physics, biochemistry) is one ofthe major challenges facing scientists working in this field.[1] The level of complexity becomes even more significant, if a miniaturized TDP is intended to be inserted in the human body. The main requirement that a conventional chemical sensor must satisfy is its selectivity to an specific chemical specie. Many efforts have been made in synthesizing new materials with enhanced selectivity to certain analytes. However, one may find that a material suitable for its use in both in-vitro and ex-vivo sensors, is not fitted to in-vivo applications. The chemical complexity of the human tissues and fluids stands in the way of miniaturized chemical sensors development. Among the additional important aspects to be accounted for, signal transduction determines its in vivo applicability. The most common strategies for signal transduction are based on electrochemical, thermal, or pressure sensing. For instance, miniaturized electrochemical sensors consisting of hybrid nanowires made of alternated segments of gold and cadiumtelluride can be used to detect specific single strand DNA sequences.[2] However such methodologies do not allow the use of untethered devices. The optical detection is an advantageous approach in this sense. Moreover, some optical methods such as luminiscence allows analytical determinations at very low detection limits. Turela et al. recently demonstrated detection of nanomolar concentrations of copper using a luminescence quenching strategy.[3]Despite some limitations arising from the fact that the waves cannot reach very deep locations inside the human body, optical methods can be benefitial for ophtalmological applications.

To perform its fundamental function, the eye needs a sufficient supply of oxygen and nutrients. Oxygen is supplied by the retinal, choroidal and ciliary vessels. By diffusion through the vitreous humor it is delivered to the surrounding tissues including the lens, the ciliary body, and the retina. This oxygen is indispensable for the tissue metabolism.[4] Inadequate oxygen supply (i.e., retinal hypoxia) is correlated with major eye diseases including diabetic retinopathy, glaucoma, retinopathy of prematurity, age-related macular degeneration, neovascularization of the retina, and retinal vein

occlusion.[5] The influence of oxygen on these diseases is not well understood and in vivo oxygen measurements are essential for better diagnosis and treatment. Measuring the oxygen tensions both in aqueous humor and vitreous humor, and particularly in the preretinal area, is of great interest in ophthalmological research. Vitreous oxygen measurements were performed on animals.[4] However, the number of studies on humans is limited mainly by the invasiveness of available methods.

In 6, the concept and prototype of a minimally-invasive wireless optical sensor device to measure intraocular dissolved oxygen concentration was presented. The proposed device consists of a luminescence sensor film that is integrated on a magnetically controlled ferromagnetic sphere with a diameter of 3.25 mm. The device can be inserted through a small incision in the sclera. Closed-loop position control within the vitreous humor can then be accomplished via applied magnetic fields and visual tracking through the pupil. The precise magnetic control of wireless microrobots was demonstrated in 7 and localization of intraocular microdevices using a single camera was presented in 8.

In this work, the sensors presented in 6 were further miniaturized and oxygen sensing using microrobots was demonstrated. A microrobot which is coated with a luminescence sensing film was analyzed and a setup that can be used in the magnetic control system presented in 7 was prepared (**Fig. 1**). Pt(II) octaethylporphine (PtOEP) dyes were used in the sensor due to their long lifetime and visible excitation and emission spectra. Polystyrene (PS) was chosen for the supporting matrix as it is transparent in the visible spectrum and highly permeable to dissolved oxygen.[9] Magnetic microrobots were first coated with gold by electroless plating for biocompatibility and then dip-coated with the oxygen sensitive luminescence film. The excitation and emission properties were characterized as well as the sensing kinetics and oxygen sensitivity of the coated microrobots. Furthermore, poly(styrene-co-maleic anhydride) (PS-MA) nanospheres containing PtOEP were synthesized and used in sensors. Instead of applying a thin coating of PS with the PtOEP, nanospheres were deposited on the surface. This method is demonstrated on gold-coated chips and was compared to sensors based on spin-coated films. Dip-coating method is also applied to coat microrobots. A microrobot coated with the luminescence film and a microrobot coated with luminescence nanospheres are shown in **Fig. 1**.

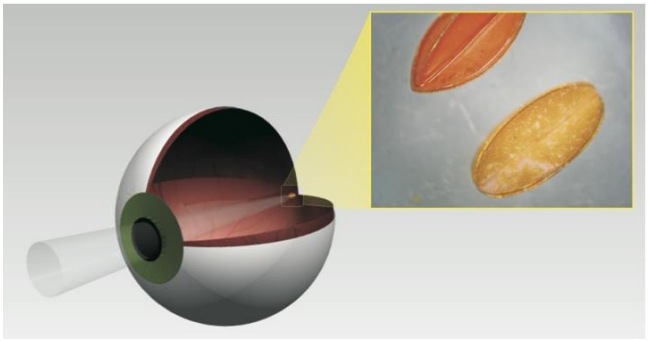

Fig. 1. The oxygen sensing microrobots can be used in the posterior segment of the eye. The inlet photo shows a microrobot coated with the PS film with PtOEP dyes (top) and a microrobot with PS-ME nanospheres with PtOEP (bottom). Both types of microrobots were first coated with gold. The length of the microrobots is 2 mm.

5.2. Luminiscente oxygen sensor

A variety of oxygen sensors have been developed, e.g. Clark electrode sensors, fiberoptic sensors. Luminescence based oxygen sensors are attractive, because they provide wireless readout, fast response, high accuracy, and they do not consume oxygen. They also do not require reference electrodes or stirring, and they can be used as disposable sensors. These sensors do not interfere with magnetic fields which is crucial for a magnetic microrobotic system.

Photoluminescence is the emission of photons from a material in response to absorption of photons. The intensity and the lifetime of emission can be decreased by a variety of processes referred to as luminescence quenching. Optical luminescence oxygen sensors work based on quenching of luminescence in the presence of oxygen, which acts as the quencher; the decrease in luminescence is related to the concentration of oxygen (**Fig. 2**). A number of devices using this principle have been demonstrated and the basic principles of different methods can be found in 10.

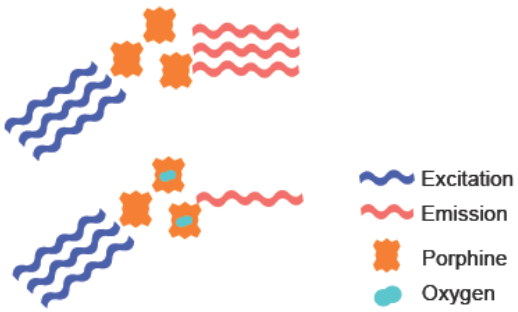

Fig. 2. Illustration of quenching of oxygen. The porphine dyes are quenched in the presence of oxygen which decreases the emission lifetime and intensity.

Luminescence sensing can be performed in different ways. A lifetime measurement approach was chosen for this work, since lifetime is an intrinsic property. The lifetime of emission decreases in the presence of oxygen as a result of the quenching process. Hence, oxygen concentration can be obtained from the lifetime of emission. There are two methods that are used for measuring luminescence lifetimes: time-domain measurements and frequency-domain measurements.[10] In time domain measurements, the sample is excited with light pulses, and the intensity signal that changes as a function of time is measured and analyzed. The time in which the intensity decays to e^{-1} (36.8%) of the initial value is the lifetime. In frequencydomain measurements the sample is excited with a periodic signal that consequently causes a modulated luminescence emission at the identical frequency. Because of the lifetime of emission, the emission signal has a phase shift (i.e., time delay) with respect to the excitation signal. The input excitation signal is used as a reference to establish a zero-phase position and the lifetime is obtained by measuring the phase shift between the excitation signal and the emission signal. The intensity of light collected by the photodetector is extremely sensitive to extrinsic conditions, which are difficult to control in such a wireless sensor application. While the sensor is steered in the ocular cavity, the optical path distance from the light source to the sensor and back to the photo detector changes. For a mono exponential decay the lifetime can be calculated: [11]

$$\tau = \frac{tan\phi}{2\pi f} \tag{1}$$

where τ is the lifetime of emission, ϕ is the phase shift and f is the modulation frequency. Owing to their intrinsic nature, the time-domain lifetime measurement approach is used to characterize with the spectrometer, and frequency-domain lifetime measurement approach is used in the proposed system.

5.2. Experimental

5.2.1. Preparation of the Film Sensor

Microrobots were made of various magnetic materials. In **Fig. 1** two assembled CoNi microrobots are shown. For biocompatibility and surface functionalization they are first coated with a thin layer of gold by electroless deposition. The PtOEP was purchased from Frontier Scientific, UT, USA. To prepare the luminescence film, 3 mg of PtOEP and 197 mg of PS were dissolved in 2 ml of chloroform by stirring. The

microrobots are dip-coated and stored 2 hours, allowing evaporation of chloroform. Gold coated silicon chips with 10mm2 were also spin-coated with the prepared solution for characterization. The thickness of the films is measured by a profiler (Tencor P10).

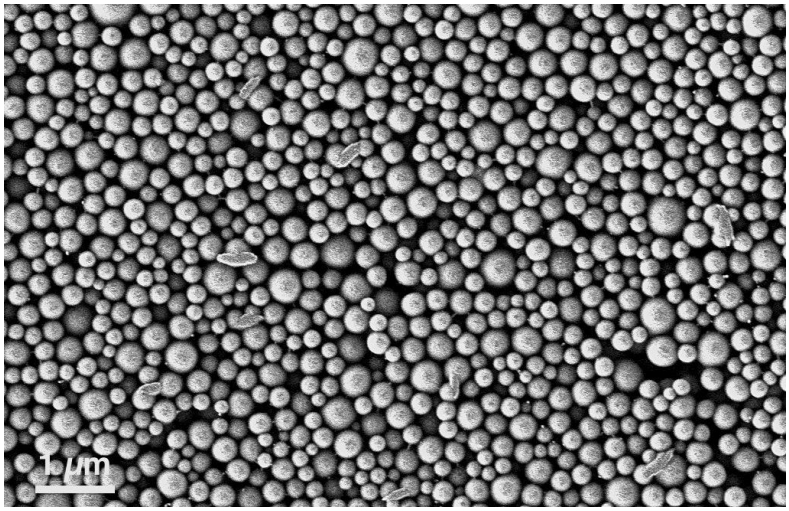

Fig. 3. SEM image of nanospheres of PS-MA containing PtOEP deposited on a gold layer.

5.2.2. Preparation of the Nanospheres Sensor

The porphyrine-functionalized poly(styrene-co-maleic anhydride) (PS-MA) nanospheres were prepared with a method reported in 12. PS-MA and PtOEP dye were dissolved in tetrahydrofuran (THF). The resulting solution was added dropwise into water under vigorous agitation and a dispersion was formed. Nitrogen was bubbled in order to accelerate the evaporation of THF. This forms an aqueous suspension of PS-MA nanospheres with PtOEP. The microrobot or goldcoated chips were first cleaned by immersing in acetone, IPA and piranha solution, consecutively, 10 minutes each. To increase the wettability of the gold substrate, they were kept in a hydrophilic thiol solution (MPS) at 50°C for one hour.[13] Lastly the suspension of nanospheres was pipette onto microrobots or chips. The nanospheres spread over the entire surface producing a uniform coating of nanospheres. **Fig. 3** shows the SEM image of the nanopheres on the gold surface. The nanospheres vary in size, but almost all of them are smaller than 140 nm a polydispersity of 0.026 This provides a sensor with a high surface area, which is generally desirable for fast response times and higher sensitivity. **Figure 4** shows the cross section of the nanospheres deposited on a gold substrate. The cut is made by focused ion beam (FIB) milling. The coating is approximately 1.5 µm thick.

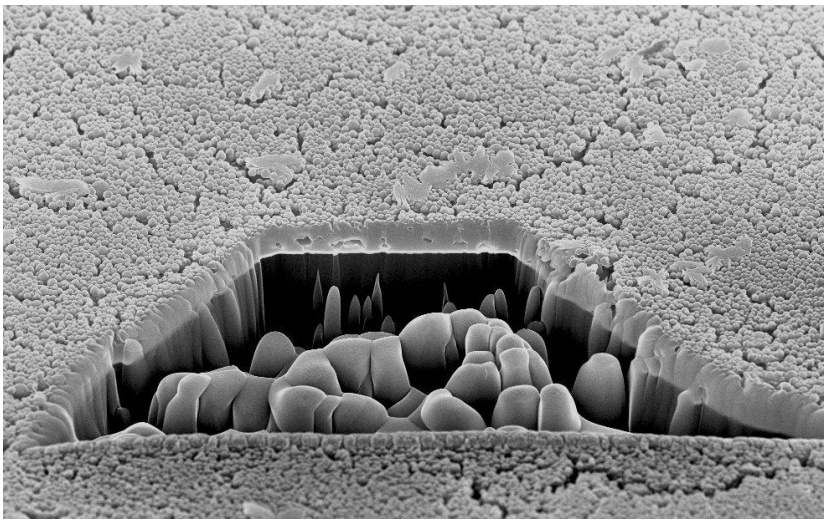

Fig. 4. SEM image showing the cross section of the nanospheres of PS-MA containing PtOEP deposited on a gold layer. The cut is made by FIB.

5.2.3. Characterization Setup

A Cary Eclipse fluorescence spectrophotometer (Varian Inc., CA, USA) was used to characterize the luminescence of the developed sensors. Excitation scan, emission scan, kinetics, and lifetime measurements were performed using this equipment. A custom flow cell which is compatible with the spectrophotometer was built and used in all experiments.

Oxygen and nitrogen was mixed at different ratios using two gas flow controllers (Bronkhorst High-Tech B.V., Netherlands) and applied to the cell. A total gas flow of 500 ml/min was maintained in all gas measurements. Before the experiments, the flow controllers were calibrated using a flow sensor. The dissolved oxygen (DO) measurements were also performed using the same chamber circulating water instead of gas. The oxygen concentration in water is changed by bubbling nitrogen or oxygen in a container. A commercial DO sensor (Oxi 340i, WTW Gmbh) was used to monitor the DO concentration in a second chamber in order to avoid possible interference by gas bubbles. The water circulated using a pump and the fluid flow rate was kept constant. **Figure 5** shows the setup used for DO measurements.

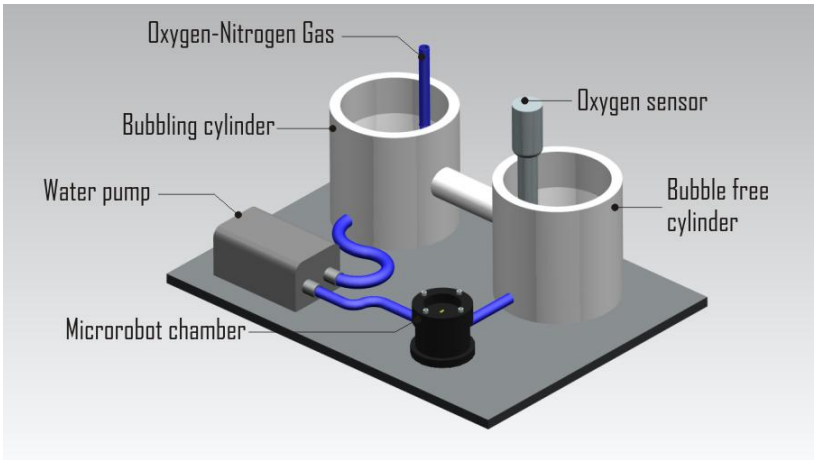

Fig. 5. Calibration setup for dissolved oxygen measurements.

5.2.4. Intraocular Sensing Setup

A custom setup was designed and built for wireless oxygen concentration measurements considering the anatomy of the eye and the control system described in 14. A UV LED and a shortpass filter were used as the excitation source, and a Si photodetector (PD-100A, Thorlabs Gmbh) with a longpass filter were used for the read out. Using a beamsplitter (Edmund Optics) two seperate optical paths were generated: one for the detecting system and the other one for the excitation system and tracking camera. An indirect non-contact ophthalmoscopy lens is needed in front of the eye for localization and tracking. **Fig. 6** shows the illustration of the measurement setup. A lock-in amplifier (HF2LI, Zurich Instruments, Switzerland) was used for the readout. Its internal signal generator modulated the excitation circuit of the led and acted as the reference signal for the detection of the photodetector signal. A bandwidth of 48 mHz was used for the detection of phase change as a function of oxygen concentration. By this method, effective noise cancellation was obtained.

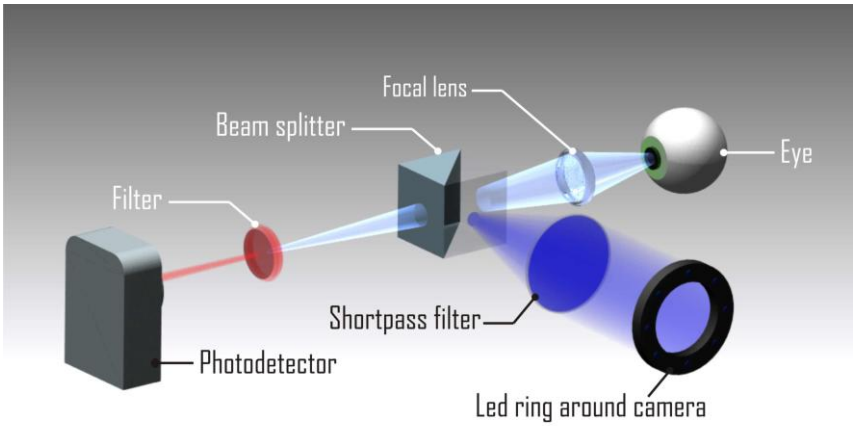

Fig. 6. Setup for detecting oxygen of the microrobot in a real scenario, and hence was placed at the end of the setup.

5.3. Results

5.3.1. Characterization of the films and nanospheres

The emission and excitation characteristics for the PS nanospheres containing PtOEP were very similar to the PS film containing PtOEP. The peak emission wavelength was found to be 645 nm. Excitation wavelengths between 300 nm to 400 nm produced high emission intensity. The excitation and emission characteristics of dip-coated microrobot are shown in **Fig. 7**). The oxygen sensitivity of spin-coated films on gold-coated Si substrate and nanospheres coated on a gold-coated Si substrate is shown in **Fig. 8** and **Fig. 9**, respectively. The lifetime of emission is measured as the oxygen concentration is varied from 0% to 10% with steps of 1%. The main difference in response was observed for the response time. To characterize the lifetime the nanospheres sample and two spin-coated film samples with thicknesses of 4 µm and 20 µm were analyzed applying cycles of 0% oxygen (100% nitrogen) and 100% oxygen (**Fig. 10**). All sensors showed faster response going towards 100% oxygen (falltime) than going towards 0% oxygen (risetime). The falltimes for the nanospeheres and 4 µm and 20 µm-thick films were found as 0.7, 1.9, and 2.5, respectively. The risetimes were found as 1, 1.5, and 11.5, respectively. The fast response of the nanospheres is most probably due to the increased surface area caused by the nanospheres.

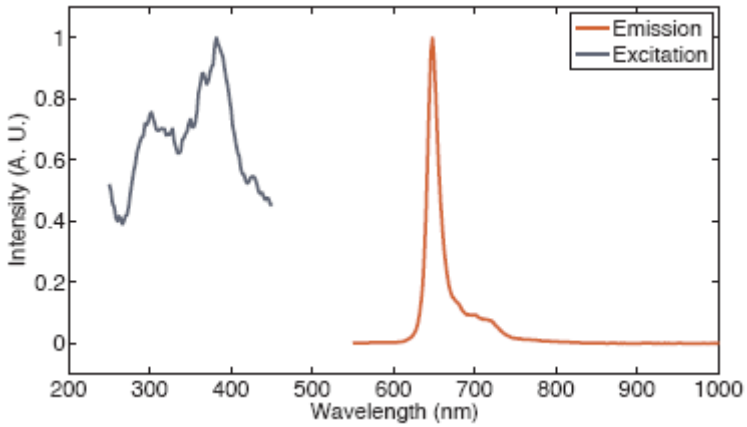

Fig. 7. The excitation and emission spectrum of the oxygen sensing film.

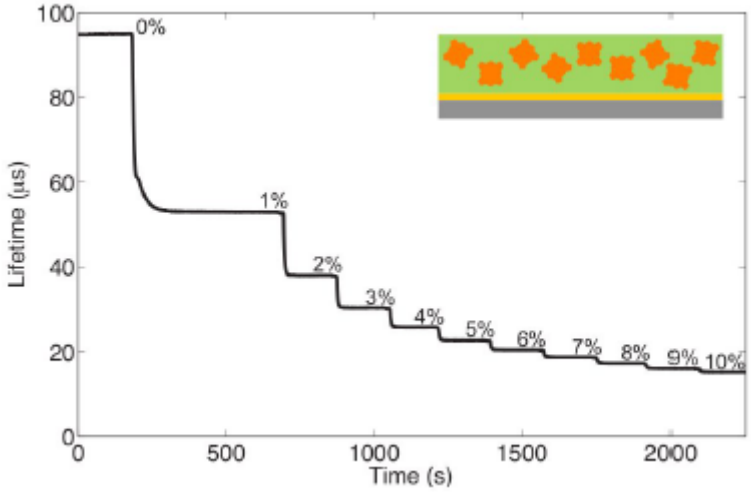

Fig. 8. The lifetime of emission is measured as the oxygen concentration is varied from 0% to 10% with steps of 1% for the 4 _m-thick spin-coated film on gold coated Si chip.

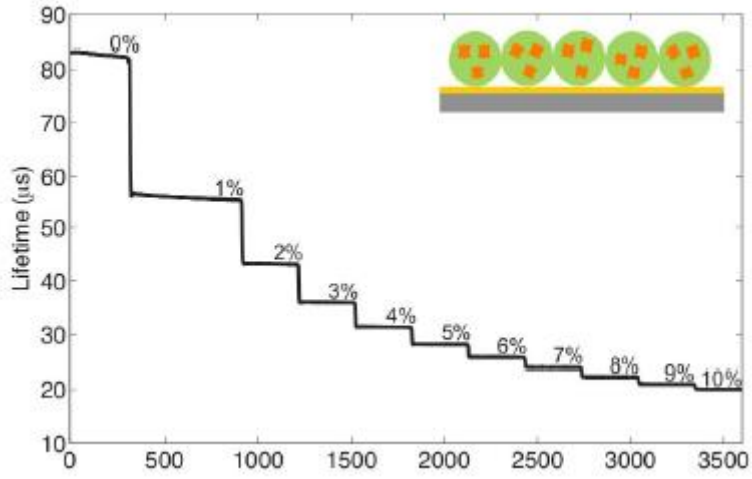

Fig. 9. The lifetime of emission is measured as the oxygen concentration is varied from 0% to 10% with steps of 1% for the 1.5 _m-thick nanospheres on gold coated Si chip.

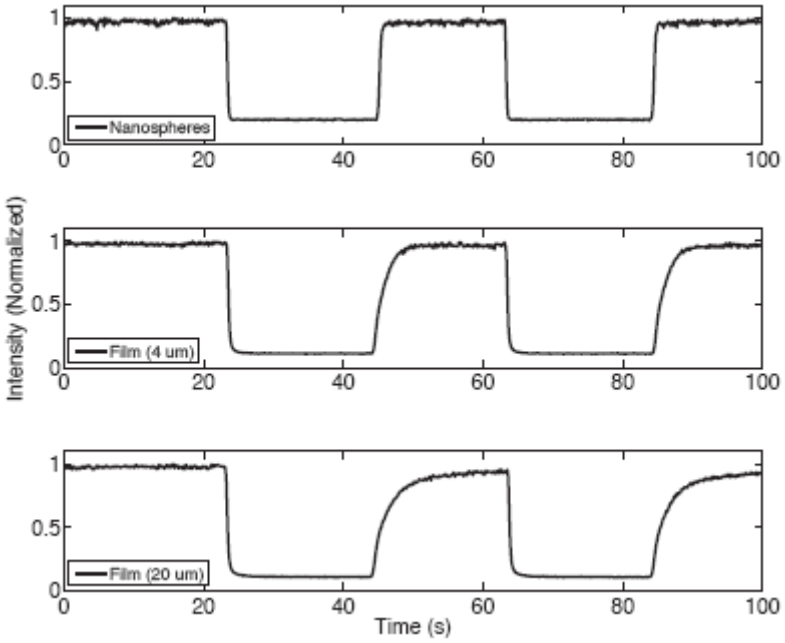

Fig. 10. Response time of the film sensor and the nanospheres sensor. The high intensity state is 100% nitrogen and the low intensity state is 100% oxygen flow.

5.3.2. Characterization of the microrobot sensor

First, the excitation and emission characteristics were obtained for the dip-coated microrobot sensor containing PtOEP (**Fig. 7**). Next, using the flow cell described, the oxygen sensitivity of the sensor was measured in gas and in water. **Fig. 11** shows the Stern-Volmer plot of the lifetime of emission of a coated microrobot in response to different ratios of oxygen to nitrogen under a constant flow of 500 ml/min. In **Fig. 12**, the Stern-Volmer plot of the lifetime of emission of the same microrobot is shown in water with a flow rate of 3.15 l/min at different dissolved oxygen concentrations observed by the commercial oxygen sensor. An unquenched emission lifetime of 100 µs was observed.

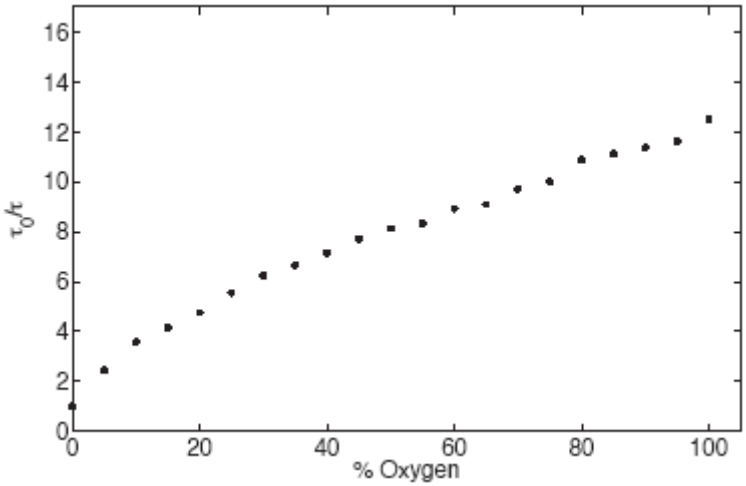

Fig. 11. The Stern-Volmer plot of the lifetime of emission of a coated microrobot in response to different ratios of oxygen to nitrogen. The total flow rate was 500 ml/min.

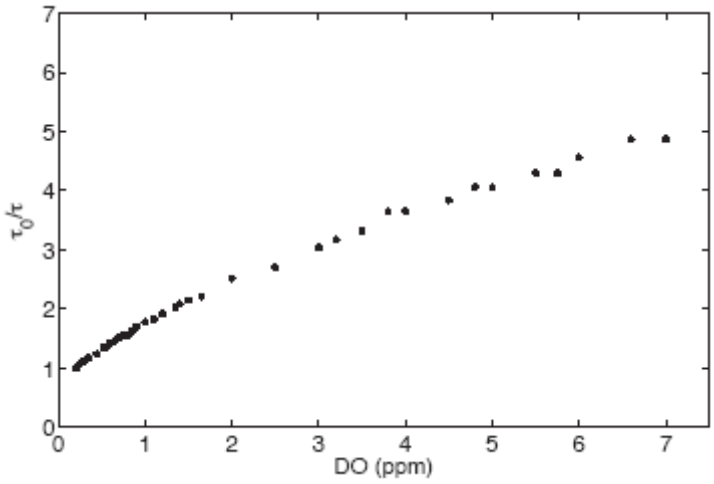

Fig. 12. The Stern-Volmer plot of the lifetime of emission of the coated microrobot at different dissolved oxygen concentrations in water. The oxygen concentration was obtained by the commercial oxygen sensor.

The reduction in either intensity or lifetime is described by the Stern-Volmer equation:

$$\frac{\tau_0}{\tau} = 1 + k_{SV}[O_2] \tag{2}$$

where τ is the luminescence lifetime, the subscript "*0*" refers to the value in the absence of quencher, k_{SV} is the Stern- Volmer constants and [O_2] is the partial pressure of oxygen. However, in many cases, there is a deviation from the linearity of the response due to the heterogeneity of the medium where the dyes are immobilized. This deviation is explained by the presence of different oxygen quenching sites within the

matrix, and therefore a multi-site model with each site having a linear behavior can be applied [15-17] The model proposed by Lehrer[18] was applied and a two-site model was found to be sufficient to describe the response of the sensor to the presence of oxygen, where only one of the two microenvironment is accessible to the quencher:

$$\frac{\tau_0}{\tau} = \left[\frac{f}{1 + k_{SV}[Q]} + (1 - f)\right]^{-1} \quad (3)$$

where f_0 denotes the fraction of the total luminophores population that the quencher is able to access, and k_{SV} is the Stern-Volmer quenching constant associated with the accessible fraction of luminophores. A Stern-Volmer constant k_{SV} of 41.89 bar^{-1} was found in gas and 31.50 bar^{-1} in water using Lehrer's model. From the results and the Stern- Volmer plot it can be observed that the site accessible to oxygen correspond to the lowest oxygen concentration, which confirms the suitability of this type of sensor to measure within the physical oxygen range of the eye.[19]

5.3.3. Measurements using Lock-in Amplifier

Lastly, the film coated microrobot sensor was used with the custom-built ophthalmologic setup. **Figure 13** shows the lifetime of emission of the microrobot in water with a flow rate of 3.15 l/min at different dissolved oxygen concentrations measured by the spectrometer. The same flow chamber was used with this setup. To mimic the optical properties of the eye, another lens was placed after the ophthalmoscopy lens in front of the flow chamber. Using the commercial sensor the oxygen concentration was observed and the phase change was acquired from the lock-in amplifier. **Fig. 14** shows the response of the sensor in the custom-built ophthalmic setup under different dissolved oxygen concentrations. There is a decrease in phase shift with the increasing oxygen concentration, indicating that DO concentration can be measured with the custom setup and the microrobot.

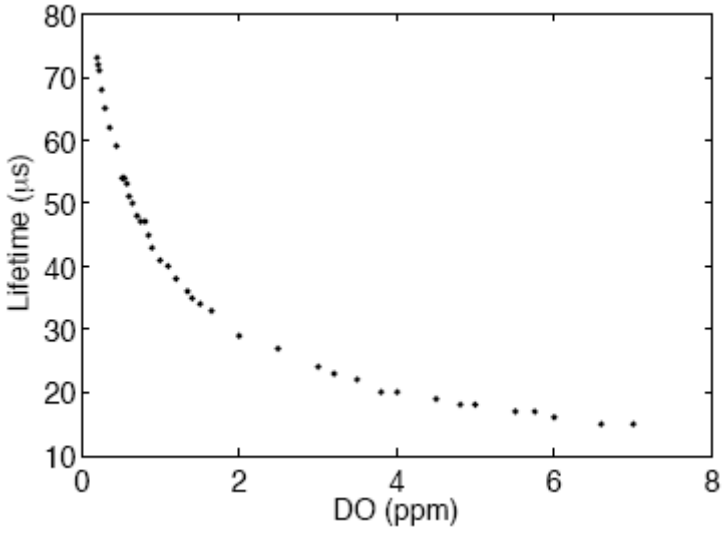

Fig. 13. The lifetime of emission of the coated microrobot at different dissolved oxygen concentrations in water. The oxygen concentration was obtained by the commercial oxygen sensor.

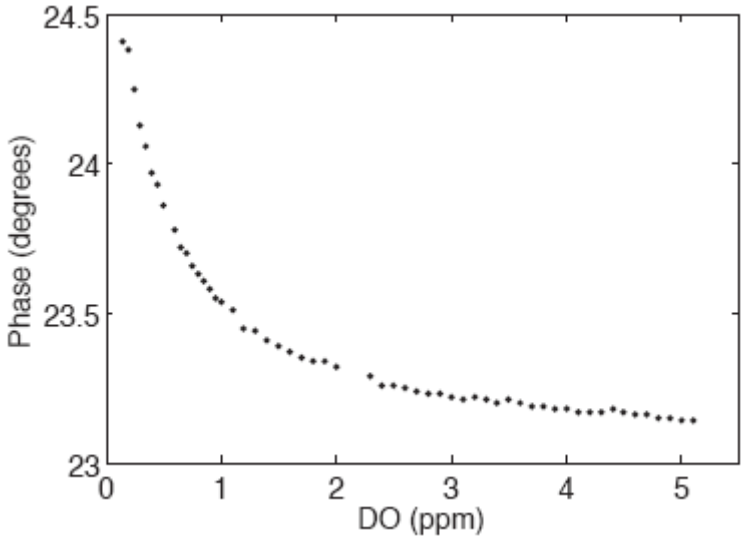

Fig. 13. The response of the microrobot sensor under different oxygen concentrations using the custom ophthalmic setup with the lock-in detection

5.4. Conclusions and future work

A wireless micro oxygen sensor was developed using a magnetic microrobot and PS film with PtOEP dye. A custom setup to excite and readout this sensor was designed and implemented. Oxygen sensing using this microrobot and setup was demonstrated. This sensor can be precisely controlled in the ocular cavity by applying magnetic fields as described in [14]. Minimally-invasive oxygen concentration measurements can be

performed using these systems. Future work will focus on using the readout system together with the control and tracking systems.

An alternative sensor coating using nanospheres of PSMA containing PtOEP was also demonstrated and improvements were obtained in response time due to the increased surface area. Microrobots were successfully coated with these nanospheres. In the future, oxygen sensitivity of the nanospheres will be explored and compared to the film sensors. The nanospheres will be further characterized (i.e., size distribution) and their effect on the sensor performance will be explored.

Acknowledgments. The authors gratefully acknowledge the contribution of Kartik Sivaraman and Prof. Sotiris Pratsinis from ETH Zurich and A.L. Medina-Castillo from University of Granada. This work is supported by the NCCR Co-Me of the Swiss National Science Foundation. The authors acknowledge the financial support of the Junta de Andaluc´ıa, Regional Government of Spain (Excellence Project FQM-02625 and Mar´ın-Su´arez del Toro's grant and financial support in Switzerland). Financial support from the Swiss National Science Foundation (Nr. 200020-126694) is kindly acknowledged.

Referencias

1. Harrison, D. J.; Mallouk Thomas, E., Chemically Sensitive Interfaces. In *Interfacial Design and Chemical Sensing*, American Chemical Society: 1994; Vol. 561, pp 1-14.
2. Wang, X.; Ozkan, C. S., Multisegment Nanowire Sensors for the Detection of DNA Molecules. *Nano Letters* **2008,** 8, (2), 398-404.
3. Turel, M.; Duerkop, A.; Yegorova, A.; Scripinets, Y.; Lobnik, A.; Samec, N., Detection of nanomolar concentrations of copper(II) with a Tb-quinoline-2-one probe using luminescence quenching or luminescence decay time. *Analytica Chimica Acta* **2009,** 644, (12), 53-60.
4. Sakaue, H.; Negi, A.; Honda, Y., Comparative study of vitreous oxygen tension in human and rabbit eyes. *Investigative Ophthalmology & Visual Science* **1989,** 30, (9), 1933-7.
5. Galloway, N.; Amoaku, W.; Galloway, P.; Browning, A., Common Diseases of the Conjunctiva and Cornea, Common Eye Diseases and their Management. In Springer London: 2006; pp 45-60.

6. Ergeneman, O.; Dogangil, G.; Kummer, M. P.; Abbott, J. J.; Nazeeruddin, M. K.; Nelson, B. J., A Magnetically Controlled Wireless Optical Oxygen Sensor for Intraocular Measurements. *Sensors Journal, IEEE* **2008,** 8, (1), 29-37.
7. Kummer, M. P.; Abbott, J. J.; Kratochvil, B. E.; Borer, R.; Sengul, A.; Nelson, B. J., OctoMag: An Electromagnetic System for 5-DOF Wireless Micromanipulation. *Robotics, IEEE Transactions on* **2010,** 26, (6), 1006-1017.
8. Bergeles, C.; Shamaei, K.; Abbott, J. J.; Nelson, B. J., Single-Camera Focus-Based Localization of Intraocular Devices. *Biomedical Engineering, IEEE Transactions on* **2010,** 57, (8), 2064-2074.
9. Wolfbeis, O. S., Materials for fluorescence-based optical chemical sensors. *Journal of Materials Chemistry* **2005,** 15, (27-28), 2657-2669.
10. Lakowicz, J. R., *Principles of Fluorescence Spectroscopy*. 2nd ed.; Kluwer Academic: New York, 1999.
11. Trettnak, W.; Kolle, C.; Reininger, F.; Dolezal, C.; O'Leary, P., Miniaturized luminescence lifetime-based oxygen sensor instrumentation utilizing a phase modulation technique. *Sensors and Actuators B: Chemical* **1996,** 36, (13), 506-512.
12. Borisov, S. M.; Mayr, T.; Mistlberger, G.; Waich, K.; Koren, K.; Chojnacki, P.; Klimant, I., Precipitation as a simple and versatile method for preparation of optical nanochemosensors. *Talanta* **2009,** 79, (5), 1322-1330.
13. Tian, S.; Wang, J.; Jonas, U.; Knoll, W., Inverse Opals of Polyaniline and Its Copolymers Prepared by Electrochemical Techniques. *Chemistry of Materials* **2005,** 17, (23), 5726-5730.
14. Kratochvil, B. E.; Kummer, M. P.; Abbott, J. J.; Borer, R.; Ergeneman, O.; Nelson, B. J. In *OctoMag: An electromagnetic system for 5-DOF wireless micromanipulation*, Robotics and Automation (ICRA), 2010 IEEE International Conference on, 3-7 May 2010, 2010; 2010; pp 1080-1081.
15. Fernández-Sánchez, J. F.; Roth, T.; Cannas, R.; Nazeeruddin, M. K.; Spichiger, S.; Graetzel, M.; Spichiger-Keller, U. E., Novel oxygen sensitive complexes for optical oxygen sensing. *Talanta* **2007,** 71, (1), 242-250.
16. Marin-Suarezdel Toro, M.; Fernandez-Sanchez, J. F.; Baranoff, E.; Nazeeruddin, M. K.; Graetzel, M.; Fernandez-Gutierrez, A., Novel luminescent Ir(III) dyes for developing highly sensitive oxygen sensing films. *Talanta* **2010,** 82, (2), 620-626.
17. Medina-Castillo, A. L.; Fernandez-Sanchez, J. F.; Klein, C.; Nazeeruddin, M. K.; Segura-Carretero, A.; Fernandez-Gutierrez, A.; Graetzel, M.; Spichiger-Keller, U. E., Engineering

of efficient phosphorescent iridium cationic complex for developing oxygen-sensitive polymeric and nanostructured films. *Analyst* **2007,** 132, (9), 929-936.

18. Lehrer, S., Solute perturbation of protein fluorescence. quenching of the tryptophyl fluorescence of model compounds and of lysozyme by iodide ion. *Biochemistry* **1971,** 10, (17), 3254-3263.

19. Abdallah, W.; Ameri, H.; Barron, E.; Chader, G. J.; Greenbaum, E.; Hinton, D. R.; Humayun, M. S., Vitreal Oxygenation in Retinal Ischemia Reperfusion. *Investigative Ophthalmology & Visual Science* **2011,** 52, (2), 1035-1042.

Capítulo 6

Electrophoretic deposition of nanoparticles for the fabrication of optical oxygen sensing materials

M. Marín-Suárez[a], S. Medina-Rodríguez[a], O. Ergeneman[b], S. Pané[b], J.F. Fernández-Sánchez[a], B. J. Nelson[b], A. Fernández-Gutiérrez[a]

[a]*Department of Analytical Chemistry, Faculty of Sciences, University of Granada, Avda. Fuentenueva s/n, E-18071 Granada, Spain*

[b]*Institute of Robotics and Intelligent Systems, ETH Zurich, Tannenstrasse 3, CH-8092, Zurich, Switzerland*

Abstract

Optical oxygen-sensitive layers have been developed by electrophoretic deposition (EPD). This deposition method allows controlling the thickness of the sensing layer and deposition to non-planar surfaces. The layers consist of poly(styrene-co-maleic anhydride) nanoparticles in which the oxygen sensitive dye Pt(II) meso-Tetra(pentafluorophenyl)porphine (PtTFPP) is entrapped. By investigation of the particle suspension, potentials and deposition times to perform EPD were optimized. The amount of nanoparticles deposited increases with both potential and time. The oxygen sensing properties of the deposits were investigated both in gas and solution, using a phase-resolved frequency-domain lifetime measurement technique. The deposits showed a k_{sv1} between 45 and 52 bar^{-1} for gas and response times of 8 seconds when changing from N_2 to O_2, and 4 seconds from O_2 to N_2. In addition, a linear k_{sv} of 0.94 bar^{-1} was found in aqueous phase, and no leaching of the nanoparticles from the surface was observed after 10 hours of continuous water flow.

Keywords: EPD; nanoparticles; oxygen; optical sensor; films; luminescence; *E-mail: mmarinst@ugr.es (M. Marín-Suárez), oergeneman@ethz.ch (Olgaç Ergeneman).*

6.1. Introduction

Molecular oxygen is one of the most important gases in our environment since it is present in a variety of reactions with industrial, medical, and biological applications.[1-5] The role of oxygen in cellular metabolism makes its supply essential for cell viability. Several pathologies such as inflammation, cancer, or diabetes can affect the oxygenation of the human tissue.[6] Like other parts of the body, the eye needs sufficient supply of oxygen to perform its primary function. The presence of hypoxia in ocular tissue is related with many common diseases, such as diabetic retinopathy, glaucoma, retinopathy, age-related macular degeneration, and retinal vein occlusions.[5, 7-9] The use of untethered microrobots have shown high potential in biomedical applications,[10, 11] including minimally invasive detection of oxygen inside the eye.[12, 13]

Different approaches can be utilized for detection of oxygen. Oxygen sensing by quenching of luminescence offers several advantages compared to electrochemical methods. [14-18] Some of them include measurements with no oxygen consumption, inertness to magnetic fields, and wireless signal transduction[14, 19], which are of great importance for biomedical applications. These sensing phases are based on a luminescent oxygen indicator embedded in a matrix, which ideally should be transparent, permeable to oxygen, and withstand mechanical stress while providing photostability.[19-21] Several oxygen probes and matrices have been reported[17-22], but polymeric matrices have demonstrated good properties in terms of solubility of the dye and selective permeability to oxygen.[19] In addition, the ease of polymeric materials to acquire different shapes and be deposited in solid supports have been exploited for the development of optical sensing films by different coating techniques such as spin-coating, electro-spinning, dip-coating, knife-coating, etc.[17, 23, 24] These methodologies allow a precise control on the thickness of the sensing layer, but either a planar surface is required in order to deposit the sensing layer, or they are difficult to adapt to micrometric scale.

The integration of polymeric films to biomedical devices, with nano and micrometer dimensions and complex shapes seems to be a crucial factor for the development of microelectromechanical systems (MEMS), nanoelectromechanical systems (NEMS), biosensors, etc. [25] Nanomaterials based on the assembly of nanometer-sized particles can overcome these limitations. The ability of nanotechnology for the development of

efficient and flexible methods to create functional assembled structures for a variety of applications has taken considerable interest in recent years.[26] These techniques are usually compatible with nanometer dimensions and complex shapes, [25-28] but not all of them provide uniform thicknesses in large domains.[26, 28-32] In this aspect, electrophoretic deposition (EPD) has demonstrated good control over the features of surface, while being easily adaptable to micrometer-sized complex devices. [33-35]

EPD is a coating technique in which charged nanoparticles suspended in a liquid move and deposit on a conductive substrate of opposite charge by the application of an external electric field.[36] Consequently, deposition can be carried out over different shaped substrates, with slight changes in the electrophoretic cell design, and the thickness of the deposited film can be controlled by simple adjusting the deposition time and applied potential.

Bearing in mind the advantages of both polymeric materials and EPD, we propose a method to develop optical sensing layers based on electrophoretic deposition of oxygen-sensitive polymeric nanoparticles. EPD has been successfully applied for a variety of materials, [33-35] including different types of nanoparticles and composites. Although some polymers and composites have been deposited via EPD for optical sensing applications,[37-40] this is the first time that EPD is performed over a suspension of doped-polymeric nanoparticles in order to develop an optical oxygen-sensitive matrix.

Polymeric nanoparticles with an oxygen indicator can be produced by several methods, such as covalent attachment to the polymer, swelling or physical entrapment of the dye. [41-44] Solvent displacement method[43] allows to easily produce nanoparticles with a good control over the properties of the particles, and therefore was selected to produced oxygen sensitive nanoparticles using poly(styrene-co-maleic anhydride) as the supporting polymer. The role of the maleic anhydride is important because when it reacts with water, the produced carboxyl groups form highly stable dispersions of nanoparticles while provide negative charges to the surface in order to perform anodic EPD. In addition, the presence of carboxyl groups may be interesting to further modify the films with enzymes or antibodies for the development of biosensing phases.[44]

In this work the characteristics of the deposition formed via EPD are analyzed according to two groups of parameters: one regarding to the suspension of

nanoparticles and other related to the process itself. [36] Therefore, the first step was focused in the properties of the suspension, where stability and particle's size can be easily tunable by varying different synthesis parameters. Secondly, different potentials and deposition times were applied in order to ensure the immobilization of nanoparticles via EPD. The evaluation of the deposits of nanoparticles was done according to the oxygen sensing properties both in gaseous and aqueous phase. The morphology, stability and response time of the sensing phases were also analyzed.

6.2. Experimental

6.2.1. Reagents

Poly(styrene-co-maleic anhydride) polymer (PSMA, 7% maleic anhydride, Mw =224000 g mol-1), tetrahydrofuran (THF), sodium hydroxide (NaOH) and hydrochloric acid (HCl, 37%) were purchased from Sigma Aldrich. Oxygen indicator Pt(II) meso-Tetra(pentafluorophenyl)porphine (PtTFPP) was purchased from Frontier Scientific.

6.2.2. *Preparation of the nanoparticles*

0.1% w/v of PSMA was dissolved in THF with 1.5% w/w respect to the polymer of the oxygen indicator PtTFPP. The cocktail was subsequently dropped over deionized water under agitation. The mixture was exposed to blowing air for 20 minutes and THF was evaporated. The resulting polymeric particles with the embedded dye formed stable dispersions. Solutions of 1 mM of NaOH and 1 mM of HCl were used to adjust the pH of the dispersion of particles.

6.2.3. Characterization of the nanoparticles

Particle mean diameter (*d*, in nm), size distribution (*PdI*), zeta potential (ζ, in mV) and conductivity (*C*, in mS cm^{-1}) of the suspension were measured with a Zetananosizer (Malvern Instrument, model Zetasizer Nano ZS, www.malvern.com), which is equipped with a laser and a dynamic light scattering (DLS) detector.

6.2.4. Electrophoretic cell

A home-made electrophoretic cell was built by placing an acrylglass box (polymethylmethacrylate) on a Titanium platinized plate sheet (purchased from www.ti-shop.com) that acts as the cathode. The suspension of nanoparticles can be

therefore placed inside the box, and a 1 cm^2 gold coated silicon chip can be inserted opposite to the Pt plate, keeping a distance of 5 mm. A schematic drawing is presented in **Fig. 1**

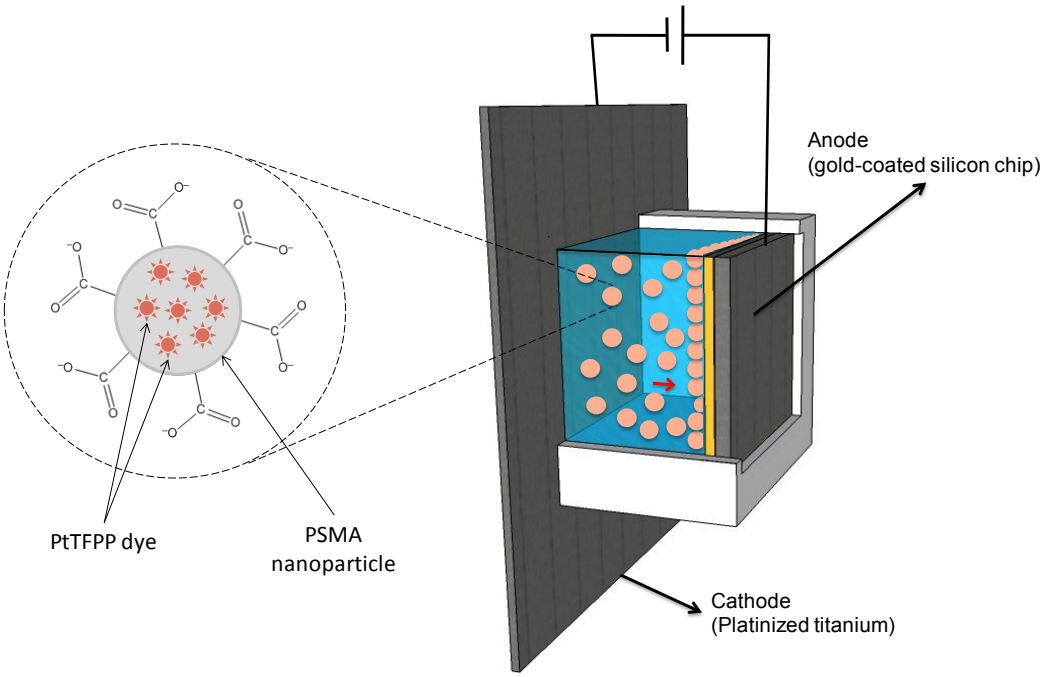

Figure 1. Schematic drawing of the electrophoretic cell and EPD process performed in order to develop oxygen sensitive layers over a gold coated chip. A single nanoparticle is reprenseted with the dye PtTFPP entrapped on the PSMA core and carboxylic acids on its surface.

The Pt cathode and the gold chip anode were connected to a programmable DC power supply (Promax Electronics, model FA-665, MA, USA) in order to perform EPD.

6.2.5. Measurement principle

Luminescence sensing can be performed in different ways: recording either intensity or lifetime at different oxygen concentrations.[14] Recording intensity of luminescence[14, 17] is relatively simple and accurate in the laboratory but highly dependent on the extrinsic conditions and suffers from photobleaching or leaching of the dye. [45] These problems can be minimized by measuring the lifetime (τ, in µs) of the oxygen sensitive layers for different oxygen concentrations.[46] The lifetime of emission can be measured either in the time domain or in the frequency domain.[14] Time-domain measurements are ideally suited to eliminate background luminescence and scattering,[47] but they usually require more sophisticated instrumentation than frequency-domain sensing.[48]

In this work, a phase-resolved method (in the frequency-domain) was selected to determine the oxygen sensitivity of the layers. The sensing layer was excited with a sinusoidally modulated light that consequently causes a modulated emission at the identical frequency. Because of the lifetime of the indicator dye, this emission exhibits a time delay (i.e. phase shift) respect to the excitation signal. Both the phase shift (Φ, in radians) or the magnitude (R, in mV) of the modulated emission signal with respect to the excitation signal (taken as a reference), can be measured using a commercial dual-phase lock-in amplifier, and used to calculate the lifetime. [14, 49]

In this case, the Φ measurements at different oxygen concentration were used to calculate the lifetime and characterize the oxygen sensitivity of the materials, while the R measurements (proportional to the emission intensity) of the modulated emission signal were employed to extract information about the amount of particles deposited and their *adhesion strength* to the gold surface.

The selection of the optimal modulation frequency for this kind of measurements should be made carefully as a compromise between increased SNR (signal to noise ratio) and a reduced phase sensitivity for low modulation frequencies.[14, 50, 51] In this work an optimal modulation frequency at 5145 Hz was experimentally found for our sensing layers considering the lower frequency that maximized the phase differences between 0 % and 30 % of oxygen [52]

6.2.6. Measurement setup

An optical fiber measurement system was designed to characterize the sensitivity to oxygen of the sensing layers using the phase-resolved method described above.[53] An ultraviolet LED (Ocean optics, model LS-450 LED-395, λ_{peak}=395 nm, angle of illumination 15º, LED diameter 5 mm, luminous power 25 µW coupled into a 600 µm optical fiber core) was used as the excitation light source. A sinusoidal signal extracted from the internal signal generator of a dual-phase lock-in amplifier (Stanford Research System, model SR830) at a fixed frequency of 5145 Hz was used to modulate the current of the LED light source. An optical bandpass filter (Thorlabs GmbH, model MF390-18, $\lambda_{central}$=390 nm, BW=18 nm) was placed after the UV LED to prevent interferences and the light was directly coupled into a bifurcated fiber optic bundle (Avantes Inc., model FCR-7xx200-2, wavelength range 200-800 nm (UV-VIS), 12 light-fibers, 1 read fiber 200 µm core, N.A. 0.22). One of the branches of the fiber optic

bundle conducted the excitation light to the sensing phase, while the other was used to guide the phase-shifted luminescent emission from the sensing phase to the detector (a photomultiplier tube (PMT) Hamamatsu Photonics Japan, model H10723-20, transimpedance 100 kΩ, BW DC-1 MHz). The emission light was previously filtered with an optical bandpass filter (Hamamatsu Photonics Japan, model A10033-03, $\lambda_{central}$=630 nm, BW=60 nm) placed before the PMT, in order to separate the reflected excitation light from the emission. The voltage signal provided by the PMT was amplified using a commercial low-noise programmable voltage preamplifier (Stanford Research Systems, model SIM911 BJT), which presented 1.8 $nV/\sqrt{Hz}$ input noise, low output noise, 1 MHz bandwidth and selectable gain from 1 to 100. Finally, the aforementioned dual-phase lock-in amplifier was also used to measure the phase shift between the reference signal and the emission signal emitted by the sensing phase as well as the magnitude of the emission signal from the sensing phase.

The additional phase shift introduced by the electronic components[51] (PMT, LED driver, amplifier, etc.) was evaluated using a reference LED (LED Supply, model L2-0-R5TH50-1, λ_{peak}=660 nm, angle of illumination 50º, LED diameter 5 mm, luminous intensity 2000 mcd typ. @ 20mA).

For the gas characterization, the sensing phases was placed inside a home-made flow-through cell and different mixtures of nitrogen and oxygen gas (supplied by 50 L gas bottles at 200 bars with nitrogen 60 and oxygen 55, Air Liquide) were passed through the cell. The flow cell was made of black polytetrafluoroethylene to prevent stray reflections and to assure the chemical inertness. Both the flow cell and the photodetector were housed in a dark room (Thorlabs GmbH, model XE25C1) to prevent interference from stray light and temperature was monitored during all the experiments. For gas mixing, two mass-flow controllers (MFCs) (Bronkhorst High-Tech, model EL-FLOW Select F-201CV) were used. After the MFCs, copper and stainless steel tubing was used to connect the MFCs with the flow-through cell. The system was fully controlled from a PC using a self-made program written in Matlab 7.10 and LabView 8.5.

For the characterization of dissolved oxygen, the same cell was filled with water at a constant flow rate of 1 ml min^{-1} using a peristaltic pump (Gilson Inc., model Minipuls 3). The dissolved oxygen present in the water was adjusted by blowing different ratios

of oxygen and nitrogen with the aforementioned gas setup. A commercial Clark electrode (Eutech Instruments, model CyberScan PCD-650) was used to monitor the oxygen concentration in the aqueous phase.

6. 3. Results and discussion

6. 3.1. Suspension of O_2-sensing nanoparticles

The proposed system for the production of nanoparticles is based on the dye PtTFPP immobilized in the polymer poly(styrene-co-maleic anhydride) (PSMA). PtTFPP is one the most widely used dyes for the preparation of the optical oxygen-sensing films due to its good photostability,[54] long lifetime of emission, wide excitation range, and large Stokes shift which allows to simplify the measurement system.[48, 55] THF was used as the organic solvent to produce the nanoparticles due to its good properties to dissolve both the dye and the polymer as well as its ease of removal from water.

For the investigation of the properties of the suspension, parameters such as size and size distribution of the particles, zeta potential, and conductivity were considered.

Several volumes of THF cocktail containing 0.1% w/v of polymer and 1.5% w/w of sensitive dye were dropped over 8 mL of water in order to find out its influence over size and polydispersity of the nanoparticles.[43] The concentration of the dye was kept at 1.5% w/w respect to the polymer in order not to exceed the solubility of the dye in the polymer, which produces aggregation and self-quenching.[16]

Figure 2a) shows size (*d*) and size distribution (*PdI*) obtained for different ratios of cocktail/water (*o/w* ratios), showing an increase in particle size when the volume dropped (and thus, amount of polymer) increased. However, polydispersity of the particles is hardly influenced by the *o/w* due to the low initial polymer concentration in the cocktail (0.1% w/v). To confirm this, 2 mL and 1 mL of cocktail containing an initial loading of 0.25% and 0.5% w/v of polymer respectively (same total weight of polymer) were dropped on water showing an increase in both *d* and *PdI* up to 238.7 nm and 0.18 respectively, for 0.5% w/v of initial polymer concentration. With the higher percentage of polymer, aggregates appeared during the synthesis even for low volume. Therefore, concentration of polymer used in the particle's synthesis was kept at the minimum in order to ensure a good size distribution of the particles, which tend to form more ordered packed area than those with a wider size distribution.[36]

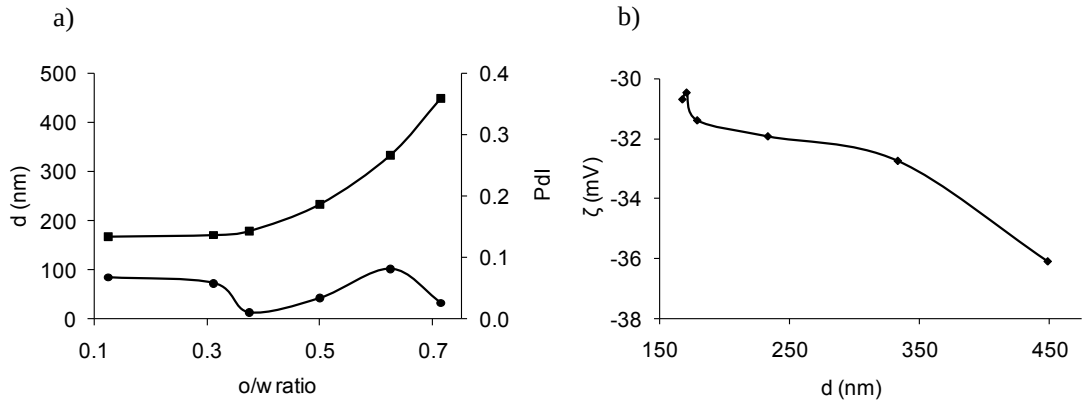

Figure 2 a) (■) Size (*d*, nm), and (●) size distribution (*PdI*) of the PSMA nanoparticles obtained by precipitation-evaporation method with different *o/w* ratios and initial polymer loading of 0.1% w/v. b) Influence of the particle size over the zeta potential.

In the same way, the zeta potential of the particles produced with 0.1% w/v was investigated. A high zeta potential (ζ in mV), in absolute value, is desirable as it improves the mobility while avoiding sedimentation of the particles during EPD.[36] Since ζ is dependent on the surface charge of the particles, particles with higher diameter are expected to possess a more negative zeta potential (see Fig 2b). Nevertheless, all the sizes present an absolute potential higher than 30 mV, which is considered inside the range of stability for EPD.[56] The final *o/w* ratio selected for the synthesis of nanoparticles was 0.6, which leads to particles of about 280 nm, *PdI* of 0.06 and a ζ of -33.0 mV.

Apart from size, pH has a stronger influence over zeta potential and its adjustment usually improves the stability of nanoparticles.[56] **Table 1** shows the zeta potential and conductivity (*C*) of the suspension of nanoparticles (*o/w*=0.6) when changing the pH. ζ of the suspension is improved from -33 to -39 mV when a base is added. Since the particles are negatively charged, the addition of acid neutralize the negative charge, while adding base increases the zeta potential in absolute value, thus increasing the stability. This change in ζ is also accompanied with an increase in the conductivity of the media. This parameter is also important since high conductivity may lead to larger agglomerate during deposition, influencing the homogeneity of the EPD.[36]

Table 1. Influence of pH over the zeta potential, and conductivity of the suspension of nanoparticles produced with an o/w ratio of 0.6.

pH	ζ (mV)	C (mS cm^{-1})
2.0	-1.87	10.7
6.5	-33.0	0.125
11	-39.1	16.0
6.5 (diluted 1:4)	-33.5	0.028

6.3.2. Electrophoretic deposition

To deposit the nanoparticles electrophoretically, a gold coated chip, which is often used in biomedical devices due its biocompatibility, is used as the conductive substrate. Potential and deposition time were screened in order to find out the appropriate range of working conditions for the stable suspension shown in Table 1.

For the nanoparticles stabilized with a base (ζ=-39.1 mV), the increase of conductivity (C=16.0 mS cm^{-1} compared to 0.125 mS cm^{-1} for the base-free suspension) lead to the darkening of the polymer when deposition was carried out, even at low potential and deposition times. In addition, a high formation of bubbles within a non-homogenous deposition was observed for the base-free solution (ζ=-33.0 mV, C=0.125 mS cm^{-1}) which suggest that a high current transport still exists.

In order to decrease the amount of particles per volume and current transport without decreasing the size and/or the ζ of the final nanoparticles, the base-free solution was diluted 1:4. With these conditions (ζ=-33.5 mV, C=0.028 mS cm^{-1}) it was found that for potentials higher than 40 V cm^{-1} or times higher than 10 min, the electrophoretic deposition of the nanoparticles led to the darkening of the deposit, probably because of Joule heating of the polymer and the electrochemical attack of the deposit.[36] Below 10 V cm^{-1} or times shorter than 1 min no homogenous deposition over the whole surface was found. Therefore, the influence of applied potential between 10 V cm^{-1} and 40V cm^{-1} and deposition time between 1 min and 10 min was studied to investigate the oxygen sensing properties of the films.

The morphology of the deposits was investigated using scanning electron microscopy (SEM). **Fig. 3** shows the SEM photographs of the chips undergoing 40 V cm^{-1} and 10 V cm^{-1}. For the chips undergoing 40 V cm^{-1}, it can be noticed that the amount of particles increases when time increases (Fig. 3 d), e) and f)). Similar trends were found for 30 V

cm^{-1} and 20 V cm^{-1} (see Electronic Supporting Information, ESI). For the chips undergoing 10 V cm^{-1} the amount of particles is hardly influenced when time is increased compared to the rest of potentials (see Fig. 3 a), b) and c)). In addition, heterogenic areas were found in the chip undergoing 40 V cm^{-1} and 10 minutes (see ESI for more SEM images).

Fig. 3 and ESI also confirm that the nanoparticles produced by the precipitation-evaporation are spherical and their *d* and *PdI* is in agreement with the DLS measurements. In addition, it can be observed that the EPD produces a homogenous distribution of the particles over the surfaces.

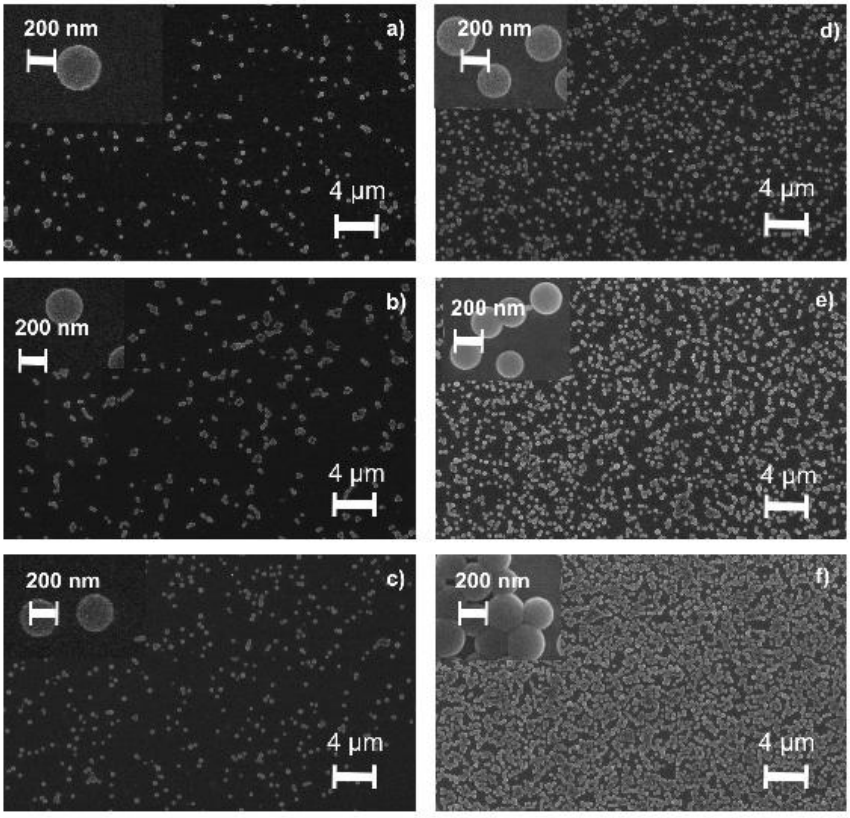

Figure 3. Scanning electron microscopy photographs for the chips undergoing a) 40V cm^{-1}- 1 min; b) 40V cm^{-1} - 5 min; c) 40V cm^{-1}- 10 min; d) 10 V cm^{-1}- 1 min; e) 10 V cm^{-1}- 1 min; f) 10 V cm^{-1}- 1 min.

Since the luminescence emission of the dye is proportional to the amount of particles, the magnitude of the *modulated emission signal* (*R*) can be used to evaluate the amount of particles deposited by EPD. **Fig. 4** shows the magnitude (*R*, in V) of the modulated emission signal registered for each chip in a nitrogen saturated atmosphere, which is proportional to the intensity emission. According to this, the amount of polymer

deposited is increased when increasing either the time or the applied potential. The deposition rate is similar for all potentials, except for 10 V cm^{-1}, where the increase in *R* with time is less pronounced. This result is in good agreement to the photographs shown in Fig. 4. As expected, the higher amount of deposited nanoparticles was obtained for 40 V cm^{-1} and 10 min.

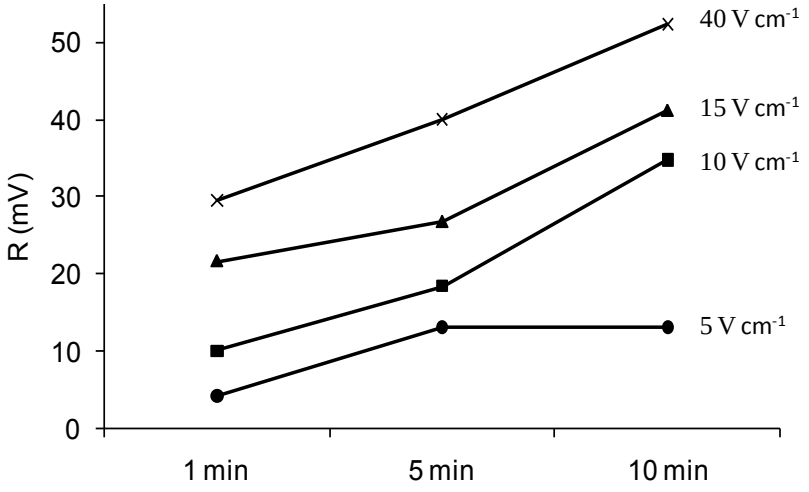

Figure 4. Magnitude (*R*, mV) of the emission collected at the different deposition times for an applied potential of 10 V cm^{-1} (●), 20 V cm^{-1} (■), 30 V cm^{-1} (▲) and 40 V cm^{-1} (**X**) in absence of oxygen.

6.3.3. Gas characterization

The oxygen sensing characterization was done by recording the phase shift at different oxygen concentrations using the phase-modulation method. Assuming that the luminescence decay is monoexponential, the relation between the phase shift Φ (in radians) and the emission lifetime τ (in seconds) is given by the expression (1), where f is the modulation frequency (in Hz).[14, 53]

$$\tau = \frac{tan\phi}{2\pi f} \quad (1)$$

Therefore, the oxygen sensing properties were evaluated by the reduction in the lifetime of emission when different quencher (oxygen) concentrations are present. This reduction in lifetime is described by the Stern-Volmer equation[14] (see Equation (2)).

$$\frac{\tau_0}{\tau} = 1 + k_{SV} pO_2 \quad (2)$$

where τ is the luminescence lifetime, the subscript "*0*" refers to the value in the absence of quencher, k_{SV} is the Stern-Volmer constants and pO_2 is the partial pressure of oxygen.

However, in polymeric films it is usual to find some deviation from the linearity of the response due to the heterogeneity of the matrix where the dye is dispersed.[16-18] In this case, the response can be explained with a multi-site model, in which different types of oxygen quenching sites are present in the matrix. The most simple one is the two-site model (with each site having a linear behavior), proposed by Demas and co-workers, the so called Demas' model[57] (see Equation (3))

$$\frac{\tau_0}{\tau} = \left[\frac{f_1}{1 + k_{SV1}\, pO_2} + \frac{f_2}{1 + k_{SV2}\, pO_2}\right]^{-1} \quad (3)$$

where f_i denotes the fractional contribution of the total luminescence emission from the luminophore located at site type i under unquenched conditions, which exhibit a discrete Stern-Volmer quenching constant given by k_{SVi}.

The value of the Stern-Volmer constant for each sensing film was determined, and it was used as a parameter to evaluate the oxygen sensitive properties of the films. Prior to this characterization, the influence of the applied potential during the EPD (which may cause changes on the indicator molecule and its properties towards oxygen) was also investigated. To rule out this issue, the particles that had remained in the EPD cell after electrophoresis were compared to original particles in terms of oxygen sensitivity. For this comparison, 50 µL of each solution of nanoparticles was simply dropped on a gold chip and dried under vacuum. The oxygen sensitivity was evaluated showing no change in the quenching ability of the dye when the suspension of nanoparticles underwent an applied potential.

Table 2 shows the response to oxygen of the gold chips covered with the sensing nanoparticles, which is practically the same for all the range of selected potentials and times. This response for all the chips, except C12, can be explained by the two sites model proposed by Demas (Eq. 3), where there is a first fraction of sites (f_1) possessing a high k_{sv1}, and a second fraction of sites (f_2), whose contribution is very small compared to f_1, which present less sensitivity. However, in chip C12 this second site is not sensitive to oxygen ($k_{sv2} = 0$). This behavior can be explained if a higher amount of

particles are deposited or because of the heterogeneity (see ESI), which avoids the penetration of the oxygen into some regions of the film.

Table 2. Oxygen sensitivity according to Demas' Model for the films obtained by EPD at different potentials and deposition times.

Chip No.	Potential	Time of deposition	Demas' Model[a]			
			f_1	k_{sv1} (bar^{-1})	f_2	k_{sv2} (bar^{-1})
C1	10 V cm^{-1}	1 min	0.82 ± 0.00	45.53 ± 0.52	0.19 ± 0.00	2.03 ± 0.21
C2		5 min	0.82 ± 0.00	46.37 ± 0.55	0.19 ± 0.00	2.12 ± 0.13
C3		10 min	0.82 ± 0.00	46.28 ± 1.17	0.19 ± 0.01	1.96 ± 0.36
C4	20 V cm^{-1}	1 min	0.82 ± 0.00	51.68 ± 2.38	0.19 ± 0.00	2.09 ± 0.22
C5		5 min	0.83 ± 0.00	48.06 ± 0.42	0.18 ± 0.00	2.11± 0.28
C6		10 min	0.82 ± 0.01	49.53 ± 5.38	0.19 ± 0.01	2.17 ± 0.06
C7	30 V cm^{-1}	1 min	0.82 ± 0.00	50.51 ± 0.31	0.18 ± 0.00	2.17 ± 0.07
C8		5 min	0.81 ± 0.00	50.66 ± 4.01	0.20 ± 0.01	1.93 ± 0.06
C9		10 min	0.80 ± 0.01	51.70 ± 2.75	0.22 ± 0.01	1.79 ± 0.26
C10	40 V cm^{-1}	1 min	0.82 ± 0.02	48.72 ± 7.06	0.18 ± 0.03	1.67 ± 0.09
C11		5 min	0.82 ± 0.01	47.32 ± 2.05	0.19 ± 0.02	1.56 ± 0.05
C12		10 min	0.86 ± 0.02	37.11 ± 1.75	0.12 ± 0.03	0.00 ± 0.00

[a] The experimental results have been expressed as the average of 3 replicas $\pm\ s \cdot t / \sqrt{n}$ (n=3, t=4.30 (2P = 0.05));

Since the physico-chemical quenching reaction is a reversible process, the complete reversibility of the luminescence emission of the films allows continuously monitoring increasing and decreasing amounts of O_2. **Fig. 5** shows the response time and operational stability for chip C10, which was conducted by measuring the phase shift during alternated nitrogen and oxygen saturated atmospheres. The time duration to achieve the response is an important feature in all chemical sensors, and a fast response is a critical factor for medical monitoring, among others. The response time (t_{95}) of optical sensors is defined as the time at which the signal reaches the 95% of the total response when the sensor is exposed to an alternating atmosphere of oxygen and nitrogen. The t_{95} for the novel sensing films showed shorter times than those reported in literature,[54, 58] with 8 seconds when changing from 0% O_2 to 100% O_2, and lower than 4 s when changing from 100% O_2 to 0% O_2.

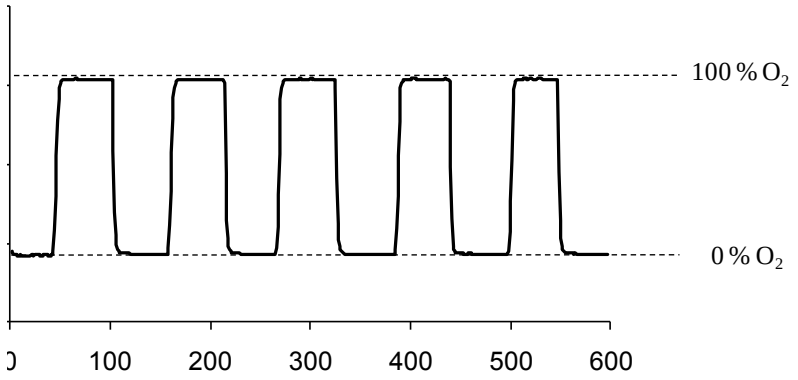

Figure 5. Response time and stability of chip C10 when changing from nitrogen to oxygen consecutively.

6.3.4. Dissolved oxygen measurements

The sensitivity to oxygen in aqueous phase was also analyzed since O_2 tension in biological fluids requires the sensing phase contacting an aqueous environment. In the sensing layers developed by EPD, the response to oxygen followed a linear behavior between 0 and 30% of oxygen bubbled into the water (a commercial Clark electrode was used to monitor the actual oxygen concentration in the water, which ranged from 0 and 11.28 ppm). **Fig. 6** shows Stern-Volmer plot which shows a k_{sv} of 0.94 bar^{-1} according to Eq. (2) .

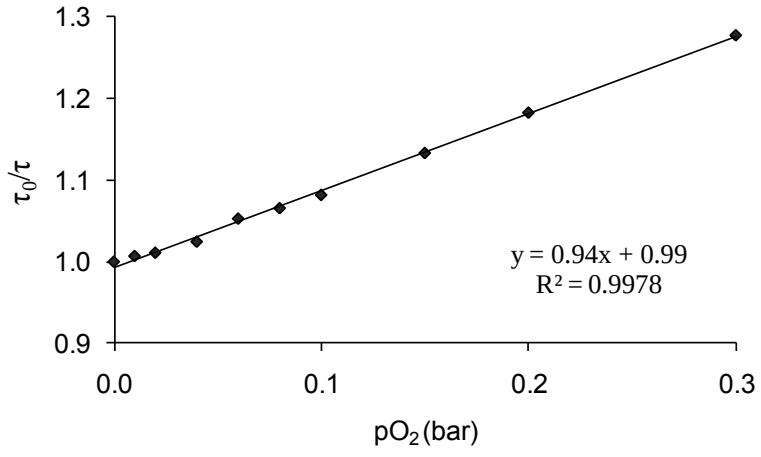

Figure 6. Stern-Volmer plot using chip C9 for different oxygen partial pressures bubbled in water.

Furthermore, in order to evaluate the attachment of the nanoparticles over the gold surface, the chips underwent a continuous water flow of 1mL min^{-1} for10 hours. The O_2 concentration in the water flow was changed from 10% to 30% O_2 consecutively, and *R*

value of the modulated emission signal was recorded during 100 seconds every 60 minutes. If the sensing nanoparticles leach out of the chip, the intensity emission (i.e. R value of the emission signal) will decrease for any of the oxygen concentration. **Fig. 7** shows the average value of the measurements at each oxygen concentration for chip C8 with its error (calculated using *Student's t* test with n=100 and a=0.025). The same level of R with a small error is reached for each concentration, confirming that the measurement is stable and there is no removal of the nanoparticles from the gold surface.

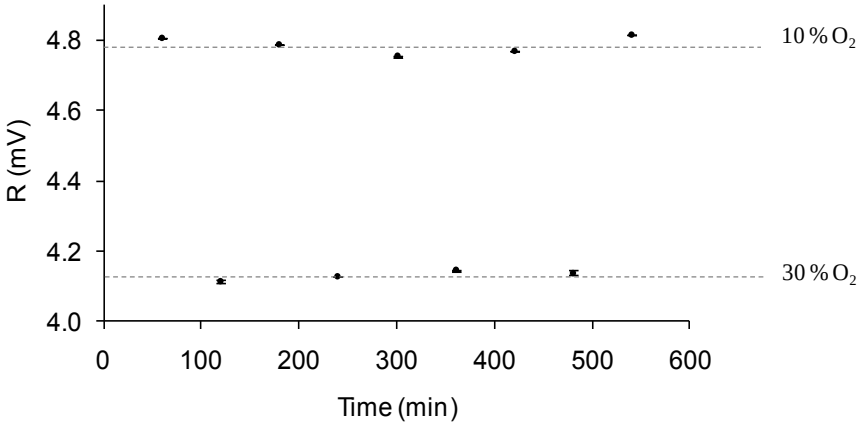

Figure 7. Magnitude of the emission signal (R, in mV) of chip C8 when undergoing a continuous flow rate of 1 ml min^{-1}, switching from 10% to 30% of oxygen every 60 minutes. Measurement at each concentration: 100 seconds taking 1 measurement per second.

6.4. Conclusions

Optical oxygen sensitive films have been developed by electrophoretic deposition of polymeric nanoparticles. The resulting films possess good oxygen sensitivity and their thickness can be tuned by changing deposition time or applied potential.

The films are based on poly(styrene-co-maleic anhydride) nanoparticles which have been synthesized by precipitation over water of a THF cocktail containing the polymer and the luminescence oxygen sensitive dye PtTFPP. The carboxylic groups present in the surface of the particles are responsible of the high stability of the nanoparticles in water and allow the performance of anodic EPD. These particles show tuneable size and zeta potential, which allows selection of the best conditions for the aqueous EPD.

To perform EPD, a gold coated chip was selected to act as the anode in order to have a biocompatible material commonly used in biomedical devices. The amount and morphology of the particles deposited was evaluated according to the SEM photographs and analyzing the magnitude *R* of the emission collected for the different times and potentials. The results show that the amount of polymer deposited is increased when increasing both deposition time and potential, while SEM confirms a homogenous distribution of the particles along the surface.

Furthermore, the oxygen characterization of the chips covered with the sensitive films was evaluated both in gas and aqueous phase. All the chips showed the same behaviour, regardless of applied potential or time, with k_{sv1} from 45 to 51.70 bar^{-1} and around 2 bar^{-1} for $k_{sv2,}$ except for the chip undergoing 40 V cm^{-1} during 10 min. The response time was also found to be around 8 seconds from nitrogen to oxygen, and less than 4 seconds from oxygen to nitrogen.

The ability of the sensing films to measure dissolved oxygen was also evaluated showing a linear k_{sv} of 0.94 bar^{-1}. Furthermore, the nanoparticles are well attached to the gold surface as they do not leach when undergoing a continuous water flow of 10 hours.

EPD of polymeric oxygen-sensitive nanoparticles has proved to be a suitable method for the development of optical sensing films that allows easy control of the amount of polymer deposited. This technique can be applied to different kinds of conductive substrates, with the advantages of adaptability to non-planar surfaces and micrometer scale, which is the main challenge for the development of appropriate sensing phases adaptable to MEMS. The use of polymers with carboxylic groups allows further enzyme crosslinking. In addition, multi-deposition of different optical indicators could be also feasible in order to develop multiparametric sensing phases for a variety of applications.

Acknowledgments. We acknowledge financial support for this work by the Regional Government of Andalusia (Excellence projects P07-FQM-2625 and P07-FQM-2738) and the Spanish Ministry of Science and Innovation (CTQ2008-01394).

.

Referencias

1. Xie, K.; Zhang, X.-W.; Huang, L.; Wang, Y.-T.; Lei, Y.; Rong, J.; Qian, C.-W.; Xie, Q.-L.; Wang, Y.-F.; Hong, A.; Xiong, S., On-line monitoring of oxygen in Tubespin, a novel, small-scale disposable bioreactor. *Cytotechnology* **2011,** 63, (4), 345-350.
2. Beshay, M.; Garon, S.; Ruiz, D.; Kempen, L. U. In *Intrinsically safe oxygen and hydrogen optical leak detector*, Photonic Applications for Aerospace, Transportation, and Harsh Environment II, Orlando, Florida, USA, 2011; SPIE: Orlando, Florida, USA, 2011; pp 802605-9.
3. Staal, M.; Prest, E. I.; Vrouwenvelder, J. S.; Rickelt, L. F.; Kühl, M., A simple optode based method for imaging O2 distribution and dynamics in tap water biofilms. *Water Research* **2011,** 45, (16), 5027-5037.
4. Jamnik, P.; Raspor, P., Methods for monitoring oxidative stress response in yeasts. *Journal of Biochemical and Molecular Toxicology* **2005,** 19, (4), 195-203.
5. Lange, C. A. K.; Stavrakas, P.; Luhmann, U. F. O.; de Silva, D. J.; Ali, R. R.; Gregor, Z. J.; Bainbridge, J. W. B., Intraocular Oxygen Distribution in Advanced Proliferative Diabetic Retinopathy. *American Journal of Ophthalmology* **2011,** 152, (3), 406-412.e3.
6. Carreau, A.; Hafny-Rahbi, B. E.; Matejuk, A.; Grillon, C.; Kieda, C., Why is the partial oxygen pressure of human tissues a crucial parameter? Small molecules and hypoxia. *Journal of Cellular and Molecular Medicine* **2011,** 15, (6), 1239-1253.
7. Galloway, N.; Amoaku, W.; Galloway, P.; Browning, A., Common Diseases of the Conjunctiva and Cornea

Common Eye Diseases and their Management. In Springer London: 2006; pp 45-60.

8. Abdallah, W.; Ameri, H.; Barron, E.; Chader, G. J.; Greenbaum, E.; Hinton, D. R.; Humayun, M. S., Vitreal Oxygenation in Retinal Ischemia Reperfusion. *Investigative Ophthalmology & Visual Science* **2011,** 52, (2), 1035-1042.
9. Barbazetto, I. A.; Liang, J.; Chang, S.; Zheng, L.; Spector, A.; Dillon, J. P., Oxygen tension in the rabbit lens and vitreous before and after vitrectomy. *Experimental Eye Research* **2004,** 78, (5), 917-924.
10. Saliterman, S., *Fundamentals of bioMEMS and medical microdevices*. Wiley-Interscience: 2006.
11. Nelson, B. J.; Kaliakatsos, I. K.; Abbott, J. J., Microrobots for Minimally Invasive Medicine. *Annual Review of Biomedical Engineering* **2010,** 12, (1), 55-85.

12. Ergeneman, O.; Abbott, J. J.; Dogangil, G.; Nelson, B. J. In *Functionalizing intraocular microrobots with surface coatings*, Biomedical Robotics and Biomechatronics, 2008. BioRob 2008. 2nd IEEE RAS & EMBS International Conference, 19-22 Oct. , 2008; 2008; pp 232-237.

13. Ergeneman, O.; Chatzipirpiridis, G.; Gelderblom, F. B.; Pokki, J.; Pane, S.; Marín Suárez del Toro, M.; Fernández Sanchez, J. F.; Sotiriou, G. A.; Nelson, B. J. In *Oxygen sensing using microrobots*, Engineering in Medicine and Biology Society (EMBC), 2010 Annual International Conference of the IEEE, Aug. 31 2010-Sept. 4 2010, 2010; 2010; pp 1958-1961.

14. Lakowicz, J. R., *Principles of fluorescence spectroscopy*. 3rd ed.; Springer: 2006; Vol. 1.

15. Wolfbeis, O. S.; Weidgans, B. M.; Baldini, F.; Chester, A. N.; Homola, J.; Martellucci, S., Fiber Optic Chemical Sensors and Biosensors: A View Back Optical Chemical Sensors. In Springer Netherlands: 2006; Vol. 224, pp 17-44.

16. Borisov, S.; Klimant, I., Luminescent nanobeads for optical sensing and imaging of dissolved oxygen. *Microchimica Acta* **2009,** 164, (1), 7-15.

17. Marin-Suarezdel Toro, M.; Fernandez-Sanchez, J. F.; Baranoff, E.; Nazeeruddin, M. K.; Graetzel, M.; Fernandez-Gutierrez, A., Novel luminescent Ir(III) dyes for developing highly sensitive oxygen sensing films. *Talanta* **2010,** 82, (2), 620-626.

18. Fernández-Sánchez, J. F.; Roth, T.; Cannas, R.; Nazeeruddin, M. K.; Spichiger, S.; Graetzel, M.; Spichiger-Keller, U. E., Novel oxygen sensitive complexes for optical oxygen sensing. *Talanta* **2007,** 71, (1), 242-250.

19. Wolfbeis, O. S., Materials for fluorescence-based optical chemical sensors. *Journal of Materials Chemistry* **2005,** 15, (27-28), 2657-2669.

20. Amao, Y., Probes and Polymers for Optical Sensing of Oxygen. *Microchimica Acta* **2003,** 143, (1), 1-12.

21. Fernández-Sánchez, J. F.; Cannas, R.; Spichiger, S.; Steiger, R.; Spichiger-Keller, U. E., Novel nanostructured materials to develop oxygen-sensitive films for optical sensors. *Analytica Chimica Acta* **2006,** 566, (2), 271-282.

22. Marín-Suárez, M.; Curchod, B. F. E.; Tavernelli, I.; Rothlisberger, U.; Scopelliti, R.; Il, J.; Di Censo, D.; Grätzel, M.; Fernandez-Sanchez, J. F.; Fernandez-Gutierrez, A.; Nazeeruddin, M. K.; Baranoff, E., Nanocomposites containing neutral blue emitting cyclometalated iridium(III) emitters for oxygen sensing. *Chemistry of Materials*.

23. Medina-Castillo, A. L.; Fernández-Sánchez, J. F.; Fernández-Gutiérrez, A., One-Step Fabrication of Multifunctional Core-Shell Fibres by Co-Electrospinning. *Advanced Functional Materials* **2011,** 21, (18), 3488-3495.

24. Burke, C. S.; Stránik, O.; McEvoy, H. M.; MacCraith, B. D., *Optical Chemical Sensors*. Springer: Dordrecht, The Netherlands, 2006; Vol. 224.
25. Charles P. Poole, J.; Owens, F. J., *Introduction to Nanotechnology*. John Wiley & Sons, Inc. : New Jersey, 2003.
26. Xia, Y.; Gates, B.; Yin, Y.; Lu, Y., Monodispersed colloidal spheres: Old materials with new applications. *Advanced Materials* **2000,** 12, (10), 693-713.
27. Madueno, R.; Raisanen, M. T.; Silien, C.; Buck, M., Functionalizing hydrogen-bonded surface networks with self-assembled monolayers. *Nature* **2008,** 454, (7204), 618-621.
28. Jiang, P.; McFarland, M. J., Large-Scale Fabrication of Wafer-Size Colloidal Crystals, Macroporous Polymers and Nanocomposites by Spin-Coating. *Journal of the American Chemical Society* **2004,** 126, (42), 13778-13786.
29. Fu, Y.; Jin, Z.; Liu, G.; Yin, Y., Self-assembly of polystyrene sphere colloidal crystals by in situ solvent evaporation method. *Synthetic Metals* **2009,** 159, (17-18), 1744-1750.
30. Reculusa, S.; Ravaine, S., Colloidal photonic crystals obtained by the Langmuir-Blodgett technique. *Applied Surface Science* **2005,** 246, (4), 409-414.
31. Li, Y.; Kunitake, T.; Fujikawa, S., Efficient fabrication of large, robust films of 3D-ordered polystyrene latex. *Colloids and Surfaces A: Physicochemical and Engineering Aspects* **2006,** 275, (13), 209-217.
32. Divliansky, I.; Mayer, T. S.; Holliday, K. S.; Crespi, V. H., Fabrication of three-dimensional polymer photonic crystal structures using single diffraction element interference lithography. *Applied Physics Letters* **2003,** 82, (11), 1667-1669.
33. Pokki, J.; Ergeneman, O.; Sivaraman, K. M.; Ozkale, B.; Zeeshan, M. A.; Luhmann, T.; Nelson, B. J.; Pane, S., Electroplated porous polypyrrole nanostructures patterned by colloidal lithography for drug-delivery applications. *Nanoscale* **2012**.
34. Dziomkina, N. V.; Vancso, G. J., Colloidal crystal assembly on topologically patterned templates. *Soft Matter* **2005,** 1, (4), 265-279.
35. Rogach, A. L.; Kotov, N. A.; Koktysh, D. S.; Ostrander, J. W.; Ragoisha, G. A., Electrophoretic Deposition of Latex-Based 3D Colloidal Photonic Crystals: A Technique for Rapid Production of High-Quality Opals. *Chemistry of Materials* **2000,** 12, (9), 2721-2726.
36. Besra, L.; Liu, M., A review on fundamentals and applications of electrophoretic deposition (EPD). *Progress in Materials Science* **2007,** 52, (1), 1-61.
37. Sun, Z.; Jin, L.; Zhang, S.; Shi, W.; Pu, M.; Wei, M.; Evans, D. G.; Duan, X., An optical sensor based on H-acid/layered double hydroxide composite film for the selective detection of mercury ion. *Analytica Chimica Acta* **2011,** 702, (1), 95-101.

38. Tada, K.; Onoda, M., Nanostructured Conjugated Polymer Films by Electrophoretic Deposition. *Advanced Functional Materials* **2002,** 12, (6-7), 420-424.

39. Yarimaga, O.; Yoon, B.; Ham, D.-Y.; Lee, J.; Hara, M.; Choi, Y.-K.; Kim, J.-M., Electrophoretic deposition of amphiphilic diacetylene supramolecules: polymerization, selective immobilization, pattern transfer and sensor applications. *Journal of Materials Chemistry* **2011,** 21, (46), 18605-18612.

40. Shi, W.; He, S.; Wei, M.; Evans, D. G.; Duan, X., Optical pH sensor with rapid response based on a fluorescein-intercalated layered double hydroxide. *Advanced Functional Materials* **2010,** 20, (22), 3856-3863.

41. Mistlberger, G.; Medina-Castillo, A.; Borisov, S.; Mayr, T.; Fernández-Gutiérrez, A.; Fernandez-Sanchez, J.; Klimant, I., Mini-emulsion solvent evaporation: a simple and versatile way to magnetic nanosensors. *Microchimica Acta* **2011,** 172, (3), 299-308.

42. Mistlberger, G. n.; Borisov, S. M.; Klimant, I., Enhancing performance in optical sensing with magnetic nanoparticles. *Sensors and Actuators B: Chemical* **2009,** 139, (1), 174-180.

43. Borisov, S. M.; Mayr, T.; Mistlberger, G.; Waich, K.; Koren, K.; Chojnacki, P.; Klimant, I., Precipitation as a simple and versatile method for preparation of optical nanochemosensors. *Talanta* **2009,** 79, (5), 1322-1330.

44. Mistlberger, G.; Koren, K.; Scheucher, E.; Aigner, D.; Borisov, S. M.; Zankel, A.; Pölt, P.; Klimant, I., Multifunctional Magnetic Optical Sensor Particles with Tunable Sizes for Monitoring Metabolic Parameters and as a Basis for Nanotherapeutics. *Advanced Functional Materials* **2010,** 20, (11), 1842-1851.

45. Gewehr, P. M.; Delpy, D. T., Optical oxygen sensor based on phosphorescence lifetime quenching and employing a polymer immobilised metalloporphyrin probe: Part 2 - Sensor membranes and results. *Medical and Biological Engineering and Computing* **1993,** 31, (1), 11-21.

46. Hartmann, P.; Leiner, M. J. P.; Lippitsch, M. E., Response characteristics of luminescent oxygen sensors. *Sensors and Actuators: B. Chemical* **1995,** 29, (1-3), 251-257.

47. Jenkins, D. M.; Zhu, C.; Su, W. W., A simple hybrid circuit for direct determination of fluorescence lifetimes. *Applied Engineering in Agriculture* **2008,** 24, (2), 259-263.

48. Trettnak, W.; Kolle, C.; Reininger, F.; Dolezal, C.; O'Leary, P., Miniaturized luminescence lifetime-based oxygen sensor instrumentation utilizing a phase modulation technique. *Sensors and Actuators B: Chemical* **1996,** 36, (13), 506-512.

49. Andrzejewski, D.; Klimant, I.; Podbielska, H., Method for lifetime-based chemical sensing using the demodulation of the luminescence signal. *Sensors and Actuators, B: Chemical* **2002,** 84, (2-3), 160-166.

50. Valledor, M.; Campo, J. C.; Sánchez-Barragán, I.; Costa-Fernández, J. M.; Alvarez, J. C.; Sanz-Medel, A., Determination of phosphorescence lifetimes in the presence of high background signals using phase-shift measurements. *Sensors and Actuators, B: Chemical* **2006,** 113, (1), 249-258.

51. McDonagh, C.; Kolle, C.; McEvoy, A. K.; Dowling, D. L.; Cafolla, A. A.; Cullen, S. J.; MacCraith, B. D., Phase fluorometric dissolved oxygen sensor. *Sensors and Actuators B: Chemical* **2001,** 74, (13), 124-130.

52. Ogurtsov, V. I.; Papkovsky, D. B., Selection of modulation frequency of excitation for luminescence lifetime-based oxygen sensors. *Sensors and Actuators, B: Chemical* **1998,** 51, (1-3), 377-381.

53. Lippitsch, M. E.; Draxler, S., Luminescence decay-time-based optical sensors: principles and problems. *Sensors and Actuators: B. Chemical* **1993,** 11, (1-3), 97-101.

54. Amao, Y.; Miyashita, T.; Okura, I., Platinum tetrakis(pentafluorophenyl)porphyrin immobilized in polytrifluoroethylmethacrylate film as a photostable optical oxygen detection material. *Journal of Fluorine Chemistry* **2001,** 107, (1), 101-106.

55. Chu, C.-S.; Lo, Y.-L., Optical fiber dissolved oxygen sensor based on Pt(II) complex and core-shell silica nanoparticles incorporated with sol-gel matrix. *Sensors and Actuators B: Chemical* **2010,** 151, (1), 83-89.

56. Hyam, R. S.; Subhedar, K. M.; Pawar, S. H., Effect of particle size distribution and zeta potential on the electrophoretic deposition of boron films. *Colloids and Surfaces A: Physicochemical and Engineering Aspects* **2008,** 315, (1-3), 61-65.

57. Demas, J. N.; DeGraff, B. A., Luminescence-based sensors: microheterogeneous and temperature effects. *Sensors and Actuators B: Chemical* **1993,** 11, (1-3), 35-41.

58. Lee, S.-K.; Okura, I., Photostable Optical Oxygen Sensing Material: Platinum Tetrakis(pentafluorophenyl)porphyrin Immobilized in Polystyrene. *Analytical Communications* **1997,** 34, (6), 185-188.

Supporting Information (SI)

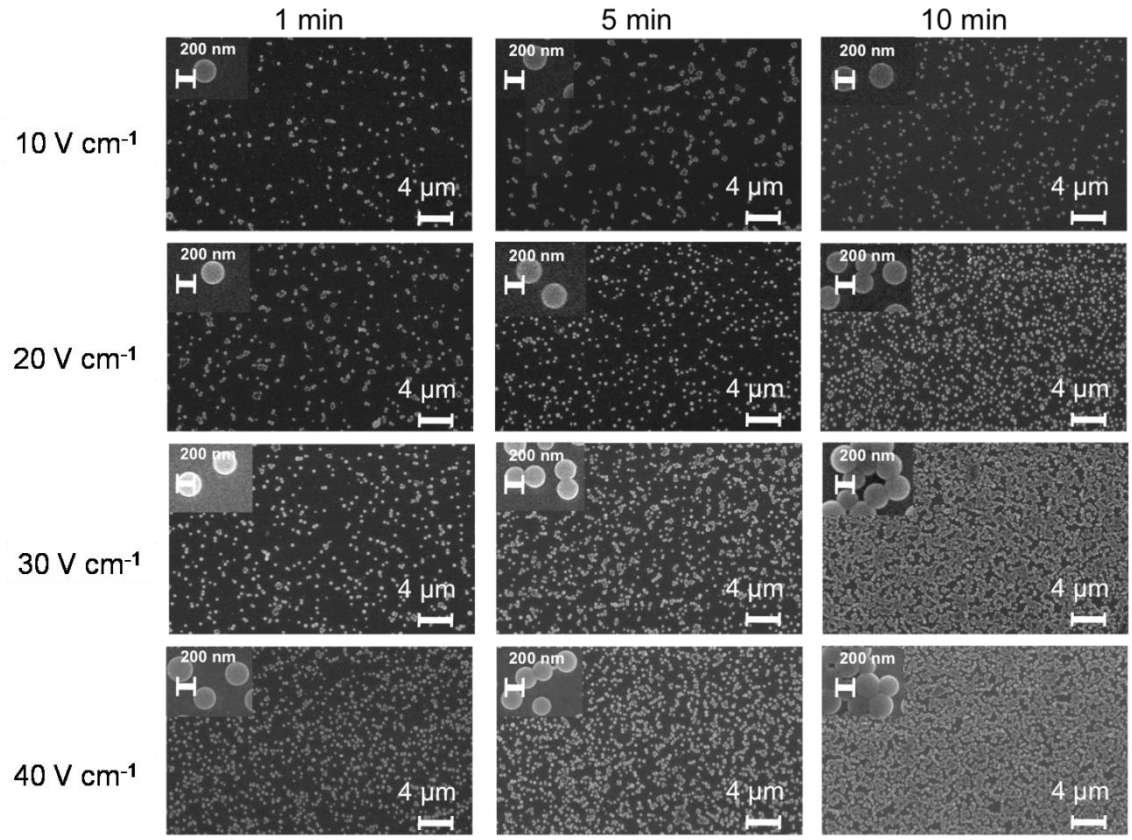

Figure S1. Scanning electron microscopy photographs for the different voltages and time applied.

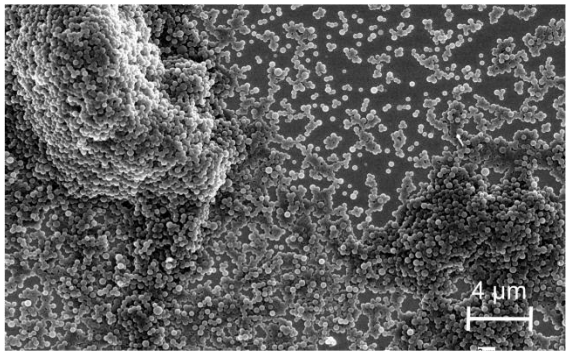

Figure S2. Scanning electron microscopy photograph of chips undergoing 20 V cm^{-1} during 10 minutes where it can be observed the heterogeneities found.

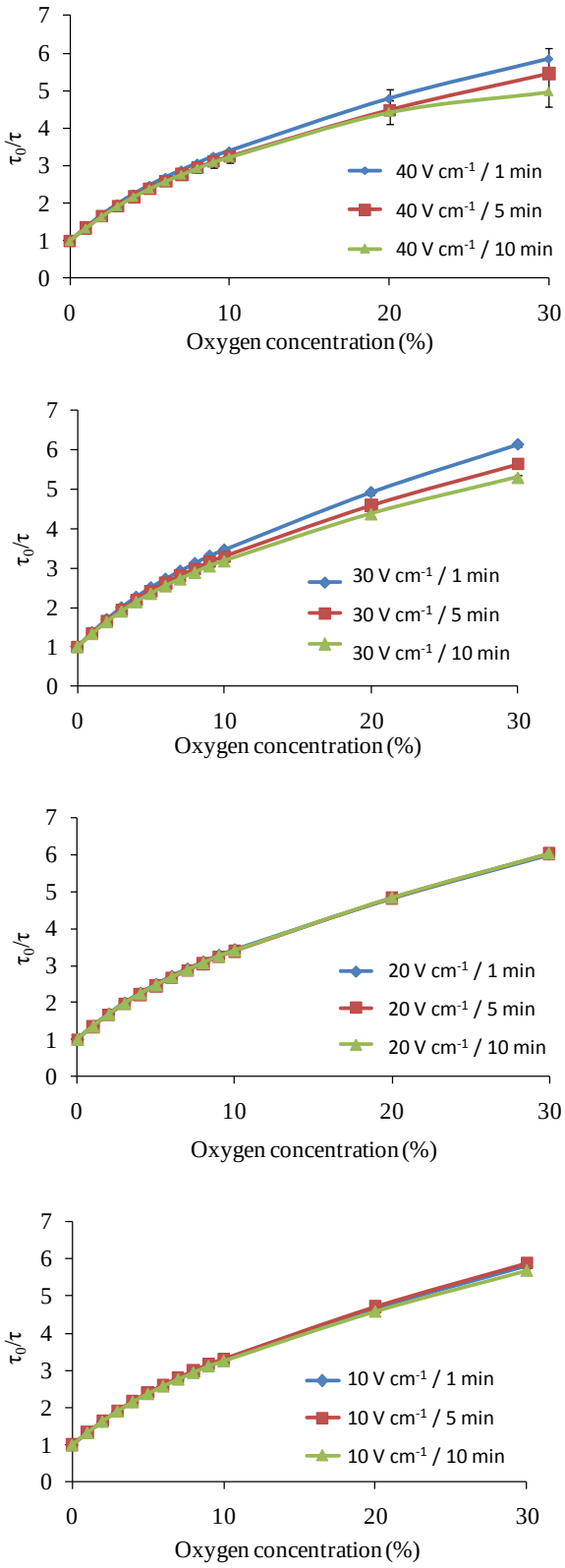

Figure S3. Stern-Volmer plots of for the different voltages and time applied. The adjustement was done using Demas' model, and the error bars are calculated by the 3 replicas using *Student's t* test (n=3, t=4.30 (2P = 0.05))

Bloque IV. Biosensores con transducción óptica de oxígeno para determinación de glucosa.

En general, un biosensor se define como un sensor que incorpora un elemento de reconocimiento biológico: ácido nucleico, enzima, anticuerpo, receptor, tejido, célula, etc., siendo ésta la única diferencia que existe con los sensores químicos comentados en la introducción. Así, el principio de detección de un biosensor se basa en la interacción específica entre la fase sensora bioquímica y el compuesto de interés. Como resultado de esta interacción se produce la variación en alguna de las propiedades físico-químicas, la cual es detectada por el transductor.

El primer biosensor fue desarrollado por Clark y Lyons en 1962 y comercializado por *Yellow Spring Instrument Company* en 1975 para la determinación de glucosa.[1] Este biosensor se denominó "*enzyme electrode*" y se basaba en el acoplamiento de la enzima glucosa oxidasa en un electrodo para oxígeno. Sin embargo, el término biosensor no empezó a usarse en literatura hacia finales de los años 70, cuando se desarrolló el primer dispositivo que utilizaba un microorganismo vivo en la superficie de un electrodo sensible a amonio[2, 3]. Este dispositivo se utilizó para detectar el aminoácido arginina y sus creadores lo denominaron "sensor bio-selectivo". Posteriormente, para acortar el nombre de este tipo de dispositivos, se empezaron a denominar biosensores y este término ha permanecido desde entonces para designar la unión entre un sistema biológico y un transductor físico. Hoy en día son muchas las definiciones de biosensor, entre ellas se puede encontrar la de "*un dispositivo analítico que incorpora a un elemento biológico (responsable de producir un reconocimiento específico) y un elemento físico (que transduce este reconocimiento), combinados de forma íntima y deliberada*".[2]

El desarrollo de biosensores empieza a crecer exponencialmente desde finales de los años 70, siendo en su gran mayoría electrodos enzimáticos o biosensores electroquímicos con aplicación en el campo clínico. Al igual que ocurrió con los sensores químicos, los biosensores de transducción electroquímica son los que más se han desarrollado y los que más relevancia y comercialización tienen en la actualidad. No obstante, el auge que sufrieron los métodos ópticos y la demostración de las ventajas de usar estas técnicas en el desarrollo de sensores, empujaron el desarrollo de biosensores ópticos, los cuales ha llegado a convertirse en el verdadero motor del incremento de dispositivos que usan este tipo de transducción. En la actualidad, existe

un gran número de dispositivos basados en interacciones de tipo bioquímico con aplicación en campos tan variados como la medicina, al análisis ambiental, la industria agroalimentaria, etc., aunque la aplicación por excelencia es la detección de glucosa, debido principalmente a su potencial en el mercado: más del 40% de los análisis de sangre detectan glucosa. [4]

En cualquier caso, este tipo de dispositivos se basan en dos tipos de interacción: interacciones de bioafinidad e interacciones biocatalíticas.

- Las **interacciones de bioafinidad** se basan en la interacción del analito de interés con la fase biosensora sin que exista transformación catalítica. Se establece, por tanto, un equilibrio donde se forma un complejo analito-receptor.[3] Para medir esta interacción, ya que no hay consumo de sustratos ni generación de productos, se suelen utilizar las características físico-químicas intrínsecas del receptor, el marcaje del receptor o bien la medida de un elemento que compita con el analito por la unión al receptor.

  De los diferentes tipos de receptores de bioafinidad existentes, los más utilizados en el desarrollo de biosensores son: anticuerpos, lectinas, células completas y ácidos nucleicos.

  Una desventaja de este tipo de interacciones es que se puede producir una saturación del receptor, lo cual no permitiría una monitorización en continuo

- Las **interacciones biocatalíticas** son las más ampliamente usadas en el desarrollo de fases biosensoras. Se basan en la utilización de biocatalizadores, es decir, elementos que favorecen que ocurra una reacción química en la cual, a partir de uno o varios sustratos, se forman uno o varios productos conocidos sin consumo del biocatalizador, el cual se regenera y puede ser reutilizado. Estos biocatalizadores pueden ser sistemas que contienen enzimas o sistemas multienzimáticos aislados, orgánulos celulares, células completas o tejidos animales o vegetales.[3] Pueden usarse para detectar la presencia de alguno de los sustratos que participan en la reacción, la desaparición de algún co-sustrato conocido distinto de aquel que se quiere detectar o bien la aparición de algún producto conocido.

Como se ha venido comentando, el oxígeno molecular es una especie que está involucrada en multitud de reacciones biológicas, bien como reactivo o como producto. Por ello, los sensores de oxígeno no sólo son relevantes para la determinación de esta especie sino que pueden ser usados como transductores de reacciones bioquímicas y, por tanto, de biosensores. Así, reacciones enzimáticas en las que estén implicadas enzimas oxidasas, oxigenasas o desoxigenasas se pueden seguir mediante el uso de sensores de oxígeno. Debido a las grandes ventajas que tienen los sensores ópticos de oxígeno frente a los electroquímicos, los biosensores ópticos basados en interacciones biocatalíticas con transducción mediante medida de oxígeno molecular han sido ampliamente estudiados[4-9]

En este bloque, se ha tomado la glucosa y la enzima glucosa oxidasa como modelos de parámetros bioquímicos para desarrollar una fase biosensora con transducción óptica de oxígeno. Para ello se ha usado el dispositivo electroforético desarrollado en el Capitulo 6, el cual permite realizar una deposición de la enzima glucosa oxidasa como elemento biocatalítico y de nanopartículas sensibles a oxígeno como el elemento transductor. Previo al estudio de las condiciones de deposición de la fase sensora, el indicado PtTFPP se unió covalentemente al polímero PSMA, el cual fue utilizado para la síntesis de las nanopartículas sensibles a oxígeno. Los resultados de este estudio están recogidos en el Capitulo 7.

Referencias

1. Clark, L. C.; Lyons, C., Electrode Systems for Continous Monitoring in Cardiovascular Surgey. *Annals of the New York Academy of Sciences* **1962,** 102, (1), 29-45.
2. Mohanty, S. P.; Kougianos, E., Biosensors: a tutorial review. *Potentials, IEEE* **2006,** 25, (2), 35-40.
3. Mello, L. D.; Kubota, L. T., Review of the use of biosensors as analytical tools in the food and drink industries. *Food Chemistry* **2002,** 77, (2), 237-256.
4. Steiner, M.-S.; Duerkop, A.; Wolfbeis, O. S., Optical methods for sensing glucose. *Chemical Society Reviews* **2011,** 40, (9), 4805-4839.

5. Moreno-Bondi, M. C.; Wolfbeis, O. S.; Leiner, M. J. P.; Schaffar, B. P. H., Oxygen optrode for use in a fiber-optic glucose biosensor. *Analytical Chemistry* **1990,** 62, (21), 2377-2380.

6. Rosenzweig, Z.; Kopelman, R., Analytical Properties and Sensor Size Effects of a Micrometer-Sized Optical Fiber Glucose Biosensor. *Analytical Chemistry* **1996,** 68, (8), 1408-1413.

7. Wolfbeis, O. S.; Oehme, I.; Papkovskaya, N.; Klimant, I., Sol-gel based glucose biosensors employing optical oxygen transducers, and a method for compensating for variable oxygen background. *Biosensors and Bioelectronics* **2000,** 15, (12), 69-76.

8. Pasic, A.; Koehler, H.; Schaupp, L.; Pieber, T.; Klimant, I., Fiber-optic flow-through sensor for online monitoring of glucose. *Analytical and Bioanalytical Chemistry* **2006,** 386, (5), 1293-1302.

9. Völkl, K. P.; Opitz, N.; Lübbers, D. W., Continuous measurement of concentrations of alcohol using a fluorescence-photometric enzymatic method. *Fresenius' Journal of Analytical Chemistry* **1980,** 301, (2), 162-163.

Electrophoretic deposition of oxygen sensing nanoparticles and glucose oxidase to developed a glucose sensing film based on optical oxygen transduction

7.1. Introduction

Glucose concentration is one of the parameters most widely detected in medicine, in special in clinical analysis where it is estimated in the 40%[1] of the blood samples. In addition, it has several applications in food industry and biotechnology. [2]

The continuous or discontinuous quantification of glucose is performed using biosensors. A biosensor consists on two elements: a recognition one which is able to selectively bind the glucose and a transduction element which provides the analytical signal. This transduction can be accomplished by detecting changes in physic-chemical properties of the media as a result of a biocatalytic interaction.[1] Such is the case of sensing glucose with oxygen transduction, where normally the enzyme glucose oxidase (GOx) catalyzes the oxidation of glucose according the following reactions:

$$\beta\text{-}D\text{-}glucose + O_2 \xrightarrow{GOx} D\text{-}glucono\text{-}1,5\text{-}lactone + H_2O$$

$$D\text{-}glucono\text{-}1,5\text{-}lactone + H_2O \longrightarrow gluconate + H^+$$

GOx has been applied in the field of biosensors for decades due to its high specificity, turn over, and stability,[3] and nowadays most commercial glucose biosensor are base in GOx.[1] The properties of GOx have allowed several authors to develop glucose biosensors by measuring the decrease in oxygen partial pressure (p_{O2}) produced during the enzyme metabolism. [1, 2, 4-6] The enzyme can be adsorbed, physically entrapped or chemically attached to the different substrates, but in any case its activity must remain constant in order to ensure the glucose detection. Particularly, the detection of changes in the oxygen concentration using optical sensors offers several advantages towards electrochemical methods such as no oxygen consumption

and inertness to magnetic fields,[7, 8] which makes its employment interesting in several areas of medicine, industry or enviroment.[9-13]

Optical oxygen sensors are based in the quenching of a luminescent dye, normally deposited in an inert matrix, when different concentration of oxygen are present in the media. The numerous biosensors with optical oxygen transduction for glucose differ from each other in the type of indicator and matrix used, immobilization mechanism and sensing configuration.[1] Besides the different materials than can be used to inmobilized the indicator, it is usually embedded in a polymeric matrix which is permeable to oxygen but not to other molecules than can act as quenchers.[7] Due to the hydrophobic nature of the polymer and the lipophilic character of most dyes, the chemical immobilization of the dye to the polymeric chain can resolve problems associated to the aggregation or leaching of the dye from the matrix, which could result in a decrease of the sensitivity to oxygen.[14]

Electrophoretic deposition (EPD) is considered as a suitable method for nanofabrication of devices with application in nanomedicine and drug delivery nanomachines.[15, 16] In addition, EPD of several types of biomaterials, including different types of enzymes, bacteria and cells, has successfully been applied. [15] In this aspect, the electrodeposition of biomolecules has proved to be a suitable method for the fabrication of microelectrodes for electrochemically based biosensors,[17] and glucose oxidase has been electrophoretically deposited from water following different strategies[2, 18, 19] where the thickness of the enzyme layer can be modified by varying the deposition parameters.

Herein we present a method for the electrophoretic deposition of both the oxygen sensitive layer and GOx enzyme. The oxygen sensitive layer consists on polymeric nanoparticles in which an oxygen sensitive dye is covalently attached to the polymeric chains. The polymer chosen was poly(styrene-co-maleic anhydride) which when used to form nanoparticles provides good stability and high zeta potential.[20] These properties are expected to improve the electrophoretic mobility of the particles and their deposition on the substrate. In the field of optical sensor, fiber-based biosensor for cholera antitoxin antibodies was developed by immobilizing biotin in a electrochemically deposited polypyrrole film.[21] However, the EPD approach has never

been applied for the production of an optical glucose sensing films with oxygen transduction.

7.2. Experimental

7.2.1. Reagents

Poly(styrene-co-maleic anhydride) polymer (PSMA, 7% maleic anhydride, Mw =224000 g mol-1), tetrahydrofuran (THF), anhydrous *N-N*-dimethylformamide (DMF), triethanolamine (TEA), glucose oxidase (GOx) from *Aspergillus niger*, and potassium phosphate dibasic and potassium phosphate monobasic were all purchased from Sigma Aldrich. Oxygen indicator Pt(II) meso-Tetra(pentafluorophenyl)porphine (PtTFPP) was purchased from Frontier Scientific. 1-Ethyl-3-(3-dimethylaminopropyl)carbodiimide hydrochloride (EDC) crosslinker for enzyme immobilization was obtained from Piercenet.

7.2.2. Covalent attachment of the dye and

The modification of the commercial polymer PSMA in order to bind the dye PtTFPP was carried out using two nucleophylic substitutions in DMF. After the reaction, the polymer (PSMAcoPtTFPP) was was washed, centrifuged and freeze-drying.

7.2.3. Luminescence intensity measurements

To obtain the intensity plot of the PSMAcoPtTFPP, a Varian Cary-Eclipse luminescence spectrometer equipped with a Xe flash lamp (peak power equivalent to 75 kW), Czerny-Turner monochromators, R-928 photomultiplier tube which is red sensitive (even 900 nm) was used. For gas mixing, two mass flow controllers (MFC) of Type EL-FLOW® model F-201CV Bronkhorst High-Tech (Ruurlo, Netherlands) were connected to copper and stainless steel tubing. The system was controlled by Cary Eclipse software for Windows 95/98/NT which fully controls the luminescence spectrometer. The O_2-gas station was controlled by a self-written LabView 8.2 program connected to a Flow Bus interface (Bronkhosrt) that fully controls the Bronkhosrt mass-flow controllers via RS-232.

7.2.4. Preparation of the nanoparticles

In order to prepare nanoparticles, 0.1% w/v of PSMAcoPtFPP was dissolved in THF. The cocktail was subsequently dropped over a buffer solution of phosphate 7.2 (50 mM) under agitation. The mixture was exposed to blowing air for 20 minutes and THF was evaporated. The resulting polymeric particles formed stable dispersions.

7.2.5. Characterization of the nanoparticles

Particle mean diameter (*d*, in nm), size distribution (*PdI*), zeta potential (ζ, in mV) and conductivity (*C*, in mS cm^{-1}) of the suspension were measured with a Zetananosizer (Malvern Instrument, model Zetasizer Nano ZS, www.malvern.com), which is equipped with a laser and a dynamic light scattering (DLS) detector.

7.2.6. Covalent binding of the enzyme

In the cases than the enzyme is attached to the nanoparticles, a zero-length crosslinking reported elsewhere is carried out using EDC.[20] The nanoparticles in the buffer solution and 2 mg of EDC are mixed during 10 minutes and continueos agitation. Subsequently, 3 mg of the enzyme are added to the mixture and the agitation in maintain during 5 hours. The particles that precipitated after the reaction and redispersed in a buffer solution of pH 7 in order to remove the unreacted enzyme and and EDC.

7.2.7. Electrophoretic cell

A home-made electrophoretic cell was built by placing an acrylglass box (polymethylmethacrylate) on a Titanium platinized plate sheet (purchased from www.ti-shop.com) that acts as the cathode. The suspension of nanoparticles can be therefore placed inside the box, and a 1 cm^2 gold coated silicon chip can be inserted opposite to the Pt plate, keeping a distance of 5 mm.

7.2.8. Glucose measurement setup

The calibration of the sensing layers was done using a phase-resolved technique.[22] A home-made holder was prepared to place the excitation source and detector forming a 90º angle while keeping the minimum distance to the measurement cell in order to avoid light losses. An ultraviolet LED (Ocean optics, model LS-450 LED-395, λ_{peak}=395 nm, angle of illumination 15º, LED diameter 5 mm, luminous power 25 μW) was used

as the excitation light source. A sinusoidal signal extracted from the internal signal generator of a dual-phase lock-in amplifier (Stanford Research System, model SR830) at a fixed frequency of 5145 Hz was used to modulate the current of the LED light source. An optical bandpass filter (Thorlabs GmbH, model MF390-18, $\lambda_{central}$=390 nm, BW=18 nm) was placed after the UV LED to prevent interferences and the light was directly pointed 45º respect to the film.

The emission light was straight forward collected by the detector (a photomultiplier tube (PMT) Hamamatsu Photonics Japan, model H10723-20, transimpedance 100 kΩ, BW DC-1 MHz) by placing it in front of the film forming another 45º. An optical bandpass filter (Hamamatsu Photonics Japan, model A10033-03, $\lambda_{central}$=630 nm, BW=60 nm) placed before the PMT, in order to separate the reflected excitation light from the emission.

The voltage signal provided by the PMT was amplified using a commercial low-noise programmable voltage preamplifier (Stanford Research Systems, model SIM911 BJT), which presented 1.8 nV/$\sqrt{\text{Hz}}$ input noise, low output noise, 1 MHz bandwidth and selectable gain from 1 to 100. Finally, a dual-phase lock-in amplifier was also used to measure the phase shift between the reference signal and the emission signal emitted as well as its magnitude when different glucose concentration were present in the media.

Assuming that the luminescence decay is monoexponential, the relation between the phase shift Φ (in radians) and the modulation frequency *f (* in Hz) is given by the expression (1).[14, 53]

$$tan\ \phi = 2\pi\tau f \quad (1)$$

where τ is the lifetime of emission (in seconds). Therefore, the modulation frequency was selected considering a compromise between a reduced sensitivity for low modulation frequencies but an increased SNR (signal to noise ratio).[14, 50, 51] Thus, *f* was experimentally fixed at 5145 *Hz*, the lower frequency that maximized the phase shift differences according to the lifetime of the sensing phase.[52]

7.3. Results and discussion

7.3.1. Chemical attachment of the dye

The covalent attachment of the dye PtTFPP to the polymer PSMA was carried out using anhydrous DMF and mild conditions by a two step reaction, which is represented in **Scheme 1**:

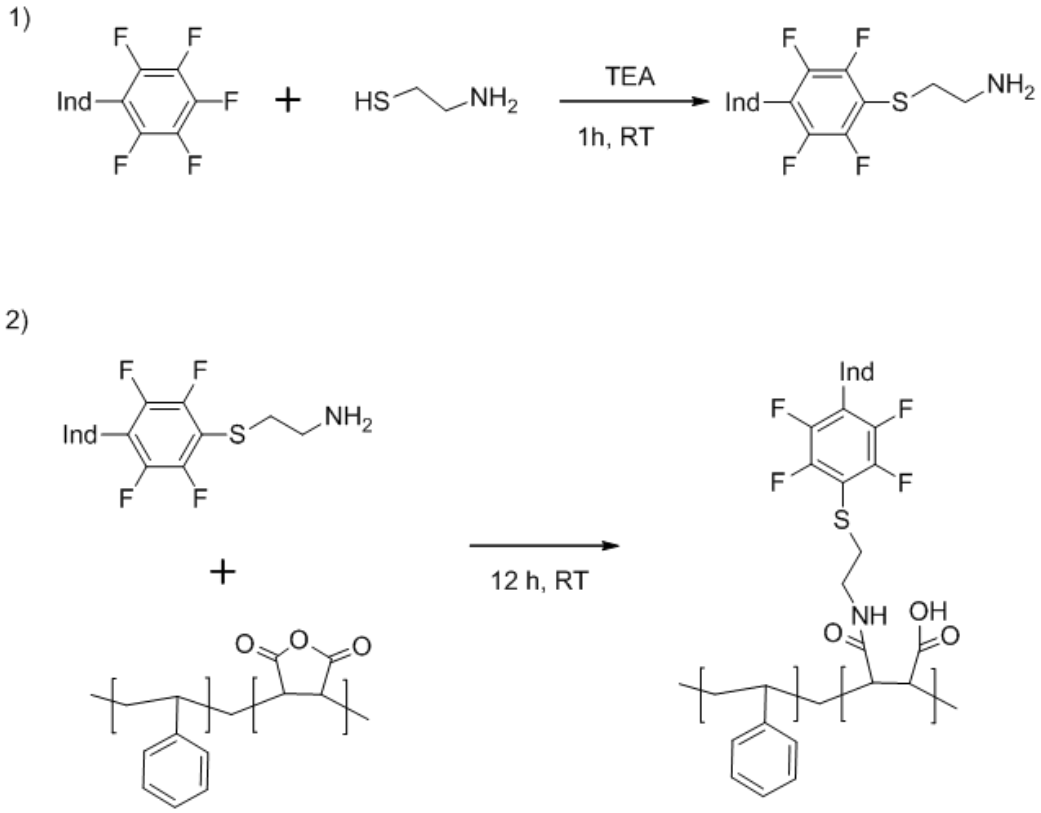

Scheme 1. Two step reaction to covalently attach the dye PtTFPP to the polymer PSMA

In the first step, 10 mg of the dye in DMF were mixed with excess of TEA and 0.53 mg of AET during one hour. Subsequently, 100 mg of the polymer PSMA were added to the mixture overnight. The resulted PSMAcoPtTFPP in DMF was precipitated 4 consecutive times in methanol order to remove the excess of TEA and PtTFFP and to confirm the covalent binding of the dye and the polymer. The polymer was subsequently dried under freeze-drying. The analysis of the absorption spectra of 0.5 g L^{-1} of the polymer in chloroform confirmed the presence on 1.59 % of PTTFFP attached to the polymer chains, considering the Beer-Lambert law and an absorption coefficient of 250000 L mol^{-1} cm^{-1} for the PtTFPP dye.

Fig. 1 shows the excitation and emission spectra for the (a) PSMAcoPtTFPP and (b) sensing layer composed of 1.5% w/w of PtTFPP immobilized in polystyrene (PS). The Soret band at 395 nm and the two Q bands between 508 and 541 nm showed no

changes in the spectroscopic behavior of the indicator when it is covalently attached to the polymer.

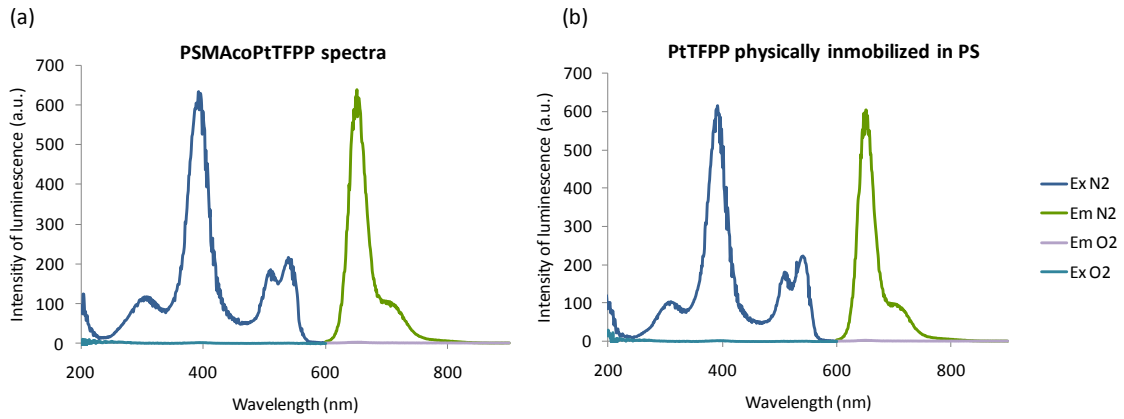

Fig. 1. Excitation (Ex) and emission (Em) spectra in presence (O2) and absence (N2) of oxygen for (a) PSMAcoPtTFPP and (b) 1.5% w/w of PtTFPP immobilized in polystyrene (PS).

7.3.2. Electrophoretic deposition

The properties of the media and the nature of the applied voltage play an important role in the electrophoretic deposition. On one side, the media is important for both the electrophoretically mobility of the enzyme and the conductivity of the media. When high potential is applied in solutions with high conductivity, the decomposition of water and the heat generation can lead to enzyme denaturation, while disrupting the deposition of both the enzyme and the nanoparticles. [19] On the other side, switching from direct current to unbalanced alternating fields is known to improve the electrophoretic deposition of enzymes.[18, 19] In addition, covalent crosslinking of the enzyme increases its stability.[1, 20]

Bearing in mind these considerations, the electrophoretic deposition under unbalanced voltage of different magnitude was carried out. Several protocols were evaluated: (1) the enzyme was first covalently bounded to the oxygen-sensitive nanoparticles via EDC and then they were deposited onto the gold coated chip via EPD; (2) nanoparticles were first deposited onto the chip via EPD and then the enzyme was covalently bounded to the immobilized oxygen-sensitive nanoparticles via EDC crosslinking; (3) both the enzyme and the nanoparticles were electrophoretically deposited at the same stage, without any crosslinking; (4) a first layer of GOx was followed by a second layer of nanoparticles, both deposited via EPD using different

applied potential; (5) GOx was electrophoretically deposited after a first layer of oxygen sensitive nanoparticles obtained via EPD.

Neither of the approaches (1) or (2) gave good results when the sensing films were exposed to glucose. It was hypothesized that the availability of enzyme was not enough to produce changes in the oxygen concentration either due to (1) the crosslinking of the enzyme to the nanoparticles destabilized the zeta potential, thus resulting a bad electrophoretic mobility and no deposition onto the gold chip, (2) the available carboxyl groups of the nanoparticles may not be enough to crosslink enough enzyme to carry out the reaction. Approaches (3), (4) and (5) showed response to glucose but were not reproducible, and the signal decreased in the first washed, suggesting the leaching of the enzyme from the chip.

Taking into account these initial results, it was decided to introduce a new strategy in which the glucose sensitivity film is produced like a *sandwich*, with alternating layers of GOx and nanoparticles. In addition, the enzyme concentration was increased up to 60 mg mL^{-1} to ensure its deposition. Therefore, four layers of nanoparticles and three layers of GOx were alternatively deposited via EPD. The chip was washed with desionized water and dried with nitrogen between each deposition step. Table 1 shows the properties of both the solutions of nanoparticles and enzyme (note that the solution of NP prepared as mentioned above was diluted with desionized water in order to apply the same conditions of potential and time than GOx).

Table 1. Properties of the solution used in EPD.

	Concentration (mg mL^{-1})	C (mS cm^{-1})	ζ (mV)	Mob	d (nm)	PdI
NP	1.5	7.96	-50	-3.9190	242.8	0.093
Gox	50	8.81	-8.92	-0.6994	-	-

Fig. 2 shows the unbalanced potential applied for the deposition of both NP and enzyme. The procedure consists of 9 cycles, each one composed of an applied potential of 2 V cm^{-1} during 45 seconds followed by 6 V cm^{-1} during 25 seconds. In this manner, it is expected not considerable change in pH or heating during the high but short potential, while the low potential ensures continuous mobility of the particles.

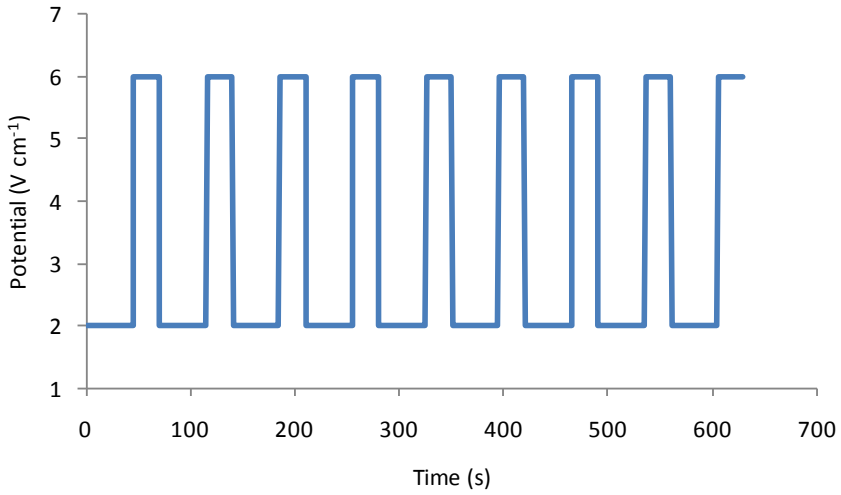

Fig. 2. Unbalanced potential applied for the deposition of each layer of enzyme and oxygen sensitive nanoparticles.

7.3.3. Figures of merits

The chip showing no lixiviation of the enzyme was calibrated by immersing it in a solution containing different amounts of glucose. The phase shift (Φ, in degrees) was detected by using the setup described above. After approximately 600 s of continuous monitoring of the oxygen consumption by the enzyme catalyzing the reaction, the chip was washed and the base line recorded before analyzing the next glucose concentration. **Fig.3** shows the response of the electrophoretically deposited chip for different glucose concentration within the physiological range (0-20mM).

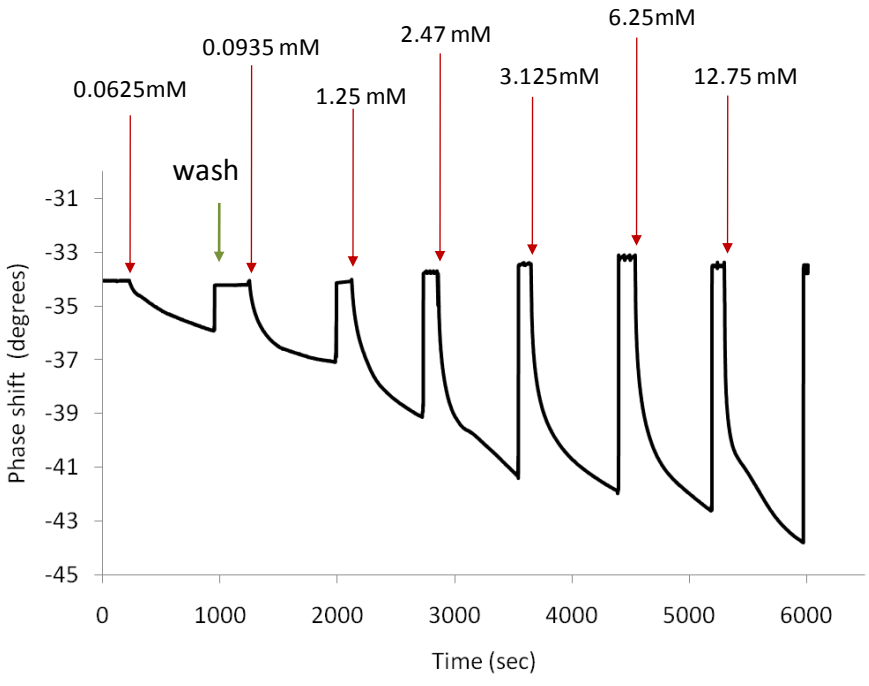

Fig. 3. Response in the phase shift of the biosensing film to different glucose concentrations.

For this type of calibration the activity of the enzyme must remain constant during all the measurement and no dye photobleaching or leaching of the particles from the chip surface should happen. However, taking into account the total time required for the sensing layer to provide a good signal, we can consider that the activity of the enzyme remains constant. On the other hand, after each measurement a small decrease of the phase shift corresponding to the baseline was detected, which suggest that either the photobleaching of the dye (for almost 2 hours with a maximum LED power) or the lixiviation of the nanoparticles from the surface, occurred.

Fig. 4 shows the normalized phase shift for each glucose concentration versus reaction time. The plot can be adjusted using a logarithm fitting following the equation:

$$y = a + b \cdot ln(x) \tag{2}$$

where y is the normalized phase shift (Φ/Φ_0) and x is time (in seconds). **Table 2** provides the slope (b) of the fitting and its corresponding correlation coefficients for each glucose concentration.

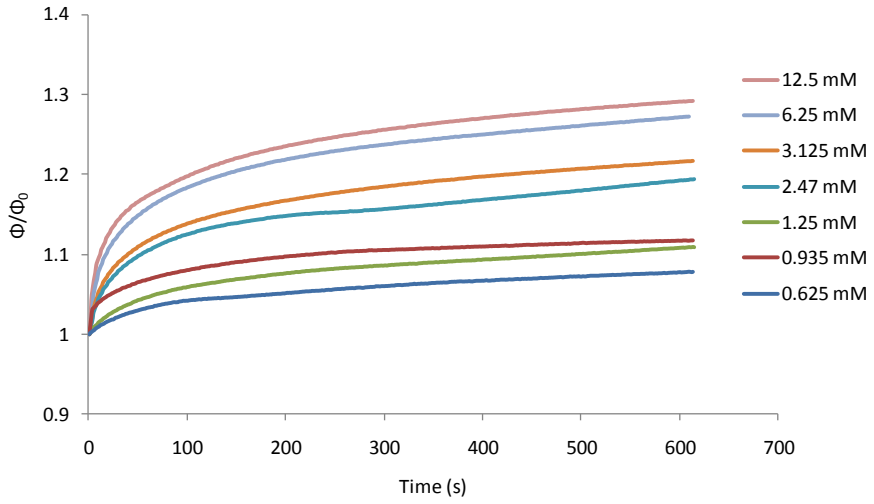

Fig. 4. Evolution of the normalized phase shift with the time for each glucose concentration.

Table. 2. Fitting of the response Φ/Φ_0 vs. time for each glucose concentration.

[Glucose] (mM)	b ($\frac{1}{\ln(s)}$)	r^2
0.625	0.0169	0.9653
0.935	0.0201	0.9920
1.25	0.0230	0.9764
2.47	0.0345	0.9885
3.125	0.0405	0.9946
6.25	0.0478	0.9983
12.5	0.0491	0.9980

The calibration of the sensing film was carried out by representing the slope of the logarithm fitting vs. glucose concentration. **Fig. 5** shows the calibration curve obtained for these conditions.

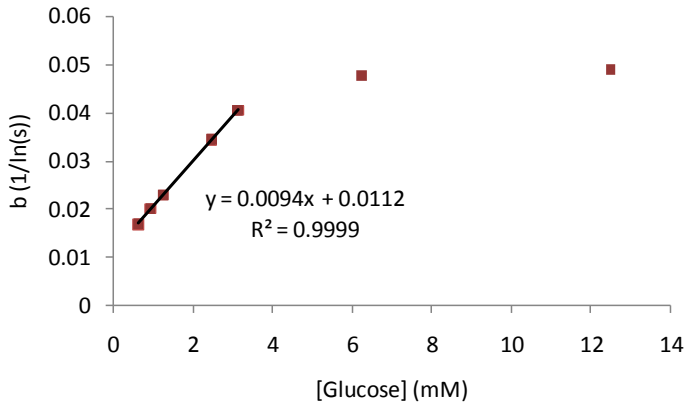

Fig. 5. Calibration curve obtained by plotting the slope of the fitting for each glucose concentration.

The saturation of the enzyme at higher concentrations is common in enzymatic systems,[23, 24] and thus, the lineal interval was found between 0.5 and 3.0 mM with a correlation coefficient of 0.9999. Nevertheless, changes in the phase shift were observed for 6.25 and 12.5 mM of glucose, allowing its detection but probably more data should be collected in order to find out an appropriate fitting model.

The illumination of the sensing phase during large periods of time may influence the sensitivity of the sensor due to either photobleaching of the dye and/or decrease of the enzyme activity, thus the time needed for the measurement was investigated. **Table 3** shows the calibration carried out by fitting Φ/Φ_0 for each concentration during different periods of time, from 100 seconds to 600 seconds. It can be observed how the goodness of the fitting increases when increasing the colleting time.

Table 3. Calibration fitting obtained by collecting the Φ/Φ_0 at different periods of time.

Colecting time (s)	a	b(1/ln(s))	r^2
100	0.0066	0.0095	0.9669
200	0.0083	0.0098	0.9735
300	0.0095	0.0095	0.9843
400	0.0093	0.0093	0.9919
500	0.0093	0.0093	0.9917
600	0.0094	0.0094	0.9999

7.4. Conclusion and future work

A glucose sensitive film with optical oxygen transduction has been developed using electrophoretic deposition. The sensing layers shows linear response between 0.5 and 3.0 mM. The transduction element of the biosensing film consisted on PSMAcoPtTFPP, which was synthesized using mild conditions, and form stable dispersion of nanoparticles. These nanoparticles can be easily deposited onto a gold coated chip by EPD. The affinity element of the biosensor is based on electrophoretically deposited GOx, which confirms the compatibility of EPD to produce sensing films with optical transduction.

The glucose sensor based of optical transduction showed a reversible behavior towards glucose, and the particles and enzyme were well attached to the gold chip, standing at least more than 20 washing cycles and illumination during 2 hours. The kinetic nature of enzymatic reactions leads to an oxygen consumption for each glucose concentration which allows its calibration.

The reproducibility of the sensing films and the influence of pH and temperature over the sensing properties will be further investigated. A deep study of the more common interferences in glucose sensing and additional optimization on the response by changing the number of layers and/or amount of enzyme and nanoparticles deposited will be carried out.

Referencias

1. Steiner, M.-S.; Duerkop, A.; Wolfbeis, O. S., Optical methods for sensing glucose. *Chemical Society Reviews* **2011,** 40, (9), 4805-4839.

2. Ammam, M.; Fransaer, J., Two-enzyme lactose biosensor based on B-galactosidase and glucose oxidase deposited by AC-electrophoresis: Characteristics and performance for lactose determination in milk. *Sensors and Actuators B: Chemical* **2010,** 148, (2), 583-589.

3. Wilson, R.; Turner, A. P. F., Glucose oxidase: an ideal enzyme. *Biosensors and Bioelectronics* **1992,** 7, (3), 165-185.

4. Moreno-Bondi, M. C.; Wolfbeis, O. S.; Leiner, M. J. P.; Schaffar, B. P. H., Oxygen optrode for use in a fiber-optic glucose biosensor. *Analytical Chemistry* **1990,** 62, (21), 2377-2380.

5. Pasic, A.; Koehler, H.; Schaupp, L.; Pieber, T.; Klimant, I., Fiber-optic flow-through sensor for online monitoring of glucose. *Analytical and Bioanalytical Chemistry* **2006,** 386, (5), 1293-1302.

6. Rossi, L. M.; Quach, A. D.; Rosenzweig, Z., Glucose oxidase–magnetite nanoparticle bioconjugate for glucose sensing. *Analytical and Bioanalytical Chemistry* **2004,** 380, (4), 606-613.

7. Wolfbeis, O. S., Materials for fluorescence-based optical chemical sensors. *Journal of Materials Chemistry* **2005,** 15, (27-28), 2657-2669.

8. Arain, S.; John, G. T.; Krause, C.; Gerlach, J.; Wolfbeis, O. S.; Klimant, I., Characterization of microtiterplates with integrated optical sensors for oxygen and pH, and their applications to enzyme activity screening, respirometry, and toxicological assays. *Sensors and Actuators B: Chemical* **2006,** 113, (2), 639-648.

9. Dmitriev, R.; Papkovsky, D., Optical probes and techniques for Oxygen measurement in live cells and tissue. *Cellular and Molecular Life Sciences* **2012,** 69, (12), 2025-2039.

10. Ungerböck, B.; Mistlberger, G.; Charwat, V.; Ertl, P.; Mayr, T. In *Oxygen imaging in microfluidic devices with optical sensors applying color cameras*, Procedia Engineering, 2010; 2010; pp 456-459.

11. Fernández-Sánchez, J. F.; Roth, T.; Cannas, R.; Nazeeruddin, M. K.; Spichiger, S.; Graetzel, M.; Spichiger-Keller, U. E., Novel oxygen sensitive complexes for optical oxygen sensing. *Talanta* **2007,** 71, (1), 242-250.

12. Papkovsky, D. B.; Chandan, K. S.; Gregg, L. S., Methods in Optical Oxygen Sensing: Protocols and Critical Analyses. In *Methods in Enzymology*, Academic Press: 2004; Vol. Volume 381, pp 715-735.

13. Pénicaud, C.; Peyron, S.; Gontard, N.; Guillard, V., Oxygen Quantification Methods and Application to the Determination of Oxygen Diffusion and Solubility Coefficients in Food. *Food Reviews International* **2012,** 28, (2), 113-145.

14. Koren, K.; Borisov, S. M.; Klimant, I., Stable optical oxygen sensing materials based on click-coupling of fluorinated platinum(II) and palladium(II) porphyrins: A convenient

way to eliminate dye migration and leaching. *Sensors and Actuators B: Chemical* **2012,** 169, 173-181.

15. Boccaccini, A. R.; Keim, S.; Ma, R.; Li, Y.; Zhitomirsky, I., Electrophoretic deposition of biomaterials. *Journal of The Royal Society Interface* **2010,** 7, (Suppl 5), S581-S613.

16. Pokki, J.; Ergeneman, O.; Sivaraman, K. M.; Ozkale, B.; Zeeshan, M. A.; Luhmann, T.; Nelson, B. J.; Pane, S., Electroplated porous polypyrrole nanostructures patterned by colloidal lithography for drug-delivery applications. *Nanoscale* **2012**.

17. Johnson, K. W., Reproducible electrodeposition of biomolecules for the fabrication of miniature electroenzymatic biosensors. *Sensors and Actuators B: Chemical* **1991,** 5, (14), 85-89.

18. Ammam, M.; Fransaer, J., AC-electrophoretic deposition of glucose oxidase. *Biosensors and Bioelectronics* **2009,** 25, (1), 191-197.

19. Ammam, M.; Fransaer, J., A study on electrodeposition of glucose oxidase from low conductivity solutions. *Electrochimica Acta* **2010,** 55, (28), 9125-9131.

20. Mistlberger, G.; Koren, K.; Scheucher, E.; Aigner, D.; Borisov, S. M.; Zankel, A.; Pölt, P.; Klimant, I., Multifunctional Magnetic Optical Sensor Particles with Tunable Sizes for Monitoring Metabolic Parameters and as a Basis for Nanotherapeutics. *Advanced Functional Materials* **2010,** 20, (11), 1842-1851.

21. Konry, T.; Novoa, A.; Cosnier, S.; Marks, R. S., Development of an "Electroptode" Immunosensor: Indium Tin Oxide-Coated Optical Fiber Tips Conjugated with an Electropolymerized Thin Film with Conjugated Cholera Toxin B Subunit. *Analytical Chemistry* **2003,** 75, (11), 2633-2639.

22. Lippitsch, M. E.; Draxler, S., Luminescence decay-time-based optical sensors: principles and problems. *Sensors and Actuators: B. Chemical* **1993,** 11, (1-3), 97-101.

23. Johnson, K. A.; Goody, R. S., The Original Michaelis Constant: Translation of the 1913 Michaelis-Menten Paper. *Biochemistry* **2011,** 50, (39), 8264-8269.

24. Pasic, A.; Koehler, H.; Klimant, I.; Schaupp, L., Miniaturized fiber-optic hybrid sensor for continuous glucose monitoring in subcutaneous tissue. *Sensors and Actuators B: Chemical* **2007,** 122, (1), 60-68.

Conclusiones

1. Se han caracterizado 7 nuevos complejos de Ir(III) tras ser depositados tanto en poliestireno como sobre un óxido metálico nanoestructurado, demostrando buena sensibilidad para detectar bajas concentraciones de oxígeno y su potencial aplicabilidad para el desarrollo de sensores luminiscentes. La nanoestructura de óxido hidróxido de aluminio he demostrado mejorar las propiedades luminiscentes de los complejos, incluso cuando estos tienen carácter neutro, si bien ésta puede influir de diferente forma sobre las características espectrales del indicador.

   En concreto, el complejo N-1001 demostró la mejor sensibilidad para detectar oxígeno entre 0 y 10% con una k_{SV} de 2848 ± 101 bar^{-1}, mientras que el N-969 posee la mejor capacidad para detectar concentraciones de oxígeno por debajo del 1% es gas, con un porcentaje de atenuación para esta concentración del 93.13% sobre el total del decaimiento de la luminiscencia

2. Se ha resaltado la utilidad de la polimerización radical por transferencia de átomo como herramienta para la síntesis controlada de nuevos materiales orgánicos, inorgánicos e híbridos con propiedades específicas. Estos materiales han permitido el desarrollo de un amplio abanico de fase sensores ópticas para diversos analitos, las cuales han sido revisadas bibliográficamente considerando los aspectos de la síntesis que más influyen sobre sus propiedades finales.

3. La aplicación de una metodología de superficies de respuesta ha permitido la síntesis, mediante la técnica de miniemulsión-evaporación, de nanopartículas híbridas sensibles a oxígeno con un tamaño objetivo de 200 nm y mínima polidispersidad. Estas nanopartículas han podido ser recolectadas sobre la punta de una fibra óptica mediante un imán especialmente diseñado, lo cual mejora la sensibilidad a oxígeno hasta en 20 veces comparado con una

membrana plana. Así, se ha demostrado la utilidad del diseño de experimentos para seleccionar las variables que presentan un mayor efecto sobre los parámetros de estudio y modelizar su respuesta. Las variables estudiadas en este caso fueron volumen de fase orgánica, concentración y peso molecular del polímero, concentración de surfactante, tiempo y amplitud de sonicación. Aplicando un *test de screening* se encontraron que para el intervalo estudiado, las variables más influyentes sobre el tamaño y la polidispersidad de las nanopartículas producidas vía miniemulsión-evaporación eran el volumen de fase orgánica, concentración y peso molecular del polímero. Así, se llevo a cabo una modelización del tamaño y polidispersidad de las nanopartículas en función de estas variables seleccionadas y en base a una metodología de superficies de respuesta. Esta modelización permitió obtener una carta tamaños y polidispersidades en función de las condiciones de síntesis y seleccionar así el volumen de fase orgánica y concentración de polímero más adecuados para obtener nanopartículas con una tamaño y/o polidispersidad determinada. Esta metodología resultó útil para predecir condiciones experimentales y controlar otros parámetros mediante un número mínimo de experimentos.

4. Se han evaluado diferentes fases sensoras para su implementación en un robot inalámbrico para la detección de oxígeno *in vivo* en el líquido ocular. Las fases sensoras basadas en el complejo PtOEP demostraron una respuesta más rápida cuando se depositaron en forma de nanopartículas, lo cual es vital para aplicaciones biotecnológicas. La sensibilidad del dispositivo recubierto con el complejo PtOEP y PS mediante dip-coating mostró una sensibilidad de 41.89 bar^{-1} en gas entre 0 y 30% de oxígeno y 31.50 bar^{-1} en agua entre 0 y 7 ppm. Además fue testado con un dispositivo de tiempo de vida en el dominio de la frecuencia especialmente diseñado para aplicaciones oculares, mostrando buena respuesta frente a concentraciones de oxígeno disuelto entre 0 y 5 ppm.

5. Se ha examinado la deposición electroforética para el desarrollo de fases sensoras ópticas nanoparticuladas, probando ser un método simple y versátil. La conductividad, potencial zeta, tamaño de partícula y polidispersidad de la suspensión de nanopartículas producida por miniemulsión-evaporación fueron optimizados variando las condiciones de síntesis. Las partículas de tamaño 280

nm y potencial zeta -33 mV fueron depositadas sobre chips recubiertos de oro. La variación del voltaje y el tiempo de deposición permite controlar la cantidad de partículas depositadas sobre los chips, aumentando para tiempo y voltajes mayores. Estas fases sensores mostraron una sensibilidad media de 48 bar^{-1} en gas para todas las condiciones experimentales de voltaje y tiempo de deposición, así como un k_{SV} de 0.94 bar^{-1} para oxígeno disuelto. Los chips se sometieron a un flujo constante de agua durante 10 horas para comprobar que no existen lixiviación de las nanopartículas de la superficie del chip. Se ha probado, por tanto, la viabilidad de la deposición electroforética para desarrollar fases sensoras, si bien esta deposición debe ser optimizada para cada caso, en especial para el desarrollo de un microrrobot inalámbrico para medidas in vivo.

6. Se ha sintetizado un polímero de poli(estireno-co-anhídrido maleico) con el complejo sensible a oxígeno pentafluorofenilporfirina de Pt(II) unido covalentemente como estrategia para evitar la lixiviación y/o agregación del indicador en el desarrollo de fases sensoras ópticas. Esta unión se llevo a cabo con condiciones suaves de reacción (temperatura ambiente durante 12 horas en DMF), obteniendo un polímero con un 1.5% en peso del indicador PtTFPP, el cual no mostró modificaciones en sus propiedades espectroscópicas y de sensibilidad.

7. Se ha desarrollado una fase sensora para la determinación de glucosa mediante trasducción óptica de oxígeno, demostrando la utilidad da la deposición electroforética para depositar dos especies de diferente naturaleza (enzima glucosa oxidasa y nanopartículas sensibles a oxígeno) y desarrollar sensores ópticos a diferentes analitos. La fase sensora obtenida fue calibrada por medidas de tiempo de vida en el dominio de la frecuencia, mostrando una respuesta lineal en el intervalo 0.5 - 3 mM de glucosa. El desarrollo de este biosensor ha permitido iniciar una nueva línea de investigación dentro Grupo FQM-297 para la determinación de parámetros bioquímicos con transducción óptica de oxígeno.

Conclusions

1. Seven Ir(III) dyes have been characterized after being immobilized both in polystyrene and in a nanostructured support. The results show good sensitivity to low oxygen concentration and demonstrate their suitability for the development of luminescent oxygen sensors. The nanostructured support based on aluminum oxide hydroxide has demonstrated to improve the luminescent properties of the dyes, even when they possess a neutral character. Specifically, the dye N-1001 showed the best sensitivity to oxygen in the range 0 to 10% with a k_{SV} of 2848 ± 101 bar^{-1}, while the N-969 has the best capacity to detect concentration below 1%, with a percentage of quenching for this concentration of 93.13% of the total luminescent decay.

2. The utility of Atom Transfer Radical Polymerization (ATRP) as a tool for controlled synthesis of new organic, inorganic or hybrid materials has been highlighted. These materials with specific properties have allowed the development of a wide range of optical sensing phases for different types of analytes. Theses sensing phases have been reviewed according to the most important parameters involved in their synthesis through ATRP and how these parameters can influence the final properties of the sensing phase.

3. Surface Response Methodology (RSM) has allowed the synthesis, via miniemulsión-solvent evaporation, of hybrid oxygen sensitive nanoparticles with a target size of 200 nm and minimum polydispersity. These nanoparticles can be easily collected on the tip of an optical fiber by means of a special magnet, which improves the sensitivity to oxygen up to 20 times compared to a planar membrane. Therefore, it has been demonstrated the utility of the experimental design to select those variables which a major effect over the parameter of study and to modelize their response. The selected variables for this case were volume of organic phase, concentration and molecular weight of

the polymer, concentration of surfactant, and sonication time and amplitude. By first applying a screening test, the variables with more influence in the range of study over size and polydispersity were organic phase volume and concentration and molecular weight of the polymer. Following this selection, a modelization of size and polydispersity as a function of these variables using a SRM was carried out. This model allowed to obtain a catalogue of size and polydispersity in order to select the best synthesis conditions (organic phase volume and polymer concentration) to obtain a specific size and/or polydispersity. In the same way, this methodology could by to explore other experimental conditions and predict the values of certain parameters by using a minimum number of experiments.

4. Two different sensing phases have been evaluated for their implementation in a wireless microrrobot for *in vivo* oxygen determination inside the eye. These sensing phases, based on the dye PtOEP, showed faster response time when they were deposited onto gold coated chip in the form of nanoparticles. The sensitivity of the wireless device covered by a PS layer and the dye PtOEP with dip-coating showed a k_{SV} of 41.89 bar^{-1} in gas and 31.50 bar^{-1} in water. In addition, the dip-coated microrobot sensor was tested with a custom-built ophthalmologic setup based on the lifetime measurement in the frequency domain, showing ability to detect changes in oxygen concentration between 0 and 5 ppm in water.

5. The electrophoretic deposition (EPD) of polymeric nanoparticles has been explored in order to develop a simple and versatile method for the production of optical sensing phases. The conductivity, zeta potential, size and polydispersity of the nanoparticles produced via precipitation-evaporation were optimized prior to the EPD. Final particles sizing 280 nm with a zeta potential of -33 mV were deposited onto a gold coated chip by applying different potential and times. This variation allows to control the amount of deposited particles, increasing with either higher times or potential. The sensing phases developed by EPD showed sensitivity to oxygen of about 48 bar^{-1} in gas regardless of the experimental conditions, and a k_{SV} of 0.94 bar^{-1} for dissolved oxygen. The sensing covered chips underwent a continuous flow rate

during 10 hours in order to evaluate the attachement of the nanoparticles to the gold surface, showing no lixiviation. The viability of EPD to develop optical sensing phases has been proved. The deposition has to be optimized for each application, especially for the development of a wireless microrrobot for *in vivo* measurements.

6. A polymer based on poly(styrene-co-maleic anhydride) with the oxygen sensitive dye Pt(II) pentafluorophenyl porphyrine (PtTFPP) covalently attached has been developed. This strategy avoids the lixiviation and/or aggregation of the dye due to incompatibilities with the matrix nature in the development of optical sensing phases. This attachment was carried out using mild conditions of reaction (room temperature during 12 hours in DMF). The polymer obtained posses a 1.5% in weight of the indicator PtTFPP, which did not show modifications in its spectroscopic properties and sensitivity.

7. An optical sensing phase has been developed for the determination of glucose through oxygen transduction. It has been demonstrated the ability of EPD to deposit species of different nature (glucose oxidase enzyme and oxygen sensitive polymer nanoparticles) and develop different types of optical (bio)sensors. The sensing phase obtained was calibrated using lifetime measurement in the frequency domain, showing a lineal resopnse in the range 0.5 – 3 mM of glucose. The development of this biosensors phase is the starting point of a new research line in the Research Group FQM-297 for the determination of biochemical parameters with optical oxygen transduction.